DEVELOPMENT OF SERS BASED METHODS FOR EARLY CANCER DETECTION

by
Sevda Mert

Submitted to Graduate School of Natural and Applied Sciences
in Partial Fulfillment of the Requirements
for the Degree of Doctor of Philosophy in
Biotechnology

Yeditepe University
2018

DEVELOPMENT OF SERS BASED METHODS FOR EARLY CANCER DETECTION

APPROVED BY:

Prof. Dr. Mustafa Çulha ....
(Thesis Supervisor)

Prof. Dr. Ertuğrul Kılıç ....

Assoc. Prof. Dr. Ali Özhan Aytekin ...........A.O.............

Assist. Prof. Dr. Hüseyin Çimen ....HC.............

Assist. Prof. Dr. Kaan Keçeci ....

DATE OF APPROVAL:.../..../2018

Dedicated to

“Kayıp Köpek Dostlarıma”…

ACKNOWLEDGEMENTS

The list I'm going to thank is quite long. First of all, I would like to dedicate this doctorate thesis to my lost dog friends. I am still in mourning. Then, the greatest thanks to the dog friends who are still living in these university boundaries and have been given the right to live because they are a great source of motivation for me to come to Yeditepe every day.

My special thanks to Prof. Dr. Mustafa Çulha because a multidisciplinary and interdisiciplinary science-based perspective that I have learned in time from him and he has given me a place in his laboratory advising me six-year.

I am also grateful to my thesis monitoring committee members Assist. Prof. Dr. Kaan Keçeci and Assist. Prof. Dr Hüseyin Çimen for their directive ideas throughout thesis work.

I would like to thanks to my lovely friends; Seda Keleştemur Demir, Zehra Çobandede, Hande Nayman, Hande Duru and Gamze Kuku for being supportive, motivating and helping me with proofreading of my thesis and defense presentation, Zeynep Işık, Merve Ercan, Melike Sarıçam and Hamide Özaydın for their lovely friendships. I also thank to Mine Altunbek, Şaban Kalay and Ertuğ Avcı for helping to solve the problems I experienced in laboratory.

Life is passing and no one can catch the time by their hands. I have learned much and experienced during the long PhD years. I learned a lot about human, respecting who you are but without confirmation, I saw the background of unconscious behaviors. I mostly felt pain due to uncontrolled situations but I realized that I cannot change everything, something just happened for an unknown reason according to us but there would be a mean in the universe. That is what I would like to believe. Most importantly, I learned what really love is from Dogs and started to apply on to my life. Such a great gain! It is more important than having PhD for me.

My Mom and Dad, be proud of yourself!

ABSTRACT

DEVELOPMENT OF SERS-BASED METHODS FOR EARLY CANCER DETECTION

The applicability of SERS in early cancer detection by means of differentiating cancerous tissue from healthy tissues was systematically investigated by employing three different sample preparation strategies. In the first approach, a 5-µm thick cryosectioned tissue specimen was placed on a PDMS layer coated glass slide before adding a volume of 20-µl 16× concentrated AgNPs containing colloidal suspension onto the tissue. Then, the colloidal suspension was dried at the suspended position to achieve optimal distribution of the AgNPs in the droplet area. In the second approach, *in situ* synthesis of AgNPs in the homogenized tissue sample was aimed. A 10-µl from each of 4.36×10^{-1} M $AgNO_3$, 3.55×10^{-2} M $HONH_2 \cdot HCl$ and 3×10^{-2} M NaOH was successively added into the 10-µl of homogenized tissue suspension to reduce Ag^+ ions into AgNPs in the homogenized tissue. Then, a 2µl of this mixture was placed onto a CaF_2 slide and dried before the SERS measurements. The first approach was optimized through parameters including substrate used to place tissue specimen (PDMS, Al-foil or CaF_2), signal collection type (random selection versus mapping), spectral range and acquired-mapping size while the latter approach optimized through the acquisition type and concentrations of $AgNO_3$, $HONH_2 \cdot HCl$ and NaOH solutions. Then, the data acquired with each sampling method was analyzed with PC-LDA classification models and the coefficients by comparing intra- and inter-method reproducibility, accuracy, and SERS performance indicators of spectral richness and SNR. Finally, the data acquired from these two methods were compared with our previously developed approach of Crashed-liquefied consisting of mixing a 5-µl 32× concentrated colloidal AgNP suspension with homogenized tissue sample by utilizing human thyroid biopsies (n=64). The results showed that *in situ* approach indicated a higher classification accuracy compared to other approaches for malignant vs. healthy tissue and benign vs. healthy tissue diagnostic combinations by using full spectra region of spectra while the best classification performance for benign vs. malignant tumors was obtained by using Cryosectioned-PDMS and Crashed-liquefied approaches. The findings of this study clearly indicate that SERS is a suitable technique to employ in cancer diagnosis.

ÖZET

KANSERİN ERKEN TEŞHİSİ İÇİN YÜZEYCE ZENGİNLEŞTİRİLMİŞ RAMAN SAÇILMASINA DAYALI METOTLARIN GELİŞTİRİLMESİ

Yüzeyde zenginleştirilmiş Raman saçılmasının (YZRS), kanserli ve sağlıklı dokuyu birbirinden ayırabilmesi sebebiyle erken kanser teşhisi için uygulanabilirliği, üç farklı örnekleme stratejisi geliştirerek sistematik bir şekilde keşfedildi. “Cryosectioned-PDMS” isimli ilk yaklaşımda, 16 X kat konsantre edilmiş kolloidal gümüş nanoparçacık (GNP) içeren solüsyondan 20-µl hacimce, PDMS ile kaplanmış bir cam slaytta üzerinde yer alan 5 µm kalınlığındaki cryostat doku kesitinin üzerine eklenir. Sonra, kolloidal suspansiyon, damla yüzeyinde optimal bir GNP dağılımı elde edebilmek için, asılı pozisyonda kurutulur. “*in situ*” olarak isimlendirilen ikinci yaklaşımda, GNP’lerin homojenize edilmiş doku içerisinde sentezlenmesi amaçlanır. Indirgeyici ajan olarak hacimce 10-µl 3.55×10^{-2} M $HONH_2 \cdot HCl$, hacimce 10-µl of 3×10^{-3}M NaOH solüsyonu ile birlikte, hacimce 10-µl doku süspansiyonun içerisine eklenmesinden sonra hacimce 10-µl 4.36×10^{-1} M gümüş nitrat çözeltisi de içerisine eklenir. Sonra, bu karışımdan hacimce 2-µl CaF_2 slaydının üzerinde yer alarak, ölçüm öncesi kurutulmaya bırakılır. İlk yaklaşım, doku örneğinin yer alacağı yüzey (PDMS, Al folyo, CaF_2), sinyal toplama türü (rastgele seçim, haritalama), spectral aralık, haritalanan yüzeyin büyüklüğü gibi parametreler yönünden optimize edilirken; *in situ* metotu, sinyal elde türü ve $AgNO_3$, $HONH_2 \cdot HCl$ ile NaOH solüsyonlarının konsantrasyon optimizasyonlarını içerir. Sonra, her bir metot, parametrelerin değişkenlik katsayıları, metot içi ve metot arası tekrarlanabilirlik, doğruluk ve zengin YZRS sinyal paterni terimleri ve PC-LDA sınıflandırma modelleri ile analiz edildi. Sonra, bu iki metot, hacimce 5-µl GNP suspansiyonun homojenize doku ile karıştırılmasını içeren bir önceki yaklaşımımız olan “Crashed-liquefied” ile, 64 adet insan tiroid biyopsileri kullanılarak karşılaştırıldı. Sonuçlar göstermiştir ki, YZRS datasının tam spectrum bölgesinin kullanılarak, kötü ve sağlıklı doku ile iyi huylu ve sağlıklı dokuyu ayırmada en iyi yöntem *in situ* iken, iyi huylu ve kötü huylu tümörleri en iyi ayıran ise Cryosectioned-PDMS ve Crashed-liquefied yöntemleridir. Bu çalışmanın bulguları, YZRS tekniğinin kanser tanısında kullanılabilir olduğunu göstermektedir.

TABLE OF CONTENTS

LIST OF FIGURES

LIST OF TABLES

LIST OF SYMBOLS/ABBREVIATIONS

A	Adenine
Ag	Silver
Al	Aluminum
Au	Gold
C	Carbon
°C	Degrees Celsius
Cu	Copper
g	Gram
G	Guanine
H	Hydrogen
h	Hour
kV	Kilovolt
min	Minute
ml	Milliliter
mW	Milliwatt
nm	Nanometer
N	Nitrogen
O_2	Oxygene
v	Volume
w	Weight

4MBA	4-Mercaptobenzoic Acid
$AgNO_3$	Silver Nitrate
AgNPs	Silver Nanoparticles
AJCC	American Joint Committee on Cancer
AuNPs	Gold Nanoparticles
a.u.	Arbitrary Units
CaF_2	Calcium Fluoride
CARS	Coherent Anti-Stokes Raman Scattering

CCD	Charge-Coupled Device
CE	Chemical Enhancement Mechanism
CO_2	Carbon Dioxide
COV	Covariance
CT	Computed Tomography
CV	Coefficient of Variations
ddH_2O	Double-Distilled Water
DLS	Dynamic Light Scattering
DNA	Deoxyribonucleic Acid
DOF	Degrees of Freedom
ECM	Extracellular Matrix
ELISA	Enzyme-Linked Immunosorbent Assays
EM	Electromagnetic Enhancement Mechanism
ER	Estrogen Receptor
FFPP	Paraffin Preservation
FN	False Negatives
FNAC	Fine-Needle Aspiration Cytology
FP	False Positives
FS	Fluorescence Spectroscopy
FT-IR	Fourier Transform Infrared Spectroscopy
FTC	Follicular Thyroid Carcinoma
FIT	Fecal Immunochemical Test
gFBOT	Guaiac-Based Fecal Occult Blood Test
h-AgNPs	Hydroxylamine Reduced Silver Nanoparticles
HSES	High Speed Encoded Stage
H&E	Hematoxylin and Eosin
IR	Infrared
IF	Immunofluorescence
IHC	Immunohistochemical
ISH	*in situ* Hybridization
LDA	Linear Discrimination Analysis
LOD	The limit of detection
LOO-CV	Leave-one-out-Cross-Validation

LSPR	Localized Surface Plasmon Resonance
MALDI-MS	Matrix-Assisted Laser Desorption Ionization Mass Spectrometry
MRI	Magnetic Resonance Imaging
MTC	Medullary Thyroid Carcinoma
NIR	Near Infrared Region
N.A.	Numerical Aperture
OH	Hydroxyl
QD	Quantum Dot
PCA	Principal Component Analysis
PCR	Polymerase Chain Reaction
PCs	Principal Components
PDMS	Polydimethylsiloxane
Phe	Phenylalanine
PO_2	Phosphate
PN	Partial Nephrectomy
PR	Progesterone Receptor
Pro	Proline
PTC	Papillary Thyroid Carcinoma
PSA	Prostate-Specific Antigen
RCC	Renal Cell Carcinoma
RIA	Radioimmunoassay
RNA	Ribonucleic Acid
ROS	Reactive Oxygen Species
S.D.	Standard Deviation
SEM	Scanning Electron Microscopy
SERS	Surface-Enhanced Raman Scattering
SORS	Spatially Offset Raman Scattering
SRS	Stimulated Raman Scattering
SNR	Signal to Noise Ratio
TCC	Transitional Cell Carcinoma
TEM	Transmission Electron Microscopy
TERS	Tip-Enhanced Raman Scattering
TN	True Negatives

TP	True Positives
Trp	Tryptophan
TRS	Transmission Raman Scattering
Tyr	Tyrosine
UV-Vis	Ultraviolet-Visible
US	Ultrasonography

1. INTRODUCTION

1.1. KIDNEY CANCER

Cancer is an abnormal growth of a cell, which is induced by genetics which regulates cell functions, especially growth and division. Genetic changes can occur either due to a person's lifestyle or/and inheritance from parents. The environmental exposures such as chemicals, tobacco smoke and ultraviolet rays from the sun can damage the DNA of the healthy cells, which eventually leads to uncontrolled cell division. The main mutated genes in healthy cells that promote their differentiation into cancer cells are proto-oncogenes, tumor suppressor genes, and DNA repair genes [1]. The alterations in these genes are the main reasons for the unlimited proliferation and survival characteristics of cancer cells. Although there are more than 100 different cancer types, the most commonly diagnosed types of cancer around the worldwide, especially in less developed regions, are lung, female breast, bowel, and prostate cancer. Lung, liver, stomach, and bowel are the types that are mostly implicated in cancer-related deaths [2]. Some cancer cells such as leukemia grow in the blood circulation even though others grow in tissue. On the other hand, not every tissue differentiation is cancerous such as hyperplasia, but untreated benign tumors can eventually tend to form cancer. The untreated cancer cells can spread from the original site of the body using body's bloodstream or lymph vessels to form new tumors in different organs. The spread of cancer cells into other tissues is referred as metastasis [1].

Kidney cancer is almost 2 per cent of all cancers worldwide, with its most common types being renal cell carcinoma (RCC) and transitional cell carcinoma (TCC). As the mortality rate due to kidney cancers increases by 2 per cent to 3 per cent per decade, about 210,000 new cases are reported each year and over 100,000 patients die due to the disease [3]. Kidney cancer is diagnosed based on the information obtained from imaging techniques, biopsy examinations, and blood and urine testing. The imaging techniques including ultrasound, intravenous pyelogram, computed tomography (CT or CAT) scan, cystoscopy/ nephro-ureteroscopy, and magnetic resonance imaging. The commonly used treatment approach for kidney cancer is surgery including radical nephrectomy, partial nephrectomy (PN), laparoscopic nephrectomy, and robotic-assisted laparoscopic nephrectomy. According to the American Joint Committee on Cancer (AJCC), the most common staging system for kidney cancer is the association between tumor stage and tumor size as T1a ≤ 4 cm, T1b > 4 cm but ≤7 cm, T2a > 7 cm but ≤ 10 cm, T2b > 10 cm [3]. Tumor size is related to the recurrence rate, the survival rate, and the choice of clinical treatment method [4, 5]. Several studies have shown that subdividing the T1 tumor stage into T1a and T1b stages is beneficial for a better estimation of the survival rate in patients with tumors in the size of 4 cm or less [6, 7]. The lower recurrence rate after the PN process for the tumors.

1.2. THYROID CANCER

Thyroid cancer is one of the cancer types having a rapid increase in the incidence especially in young people [8]. Focal thyroid lesions are one of the most mutual issues for endocrinologists and surgeons. The gold standard for identification and therapeutic process of thyroid lesions generally depends on the following methods, high-resolution ultrasonography (US), fine-needle aspiration cytology (FNAC) under US and surgery. The use of gold standard of pathological examination for the abnormal thyroid tissue in 7 percent to 16 percent of detected nodules are reported as malignant with a diagnostic sensitivity of 83 to 98 per cent and specificity of 70 to 92 per cent in the literature [9, 10].

Papillary thyroid carcinoma (PTC) is the most common cancer type in the incidence of all thyroid cancer cases with a range of 70 to 80 per cent , follicular thyroid carcinoma (FTC) with an incidence rate of 15 to 20 per cent , medullary thyroid carcinoma (MTC) and anaplastic thyroid cancer that constitutes 5-10 per cent and 2-5per cent of thyroid cancer patients, respectively [11, 12]. Minimally invasive carcinomas are generally indistinguishable from benign adenomas in terms of their architectural and cytological properties. The diagnosis of malignancy depends on capsular and/ or vascular invasion [13]. Thyroid cancer is generally first recognized by a lump or nodule in the thyroid gland. FNAC can be inadequate to provide differential diagnosis for benign and malignant lesions. Delay in diagnosis, sampling error, high rate of false-negative results lead to delayed effective treatment protocol for the patients with a traumatic process [14]. A 7-gene panel of genetic mutations and rearrangements (BRAF, RAS, RET/PTC, PAX8/PPARγ) gives an information platform for decision-making of primary thyroid surgery evaluating molecular markers in patients. The sensitivity of the 7-gene mutational panel testing in indeterminate cytology thyroid nodules has been reported to vary from a range of 44 per cent to 100 per cent [15-17]. Even though mutational testing has been suggested to provide optimal molecular malignancy detection for the cases of indeterminate cytology, it has been yet placed in the routine clinical protocol. Alternative or supportive methods are crucial to reduce the cost of diagnosis, to gain time, and to increase the quality of diagnosis.

1.3. CONVENTIONAL METHODS OF CANCER DIAGNOSIS AND THEIR DRAWBACKS

The physician firstly evaluates the sematic symptoms of the patient with the imaging techniques such as ultrasound, computed tomography (CT or CAT) scan, mammograms, magnetic resonance imaging (MRI) and endoscopy with marker detection-based blood and urine tests. For instance, Flexible sigmoidoscopy, colonoscopy, Double-contrast barium enema, CT colonography, guaiac-based fecal occult blood test (gFOBT), fecal immunochemical test (FIT) and stool DNA test (sDNA) are the screening tests used in early detection of colon cancer [18]. Pap test and HPV test are used in early detection of cervical cancer [19]. Yearly endometrial biopsy sometimes is used for the person who has a genetic predisposition for early detection of endometrial (uterine) cancer. Prostate-specific antigen (PSA) test with or without a rectal exam may be successful to detect prostate cancer. Complete skin examination is another screening test used for early detection of skin cancer. There are a few more cancer screening tests and techniques such as bone marrow and bone scan that are more specific and related to certain cancer types. Although marker detection can be helpful in the early diagnosis of cancer cases supposing to increase the survival rate and decrease the cancer deaths but not all cancer types have related biomarkers, and some invasive screening tests can have harmful effects on patients such as bleeding, health problems, as well as false-negative and false-positive results [20]. However, screening tests and imaging techniques can provide background information about the size and location of cancer but they cannot provide information about the grading status of the lesions. The routine clinic application of the techniques varies among the countries related to their economic and socials status. The imaging and screening techniques are followed by a biopsy or complete surgical removing of the suspicious neoplasm "*new growth*" from the patient. Biopsy samples are diagnosed by a group of pathologists related to histological information of cells and extracellular matrixes under a microscope. For this, a series of steps of a gold standard approach of pathological examination protocol fixating, embedding, slicing and staining were followed to examine tissue morphology, architecture and composition. Hematoxylin and Eosin (H&E) for nuclei and remaining cell components, Mason's Trichrome for nuclei, collagen and cytoplasm, Verhoeff and Van Gieson for elastin, Verhoeff and Van Gieson for calcification and Safranin-O for glycosaminoglycans are the common dyes used to stain and evaluate the pathology [21]. There are differences in histological grading systems depending on the parameters such as cell nucleus, size, uniformity, nuclear margin, chromatin, mitotic count..etc. Fisher's modification of Black nuclear grading, Mouriquands's grading, Robinson's grading, P. Scarff-Bloom-Richardson (SBR) grading (mostly used one), a grading system proposed by Khan et al and another grading system proposed by Taniguchi et al. are the well-known developed grading systems using for cancer grading studies seem to be accurate having a key problem with different classification results using different grading systems on the same biopsy samples [22]. Fluorescence or chromogenic enzymatic reactions (immunofluorescence (IF), immunohistochemical (IHC) analysis are the biological assays used in pathology, which uses the tagged proteins and their localization on the sectioned tissues while *in situ* hybridization (ISH) defines specific gene expression. However, to overcome the main shortfall of biomarkers assays having low sensitivity, a specific biomarker group should be selected immediately because poor selection causes missing diagnosis with inadequate sensitive analysis of the tissue. Estrogen receptor (ER), progesterone receptor (PR), HER2, BRAF V600, cMET, IDH1, mutant, and MMR panel, are the global markers used for cancer diagnosis. For the IHC technique in use, one needs to know in advance which specific proteins are related to the type of cancer, which is a complex disease system that it cannot have a precise diagnosis only with the most accurate detection of a particular protein but it helps for preliminary prognosis of the tumor sample. IHC tests combined with histology-based information and grading systems are the main parameter used by the pathologist finally to give a "predicted" diagnosis, which is still depends on the subjective decision of a group pathologist. The last predicted pathology report given by a group pathologist instead of a pathologist seems to increase the objectiveness of the diagnosis by decreasing the incorrect and non-diagnosis cases.

Likewise, time consuming steps such as stabilization and preservation of the tissue using the routine pathology protocols have challenges underlying the effects of chemical processing, which produce selective antigenic loss and nucleic acid fragmentation thereby reducing the likelihood of correct recognition of the biopsied tissue sample [23, 24].

Fixation with formaldehyde is a standard procedure used in clinics for long-term storage of biopsies to protect the morphological structure of the tissue to prevent the decay of the tissue components and to avoid the autolysis of cells. However, formaldehyde as being a biohazard for the laboratory affects the quality of DNA / RNA blocking retrieval from the block degrades the nuclear material and modifies the sequences, which decrease the applicialbity and reliability of molecular based detection tests [23, 25-27].

Paraffin-embedding is another conventional process used in routine pathology, which is applied after formalin fixation. Paraffin embedding is an advantage in that the tissue section taken from the fixation can be maintained for many years and the possibility of reaching the tissue sections when the pathologist wants to see, which means the re-diagnosis is possible. However, IHC techniques utilize tissue sections without paraffin-embedding which means the dewaxation process is employed on the tissue to remove the paraffin. However, whole paraffin never removed almost from the tissue structure with the main downside of distortions in the tissue components, and paraffin remnants which in turn can affect the correct recognition significantly leading to specific antigen loss.

The main aim of tumor surgery is to maximize tumor removal nearby healthy tissue with a well-known criticism of having undifferentiated abnormal cell and tissue from healthy tissues. The surgeon that examines tumorous and healthy tissues to determine the tumor-positive resection margins uses ocular observation. Pathologists that follow intraoperative pathological analysis use frozen section procedure, which is the examination of tissue while surgery is taking place. This process is time-consuming, requires highly skilled personnel, and the interpretation is often subjective [28]. Therefore, tumor tissues are not often removed from tumor margins efficiently, and the remaining tumor cells lead to recurrence by failing the treatment.

These conventional methods need to be improved for early diagnosis of cancer, as they are not conclusive enough. There are several spectroscopy based advanced techniques have been studied to improve the sensitivity for tissue analysis, such as matrix-assisted laser desorption/ionization imaging mass spectrometry (MALDI IMS), fluorescence spectroscopy, infrared (IR) and Raman spectroscopy (RS), which are not counting on specific antigens during the tissue analysis. A brief explanation with their promising usage in the clinics was given in the next section but the technical details with working principles can be found elsewhere [29-32].

1.4. ALTERNATIVE CANCER DIAGNOSIS APPROACHES

There are a number of recent reviews about the alternative advanced methods for cancer detection to increase the sensitivity of disease diagnosis [33-38]. Fluorescence spectroscopy (FS) is one of the techniques to investigate more precise diagnosis result by improving the detection sensitivity of specific antigens bounded a fluorescence-labeled antibody [39]. It has high sensitivity but broad bandwidth of fluorescence emission prevents the multiplex detection. In RS, dependently SERS, spectral bandwidth is much narrower allowing the detection of multiple analytes at the same time. With the increased sensitivity in SERS, it can be considered an excellent technique in a range of applications. The recent FS studies focus on using a nanoparticle to increase sensing and imaging ability of the system and its development is still in progress [40, 41].

Matrix-assisted laser desorption/ionization imaging mass spectrometry (MALDI IMS) based tissue analysis refers to differentially expressed molecules in cancer and healthy pathological biopsies [29]. It is a promising technique having a high sensitivity and the advantages of direct measurement of peptides from tissues with no antibody requirement compared to the conventional IHC methods. However, it has practical limitations due to being time-consuming, labor intensive, expensive, and analytical limitations in protein detection because sensitivity of MS decrease as protein mass increases [42].

IR, on the other hand, is an applicable technique for cancer and healthy tissue differentiation but the key problem is its inherently low spatial resolution which limits the use of technique. On the other hand, the RS with a higher spatial resolution obtained from a molecule or molecular structure is considered as its fingerprint that means Raman spectrum can be used for the label-free and identification of a molecule or molecular structure. The technique with narrow spectral bandwidth and minimal interference from water can provide very rich molecular information from cells or tissues, which has the utility of in vivo applications using a fiber optic. There are many reports demonstrating the possible use of RS in cancer diagnosis [33, 43-45]. For instance, breast cancer diagnosis was studied using RS providing a high predicted classification sensitivity and specificity of up to 99.6 per cent [46]. Furthermore, the squamous cell carcinoma (SCC) tissues were differentiated from oral healthy tissues using RS based on the tissue water content providing all cancerous tissues removing nearby healthy tissue during the oncological surgery [47]. The salivary gland cancer was also studied with RS [48]. The cancer and healhty tissues were differentiated based on the differences in the their lipid composition and secondary structure of proteins. However, breast cancer and healthy tissues were classified based on the differences in the intensity of Raman bands related to carotenoids, fatty acids and proteins [49].

Along with its weak scattering nature, RS is rather slow technique compare to IR spectroscopy, its closest competitor. The necessity to collect spectra from an area rather than a point further slows down the spectral collection, which diminishes its applicability in clinics. To overcome the key problems of RS, its novel modes were developed with clinical applicability in cancer diagnosis, which are Coherent anti-Stokes Raman (CARS) microscopy, stimulated Raman spectroscopy (SRS), spatially offset Raman spectroscopy (SORS), transmission Raman spectroscopy (TRS) and surface-enhanced Raman scattering (SERS). The techniques are briefly mentioned here but the details can be found elsewhere [33, 50-52]. CARS technique, which represents a valuable alternative to RS with the improved spatial resolution, shorter analysis time, enhanced scattering without using any external particles and lower background, was demonstrated for cell and tissue analysis in the literature [53-55]. However, it has limited spectral information due to possibility of acquiring Raman spectra from the selected vibrational frequencies. Furthermore, the non-resonant background problem of CARS was handled by using SRS technique having less background noise [56]. On the other hand, SORS technique provides the collection of spectra up to 10 mm deep, whereas TRS technique was ideally suited for bulk analysis of opaque/turbid [52, 57]. However, after SERS for the detection of a range molecules and molecular structures down to even single molecule was reported, SERS-based studies have been increased in the literature [58]. SERS-based cancer diagnosis has emerged as a powerful approach to detect many cancer types such as esophageal, nasopharyngeal, gastric, breast, ovarian, thyroid, bladder, lung, colorectal and renal cancer [59-68].

1.5. VIBRATIONAL SPECTROSCOPY

The spectroscopic techniques are associated with the interaction of electromagnetic radiation with matter. Figure 1.1 shows the diagram of energy absorptions with frequency. Longer wavelengths have lower energy and cause molecular rotation and vibration in the microwave and infrared regions, respectively. The shorter wavelength radiations such as Ultraviolet-Visible (UV-Visible) and X-rays, have the highest energies causing electronic excitation removing electrons to a higher energy state and bond breaking and ionization.

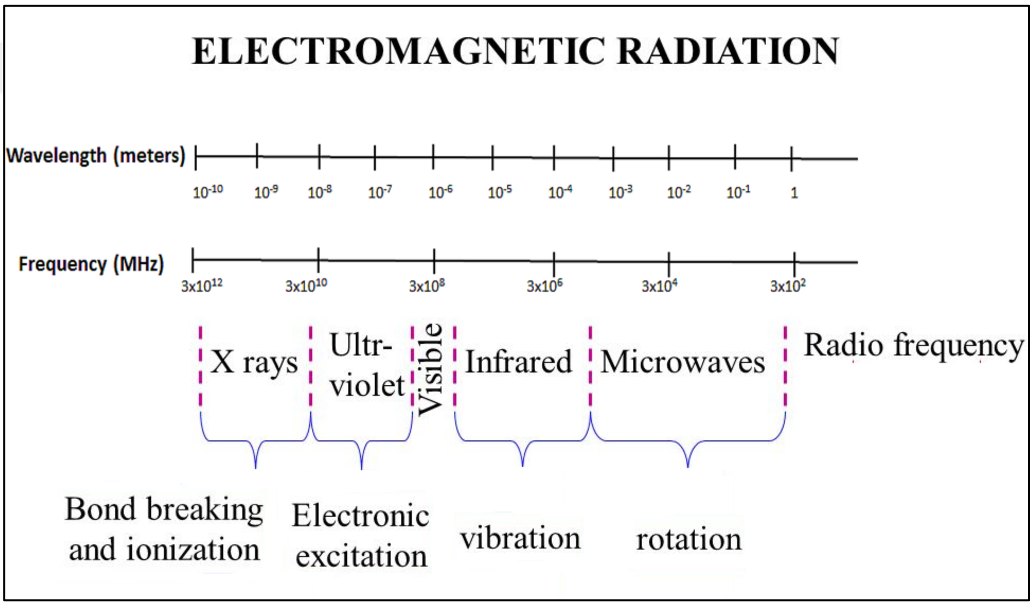

Figure 1.1. The schematic diagram of electromagnetic spectrum.

Radiation-matter interactions resulted in ionization can be observed by X-ray spectroscopy, electronic transitions by UV-Visible or fluorescence spectroscopy, vibrational changes in molecules by IR or Raman spectroscopy while rotational changes can be detected by microwave rotational spectroscopy. As mentioned above, IR and Raman spectroscopy, which are interested in molecular vibrations, are two complementary techniques due to differences in working principles. The principles of vibrations of these two techniques and their mechanisms are summarized below in "Section 1.5" and its subheadings, using general chemistry books and related references [69-72].

1.5.1. Molecular Vibrations

Molecules in space retain three types of degrees of freedom (DOF) known as translational, rotational and vibrational, that are movements as a whole on x, y, and z-axes, on orthogonal axes, and in the molecular bonds. Moreover, a diatomic molecule has one DOF, a polyatomic molecule with “N” atoms has “3N” DOFs. Furthermore, there are three transitional DOFs and two rotational DOFs in a linear molecule (3N-5 vibrational modes), whereas there are three rotational and three transitional DOFs in a nonlinear molecule (3N-6). The vibrational modes of the molecule can be bending (deformation) or stretching, cause alterations in bond length and bond angle, respectively. Stretching vibrations can be observed as symmetric or asymmetric, whereas bending vibration can be both in-plane as scissoring and rocking, and out-of-plane as wagging and twisting as seen in the Figure. 1.2

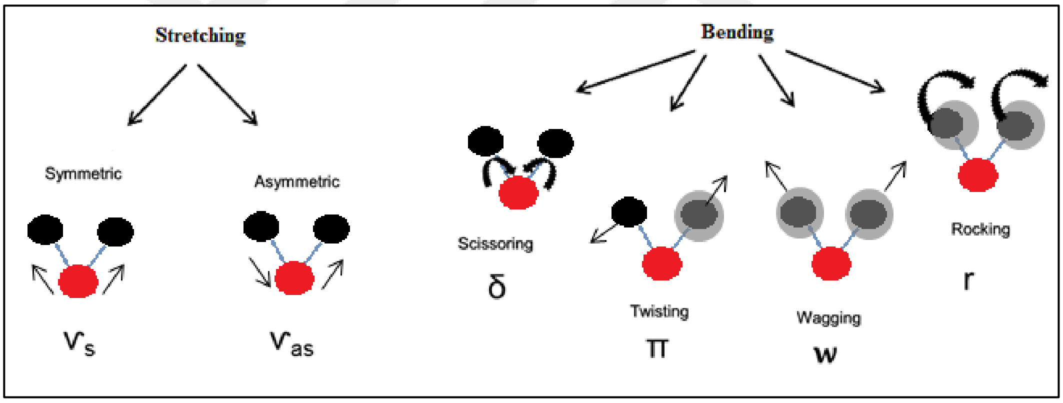

Figure 1.2. Vibrational modes of stretching and bending.

1.5.2. IR Spectroscopy

The principle of IR spectroscopy is based on absorption of a certain amount of the incident light, which cause a change in the dipole moment of a molecule at specific frequencies coming in resonance with the frequency of its bond vibrations. The molecular structure can be analyzed by the contribution of IR spectral information with the percentage of the transmitted light at certain wavenumbers (cm^{-1}). For instance, in the Figure.1.3 at wave number 1721 cm^{-1} assigned to C=O stretching vibration, about 100 per cent of the incident light was absorbed, and the frequency of the band vibration is matched with the frequency of the light. However, 50 per cent of the light was absorbed while 50 per cent was transmitted at wave number 1419 cm^{-1}.

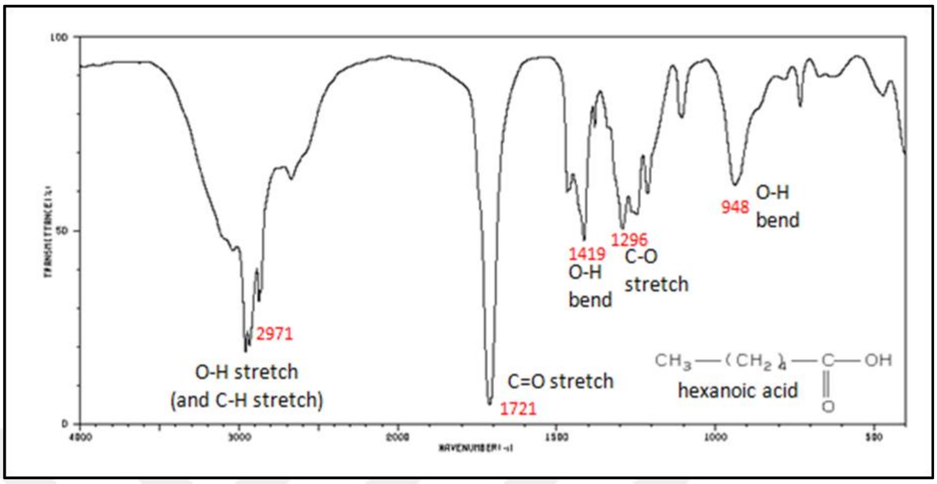

Figure 1.3. The IR spectrum of hexanoic acid [73].

There are differences between IR and Raman technique due to the electrostatic characteristic of the vibration. As a brief explanation of the differences, Raman methods are associated with the scattering of the incident light by the vibrating molecules, whereas IR is the result of the adsorption of the incident light by vibrating molecules. Raman active vibrations are corresponded to a change in the bond polarizability while IR active vibration is related to the dipole moment change of the bond. Water cannot be used in IR spectroscopy since it has an intense absorption but it is possible to use as a solvent in Raman spectroscopy. Raman signal gives information about the covalent character of the molecules while IR spectrum indicates the ionic character of the molecule.

1.5.3. Raman Scattering

As mentioned in the previous section, Raman spectroscopy is based on the inelastically scattered photons upon collusion of light with molecules while IR corresponds to the absorption of the photons. Scattering is the result of the re-emission of the light during the return of the bond to its initial position after the electric field of the light induces the electron cloud of a bond causing sudden deterioration of the distribution of electrons. Raman scattering is directly interrelated to the bond polarizability affected by the distribution tendency of the electrons.

The scattering phenomenon taking place simultaneously during Raman scattering is shown in Figure.1.4. Rayleigh scattering, inelastic in nature, occurs at the same wavelength with the excitation wavelength during the bond electrons return to back to their initial state after the electrons are excited to a virtual state as a result of the interaction of incident light. Thus, there is no energy change in the excitation photons in this scattering type. The other two types of scattering taking place meanwhile are Stokes and anti-Stokes. Some photons loose energy during the process and their wavelength sifts to a longer wavelength and called "Stokes shift" referring to the same phenomena observed in fluorescence spectroscopy. Since some photons gain energy as the vibrational mode returns to its ground state, it is called "anti-Stokes shift" as it is the opposite process of "Stokes shift"..

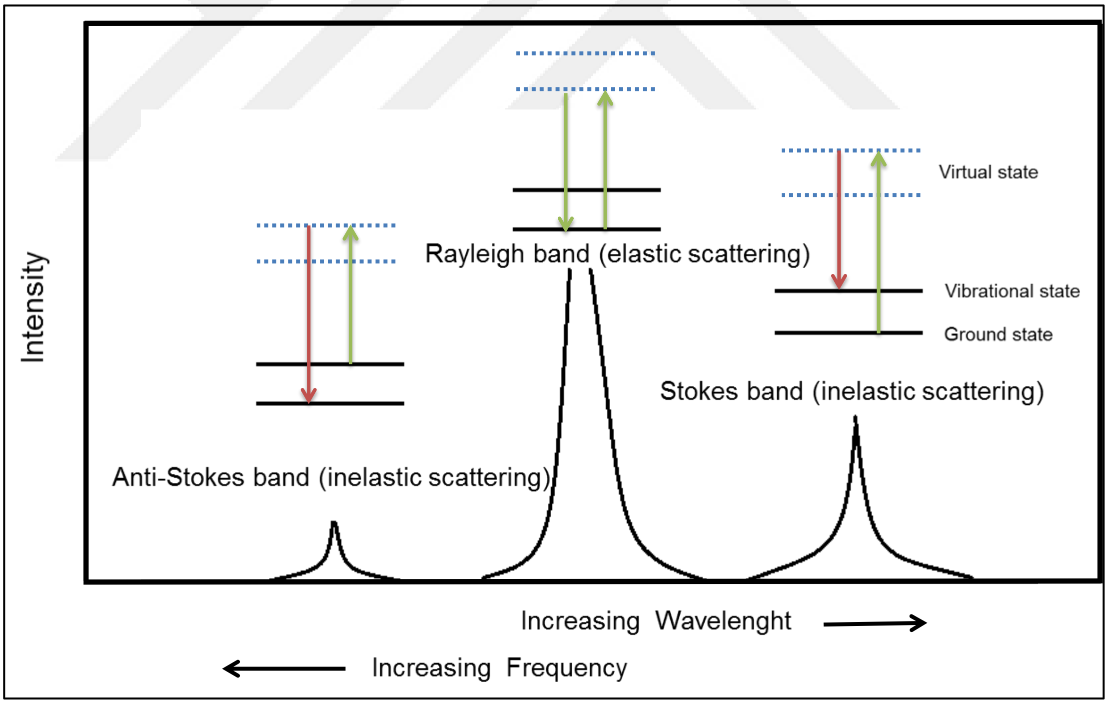

Figure.1.4. Schematic diagram of scattering types; Rayleigh, Stokes, and Anti-Stokes

Since Raman spectroscopy provides information about molecular structure through bond vibrations, it can be considered as "fingerprint". Easy sample preparation and minimum interference from water are the other advantages of the technique. However, weak nature oof scattering is the major disadvantage. The development of powerful laser and sensitive detectors helped the advancement of technique but increased laser power and exposure time can damage the sample. The RS modes of SERS, TERS, CARS, SERRS, SRS, SORS, and TRS mentioned, in the previous sections, were developed to overcoming the drawbacks of RS.

1.6. SURFACE-ENHANCED RAMAN SCATTERING (SERS)

The phenomenon of bringing the analytes into proximity of a rough metal surface or NP colloids to overcome weak scattering of RS was called as Surface Enhanced Raman Scattering (SERS). The SERS was discovered in the 1970s. Richard P. Van Duyne, who is one of the pioneers of the field, firstly calculated theoretically that if pyridine molecule adsorbs on the electrode surface, the signal intensity would be as 25 counts. While he was writing a research article based on his suggestion and explanation in May 1974, he realized that a report was published in the journal Chemical Physics Letters by Fleischmann's group indicating the enhanced signal up to 1000 counts from absorbed pyridine molecule on a roughened silver electrode [74]. In that report, Fleischmann and McQuillan also stated that anodic potentials of electrodes caused the bands shifted with the observation possibility adsorbing on a noble metal surface or bringing pyridine molecules into close proximity of the metal surface. After Van Duyne had a conversation about the study in Fleischmann's laboratory with McQuillan, he recognized that increased surface roughness of the electrode would provide more pyridine adsorption on the electrode increasing the signal intensity coming from the molecule. After he and his colleagues were studied on the optimization of surface roughness, they noticed that not only roughness of the metal surface is responsible for the increased signal intensity but also an electromagnetic field is effective, which is a result of induction of conductive electron of the metal to oscillate, Finally, he published was his findings in the Journal of Electroanalytical Chemistry, 1977 [75]. Later, Van Duyne met with physicists in the Optics at the Solid-Liquid Interface Conference to explain more about the surface plasmons and their effects with proposed electromagnetic field enhancement (EM) theory of SERS [76].

In the same year of EM theory was supposed to be identical for increased signal intensity, Albrecht and Creighton were published a report indicating a different proposition which is responsible for the increased scattering called as “chemical effect” (CE) originating from the charge transfer between the metal surface and analytes affecting the polarizability of the molecular bonds [77]. Three different proposed mechanisms for CE were suggested; resonances from molecular excitation or charge transfer between the metal substrate and analytes, and non-resonant changes in the polarizability of the molecules [78-80]. Two theories, which are responsible for the SERS; EM and CE were accepted by the SERS community in 1979 [81]. While EM was reported as more efficient with an enhancement factor about 10^5-10^6 times than CE with enhancement factor between 10^0 to 10^3 to provide enhanced Raman scattering with many comparative studies [82, 83].

The interaction of light with noble metals causes oscillation of the conductive electrons, and these oscillating electrons are known as surface plasmons [84]. The connection of surface plasmons with enhanced Raman scattering was first mentioned by Moskovits in 1978 [85]. There are two types of surface plasmon resonance known as localized surface plasmon resonance (LSPR) and surface plasmon polaritons (SPR). In LSPR, when coherent oscillation of conductance electrons of noble metal nanoparticles and frequency of light come into resonance, surface plasmons are formed as seen in Figure 1.5.

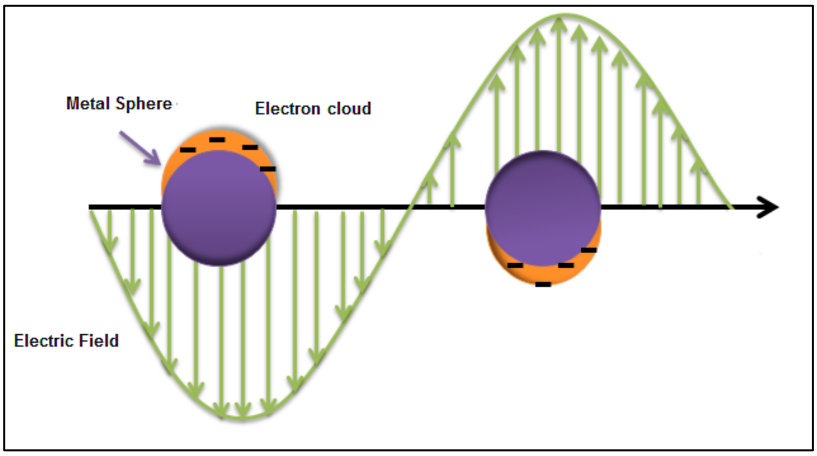

Figure 1.5. Schematic illustration of surface plasmon resonance on metal nanoparticles [86] .

SPR is a surface electromagnetic wave that forms at interface of metal and dielectric medium due to coherent oscillations of noble metals electron system and impinging light [87, 88]. Localized surface plasmons are formed around 10-200 nm size of NPs with a few nm of depth [88, 89]. The localization surface plasmons change depending on size, shape, and assembly of nanoparticles [90].

The sharp edged nanostructures such as triangular and rod compared to spherical ones have a more effective electric field at the sharp edges but the synthesis procedure of such nanostructures is more difficult compared to spherical NPs [91]. SERS can be considered as one of the application area of plasmonics [92]. The clusters/aggregates of NPs can provide intense SERS enhancement due to the plasmonically coupled metallic dimeric nanostructures named as plasmonic hybridization (also called “hot-spots”) [93]. Metal nanoparticles Ag, Au, Cu, Li and Al maintain surface plasmon due to their dielectric function in the UV/Vis and near infrared region (NIR) [92]. However, AgNPs and AuNPs are different from other metal nanoparticles with their support surface plasmons in the region of 300-1200, mostly covering the visible region of the spectrum [90]. Due to their high SERS activity, colloidal AgNPs as SERS substrates were used in this thesis study.

1.7. USE OF SERS FOR TISSUE BASED LABEL-FREE CANCER DIAGNOSIS

SERS is used in numerous applications employing both label-free and labeled approaches including detection and identification viruses, bacteria, yeasts, cell surface markers on cells and tissues, and monitoring drug release [94-99]. As mentioned earlier, even detection of single molecules with the technique was reported [58]. With its high sensitivity, simplicity, labeled and label-free detection schemes, SERS is a promising technique for cancer diagnosis. Both labeled and label-free approaches were demonstrated in the literature [38, 48, 68, 100-103]. In most labeled applications, a SERS active label was used by replacing the fluorescence detection scheme to increase the sensitivity. The conventional immunoassays based approaches used for detection of various species including proteins and viruses in clinics such as enzyme-linked immunosorbent assays (ELISA) have significant drawbacks of labor intensive sample preparation, small sample size, high cost and low sensitivity [104]**.** SERS can significantly improve the sensitivity while using a small volume of sample with minimum analysis steps. For example, the expression of a pancreatic cancer biomarker glycosylated large protein known as mucin was detected by a SERS-based immunoassay at low concentration overcoming the limitation of decreased detection sensitivity of conventional methods of ELISA and radioimmunoassay (RIA) [105]. More

SERS labeled methods were developed for the detection of cancer biomarkers such as haptoglobin (Hp) for prognosis of ovarian cancer, and p53 -p21 with 4-Mercaptobenzoic acid (4MBA) for early cancer diagnosis [102, 106]. SERS was also utilized for circulating tumor cell detection, obtaining organelle dependent cellular compartment information by conjugation of magnetic beads and SERS tags to EpCAM and her2 antibodies [107]. Besides, label-free SERS based detection of cancer cells not only utilizing cell surface properties but also dynamic process within cells was used for *ex-vivo* biopsy analysis [38, 108-110]. Many cancer types such as esophageal, nasopharyngeal, gastric, breast, ovarian, thyroid, bladder, lung, colorectal and renal cancer were evaluated by SERS [59-68].

SERS substrate has a critical effect on the quality of a measurement. The requirement that a substrate and molecule should be in contact or the distance between them should be less than 3 nm to for molecules to feel the surface plasmons defining the quality of spectrum [88, 89]. Note that the spectral quality refers to rich spectra with high reproducibility. Due to the fact that a tissue sample is not easy to bring into contact with a nanostructured noble metal surface, colloidal noble metal particles are more convenient to use. However, there are only a few SERS-based tissue sampling approaches using colloidal noble metal particles such as AgNPs or AuNPs. The colloidal noble metal NPs are either added onto the sectioned tissue surface or mixed with homogenized tissue sample [28, 111-113].

Another important point in tissue based cancer diagnosis is the storage and preservation of biopsied tissue used in SERS studies. The paraffin embedding and quick-freezing are the two conventional methods for long-term storage of biopsies used in the clinics. Furthermore, fixation is a standard procedure used in clinics for long-term storage of biopsied tissue samples to protect the morphological structure of the tissue preventing the decomposition. Formaldehyde and paraffin are two chemicals used in the fixation procedure. Formaldehyde is not only a biohazards chemical but also affects the quality of DNA / RNA by degrading the nuclear material and modifies the sequences [114]. Paraffin preservation (FFPP) is one of the main preferred procedures for the histological examination of tissue sections but the use of paraffin embedded-tissue sections is not preferred due to the spectral interference and possibility of degrading tissue structure. Thus, the evaluation of different fixative agents and tissue type were studied by Tfayli et al. comparing the effect of using fixated-tissues with two fixatives, ethanol and glycerol, and embedding tissues with different embedding media [115]. Moreover, Wills et al. demonstrated that Raman scattering obtained from cryopreserved (banked) tissue compared to fresh samples resulted in a high correlation indicating that frozen tissue from tissue banks could be used to develop diagnostic algorithms [46, 115]. Many recent studies used fresh and snap frozen tissues instead of fixated or paraffin embedded due to drawbacks mentioned above [116]. Thus, snap frozen tissues were used during the study of this thesis.

In a SERS experiment, the substrate used to place the tissue specimen has a critical importance due to the strong background originating from the substrate where tissue sample placed upon exposure to laser light. In order to minimize the background signal, Raman and SERS-based tissue analysis studies performed on the glass slides with a thicker sectioned tissue, CaF_2 slides, aluminum coated microscope slides, or quartz flats [87, 90, 117]. In this thesis, the possible alternative substrates were also evaluated.

1.8. SERS SIGNAL QUALITY

An analytical spectroscopic measurement has two components; signal and noise. The limit of detection (LOD) in quantitative analysis is usually determined as the concentration of analyte yielding a signal to noise ratio (SNR) of 3 [118]. SERS signal quality refers to high SNR and rich spectra with high reproducibility. The SNR for the peak intensity of a SERS band is the average peak height ( ) divided by the standard deviation of the noise (Q_B) used the equation below [118]:

$$SNR = \frac{\overline{S}}{\mathrm{Q_B}} \tag{1.1}$$

Figure 1.6 visualizes the differences in the SNR of two spectra belong to Na_2SO_4 in water.

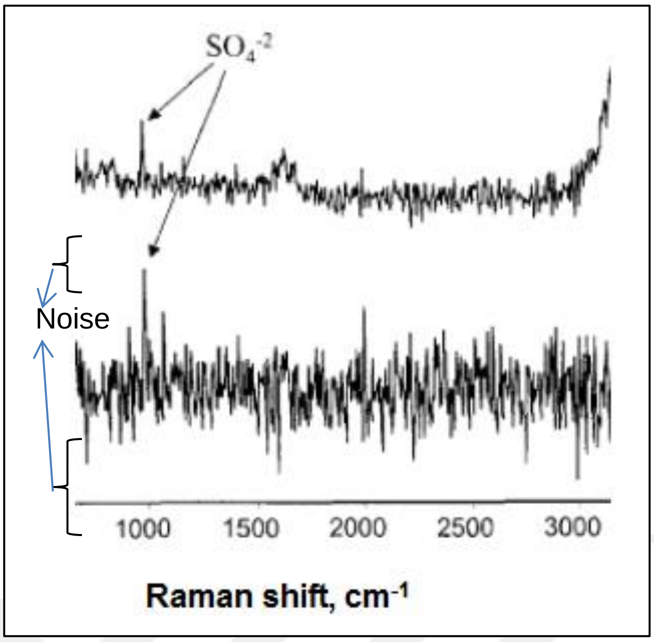

Figure 1.6. Spectra of 0.1 M Na2SO4 solution by using different laser powers [118].

It is clear that the SNR of the first spectrum is lower than the second one. The SNR in the SERS spectra was used as a comparative parameter to determine the optimized conditions during the method development. Richness in the spectral pattern is the second parameter which affects the signal quality. It means that the increased number of prominent bands on the spectrum possesses much more characteristic information about the sample. The last important factor is signal reproducibility which is the key limitation of the SERS is the other important point needs to be increased for the intra-and inter method application of a SERS-based approach. The developed SERS-based approaches also need to be optimized by their experimental and instrumental parameters. High intra-method reproducibility (point-to-point/ spot-to-spot and sample-to-sample) means that the SERS measurements obtained under the same conditions at same time having low variation while high inter-method reproducibility (point-to-point/ spot-to-spot and sample-to-sample) refers to the decreased variation in the SERS measurement performed at same conditions but by a different observer or at different times. To evaluate the inter-and intra-method reproducibility, coefficient of variation (CV), which is the ratio of standard deviation and the overall mean, was calculated to express the maximum differences for each SERS measurement using the equation below [119]:

$$C = \frac{S}{\overline{X}} = \frac{1}{\overline{X}} \left[\frac{\sum_{i=1}^{n} (X_i - \overline{X})^2}{n-1} \right]^{1/2} \tag{1.2}$$

X$_i$= exposure measurement;   = mean of the exposure measurements; n= number of the exposure measurements.

Higher CV values indicate that the variation of the exposure measurements is increased while the reproducibility of the spectral measurement was decreased for that method, parameter, condition, etc. During the method evaluation, CV values of the measurement were calculated to determine the optimized experimental and instrumental parameters.

1.9. CHEMOMETRIC ANALYSIS OF SERS DATA

The SERS data treatment is one of the important parts of the approach due to the high dimension features of spectra need to be evaluated by for inter-and intra-variability of the samples. Principle Components Analysis (PCA) is the most popular statistical methods used in different disciplines. PCA provides a new way to identify the data by extracting the patterns in the data regarding to their similarities and differences. The data relevant components are the reduced variations from the high dimensions without much loss of information. First, PCA calculates a mean from the each dimension (x➔ $\overline{x}$) [120]. Then, a covariance matrix relating to the number of the data dimension is created. Covariance matrix is used if the number of the variables in the data is more than one to standardize the data. It determines the shape of the data. The equation below is used to obtain covariance matrix from the data (n is the number of the dimension) [121]:

$$cov(X,Y) = \frac{\sum_{i=1}^{n} (\overset{\omega}{Xi} - \overline{X})(Yi - \overline{Y})}{(n-1)} \tag{1.3}$$

Then, the eigenvectors and eigenvalues were obtained from the covariance matrix. Eigenvectors corresponding to an eigenvalue indicates the characteristic roots in the data in which useful directions. The eigenvector with the highest eigenvalue generates the principle component. The method orders the eigenvectors with highest values to the lowest. The order provides to eliminate insignificant eigenvectors which consist not much of information. It should be note that "factor" is also used as the term of component. Factor loadings or component coefficients also called as component loadings in PCA provide statistically calculated information about the variances in the original data. The factor loadings of SERS spectra underlie the biological differences representative of tissue sample displaying positive and negative bands on the loadings are related to which assigned bond vibration if the SERS spectra of each samples was used together in the preforming analysis. The positive and negative bands appeared on the loadings corresponds to rising SERS signals in the original spectra and reduced contribution of the signals in the acquired SERS spectra. It should be note that PCA considers generating directions that maximize the variance in a data set is without using class labels and while LDA differentiates the variability within the dataset of the sample groups and the variability between the sample groups by maximizing the components for class separation [122]. That is why LDA used in order to generate a diagnostic model for tissue differentiating. LDA, which is a supervised method, is one of the most common pattern recognition algorithm used in the biological data treatment. First, the d-dimensional mean vectors ($m_{i)}$ are obtained from the data for different classes with *i*= 1, 2, 3 (number of the spectra) [121]:

$$m_i = \begin{bmatrix} m_{wi} \\ m_{wi} \\ m_{wi} \\ m_{wi} \end{bmatrix} \tag{1.4}$$

Then, the scatter matrices both within-class (S_w) and between-class (S_B) are computed by the following equation:

$$Sw = \sum_{i=1}^{c} S_i \tag{1.5}$$

$$Si = \sum_{x \varepsilon D_i}^{n} .(x - m_i)(x - m_i)^T \tag{1.6}$$

$$m_i = \frac{1}{n_i} \sum_{x \varepsilon D_i}^{n} x_k \tag{1.7}$$

n_i= sample size of the class; m: overall mean; m_i: sample mean; c: number of class labels

$$S_B = \sum_{i=1}^{c} N_i (m_i - m)(m_i - m)^T \tag{1.8}$$

The eigenvectors and corresponding eigenvalues for scatter matrices are obtained before the number of the eigenvectors are reduced to top “k” number vectors with the largest eigenvalues. In addition, k x d –dimensional eigenvector matrix (W) is computed by reducing the dimensional feature spaces into subspaces which means LDA not only -improve the class separation but also reduce the space’s dimensionality. New subspaces (W) are computed by transforming the samples (Y) using the equation below. (X= n x d-dimensional matrix; n: number of samples) [120, 123]:

$$\text{Y}= XxW \tag{1.9}$$

The scatter plot of the LDA vectors provides to visualize clustering performance but the performance of that classification model needs to be tested. For this reason, leave-one-out and cross-validation (LOO-CV) method is commonly used to obtain a predicted classification result of using PC-LDA classification model on the SERS data. LOO-CV provides multivariate classification predicting class between the training set and record SERS signal omitted from the training set. It is almost used in diagnostic algorithm providing an idea of how to generalize the model within an independent data set [124]. The outcome of LOO-CV (disease/healhty) style predictor is often presented in a 2x2 contingency table detailed in the Table 1.1. The number of correctly predicted diseased and healhty cases are indicated by TP (true positives) and TN (true negatives), and the number of incorrectly predicted diseased and healthy cases are FN (false negatives) and FP (false positives), respectively.

Table 1.1. Outcomes of the prediction methods in a classification model.

Presence of Disease Status		**Disease (number)**	**Healthy (number)**	**Measures**
LOO-CV Outcome- Predicted Class	Positive (number)	True Positive-TP (a)	False Positive- FP (b)	Positive predictive value a/ (a+b)
	Negative (number)	False Negative- FN (c)	True Negative-TN (d)	Negative predictive value d/(c+d)
Measures		Sensitivity a/ (a+c)	Specificity d/ (b+d)	Accuracy a+d/(a+b+c+d)

LOO-CV, which is the two class prediction method minimize the misclassifications due to overlapping positive cases to negative cases by a cut off seperationg the two classes as seen the Figure 1.7.

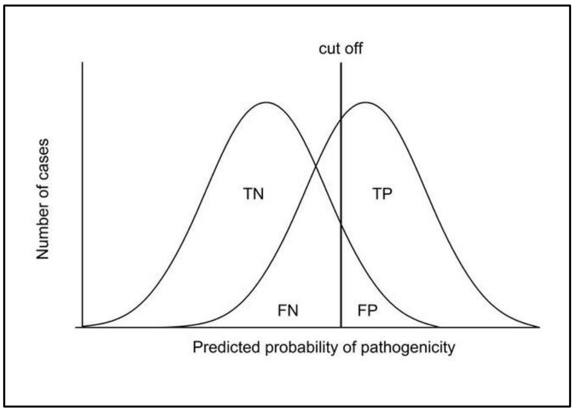

Figure 1.7. Seperation of classes based on their descriptors [125].

2. OBJECTIVES OF THE STUDY

Today, cancer is the second most common cause of death around the world. The researchers have still been working on understanding of the molecular mechanisms behind its reasons, studying on new screening and detection methods, and new treatments. Diagnosis is directly proportional to the survival time of the patients. However, the routine clinical protocols involve many time-consuming steps and artifacts during the laboratory processes, which lead to uncertain and incorrect diagnosis. The pathology protocol is based on the subjective decision of a group of pathologists used the morphological information from the stained biopsied tissue sections. There is a need for faster and more accurate approaches to remedy the problems of the conventional diagnosis approach. The surface-enhanced Raman scattering (SERS) as a highly sensitive technique can deliver more accurate and faster results compared to the conventional vague cancer diagnosis process. Alternative cancer diagnostic methods spread over a much extended period, even if promising, that routine clinical protocols can undergo radical changes. For this reason, it would be ideal to develop an easy-handled method, which is parallel to the pathology procedure. In this thesis, a systematic study based on SERS was undertaken. Glass slides and cryosectioned tissue sections with the intention to facilitate the integration of the approach into pathology were used in the methods. However, a PDMS layer on glass substrate was necessary to eliminate the background signal originating from the glass slide. The distribution of SERS active AgNPs has critical importance for reproducibility of SERS spectra. The study aimed to develop a better SERS-based approach with the expectation of a high reproducibility, rich spectrum, low cost, minimal sample preparation steps and high accuracy. Thus, two tissue sampling methods, Cryosectioned-PDMS and an *in situ* AgNP synthesis in homogenized tissue, were investigated. The parameters for Cryosectioned-PDMS method were evaluated involving the substrate cross-sectioned tissue sample placed, tissue thickness, objective lens, laser power, acquisition type (randomly selection/mapping), mode (StreamHR/Line focus), acquired-mapping size, spectral range, SERS substrate concentration and the droplet position (suspended/sessile). Moreover, the parameters such as concentration of the chemical agents used for *in situ* synthesis, and spectra collection method for in situ based method were optimized. Thyroid cancer was selected as the model system in this systematic study. Two developed SERS-based approaches were compared with the method of crashing and liquefying, which is previously developed in our laboratory. Three SERS-based tissue sampling methods were applied on the thyroid biopsies (n=64). The performance evaluation comparing the methods through the spectral pattern, principal component based linear discriminant analysis (LDA) classification accuracy, and method-reproducibility was obtained to predict the best SERS-based method for tissue differentiation for cancer diagnosis. Indeed, it was aimed to demonstrate the diagnostic power of SERS with the developed approaches whereas performing a systematic study to provide translation of Raman Spectroscopy into clinics.

3. MATERIALS AND METHODS

3.1. CHEMICALS

Solutions of silver nitrate ($AgNO_3$) (Sigma-Aldrich), hydroxylamine hydrochloride ($HONH_2 \cdot HCl$) (Merck), sodium hydroxide (NaOH) (Sigma-Aldrich) and trisodium citrate ($Na_3C_6H_5O_7$) (Sigma-Aldrich) were prepared with double distilled, deionized water from Millipore DirectQ-ultraviolet [21] system. Sylgard 184 silicone elastomer base and Sylgard 184 silicone elastomer curing agent manufactured by Dow Corning (Midland, MI). The cryostat embedding medium for frozen tissue specimen (Optimal cutting temperature-O.C.T compound) was purchased from PELCO®.

3.2. TUMOR SAMPLES

Bovine liver tissue as a model was used in the optimization studies during the development of the approaches. Fresh bovine tissue samples were stored in a deep freeze at -80°C until used for analysis.

The human biopsy samples were obtained from the cancer patients with consent of the ethical approval from Yeditepe University Hospital. The tissue specimens stored at −80°C in plastic tubes until the samples were prepared for the SERS measurements.

3.3. PREPARATION OF SERS SUBSTRATES

The colloidal AgNPs from $AgNO_3$ were synthesized using two different reducing agents; $HONH_2 \cdot HCl$ and $Na_3C_6H_5O_7$ [126, 127]. Briefly, citrate reduced AgNPs (c-AgNPs) were prepared according to method of Lee and Meisel, which involves dissolving 18 mg of $AgNO_3$ in 100 mL of distilled water, heating to boil, and adding 2 mL of 1 per cent (w/v) $Na_3C_6H_5O_7$solution slowly dropwise into this boiling solution. The suspension was kept boiling until it reached to the half of its initial volume. The suspension was concentrated by centrifugation at 5500 rpm for 30 min, and one-third of the supernatant was decanted to increase the final concentration of the AgNPs colloidal suspension to four times, which was called 4×. The concentrated AgNP suspension was used in the study of SERS-based kidney tumor staging.

Leopold and Lendl based synthesis method provides the synthesis of hydroxylamine reduced silver nanoparticles (h-AgNPs), which were used in SERS-based studies in this thesis for thyroid tumor differentiation. Briefly, a total volume of 10 ml including 1.5 x 10^2 M $HONH_2 \cdot HCl$ and 3x 10-^2 M NaOH was added in to 90 ml 1.11 x 10^3 M $AgNO_3$ solution and stirred for 15 min at room temperature. The synthesized colloidal nanoparticles were characterized with UV-Vis Spectroscopy, and Transmission Electron microscopy [128]. The average size of h-AgNPs was approximately 30 nm. Then, the colloidal suspension was centrifuged at 5500 rpm for 30 min and was and a portion of the supernatant was removed to increase the concentration of the colloidal suspension. 8×,16× and 32 AgNP colloidal suspensions were prepared by removing appropriate volume of the supernatant after the centrifugation.

3.4. RAMAN SYSTEM AND SERS MEASUREMENTS

The SERS spectra of tissue specimen were collected using a Renishaw (Wotton-under-Edge, UK) InVia Reflex spectrometer equipped with a diode laser at 830 nm, CCD detector, edge filter, holographic grating (1200 grooves/mm) with ultra-fast imaging Renishaw's StreamHR™ technology. The fast imaging mode, StreamHR with a high-speed encoded stage (HSES) and synchronized readout of the CCD detector were used in the mapping configuration and the Raman system was calibrated by using the silicon phonon mode at 520 cm^{-1} before SERS measurement. The incident laser power was adjusted to 30 mW on the sample and the spectral data acquisition time was 2 s for the Cryosectioned-PDMS method. SERS spectra over a spectral range of 582-1653 cm^{-1} (1100 cm^{-1} median value) were collected using the StreamHR point mapping acquisition method from a square grid of 10 × 10 scanned points from a total area of 22.5 µm × 22.5 µm (506.25 μm^2).

For *in situ* method, randomly selected ten spectra from the droplet surface were acquired using 830 nm laser (as adjusted in the software to 15 mW) equipped with 20× (NA: 0.40) objective, and 5s exposure time.

For the crashed-liquefied method, randomly selected ten spectra over a spectral range of 400 - 1800 cm^{-1} from the droplet surface were acquired using 830 nm laser (as adjusted in the software to 30 mW) using 20x objective (NA: 0.40) and 5s exposure time.

In the study of kidney tumor staging study, the spectra were acquired over a spectral range of 400 - 1800 cm^{-1} with a 50× microscope objective (NA: 0.50) from randomly selected points on the sample using the “map image acquisition method” function in WIRE 2.0 software, and the WIRE 2.0 software was used to carry out the spectral analyses.

3.5. EXPERIMENTAL

3.5.1. Cryosectioned-PDMS Method

The so-called Cryosectioned-PDMS sampling method includes the following steps; Tissue cryosectioning, placing it on PDMS covered slide, dropping a 20 microliter volume of 16 X colloidal AgNP suspension on the tissue surface, drying at suspended position, spectral acquisition and data analysis. The experimental design of the method is shown in Figure 3.1.

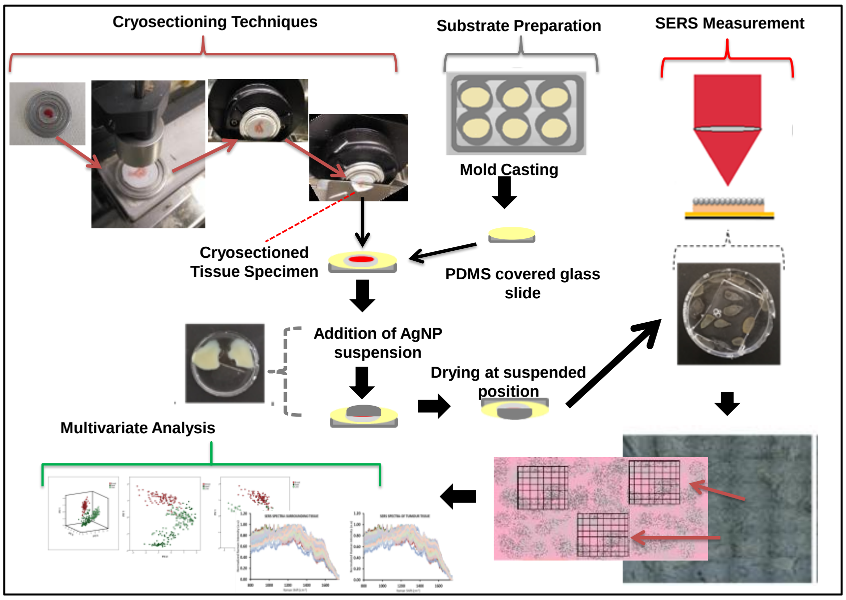

Figure 3.1. A schematic illustration of experimental design for Cryosectioned-PDMS method.

3.5.1.1. Preparation of PDMS Layer

Sylgard 184 silicone elastomer base and Sylgard 184 silicone elastomer curing agent were used to produce the polydimethylsiloxane (PDMS) layer on the glass slide. PDMS substrates were made by directly mixing corresponding elastomer base and the curing agent in a polystyrene beaker (base/agent mass ratio, 10:1). Then, approximately 0.5, 1, 1.5, 2, 2.5 and 3 ml volume of the viscous gel were added into six-well plates and was kept in an oven at 70^0 C for one hour.

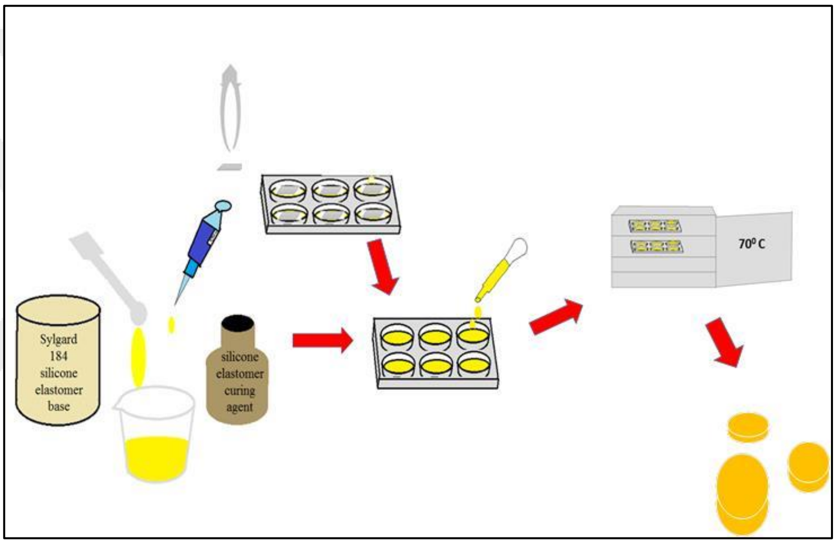

Figure 3.2. A Shematic illustration for preparation of PDMS covered surfaces.

3.5.1.2. Preparation of Tissue Sections

After tissue sample was removed from the deep freeze, it was thawed before placing on cryostat chuck and embedded in optimal cutting temperature compound medium (OCT) for cryostat sectioning. Then, the tissue embedded in OCT medium on chuck were left on the freeze bar of the cryostat.

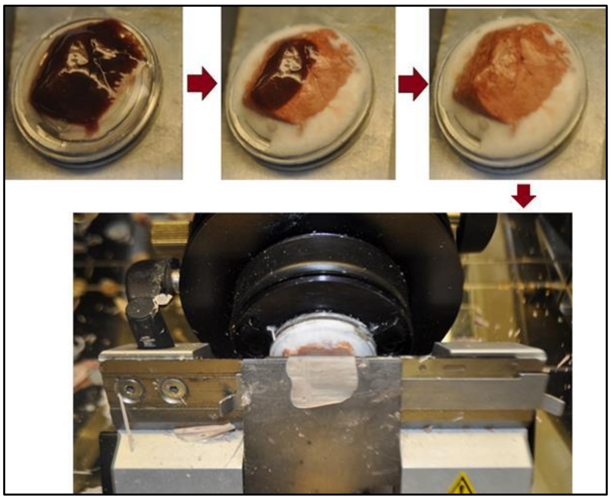

Figure 3.3. An illustration of O.C.T medium embedded bovine liver tissue sample on the chuck after frozen in the cryostat freeze bar with cryossectioning process.

Cryostat chucks provide fast freezing of tissue specimens eliminating ice crystal formation (freeze artifact), which destroys cellular morphology. The frozen tissue was cryosectioned in desired thickness using a Shandon Cryotome SME Cryostat (Thermo Electron, UK) device.

3.5.2. *in situ Based* Sampling Method

The so-called *"in situ"* method consists the steps of cutting a piece of 2x2x2 mm^3 from the biopsy sample, placing in a test tube, adding 50-µl distilled water into tube and homogenizing it by ultrasonic homogenizator (Omni International, Kennesaw, GA, USA). Then, a 10-µl volume of $3.55x10^{-2}$ M $HONH_2·HCl$ reducing agent and a 10-µl volume of $3x10^{-2}$M NaOH were added into a 10-µl volume of homogenized tissue suspension. Then, a 10-µl volume of $4.36x10^{-1}$ M $AgNO_3$ solution was added, and a 2-µl volume of mixture was placed on CaF_2 slides leaving it to dry at suspended position until SERS measurements. Then, SERS spectra collected from randomly selected ten points before pre-processing of the SERS data. A brief of experimental design of the *in situ* method can be seen in Figure. 3.4.

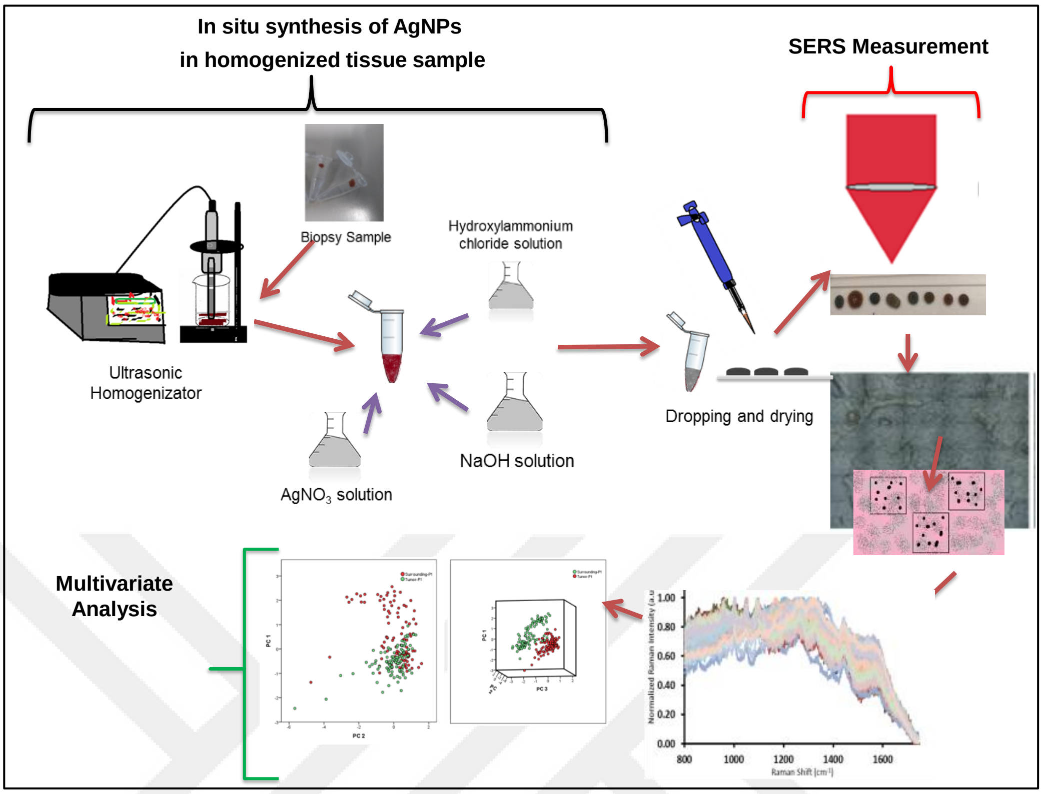

Figure 3.4. A schematic diagram of the experimental design for *in situ* based SERS approach.

3.5.3. Crashed-Liquefied Method

In “Crashed-liquefied” method, the following steps are followed. A piece of tissue approximately in the size of 2 × 2 × 3 mm^3 was cut from the fresh tissue or frozen tissue and thawed tissue. This tissue was snap frozen in liquid nitrogen and crashed with a mortar. The homogenized tissue was mixed with the AgNP colloidal suspension. A 5 µL volume of this mixture on a CaF_2 slide and dried at the suspended position before SERS measurement.

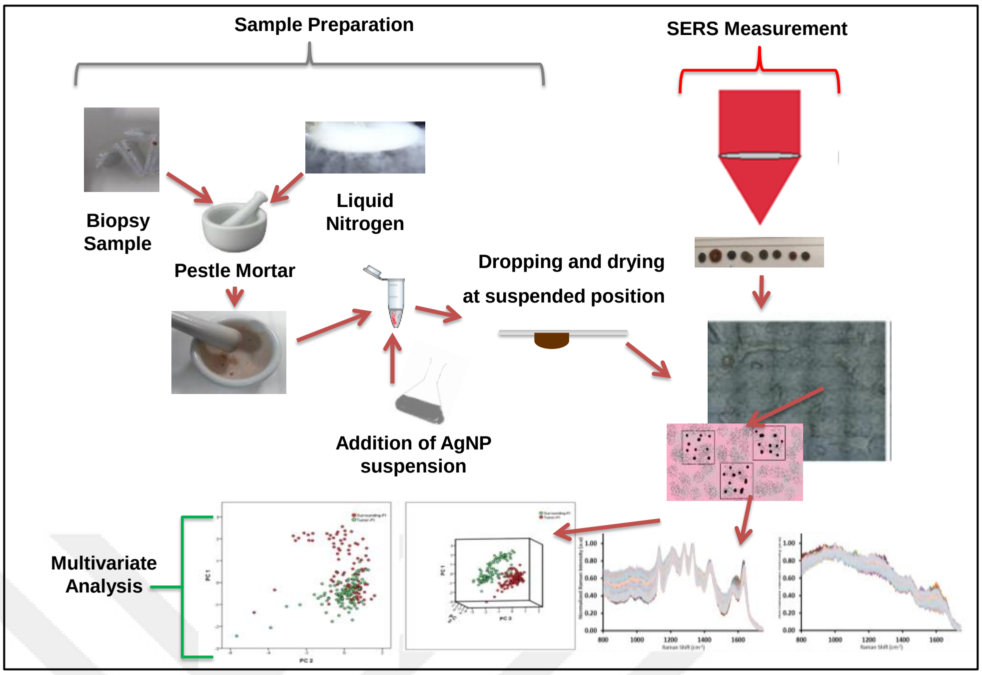

Figure 3.5. A schematic diagram of the experimental design for Crashed-liquefied method.

3.6. DATA PRE-PROCESSING

Wire 4.1 software was used for pre-processing of the SERS data. First, cosmic ray removal was applied to each spectrum, and the SERS spectra were normalized to be equal to 1 before the data was used in classification algorithms. Baseline subtraction and smoothing method were only applied to visualize the differences in the spectral patterns on the plots but not used in the classification models that means cosmic removed and normalized raw data with minimal pre-processing was used in the diagnostic classification algorithms.

3.7. STATISTICAL ANALYSIS

The pre-processed spectral dataset for statistical analysis was used in the statistical package for the social science (SPSS) package (SPSS Inc., Chicago, Illinois), which contains PCA and LDA algorithms to clarify the significant spectral characteristics of each tissue type and differentiate tissue types from each other according to their variances. PCA was applied before LDA to reduce the number of dimensions in the original high-dimensional dataset and to derive PC loading vector, which indicates the significant variances in the data. To apply PCA, the spectral data observations having high predictors were placed into a data matrix using SERS spectra acquired for each method. The eigenvalue decomposition was performed on the covariance matrix of the spectral data matrix. The resultant eigenvectors were obtained, and the original spectral dataset was projected into the new coordinate system defined by the principal directions of variance, called the principal components (PCs), which are the linear combination of the original data variables [129]. Then, the obtained regression (REGR) factors were used for classification the tissue specimens with PC-LDA. Leave one out-cross validation (LOO-CV) methodologies were applied to demonstrate the accuracy of the classification [130].

3.8. UV-VIS SPECTROSCOPY ANALYSIS

Colloidal AgNP suspension was analyzed using Lambda 25, Perkin Elmer Ultraviolet-Visible (UV-Vis) spectrometer.

3.9. SCANNING ELECTRON MICROSCOPY ANALYSIS

For scanning electron microscopy (SEM) analysis, cross-sections from PDMS substrate were taken to measure the thicknesses. The SEM images were obtained by using a Carl Zeiss Evo 40 instrument at under high vacuum with a potential of 10 kV after coating with gold in a Polaron SC 502 sputter coater.

3.10. TEM ANALYSIS

The images of AgNPs were obtained using a JEOL 2100 Transmission Electron Microscopy equipped with an Oxford Instruments 6498 EDS system.

4. RESULTS AND DISCUSSIONS

4.1. CHARACTERIZATION OF NANOPARTICLES

The citrate reduced colloidal silver nanoparticle (c-AgNPs) suspension was used in the kidney tumor analysis with the homogenized tissue sampling method where the tissue sample was frozen, crashed and mixed with the AgNPs colloidal suspension . Figure 4.1 shows the SERS spectrum (background) from a dried droplet of colloidal suspension (a), UV/Vis spectrum of the colloidal suspension containing c-AgNPs (b) and TEM image of c-AgNPs (c).

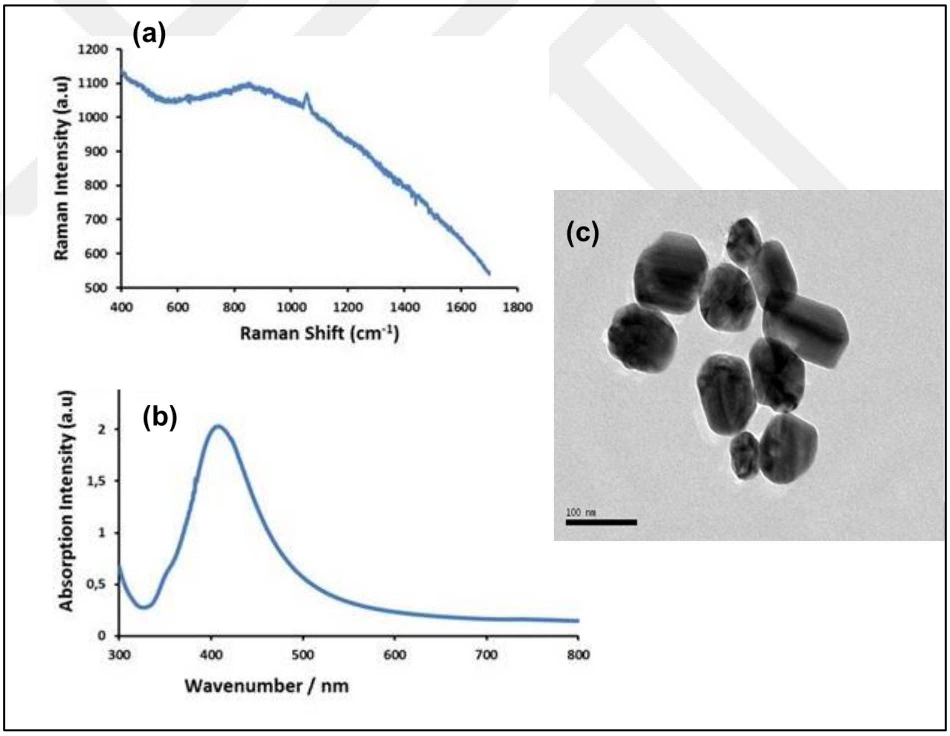

Figure 4.1. SERS spectrum of colloidal c-AgNPs (a), UV/visible absorption spectra of suspension containing colloidal c-AgNPs (b), and TEM image of AgNPs.(c).

The absorption maximum of the UV/ visible spectrum obtained from c-AgNP suspension was at 420 nm indicating the average size of the AgNPs is around 50 nm. The final density of the AgNPs used in the study of kidney tumor staging with 4× concentrated suspension was calculated as 2.08×10^{11} particles ⁄ ml [120].

The type of substrate is important in a SERS measurement since it affects the quality of spectra. The AgNPs or AuNPs are routinely used in SERS experiments due to their simple preparation, low cost, and high enhancement effect [131]. The c-AgNPs are widely used as SERS substrates but it is difficult to synthesize without having anomalous peaks originating from the molecular debris formed during synthesis [132]. Thus, hydroxylamine reduced silver nanoparticles (h-AgNPs), detailed in "*Section 3.3*", was used in the most part of this thesis due to having the benefits of increased reproducibility, minimal spectral background, high SERS activity and long-term stability, nearly 4 months [133].

The colloidal suspension containing h-AgNPs was characterized using UV-Vis spectroscopy and TEM [Figure 4.2 (a) and (c)]. The maximum absorbance of the UV-Vis spectrum of the AgNPs colloidal suspension was observed at 413 nm, and the average diameter of the colloidal AgNPs determined to be approximately 30 nm supported by TEM images. The SERS spectra of colloidal AgNPs was obtained with minimum spectral background coming from the suspension after a droplet of the suspension was placed on CaF_2 slide (Figure 4.2 (b)) and dried compared to the c-AgNPs case as seen Figure 4.1 a.

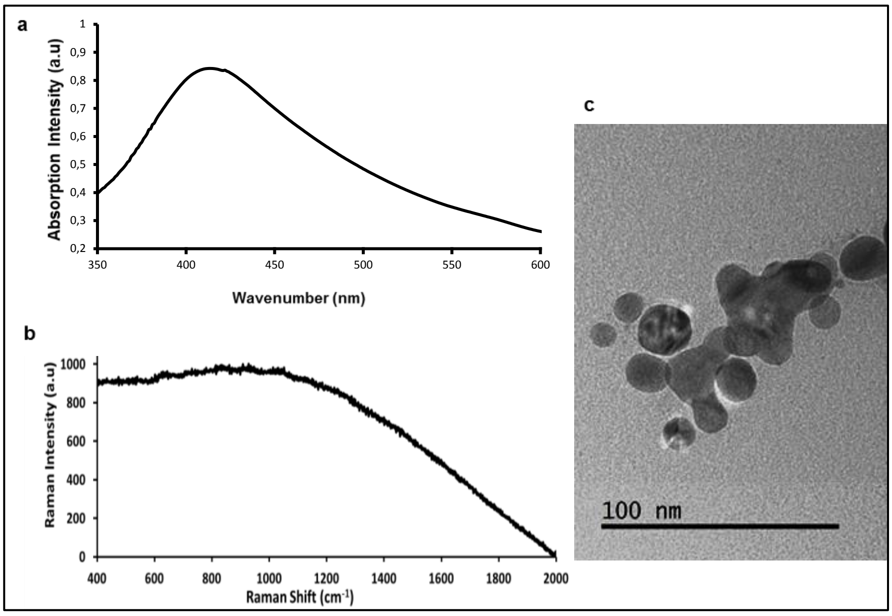

Figure 4.2. UV-Vis spectrum (a), a SERS spectrum of colloidal suspension of AgNPs (b) and TEM image (c).

4.2. CRYOSENTIONED-PDMS METHOD

The histology-based diagnosis includes several steps such as sectioning, mounting sectioned tissues on glass slide after fixation and embedding into paraffin. It would be ideal to use the tissue section prepared for the same procedure but the steps in protocols are time consuming, and the artifacts during the sample preparation affects the chemical composition thereby reducing the likelihood of correct recognition of the biopsied tissue sample. This is why the tissue without fixation is studied with snap-freezing method in molecular-based studies [134, 135]. Recent Raman and SERS studies mainly used snap frozen tissues without fixation and paraffin embedding due to the interfering peaks originating from paraffin wax at 1062, 1171-1175, 1130 and 1436 cm^{-1}. There is a systematic study performed in 2008 by a group of researchers demonstrating the effect of fixation processes on the Raman spectra [116]. In that study, different fixative agents were used to fix cells. Then, the spectral variances between fixated and unfixed cells were compared using classification models. The observations clarified that fixation process affected the cell chemistry reflected by the spectral changes. Moreover, the classification accuracy was decreased in the fixated cells compared to unfixed cells leading the misclassification of cancer and normal cells. In this thesis, the use of fresh or frozen tissue samples without fixation was aimed. However, it would be ideal to use a similar tissue section procedure applied in clinics.

Tissue thickness placed onto the substrate is an important point in Raman measurements since the laser light can easily penetrate and reach to the glass substrate generating a background signal, which can suppress signal originating from the tissue sample. In order to eliminate the background, a layer of PDMS is decided to use. A systematic optimization process was employed to assure that the approach could practically be used in clinical applications.

Bovine liver tissue was used during the optimization studies. Several parameters including the substrate where the cross-sectioned tissue sample is placed, tissue thickness, laser power, acquisition type (random selection vs. mapping) and mode (StreamHR vs. Line focus), mapping size (22.5 x 22.5/ 112.5x22.5/ 562.5 µm x 22.5-µm), spectral range, SERS substrate concentration and the droplet drying position (suspended vs. sessile) were investigated. Then, the Cryosectioned-PDMS method with other two sampling methods of SERS-based approaches was evaluated using human thyroid tumor and healthy tissue biopsies as a preliminary study. The optimization of the parameters in the Cryosectioned-PDMS method was given in the following section.

4.2.1. Experimental Optimization

In order to achieve optimal signal collection from sliced tissue, the substrate used to place the tissue. Substrate thickness, tissue thickness, objective type, laser power, focus adjustment, acquisition type, number of spectra and mode, mapped area size, spectral range, drying configuration of droplet including AgNP suspension, AgNPs concentration, and region dependent spectral reproducibility in the dried droplet area were evaluated. The subtitles below involve the experimental optimization for each parameter of the Cryosectioned-PDMS method.

4.2.1.1. Substrate Used to Place Tissue Sample

The cryosectioned tissue slices in 5-μm thicknesses were used similar to the pathology routine. However, fixation and paraffin-embedded processes were not applied due to spectral interference. The routine pathology laboratory uses glass slides to place tissue sections. The tissue sections were placed on glass slides, a 20-μl of the 8 × concentrated colloidal AgNP suspension was added on the tissue surface, and dried at the suspended position before the SERS measurements. A strong fluorescence background originating from the glass slides suppressed the SERS spectra of the tissue specimen. This strong fluorescence background was aimed to eliminate by covering the glass with polydimethylsiloxane (PDMS), which is an silicone-based elastomeric polymer with mechanical and chemical stability and widely used in a variety of applications [1, 39]. First, the microscope glass slides were attempted to coat with spin coating but it was not possible to achieve a uniform and controlled PDMS thickness on the glass surface due to high viscosity of PDMS gel. Thus, another approach called mold-casting was used for the PDMS coating [136]. Figure 4.3 shows the comparison of the spectra obtained from the same tissue sample on three different substrates where tissue specimen was placed. As seen, the substrate has a dramatic effect on the spectra. CaF_2 slides are routinely used in Raman measurements due to the low background. Although placing the PDMS layer between tissue and glass slide helps to eliminate the background from glass, it is not as good as CaF_2 slide. However, CaF_2 slides are expensive. Therefore, an approach eliminating the glass background in such application is necessary.

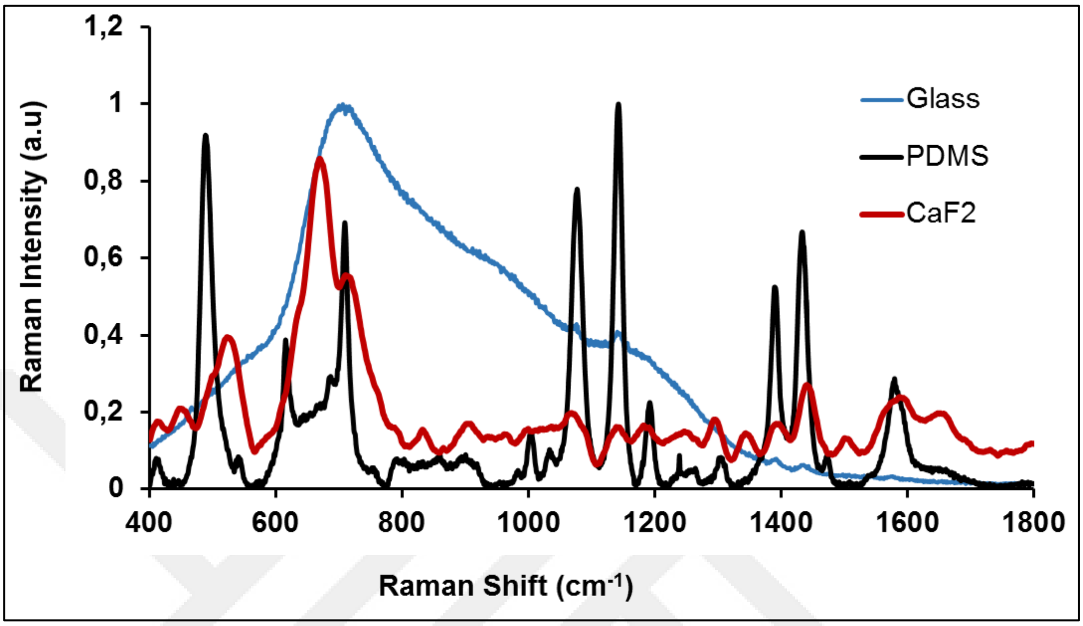

Figure 4.3. SERS spectra of bovine liver cryosectioned tissue specimen placed on glass, PDMS, and CaF_2 slide.

It is necessary to optimize the thickness of PDMS on the glass slide to prevent supressing signal coming from the glass slide. PDMS covered glass slides in different thickness were prepared using six-well plate molding method (detailed in “Section 3.5.1.1"). Then, PDMS thicknesses on the glass slides were measured from the SEM images.

Meanwhile, SERS spectra of PDMS covered glass slides were obtained after a 5-µl volume of 8 × concentrated AgNP suspension dropped onto the PDMS surface and left to dry at the suspended position. After several attempts, at least 1.8 mm thick PDMS layer was found to be optimal and decided to use in the studies. Figure 4.4 shows the comparison of the spectra obtained increasing thickness of the PDMS layer.

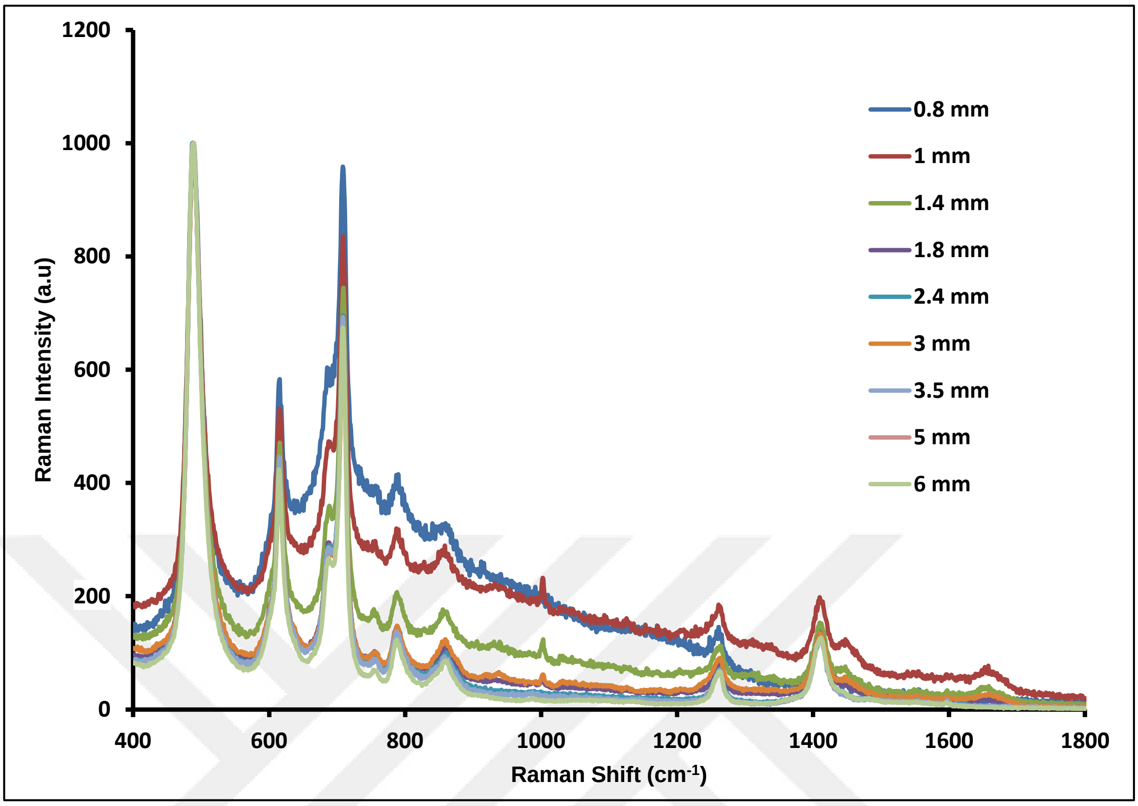

Figure 4.4. SERS spectra obtained from different thickness of PDMS coated glass slides.

As seen in Figure 4.4, the minimum thickness should be 1.8 mm or greater for a weakest background while the layers with 0.8, 1 and 1.4 thicknesses have still an intense background originating from the glass. Thus, a PDMS layer thickness at least 1.8 mm requires on the glass slide to suppress the background.

As the tissue slice is placed onto PDMS layer and the spectra are acquired, the obtained spectra can contain both Raman and SERS. Thus, both Raman and SERS spectra of PDMS were acquired to evaluate whether there are significant differences in the band position and the intensity of the spectra originating from PDMS. The comparison of the mean spectra of Raman and SERS from PDMS are given in Figure. 4.5. As seen, only difference is the intensity of the bands. However, it is clear that SERS spectra may be the mixture of both Raman and SERS.

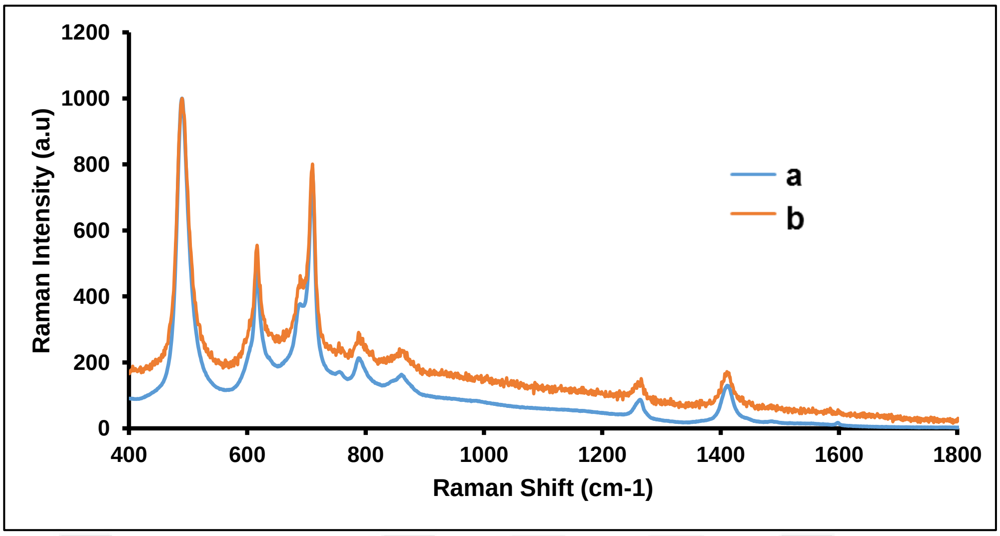

Figure 4.5. Comparison of Raman spectrum (a) and SERS spectrum (b) of PDMS.

Another alternative substrate as six-well plate was evaluated by using instead of cut glass pieces for PDMS covering because PDMS coating into the wells of a plastic (polystyrene) six-well plate was simpler. Tissue samples were sectioned on two prepared substrates. The spectra were acquired. Figure.4.6 shows the comparison of spectra obtained from PDMS on glass surface and polystyrene. As seen, there are a few less peaks on the PDMS spectrum compared to the polystyrene plastic. Thus, the PDMS coating on the glass was thought to be a better option.

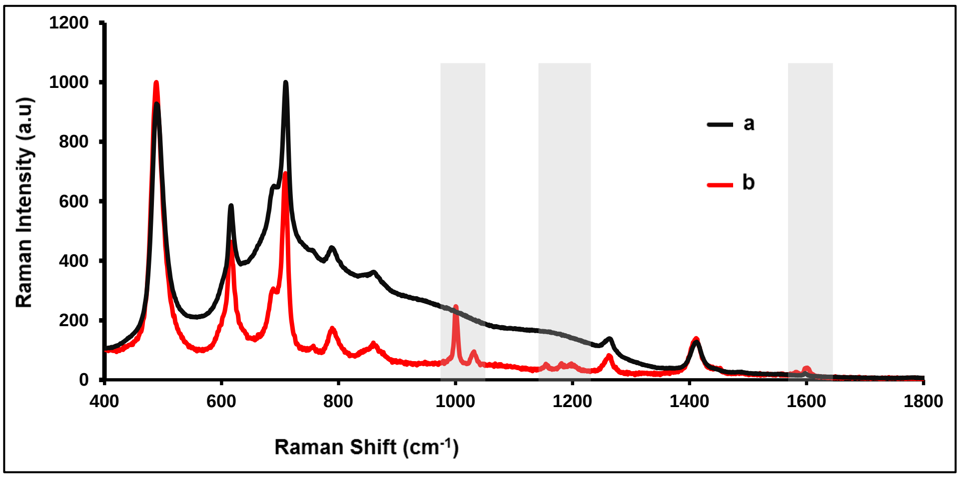

Figure 4.6. Mean SERS spectra of PDMS placed on glass slide (a) and plastic material (polystyrene) (b).

4.2.1.2. Tissue Thickness

The sectioned tissue in the range of 3 to 10 μm depending on the type of tissue is used in routine pathological procedure. The best diagnostic definition has been mostly given using sectioned tissues at around 5-μm thickness because the tissue sections should be transparent rather than opaque so that the light can pass through the tissue specimen to be successfully examined under bright field microscopy. The ten SERS spectra acquired from the sectioned tissues with different thicknesses after a 20 μl volume of 8× AgNP suspension was placed and dried at suspended position. The SERS spectra obtained to realize whether there are significant differences between the spectral patterns. Figure 4.7 demonstrates the mean SERS spectra of each sectioned tissue thickness with separated plotting of the spectra from each other to visualize the differences more clearly. As seen, from figure, the spectral patterns are quite similar to each other. There is a slight increase in intensity of the band at 721 cm^{-1}, which was attributed to DNA [137]. An increase in the nucleic acid concentration due to the increased cell population was an expected result due to increased tissue thickness. The proportional increase in the band intensity may be a supportive reason for the method with increased signal reproducibility related to more uniform distribution of AgNP aggregates.

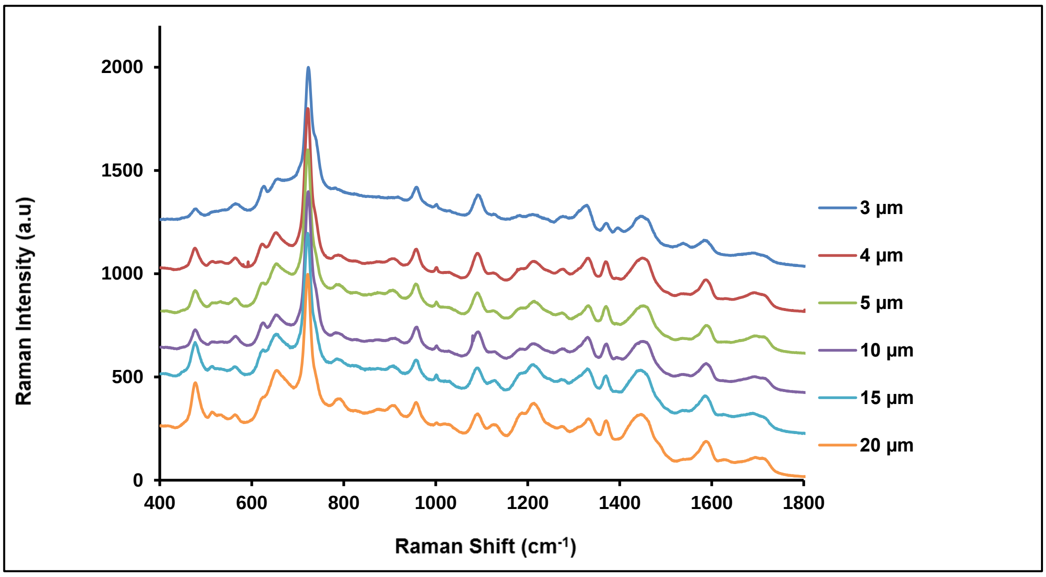

Figure 4.7. Mean SERS spectra obtained from increasing tissue thicknesses.

A 5-µm thick tissue section was selected as the optimum thickness by also considering that about a monolayer of cells in the sectioned tissue would be ideal by preventing interference from healthy or cancerous cell above or below of the cells in the monolayer.

4.2.1.3. Objective, Laser Power and Focus Adjustment

Other instrumental parameters should also be evaluated for optimal signal collection. First, objective lenses of 5×, 20× and 50× were evaluated. Each objective has a different collection efficiency and spot size at the focal point depending on their numerical aperture (NA) and the selected laser wavelength. The laser spot diameter was calculated using the formula of 1.22 λ / NA [138]. Table 4.1 shows the theoretical spot sizes of the three objectives evaluated in the study.

Table 4.1. Laser wavelength, laser power at sample, theoretical laser spot size of objective lenses with N.A.

Laser wavelength: 830 nm Laser power at sample: mW		
Objective	**N.A**	**Laser spot size (µm)**
5×	0.15	0.67
20×	0.40	0.25
50×	0.50	0.20

With a 5x objective, it is possible to scan a larger area but the background originating from the sample hampers the measurement. However, using higher magnification objectives with higher numerical aperture (N.A) provides higher spatial resolution. A 20× objective has larger spot size than a 50× objective and was chosen for further studies because their spectral patterns were quite similar with each other as seen in Figure 4.8.

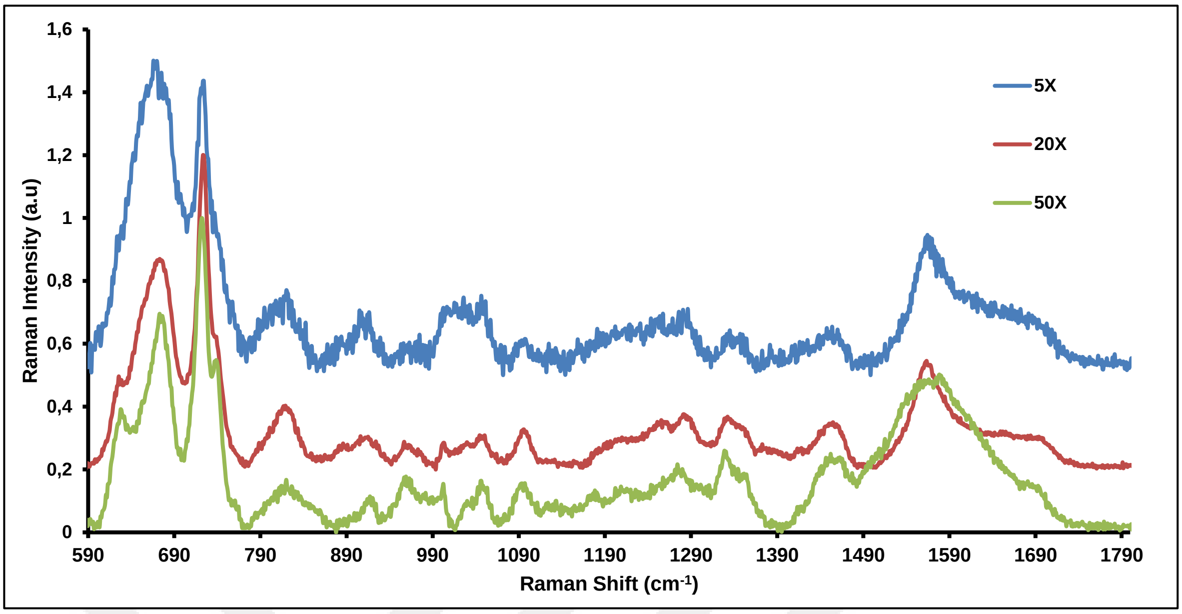

Figure 4.8. Mean spectra of tissue specimen obtained using 5 ×, 20 × and 50 × objectives.

The other parameters that affect the signal quality are laser power and exposure time. The laser powers were set in the Raman software as 3mW, 15mW, 30mW or 150 mW. The exposure times of 2, 3 and 5 s were evaluated for signal quality. In addition, five seconds to the first exposure time (which makes the total exposure time 7, 8, 10 s) were added as soon as SERS signal appeared to see whether there will be any improvement in the signal quality. Figure 4.9 compares the spectral patterns depending on laser power (as adjusted in the software) and exposure time. As seen, the richest spectrum is obtained with the use of laser power of %10 (of 30 mW) and the exposure time of 2 and 7. Although 7 s of exposure time generates higher SNR, 2 s of exposure time can also be considered as satisfactory since choosing 2 s exposure time reduces the analysis time. Further, the spectral pattern changes with traditional point mapping and StreamHR mapping were studied and found that the StreamHR point-by-point mapping was satisfactory for Cryosectioned-PDMS method. For comparison, the first spectrum from the top in Figure 4.9 was obtained using traditional point mapping. As seen, SNR ratio is lower than StreamHR point-by-point mapping and the mapping time is significantly higher, about 70 min for 10x10 points array.

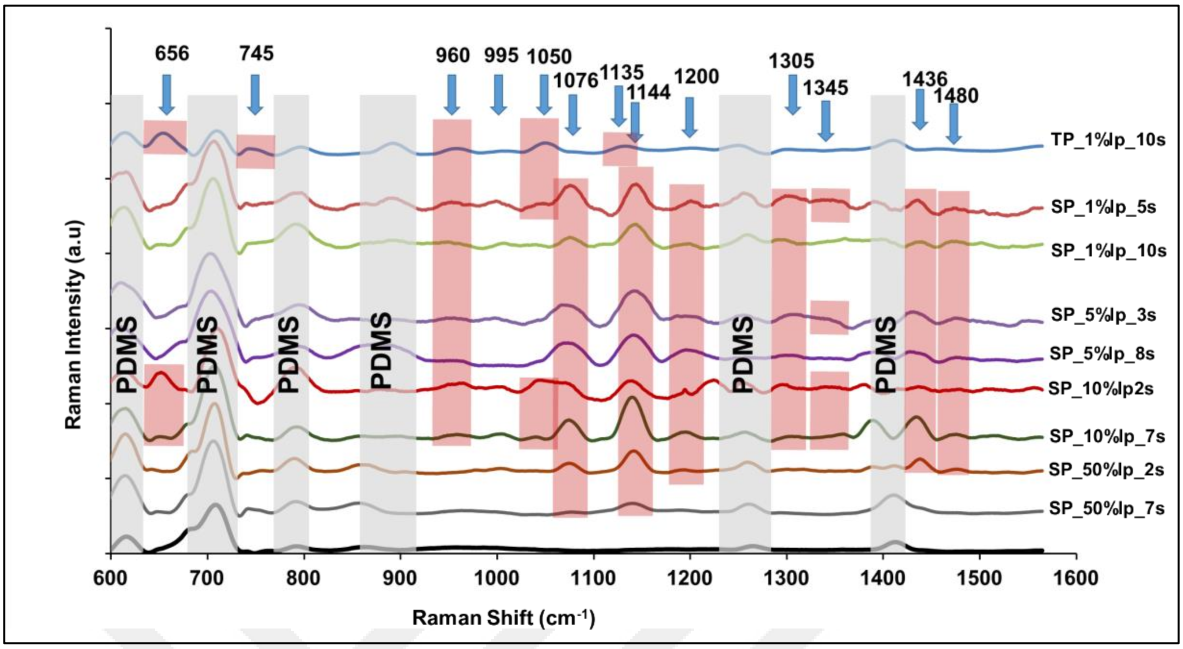

Figure 4.9. Mean SERS spectra of tissue sample obtained using different parameters of laser power and exposure time. (TP: Traditional point mapping; SP: StreamHR point mapping; lp: laser power; e: exposure time; s: second)

4.2.1.4. Acquisition Type, Number and Mode

Two acquisition approaches, mapping and random selection, can be employed to collect spectra from a sectioned tissue. Since tissue is very heterogeneous in nature possessing healthy and cancerous cells, scanning a large area of tissue can be a good strategy. However, it can take a long time to scan an area where can provide good spectra representing the biochemical characteristics of tissue. Another approach is to collect several spectra from arbitrarily chosen points on the tissue sample. In this part of the study, these two approaches were evaluated by acquiring spectra following these approaches. For fast scanning, StreamHR point acquisition is used. StreamHR acquisition method provides fast and high-resolution mapping because sample movement, data collection, and data readout occur simultaneously by using Renishaw's High Speed Encoded Stage (HSES).

SERS spectra were collected from ten randomly selected points by using two modes of StreamHR point acquisition and traditional point acquisition. The comparison of mean

SERS spectra obtained with these two modes are shown in Figure 4.10. As seen, both spectra have a quite similar pattern and SNR.

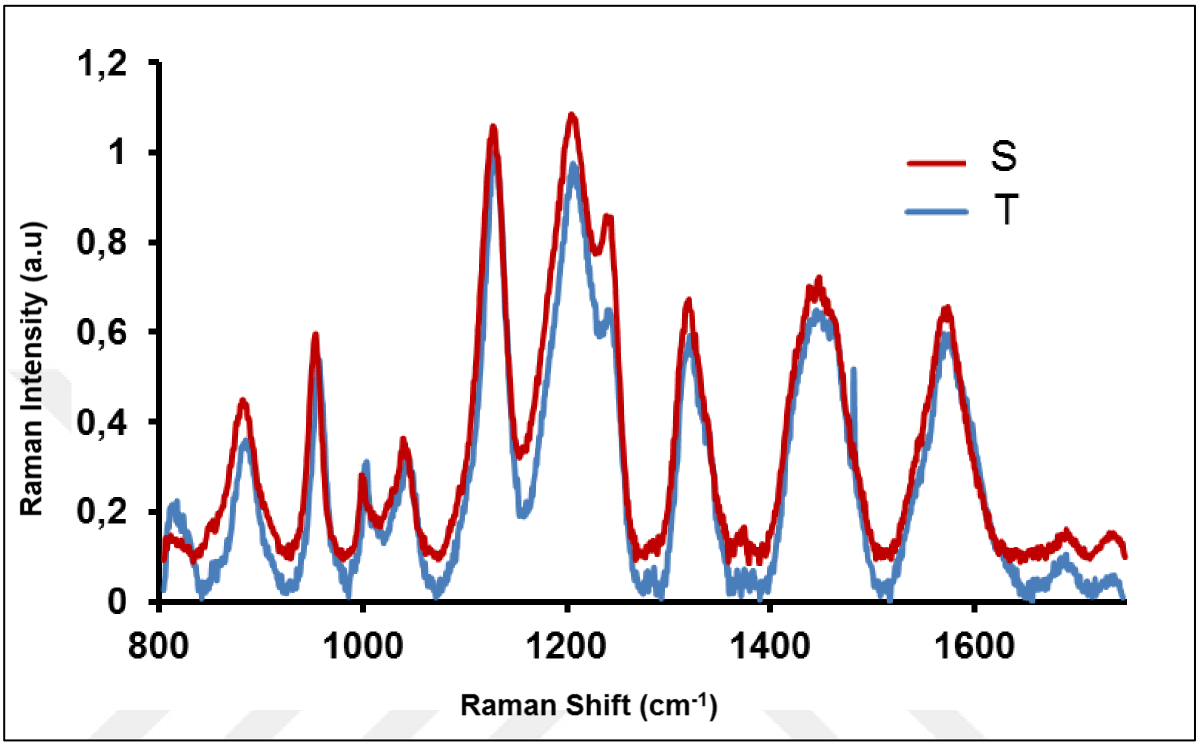

Figure 4.10. Mean SERS spectra of liver tissue acquired using StreamHR and traditional point acquisition method. (S: StreamHR acquisiton; T: Traditional acquisiton)

Then, the coefficient of variation (CV) was calculated for each measurement and repetition for a comparison of intra-and inter-method repeatability and reproducibility. Ten spectra for each mode were used to calculate intra-method repeatability to obtain the maximum variances between the spectra for all measurements combined while the averaged SERS spectra of each collection from three repetitions were used to calculate the inter-method reproducibility for the observations at different times.

The reproducibility is the maximum difference that is likely to transpire between observations at different times while the repeatability is the maximum difference that is likely to transpire between repeated experiments at the same time. Table.4.2 compares the calculated CV values of SERS spectra from three experimental repetitions.

Table 4.2. CV values of SERS measurements obtained using traditional and StreamHR acquisition method.

Bovine liver	**1st Experiment**			**2nd Experiment**			**3rd Experiment**		Average
	Traditional	StreamHR	Average	Traditional	StreamHR	Average	Traditional	StreamHR	
	4.47	7.51	8.5	8.38	1.72	0.5	8.5	8.38	1.72

The CV value for StreamHR as 7.51 per cent, which shows the maximum difference between the spectra for the first repeat of experiment, was slightly more than CV value of 4.47 per cent for Traditional method. However, the CV values of the spectra obtained using Traditional method was slightly higher compared to StreamHR method for the second and third experiments. The average CV values indicate the maximum differences between the method of Traditional and StreamHR by their mean-centered spectra. The first calculated CV value was 8.5 for the first experiment whereas the second and the third ones showed 0.50 and 1.72 per cent differences between the methods. However, this comparison is not enough to determine the optimum conditions for acquisition. The total analysis time for 10 points acquisition was 7 minutes for traditional point acquisition method while it was 30 seconds for StreamHR acquisition. This is a quite significant difference. Thus, StreamHR point acquisition type was used for collection of spectral information from the tissue specimen in Cryosectioned-PDMS sampling method. After the random selection mode was optimized, mapping modes also need to be optimized to compare. Next, the traditional point mapping, line focus and SteamHR point mapping were compared for their performance. For this, one hundred SERS spectra were collected from the same region of crytosectioned tissue using three types of mapping modes. The spectra obtained with each mode and their average is presented on Figure. 4.11.

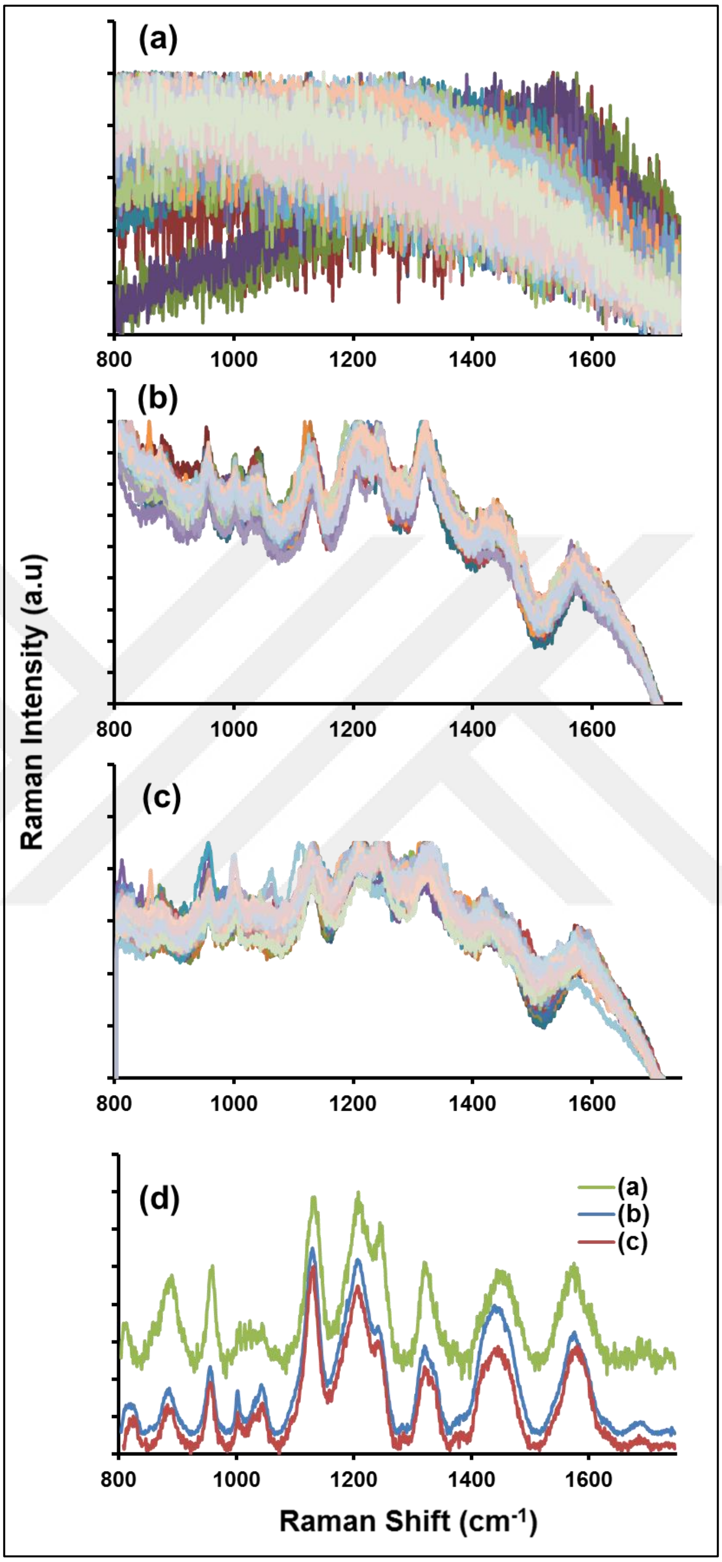

Figure 4.11. SERS spectra from a 10x10 points grid on tissue surface by using line (a), traditional point (b), and StreamHR point (c) mapping, and comparison of their average spectra (d).

In the line-mapping mode, laser spot has a shape of a line rather than a spot providing wide-field sample area illumination. With this method, it is possible to use higher laser power without damaging biological samples, and this method provides the collection of spectra from multiple location on the sample saving time. This mapping acquisition method was also optimized for this study. Even though the collected SERS spectra were noisy, the mean spectrum of the data was obtained with an increased quality due to the robust optimization of the noisy data by the WIRE.4.1 software.

The comparison of three approaches can be seen in Figure 4.11. Two experimental conditions can be given to collect a satisfactory signal collection. In the first case, the minimum laser power should be adjusted to 30 mW with at least 10 s exposure times. In the second case, laser power should be adjusted to 150 mW with at least 3 s exposure to reduce the time. After the spectral collection, the spectra were normalized. The CV values were calculated and compared to determine the reproducibility of each mode and are detailed in Table 4.3.

Table 4.3. CV values obtained using three type of mapping methods.

Line Focus Mapping				**StreamlineHR Point Mapping**				**Traditional Point Mapping**			
1st	**2nd**	**3rd**	**Average**	**1st**	**2nd**	**3rd**	**Average**	**1st**	**2nd**	**3rd**	**Average**
26.29	19.32	23.43	15.99	8.85	10.22	7.54	9.70	10.29	7.13	12.96	6.51

The CV values were obtained as 26.29, 19.32 and 23. 43 by calculating the SERS spectra obtained with three repeats. The greatest difference was observed in the CV values of the data collected with Line mapping. The values of 8.85, 10.22 and 7.54 indicate a higher repetability of using StreamHR mapping compared to Line mapping. However, the CV values calculated from the mean spectra of each experiments were found as 6.51, 9.70 and 15.99 for Traditional point, StreamHR point and Line mapping methods, respectively indicating that Traditional mapping has the the lowest CV values refering to the highest reproduciblity with a 3.19 than the StreamHR method. However, another significant point is the analysis time for the collection of 100 spectra. It was 5 min for StreamHR and 70 min for Traditional one.

Table 4.4. Analysis times and parameters used in mapping methods.

	Line Focus Mapping **10 % laser power** **10 s exposure time**	**StreamHR Point Mapping** **10 % laser power** **2s exposure time**	**Traditional Point Mapping** **5 % laser power** **10s exposure time**
Total Analysis Time	2 minutes	5 minutes	70 minutes

Based on the results presented in Table 4.3 and Table 4.4, the StreamHR point mapping method was selected as the optimum acquisition method for the spectral collection due to low analysis time and high reproducibility.

Further, the random selection of the acquisition point on the tissue sample and mapping type was optimized. The random selection and mapping was compared calculating the CV values and signal quality. Thus, the spectra from ten randomly selected points on the tissue surface were collected using StreamHR point acquisition method, and a 10x10 grid point area was mapped using StreamHR point acquisition. Then, the CV values of the spectra were calculated for each experiment and are given in Table 4.5. The SERS spectra by each method with their mean spectra are shown in Figure.4.12 as a comparison.

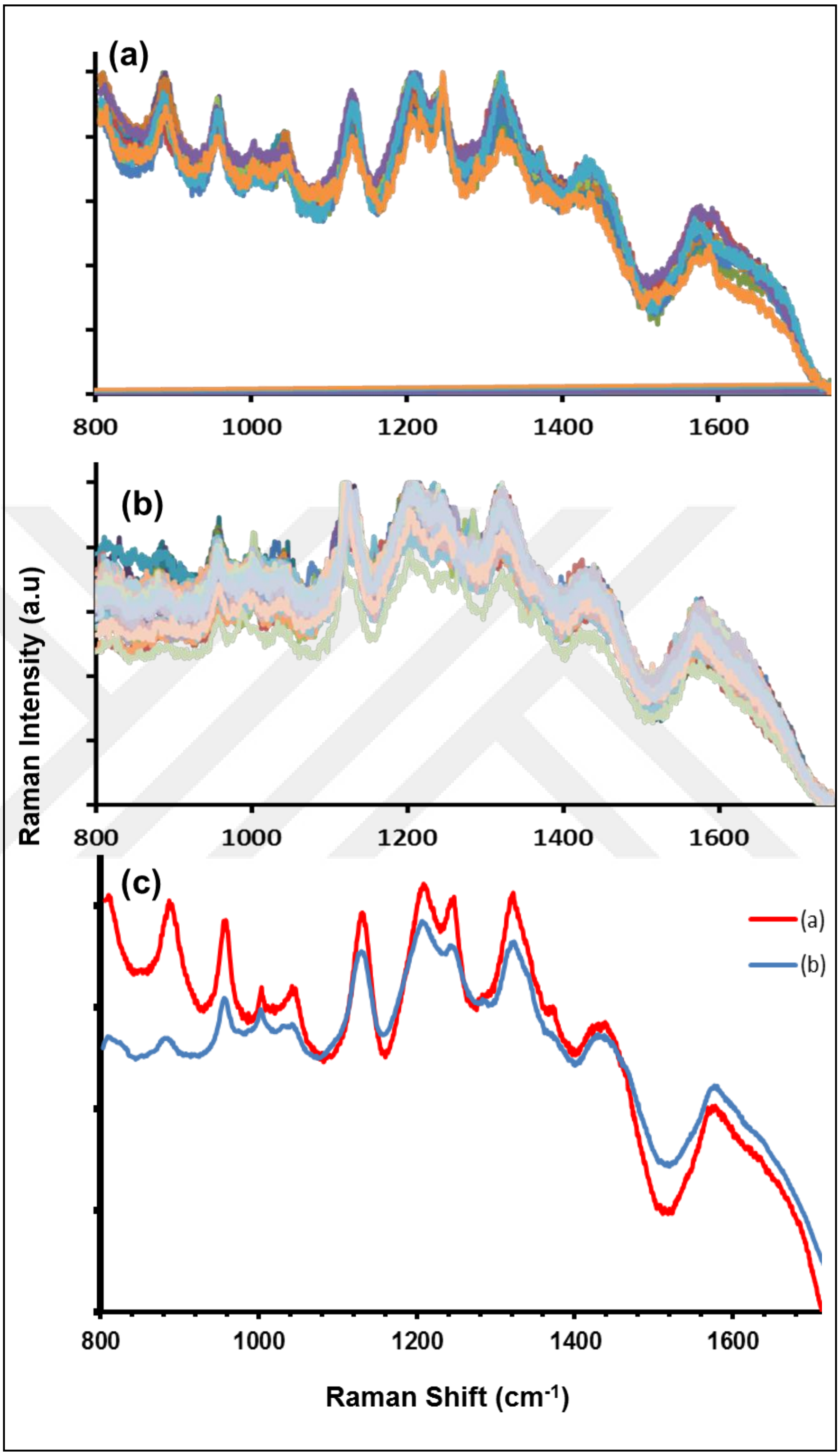

Figure 4.12. SERS spectra of tissue specimen acquired from randomly selected ten points (a) and a 10x10 points grid area (b) using StreamHR point mapping method, and comparison of their mean spectra (c).

Table 4.5. CV values of SERS spectra obtained using StreamHR point mapping and random selection of ten points.

Model tissue	1st Experiment				2nd Experiment				3rd Experiment			
	Randomly selected ten points (R)	StreamHR point mapping (S)	Average 1st Exp.		R	S	Average 2nd Exp.		R	S	Average 3rd Exp.	
			R	S			R	S			R	S
Bovine liver	7.51	7.54	8.82	5.46	13.37	9.10	7.31	4.44	10.22	9.66	5.08	2.81

Table 4.6. Analysis time and parameters used in the methods.

	Random Selection of 10 Points 10 % laser power-2s exposure times	**StreamHR Point Mapping 10 % laser power-2s exposure times**
Total Analysis Time	6.5 minutes	3 minutes

As seen, the CV values are lower for StreamHR mapping compared to the random selection acquisition for both point-to-point variations and sample-to-sample variations. The point mapping by StreamHR technology as an optimum data collection method for Cryosectioned-PDMS method was selected not only resulting in high reproducibility but also short analysis time.

4.2.1.5. Size of Mapping Area

The size of mapping area also needs to be optimized. Thus, a 10 x 10 points grid, a 50 x 10 point grid and a 250 x 10 points grid were selected on the same sectioned tissue surface for spectral collection. The mean SERS spectra of each collection are demonstrated in Figure. 4.13.

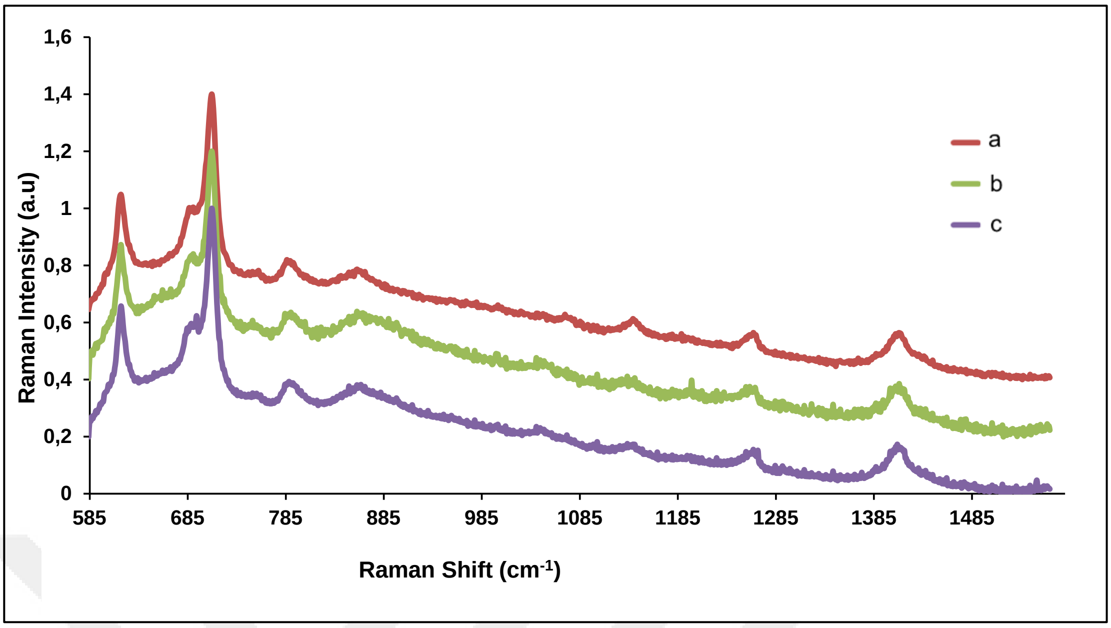

Figure 4.13. Mean SERS spectra of tissue obtained by selecting three different point arrays from the same tissue surface of 22.5-µm x 22.5-µm (a), 112.5- µm x 22.5-µm (b), and 562.5 µm x 22.5-µm (c).

As seen, the spectral patterns are obtained quite similar to each other. Thus, a 10x10 points grid area was selected as the optimum one for the Cryosectioned-PDMS method.

4.2.1.6. Spectral Range

The Raman shift range of the acquisition also needs to be optimized because it is possible to select a wide range using the traditional point-by-point method (slowest one) but the fast acquisition method of StreamHR point uses a median value for the spectral range arrangement which reduces the obtained spectral range. Thus, 400-1800 cm^{-1} range, which has the characteristic bands related to the tissue specimen, was divided into two spectral regions is included in the median value of 1100 (~580-1560 cm^{-1}) and 1400 (~480-1860 cm^{-1}). The mean spectra of each divided spectral range are given in Figure. 4.14 including PDMS spectra as a comparison.

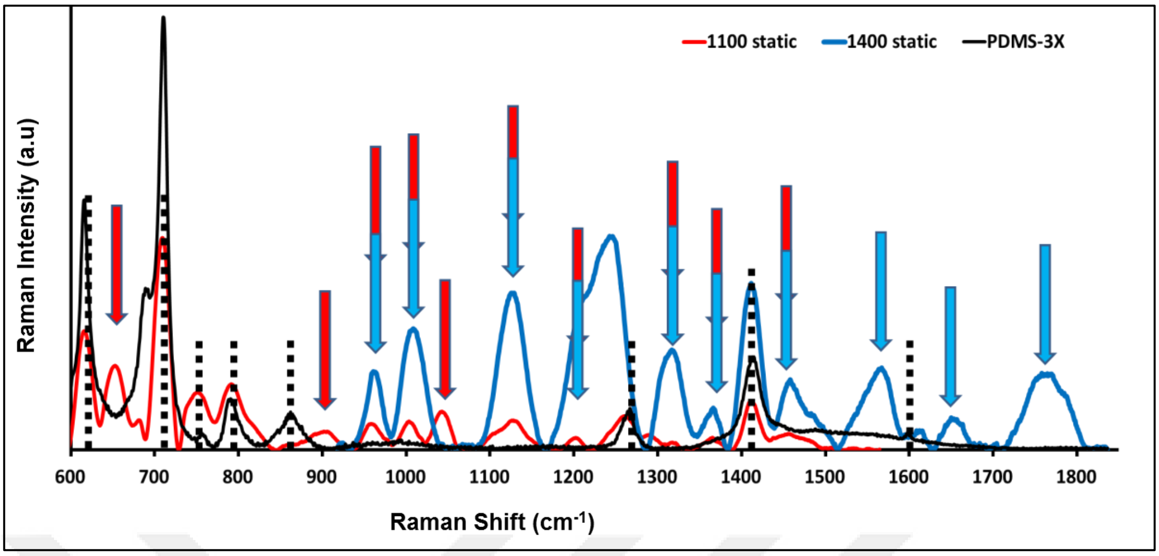

Figure 4.14. A comparison of mean SERS spectra of tissue by two divided Raman shift range obtained given median values of 1100 cm^{-1} and 1400 cm^{-1}, and the SERS spectrum of PDMS.

The number of major SERS bands originating from bovine liver tissue is the same for each spectral range; 1100 (~580-1560 cm^{-1}) and 1400 (~480-1860 cm^{-1}). The spectral range selection may vary depending on the tissue type and analyst. Thus, thyroid biopsies were studied in the range of 582 to 1563 cm^{-1} by selecting 1100 as a median value due to having rich band assignments to proteins, lipids, carbohydrates and metabolites. Although the restricted spectral range choice is a disadvantage for StreamHR fast mapping, it is much faster than the traditional mapping. Mapping the same area takes only 5 min with StreamHR fast mapping but 70 min for traditional mapping.

The distribution and packing of AgNPs aggregates on the tissue surface effect the signal reproducibility and quality as well. The suspended drying position of the droplet including colloidal AgNPs indicated an increased scattering and higher reproducibility in our previous studies [68, 139, 140]. However, the droplet drying configuration for the Cryosetioned-PDMS method was needed to be optimized. For this reason, the sessile and suspended positions were compared with each other.

4.2.1.7. AgNP Suspension-Droplet Position

The SERS spectra acquired from the mapped area on both sessile and suspended dried droplets after a 20 -µl volume of 8× colloidal AgNP suspension was placed on tissue specimen. In order to assess the distribution of AgNPs and their aggregates on the tissue surface, SEM images were obtained from the droplet area. Figure 4.15 shows the droplet configurations and SEM images. The zoomed areas are marked in the SEM image of the whole droplet area to visualize the AgNPs and their aggregates.

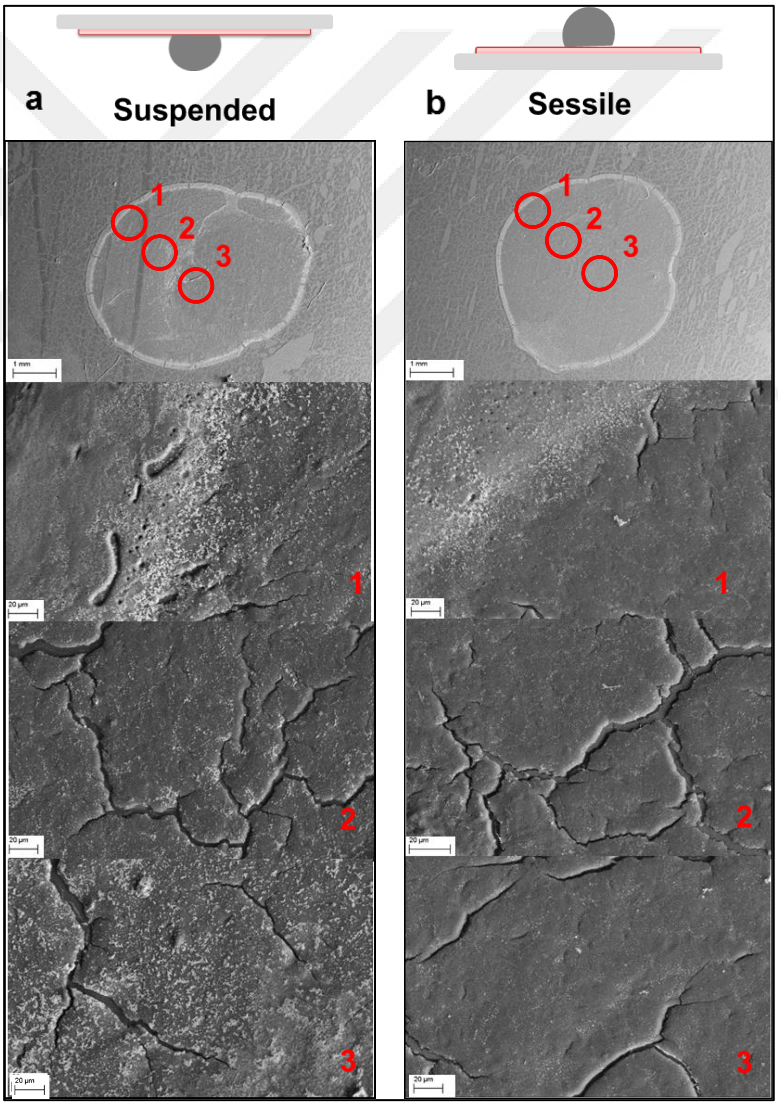

Figure 4.15. SEM images of dried droplet areas on tissue surface with suspended (a), and sessile (b) configurations.

The numbers 1, 3 and 2 refer to the middle, edge and in between. As seen, as a result of “coffee-ring” phenomenon, some of the AgNPs is packed at the edges while some are distributed though the droplet areas as single AgNPs or aggregates. The “coffee-ring” formation is a phenomenon that takes place in a drying droplet and jams most of the particles at the liquid–solid–air interface [141]. he SERS spectra were acquired from a 10x10 points grid from three different spots on the droplet area. As an example, a set of SERS spectra is shown in Figure 4.16.

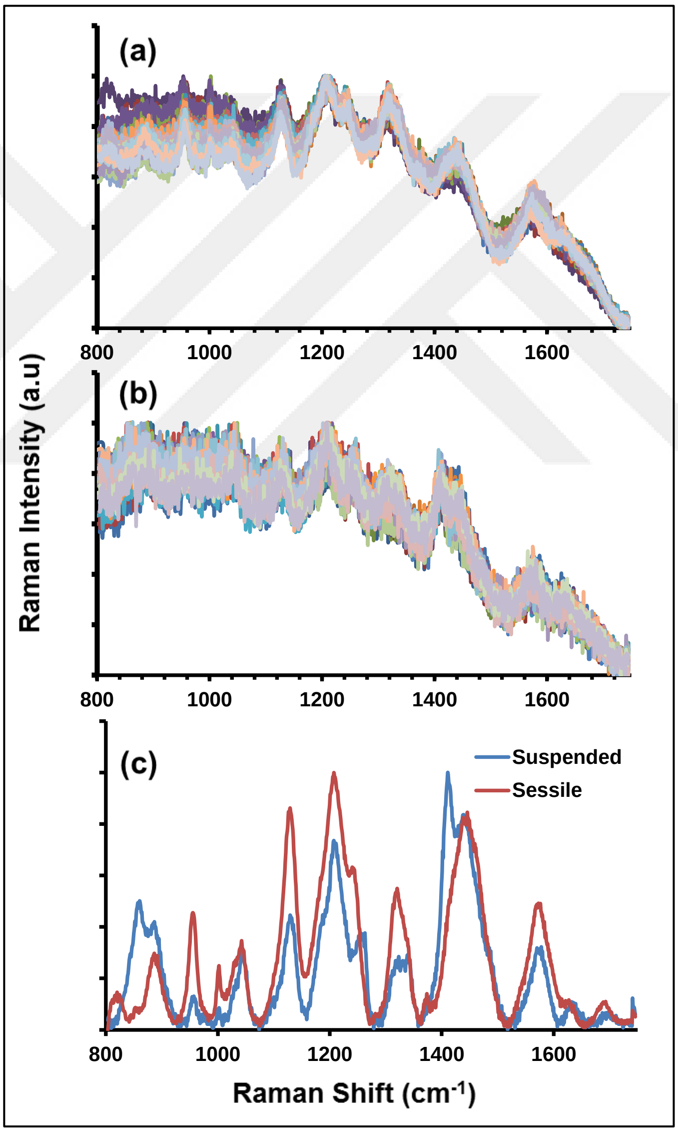

Figure 4.16. SERS spectra of tissue specimen obtained from the droplet area dried at suspended (a) and sessile position (b), and their mean spectra (c).

The averaged spectra to compare the spectral richness for each type of droplet position are also shown in Figure 4.16 (c). In general, the spectra obtained from the area where droplet is dried at the sessile position were nosier.

The averaged SERS spectra obtained from the tissue where the suspension was dried at the suspended position showed richer spectral pattern than the sessile position provided, which means more characteristic bands related to the tissue specimen. This could be both due to the difference in distribution of AgNPs in the droplet area and/or the difference in metabolic species diffusing into the droplet during drying. As the colloidal suspension is placed onto the tissue sample, cellular or metabolic species soluble in aqueous medium can be quickly diffuse and come into contact with AgNPs. What is observed on the SERS spectra could also be related to this phenomenon. Further, the CV values of the spectra obtained to address to the reproducibility of the sampling approach. Table 4.7 shows the CV values of the SERS spectra obtained from each sampling method. The spot-to-spot and sample-to-sample variations were calculated to compare the configuration dependent reproducibility.

Table 4.7. CV values of SERS measurements obtained from different region of sessile and suspended dried droplets with three repetitions.

1st Experiment								**2nd Experiment**								**3rd Experiment**							
Sessile (SES)			Suspended (SUS)			Average		Sessile (SES)			Suspended (SUS)			Average		Sessile (SES)			Suspended (SUS)			Average	
						SES	SUS							SES	SUS							SES	SUS
10.8	10.01	10.33	8.00	7.20	6.64	10.10	7.78	11.74	10.76	8.04	7.20	7.33	8.26	11.47	8.12	12.77	14.87	13.46	7.87	9.61	9.50	7.30	8.22

The spot-to-spot variations and sample-to-sample variations were obtained by calculating the CV values of the spectra. As a result, the CV values of the spectra from the suspended position were lower than the ones obtained from sessile droplet position. Thus, the suspended configuration was selected as optimum configuration for Cryosectined-PDMS approach. Then, the suspension concentration was optimized by comparing the signal quality.

4.2.1.8. SERS Substrate Concentration

The density of the colloidal suspension containing AgNPs was optimized to increase the reproducibility and quality of the spectra by covering the tissue surface as many as AgNPs and its aggregates. The concentration of the suspension was increased 8×, 16× and 32× before a 20-µl volume of the suspension from each concentration was dropped onto tissue surface, and left to dry at suspended position until SERS measurements were performed. The details for the synthesis and concentration of the AgNP suspension can be found in "*Section 3.3*". Then, the SERS spectra were collected from three different droplets areas where 8×, 16× and 32× concentrated suspensions were placed. The comparison of the mean spectra obtained with three different colloidal suspension concentrations is provided in Figure 4.17.

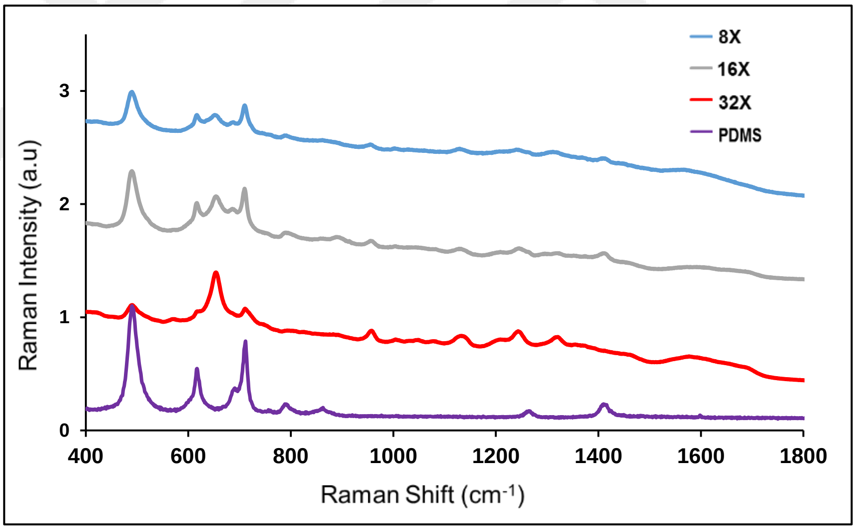

Figure 4.17. Mean SERS spectra of tissue specimen obtained from suspended dried droplet using (a) 8×, (b) 16× and, (c) 32× concentrated AgNP suspension.

The use of 16× concentrated colloidal AgNP suspension resulted in a better signal quality with increased band richness in spectral pattern compared to other mean spectra obtained from 8× and 32× concentrated suspensions. Thus, 16× concentrated suspension was selected as the optimum density for the Cryosectioned-PDMS method.

4.2.1.9. Spectral Reproducibility of Region Dependent Acquisition

The spectral reproducibility is a major problem for SERS due to the chaotic nature of the interactions of analytes and noble nanoparticles. As the colloidal suspension of AgNPs was added onto tissue, the interaction of AgNPs with the tissue components is governed by several parameters including the dynamics in a drying droplet. The distribution of the AgNPs and their aggregation status influences the SERS activity and dependently the spectral reproducibility. To understand the region dependent signal reproducibility and the influence of addition of colloidal AgNPs by dropping on to tissue surface, the spectra obtained from different regions on the dried droplet at the suspended position. The CV values of the spectra were calculated. Each spot labeled as 1, 2, 3, and 4, also shows the direction of acquisition. Each spot includes mapping of a 10x10 points grid area from the sample surface. The CV values of the spectra to calculate spot-to-spot variations were also obtained. Then, the CV values for each averaged spectrum of each region were calculated to understand the region-to-region variations. The CV values of each region detailed in Table 4.8. A total of sixteen spots from four divided regions on the droplet were evaluated as highlighted in Figure 4.18.

Table 4.8. CV values of SERS measurements obtained from different mapped areas on the same sample.

1st Region					**2nd Region**				
1st spot	2nd spot	3rd spot	4th spot	Average	1st spot	2nd spot	3rd spot	4th spot	Average
6.88	8.53	8.17	11.19	10.54	13.17	11.21	13.28	12.75	10.21
3rd Region					**4th Region**				
1st spot	2nd spot	3rd spot	4th spot	Average	1st spot	2nd spot	3rd spot	Average 4th spot	Total Average
6.41	14.90	15.39	13.89	13.20	6.01	13.45	18.76	14.21	12.34

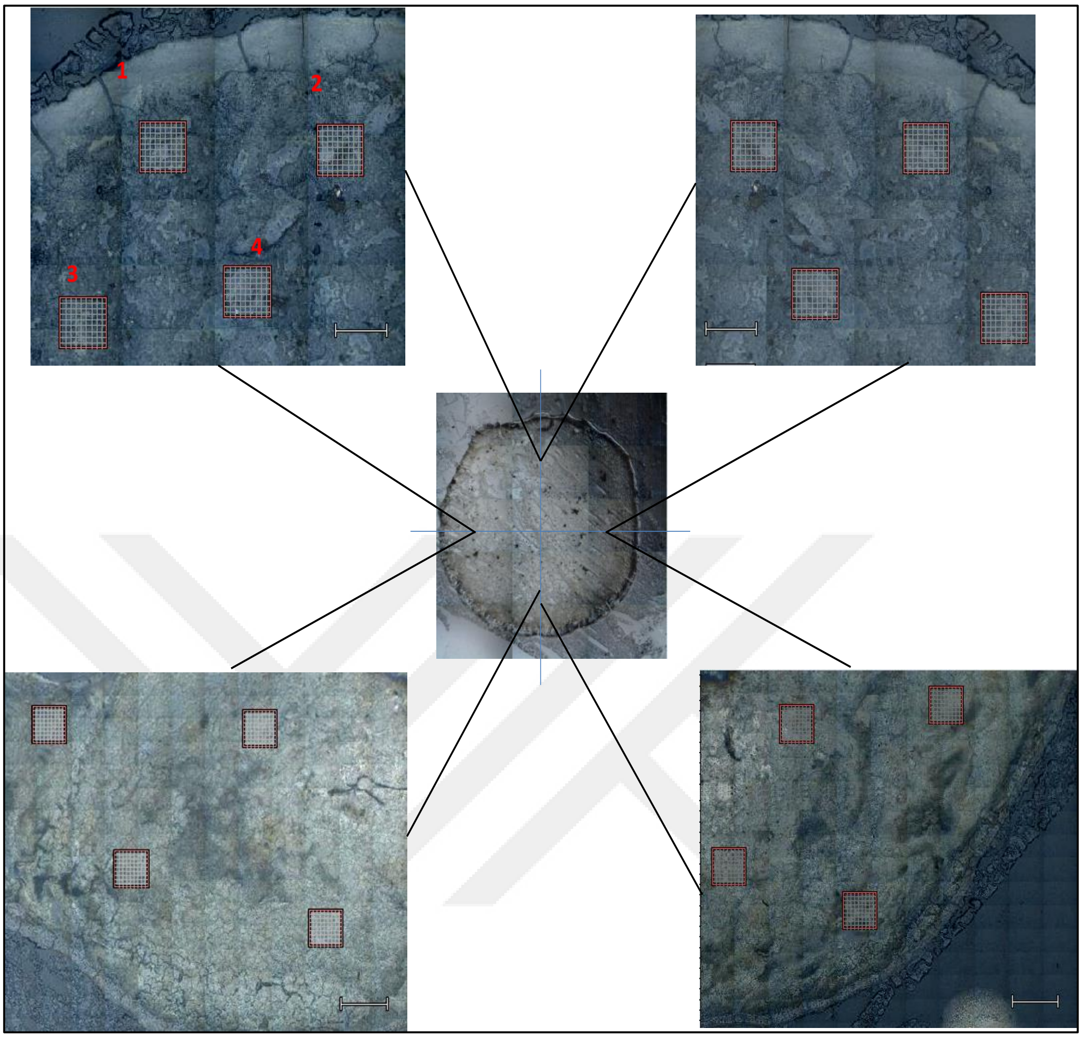

Figure 4.18. Light microscope images of selected sixteen-mapped areas from a droplet area.

The point-to-point variation was obtained between 7 and 19 per cent while the spot-to-spot variation was between 11 and 15 per cent, and the region-to-region variation was 12 per cent. The results indicated a close CV value between the spots except the first spot. However, the CV values between the regions were somewhat similar, which means the spectral collection could be selected from any regions on the droplet surface. The sample to sample variations to understand the inter-method reproducibility were calculated and interpreted in the following section.

4.2.2. Intra-Method Reproducibility

The CV values of SERS measurements regarding point-to-point, spot-to-spot and sample-to-sample variations obtained from the three different spots by scanning a 10x 10-points grid area on the droplet surface were calculated. The CV values of the 100 spectra were calculated to obtained point-to-point variations. Then, the CV values of averaged spectra obtained from 100 spectra for each spot were calculated to understand the spot-to-spot variations. Finally, an average CV value of the averaged spectra obtained from each experiment was calculated to obtain the sample-to-sample variations. The intra-method reproducibility of the Cryosectioned-PDMS sampling method depends on the CV values among the points, spots and samples studied at the same time while inter-method reproducibility depends on the results obtained at the different times.

Table 4.9. CV values of SERS measurements obtained from different mapped areas on three samples at different times. (Av.; Average)

1st Experiment				**2nd Experiment**				**3rd Experiment**				**Total Av.**
1st spot	2nd	3rd	Av.	1st spot	2nd	3rd	Av.	1st spot	2nd	3rd	Av.	
10.50	8.15	7.12	4.03	5.90	8.01	6.15	2.09	7.02	10.8	5.81	3.09	3.50

The obtained CV value as 3.5 calculated from the mean spectra belongs to each experiment indicated that the intra-method reproducibility for the newly developed method was significantly high.

4.2.3. Comparison of Substrate Dependent Classification

The problem of background signal originating from the glass was mentioned in the previous section. To overcome this problem, PDMS was selected to cover glass slides due to its chemical stability, easy preparation, low cost compared to CaF_2 substrates, which is commonly used in Raman and SERS measurements. Moreover, PDMS surface is hydrophobic preventing aqueous samples to spread. The background originating from the PDMS is a disadvantage but PC loading vector, which represent the PDMS, can be removed before its use in the classification algorithm when necessary.

The influence of the substrates on the classification accuracy can be calculated comparatively between CaF_2 substrates and PDMS whether there is a significant limitation on the classification accuracy due to the background of PDMS. On the other hand, there is an alternative substrate, which is Aluminum foil (Al-foil) covered slides, having more straightforward preparation compared to PDMS covered slides, and it was used in many SERS studies due to the its low cost and SERS enhancement ability [142, 143]. Al-foil covered substrate was also compared to the other substrates used in this study through calculating the CV values and classification accuracy results. Thus, the tissue specimen was prepared on the Al-foil covered slide and compared to PDMS and CaF_2 cases. Figure 4.19 shows the comparison of the mean SERS spectra obtained with three approaches.

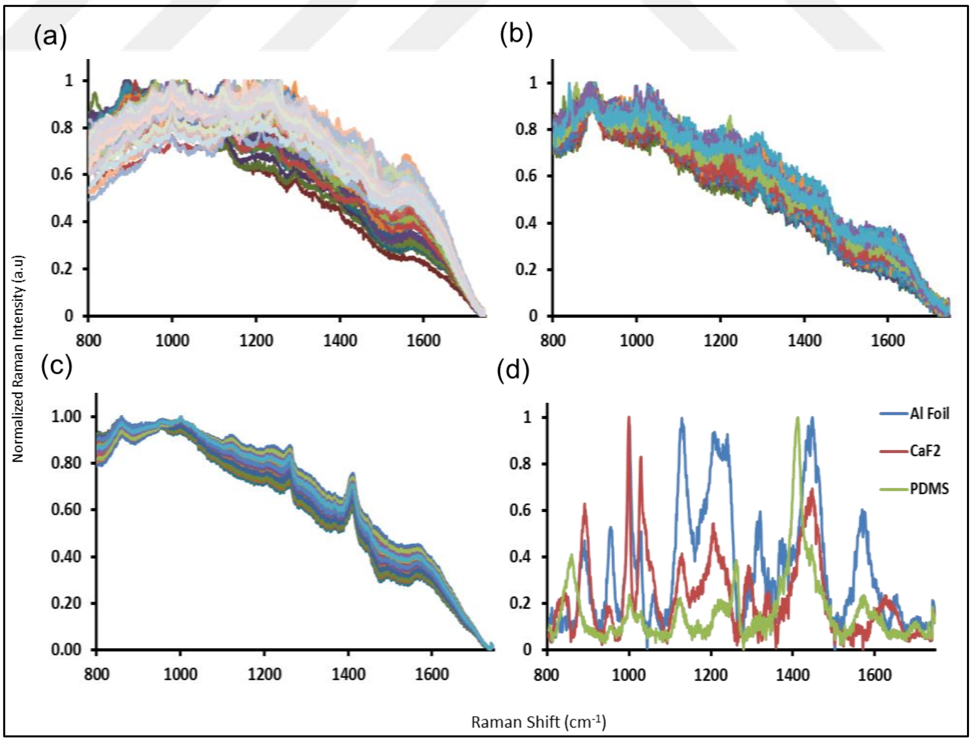

Figure 4.19. SERS spectra of bovine liver specimens placed on substrates of Al foil (a), CaF_2 (b), and PDMS substrate (c), and their mean spectra (d).

From Figure 4.19, it is apparent that the SNR and signal reproducibility is higher in the spectra collected from the tissue placed on PDMS covered slides. However, the signal quality is better for the Al-foil substrate compared to the CaF_2 slide. This may be due to the enhancement effect of Al foil [144].

A comparison of the classification accuracy related to the substrates was needed to obtain for the choice of a favorable substrate to be used in the Cryosectioned-PDMS method. Thus, this sampling method was applied to breast, liver and heart tissue of chicken. Figure 4. 20 shows the raw and the mean spectra obtained from breast, heart and liver tissue of chicken placed on CaF_2 slide.

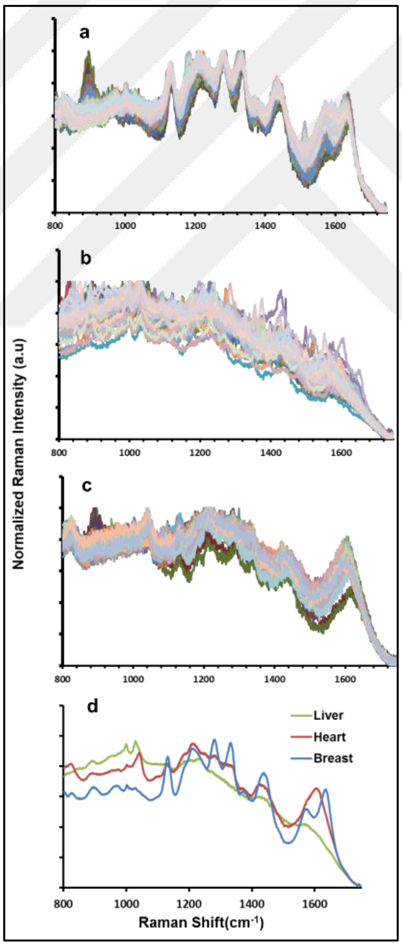

Figure 4.20. Raw SERS spectra of chicken breast (a), liver (b) and heart (c) tissue specimen placed on CaF_2 slides, and their mean spectra (d).

The high dimensional spectral data needs to be mined before using in the classification algorithms. PCA analysis method of Statistical Package for the Social Science (SPSS) was used to reduce the spectral dimension (d=1014). Thus, thirty-five PC was extracted from the collected spectra. Then, first five PCs including 87.11 per cent of the variance related to the tissue specimen as detailed in Table 4.10 was used in PCA classification algorithm.

Table 4.10. Eigenvalues and the percentage of explained variation of PCs.

PC	**Eigenvalue**	**Explained Variation %**
1st PC	4.36E+01	43.58
2nd PC	3.39E+01	77.48
3rd PC	5.05E+00	82.52
4th PC	1.88E+00	85.23
5th PC	1.35E+00	87.11

The 2D and 3D PCA scatter plots were obtained as seen in Figure 4.21 after first five PCs were used in PCA classification algorithm. The classification results were obtained by using leave-one-out cross-validation (LOO-CV) in the PC-LDA classification model. The predicted classification results is given in Table 4.11.

Table 4.11. LOO-CV classification results of breast, heart and liver tissue using PC-LDA model.

Classification Groups	**Sensitivity %**	**Specificity %**	**Accuracy %**
Breast- Heart	100.0	99.0	99.5
Breast-Liver	99.0	100.0	99.5
Liver-Heart	100.0	97.0	98.5

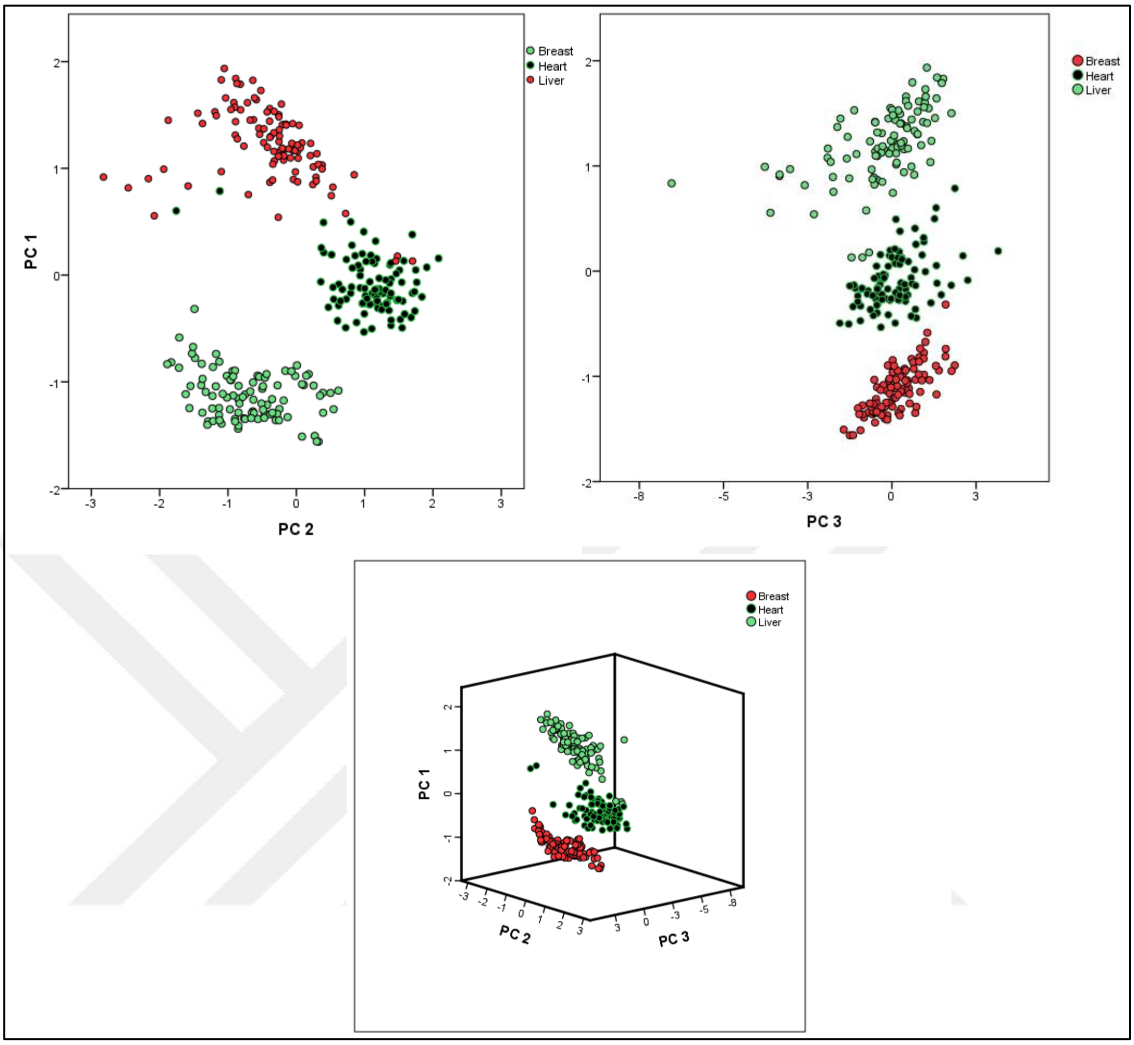

Figure 4.21. 2-D scatter plots of PC1-PC2 (a) and PC1-PC3 (b), and 3-D scatter plots of PCs in PC1 to PC3 components related to the SERS spectra acquired from breast, liver, and heart tissue specimen placed on CaF_2 substrate.

Second, the spectra were collected from breast, heart and liver tissue of chicken placed on PDMS to evaluate the performance of PDMS substrate on the classification accuracy. The raw and mean spectra of these tissues are provided in Figure 4.22.

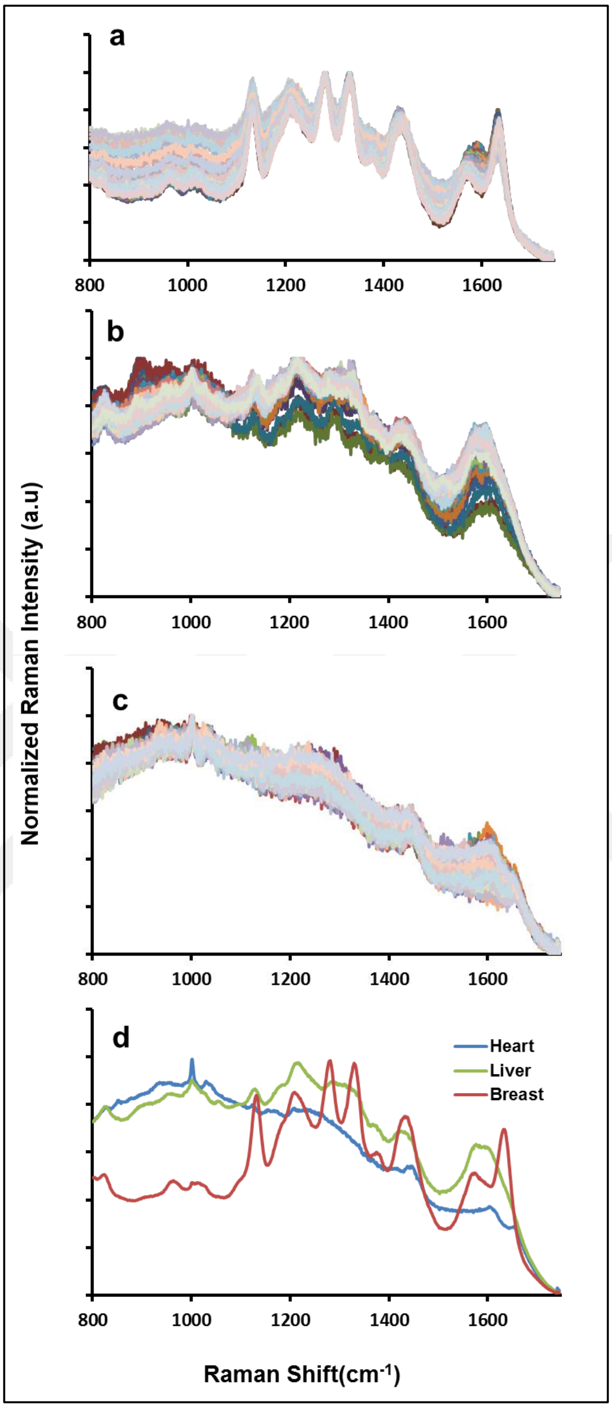

Figure 4.22. SERS spectra obtained from chicken breast (a), liver (b), and heart (c) tissue on PDMS covered slides, and their mean spectra (d).

As seen, the noise level of the spectra obtained from the tissue placed onto PDMS covered slides is lower when compared to the spectra obtained from the samples placed on CaF_2 slide. Then, PCA was applied on the spectra to reduce the dimension (d=1014) to sixteen

PCs. First five PCs including 93.77 per cent of the total variance, which are detailed in Table 4.12, were used in PCA classification algorithm.

Table 4.12. Eigenvalues and the percentage of explained variation of PCs.

PC	Eigenvalue	Explained Variation %
1st PC	5.25E+01	52.45
2nd PC	3.80E+01	90.42
3rd PC	1.40E+00	91.82
4th PC	1.02E+00	92.84
5th PC	9.33E-01	93.77

The 2D and 3D PCA scatter plots were obtained and provided in Figure 4.23 after the first five PCs were used in PCA classification algorithm. The classification results were obtained by LOO-CV in the PC-LDA classification model, and the classification results of PC-LDA model are given in Table 4.13.

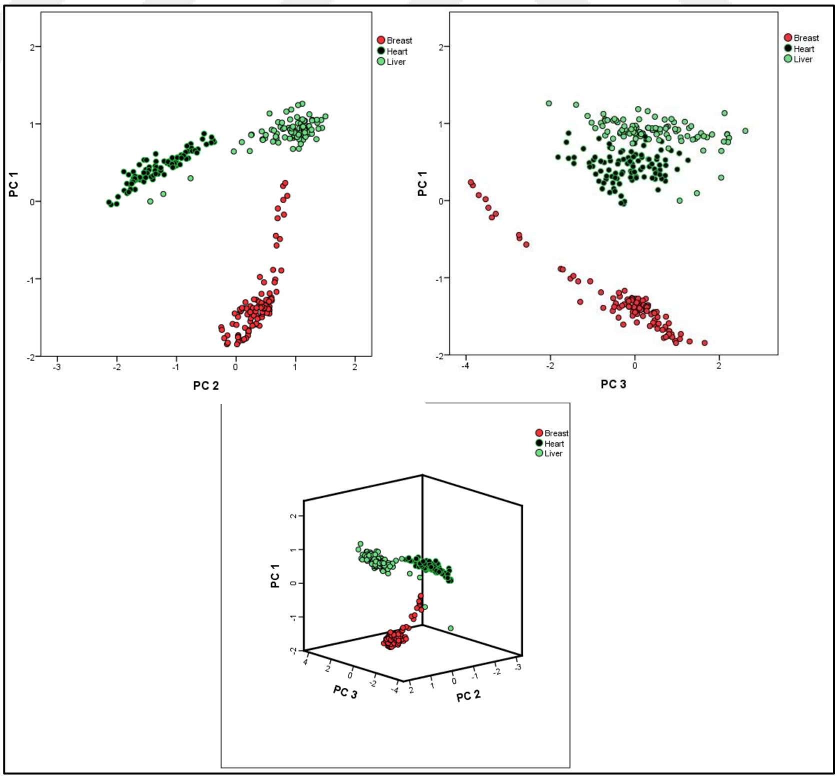

Figure 4.23. 2-D scatter plots of PC1-PC2 (a) and PC1-PC3 (b), and 3-D scatter plots of PCs in PC1 to PC3 components related to the SERS spectra acquired from breast, liver, and heart tissue specimen placed on PDMS covered slides.

Table 4.13**.** Classification results of breast, heart and liver tissue using PC-LDA model.

Classification Groups	Sensitivity %	Specificity %	Accuracy %
Breast- Heart	100	94	97
Breast-Liver	100	100	100
Liver-Heart	96	94	95

The classification accuracy was higher than the results obtained using the CaF_2 slide for the breast and liver tissue, which means the differences in the variances of the PCs were higher between breast and liver tissue specimen placed on the PDMS covered slide. The measurements were simultaneously performed to avoid possible variation due to the sampling errors. The same experiments were also repeated on Al-foil using the breast, heart and liver tissues from chicken. Figure 4.24 shows the raw spectra from each tissue sample and their mean spectra as a comparison with the mean and collected spectra obtained using Al-foil substrate.

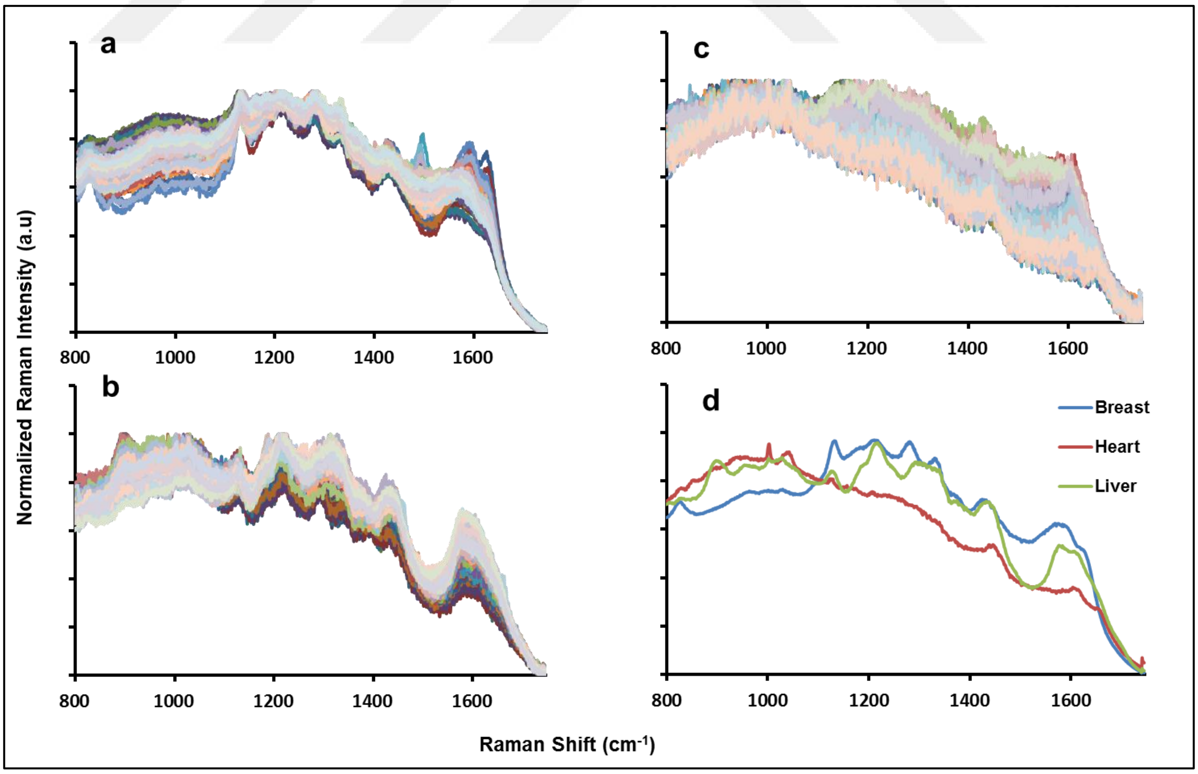

Figure 4.24. SERS spectra from chicken breast (a), liver (b) and heart (c) tissue specimen placed on Al foil covered slides, and their mean spectra (d).

PCA was applied on the spectra and sixteen PCs were extracted to reduce the spectral dimension (d=1014) before the first five PCs including 88.09 per cent of the variance were used in PCA classification algorithms. The per cent of variances related to the PC components were detailed in Table 4.14. Then, the classification results were obtained by using LOO-CV method in PCA based LDA classification algorithm as indicated in Table 4.15. The PCA scatter plots were also obtained and are given in Figure 4.25.

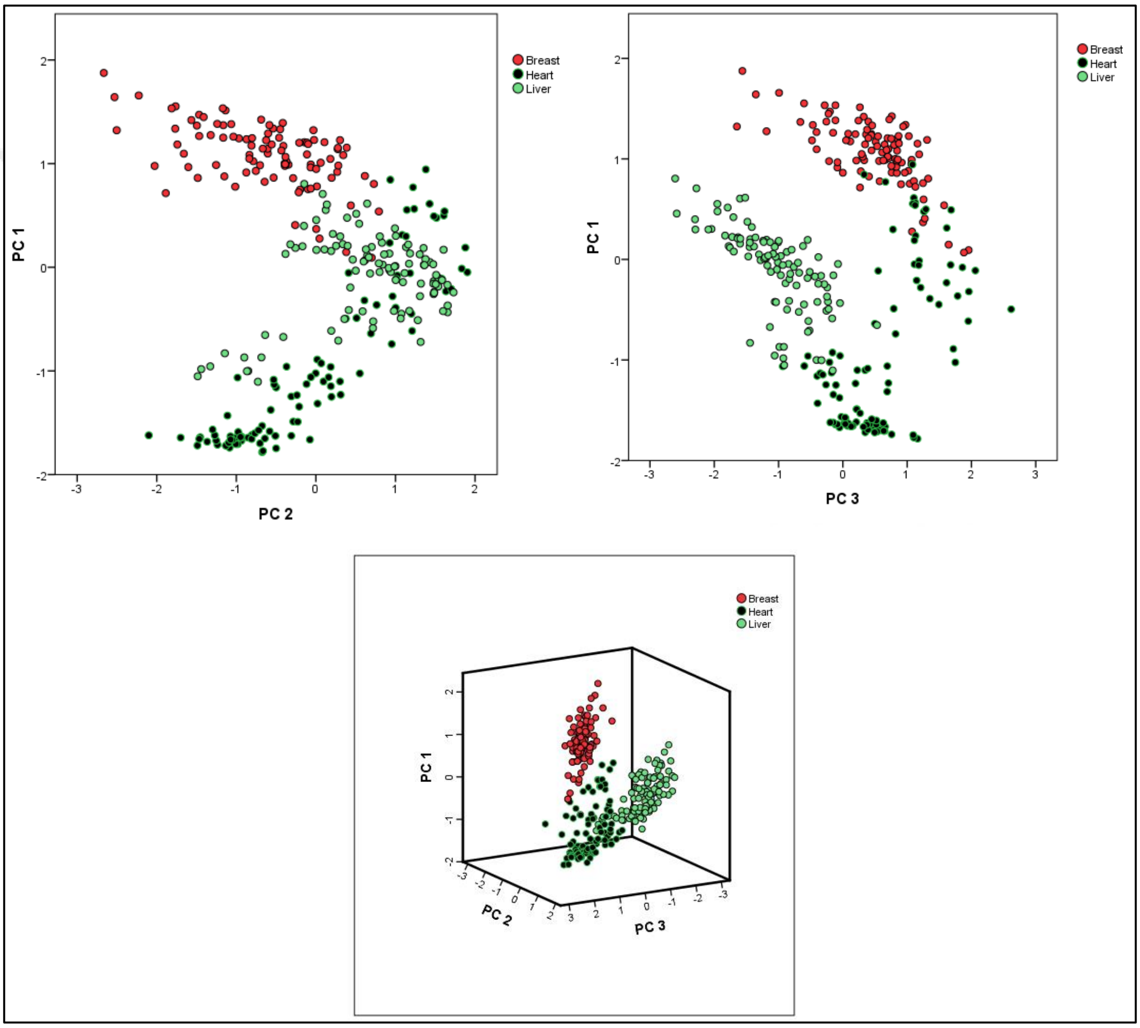

Figure 4.25. 2-D scatter plots of PC1-PC2 (a) and PC1-PC3 (b), and 3-D scatter plots of PCs in PC1 to PC3 components derived from the spectra acquired from breast, liver, and heart tissue specimen placed on Al-foil covered slides.

Table 4.14. Eigenvalues and the percentage of explained variation of PCs.

PC	**Eigenvalue**	**Explained Variation** %
1st PC	5.77E+01	57.69
2nd PC	1.55E+01	73.15
3rd PC	1.04E+01	83.54
4th PC	2.74E+00	86.28
5th PC	1.81E+00	88.09

Table 4.15. Performance of the PC-LDA models using Al-foil covered glass slides for chicken tissue types; breast, liver, and heart

Classification Groups	**Sensitivity %**	**Specificity %**	**Accuracy %**
Breast- Heart	100	96	98
Breast-Liver	100	94	97
Liver-Heart	94	96	95

Finally, the classification accuracy for each substrate preparation method was shown in Table 4.16 as a comparison.

Table 4.16. Performance measurements of the PCA models using different substrates forchicken tissue types; breast, liver, and heart.

Substrates	**Sensitivity %**	**Specificity %**	**Accuracy %**
Al-foil	98.0	95.3	96.6
PDMS	98.6	96.0	97.3
CaF_2	99.6	98.6	99.1

In conclusion, even though the use of CaF_2 as a substrate provides the highest classification sensitivity, specificity, and accuracy compared to other substrates, PDMS and Al-foil covered glass substrates have significant classification accuracy between 97 and 98 per cent probabilities. Although the difference in the performance measurement of classification models was minimal, the PDMS covered slide could be more suitable one to use in clinics. It has the advantages of low cost, high mechanical strength and the flexibility, which is detailed in Table 4.17, compared to Al foil and CaF_2 slides.

Table 4.17. A summary of comparison of the three substrates: PDMS, Al foil and CaF_2.

Proporties	**CaF_2**	**PDMS**	**Al Foil**
Mechanical strength	Fragile	Flexible and strong	Easy tearing
Surface	Hydrophobic	Hydrophobic	Hydrophilic
Cost	Quite expensive	Lower costs	Very economical

The substrate dependent signal reproducibility were also obtained by calculating the CV values.

4.2.4. Comparison of Substrate Dependent Signal Reproducibility

The spectral reproducibility is one of the major problems of the SERS technique due to the heterogeneity of the tissue structure and the chaotic distribution of nanoparticles on the tissue surface. Thus, to understand the substrate dependent signal reproducibility, three substrate platforms were used in the Cryosectioned-PDMS method with three repetitions. Table 4.18 shows the CV values of the spectra obtained by using three different substrates.

Table 4.18. CV values of the spectra obtained from model tissue specimen using different substrates.

CaF_2				PDMS				Al Foil			
1st Exp.	2nd Exp.	3rd Exp.	Average	1st Exp.	2nd Exp.	3rd Exp.	Average	1st Exp.	2nd Exp.	3rd Exp.	Average
12.98	11.17	13.13	14.99	4.03	2.09	3.09	2.73	9.88	12.05	8.76	11.75

The PDMS layered slide showed 2.7 per cent variation while CaF_2 and Al-foiled slides displayed 14.9 and 11.7, respectively. It is obvious that the PDMS coating is more suitable based on the CV values and decided to use in the Cryosectioned-PDMS method.

4.2.5. A Preliminary Study with Thyroid Tumors

The optimized approach finally tested on real human benign thyroid tumor and the tissue surrounding thyroid tumor (healthy). Thus, two biopsy samples using the Cryosectioned-PDMS method were prepared for SERS measurements. The protocol of Cryosectioned-PDMS approach is summarized in the following paragraph with the optimized parameters.

The cryosectioned tissue sample placed on a cover slide was used for SERS measurements by placing the AgNPs colloidal suspension on the sectioned tissue. Then, a layer of PDMS with 1.8 mm was placed between the sliced tissue and the cover slide to overcome the suppressing background. A 5- µm thick tissue was placed onto the PDMS surface. A 30 mW laser power (as adjusted in the software) with 2s exposure time was used. A 10 x 10 points array was mapped with StreamHR fast point mapping. The colloidal suspension concentration was 16×. Raman shift range was set to 582- 1563 cm^{-1} by given a median value of 1100 cm^{-1}, which was found to be optimum for thyroid tumor samples. Finally, the collected spectra were reduced to new variables using PCA algorithm, and PC-LDA classification model was performed with LOO-CV method.

The collected SERS spectra from the benign tumor and surrounding tissue (healthy), and their mean spectra are shown in Figure 4.26.

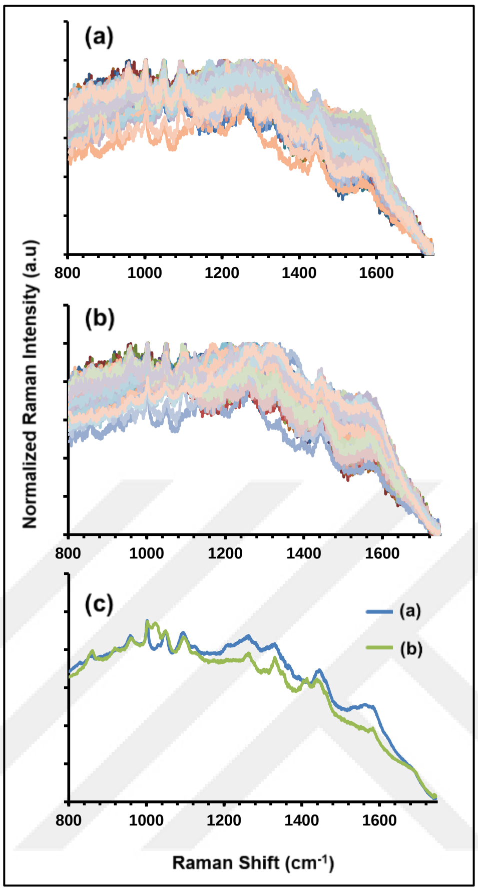

Figure 4.26. SERS spectra obtained from tissue samples pathologically confirmed as healthy (tissue surrounding tumor) (a) and benign tumor (b) placed on PDMS, and their mean spectra (c).

The high dimenional data was reduced to sixty-five PCs, which were extracted using PCA algorithm. The first five PCs including 81.09 per cent of variance as detailed in Table 4.19 used in PC-LDA classification model.

Table 4.19. Eigenvalues and the percentage of explained variation of PCs.

PC	**Eigenvalue**	**Explained Variation %**
1st PC	4.94E+01	49.42
2nd PC	2.13E+01	70.74
3rd PC	4.72E+00	75.46
4th PC	4.07E+00	79.53
5th PC	1.56E+00	81.09

The 2-D and 3-D PCA scatter plots were obtained as shown in Figure. 4. 27. Then, the classification results were calculated by using LOO-CV method and detailed in Table 4.20.

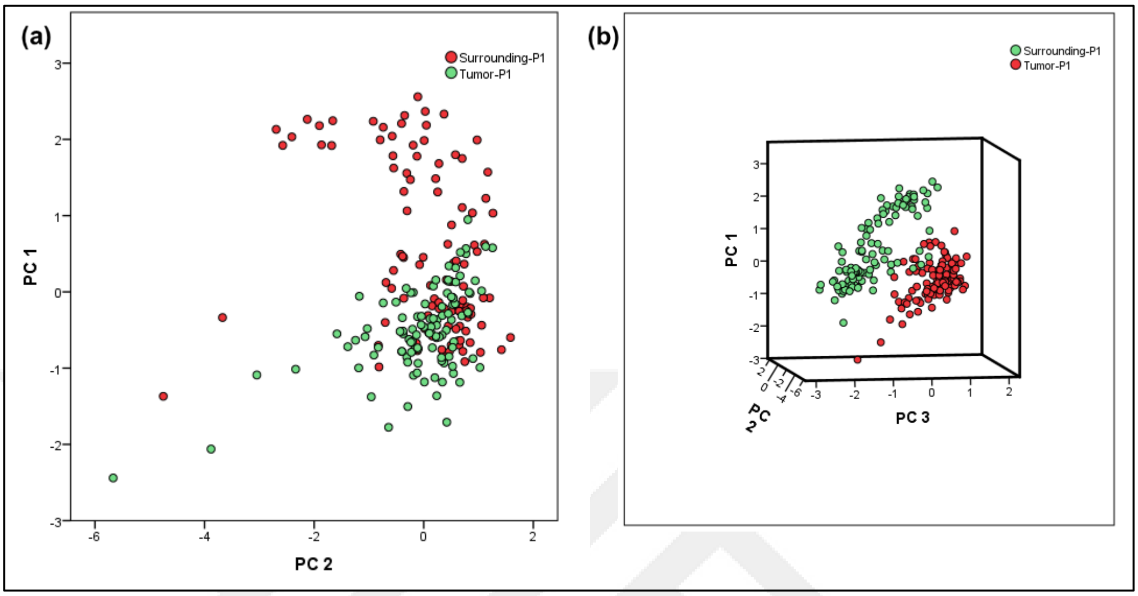

Figure 4.27. 2- D (a) and 3-D (b) PCA scatter plots related to the SERS spectra acquired from surrounding (healthy) and tumor tissue specimen placed on PDMS covered glass slides.

Table 4.20. Performance measurements of the PC-LDA model using PDMS covered glass slides for the differentiation of benign tumor and surrounding tissue specimen.

Classification Tissue Groups	**Sensitivity %**	**Specificity %**	**Accuracy %**
Healthy vs Tumor	100	100	100

Applying newly developed Cryosectioned-PDMS approach displayed successfully diagnosis of tumor and healthy thyroid biopsies with an accuracy of 100 per cent.

4.2.6. Diagnosis of Thyroid Tumors

In this part of the study, SERS-based Cryosectioned-PDMS method was applied on 31 normal and 33 abnormal pathologically evaluated tissue samples obtained from thyroid disease patients to differentiate sample groups. Table. 4. 21 shows the tissue type, collected spectra per sample and pathological diagnostic results of tissue specimen examined in the clinic. The tissue samples were marked as tumor (benign/malignant) and healthy (the tissue surrounding the tumor). Although the tissue surrounding the tumor marked healthy and phatologically verified healthy, it might still have tumorus cells.

StreamHR point mapping acquisition from a square grid of 10 × 10 scanned points, a total area of 22.5 µm × 22.5 µm (506.25 µm^2), was performed with the optimized parameters of Cryosectioned-PDMS approach. One hundred spectra per biopsy sample (total of 6400 spectra for 64 biopsy sample) were collected. The mean spectrum of each tissue type (benign, malignant and healthy) obtained from one hundred spectra, which is presented in Figure 4. 28 and Figure 4.29.

Table 4.21. Pathological evaluation of the specimens, number of biopsies, and number of spectra obtained per biopsy.

Sample type	**Sample Number**	**Spectra Number**
Adenomatous Nodule	16	1600
Follicular Adenoma	3	300
Papillary Thyroid Carcinoma	9	900
Hürthle Cell Adenoma	3	300
Multifocal Papillary Thyroid Carcinoma	1	100
Minimally Invasive Follicular Carcinoma	1	100
Normal Thyroid Tissue	31	3100
Benign Tumor	22	2200
Malignant Tumor	11	1100
Total	64	6400

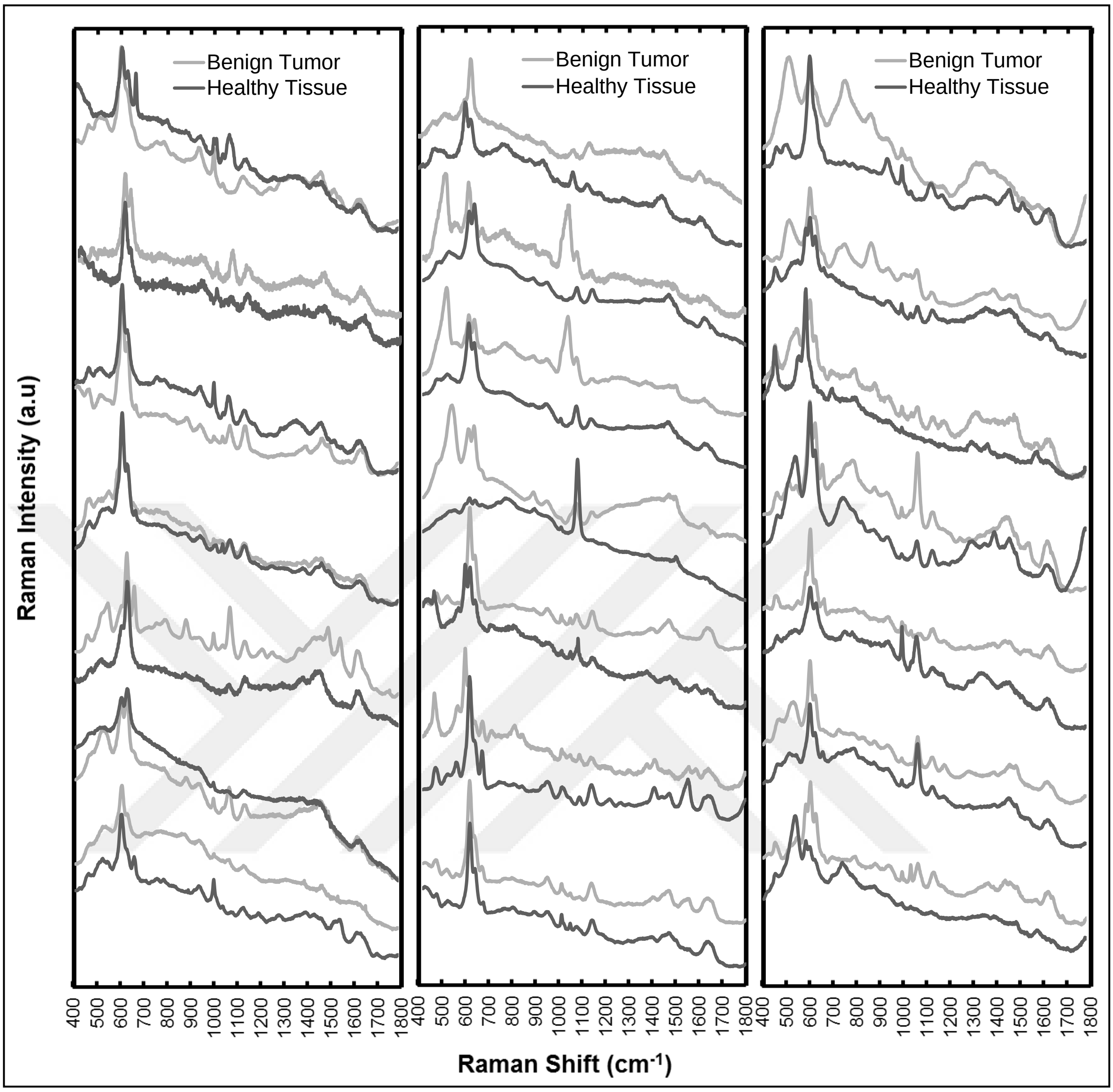

Figure 4.28. Mean SERS spectra of benign (n=22) and healthy (n=22) tissue specimen prepared by using Cryosectioned-PDMS sampling method.

The cosmic ray filtering and min-max normalization processes through the WIRE.4.1 software were applied to the spectral data. The baseline correction and smoothing were not applied to the spectral data used in the classification model because variations in band intensity and localization could be appeared affecting the reliability of results.

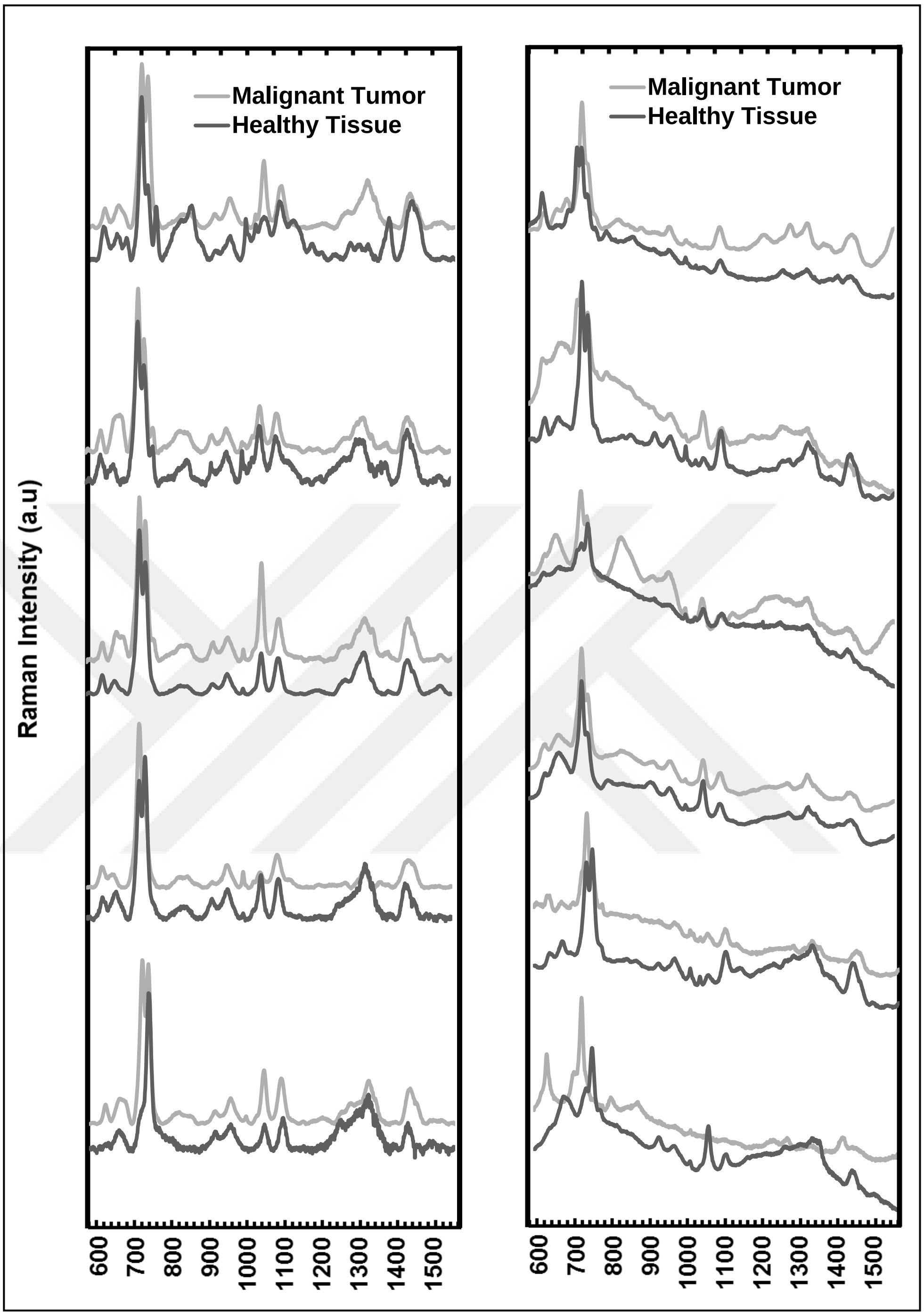

Figure 4.29. Mean SERS spectra of malignant (n=11) and healthy tissue specimen (n= 11) prepared by using Cryosectioned-PDMS approach.

The same pre-processing steps, cosmic ray filtering and min-max normalization processes were applied also to the spectral data belonging to malignant and healthy tissue specimen. Baseline correction using cubic splines and smoothing through the WIRE.4.1 software were applied on the averaged SERS spectra related to malignant and healthy tissue samples to increase the visibility of the differences between the spectral patterns but original data without baseline correction was used in the classification model.

As seen, there are similarities between the average spectra of malignant tumor and healthy tissue. However, significant differences in the spectra of tissue samples from different patients were also observed. This is possibly due to the variation of the tissue from patient to patient. The variations in the spectra were statistically observed by using PCA method.

PCA was performed in the thesis study due to two primary reasons. First one is to minimize high dimensional spectral data to new relevant scores to be able to use in LDA based diagnostic algorithm to serve the purpose of comparison on classification accuracy between the tissue sampling methods of Cryosectioned-PDMS, *in situ* method and Crashed-liquefied. The second one is to indicate the variability in the spectral data by extracted loading vectors, which represent the variances of each variable (wavenumber). The variations in the molecular components of tissue specimen were reflected on the spectra, and the variances can be observed by analyzing the loading vectors of the PCs with the positive and negative contributions related to prominent SERS bands.

The average spectra for each one hundred spectral data was estimated to represent each biopsy tissue specimen before using this multidimensional data (dimension=64x1015) to construct loading vectors and regression (REGR) factors by using PCA algorithm. After the data processing, the average spectra were reduced into new relative variants called as principle components scores (PCs). Nineteen significant PCs (eigenvalues greater than > 1) were obtained by PCA method in the SPSS software as seen in Table 4.22 with the per cent value of explained variances in each PC.

The REGR factors derived by using PCA method, and the factors were then used in PC-LDA classification model. The scatter plots of PCA and PC-LDA analysis are shown in Figure 4. 30.

The PCs of first three factors were used in PCA scatter plot but it does not indicate well-separated clusters for each group. Then, LDA classification algorithm was applied on PCs with LOO-CV method to increase the classification accuracy by maximizing the differences within the groups, and obtaining a predicted classification result explained in the terms of sensitivity, specificity and accuracy. However, PC-LDA scatter plot (b) indicated better classified groups compared to the PCA scatter plot (a). Table 4.23 gives the detailed classification results obtained after the LOO-CV method applied on the PCs (1, 2 and 3 assigned healthy, benign and malignant type, respectively).

Table 4.22. Total variance explained PCs with percentage of explained variation of PCs for 64x1015 dimensional spectral data set.

Total Variance Explained			
PC	Total	% of Variance	Cumulative %
1	718.88	71.11	71.11
2	96.27	9.52	80.63
3	60.95	6.03	86.66
4	34.83	3.45	90.10
5	21.83	2.16	92.26
6	17.04	1.69	93.95
7	15.07	1.49	95.44
8	8.39	0.83	96.27
9	6.25	0.62	96.89
10	5.74	0.57	97.45
11	4.17	0.41	97.87
12	3.48	0.34	98.21
13	3.11	0.31	98.52
14	2.11	0.21	98.73
15	1.77	0.18	98.90
16	1.52	0.15	99.05
17	1.27	0.13	99.18
18	1.18	0.12	99.30
19	1.02	0.10	99.40

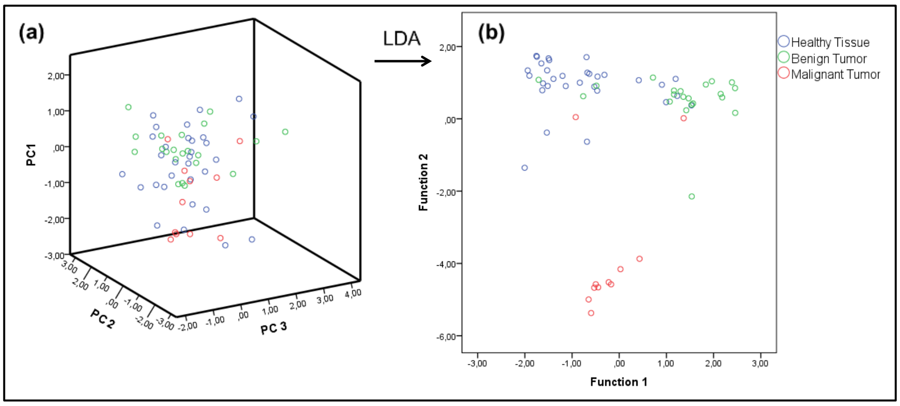

Figure 4.30. Scatter plots of PCA (a) and PC-LDA (b) with the PC scores related to the spectra of healthy, benign and malignant tissues.

Table 4.23. Classification results for healthy, benign and malignant tissue samples.

			Predicted Group Membership			**Total**
			1	2	3	
Original	Count	1	22	6	3	31
		2	6	15	1	22
		3	0	1	10	11
	%	1	71	19.4	9.7	100
		2	27.3	68.2	4.5	100
		3	0	9.1	90.9	100
Cross-validated	Count	1	22	6	3	31
		2	6	15	1	22
		3	0	1	10	11
	%	1	71	19.4	9.7	100
		2	27.3	68.2	4.5	100
		3	0	9.1	90.9	100

73.4 per cent of original grouped tissue specimens and 73. 4 per cent of cross-validated grouped tissue specimens were correctly classified based on the result presented in Table 4.24. Then, the loading vectors were extracted from the data using PCA to highlight the most prominent diagnostic variables among the spectra belongs to differently diagnosed tissue samples. The first 8 loading PC vectors, which have the most prominent bands on it, were shown in Figure 4. 31 and Figure 4.32.

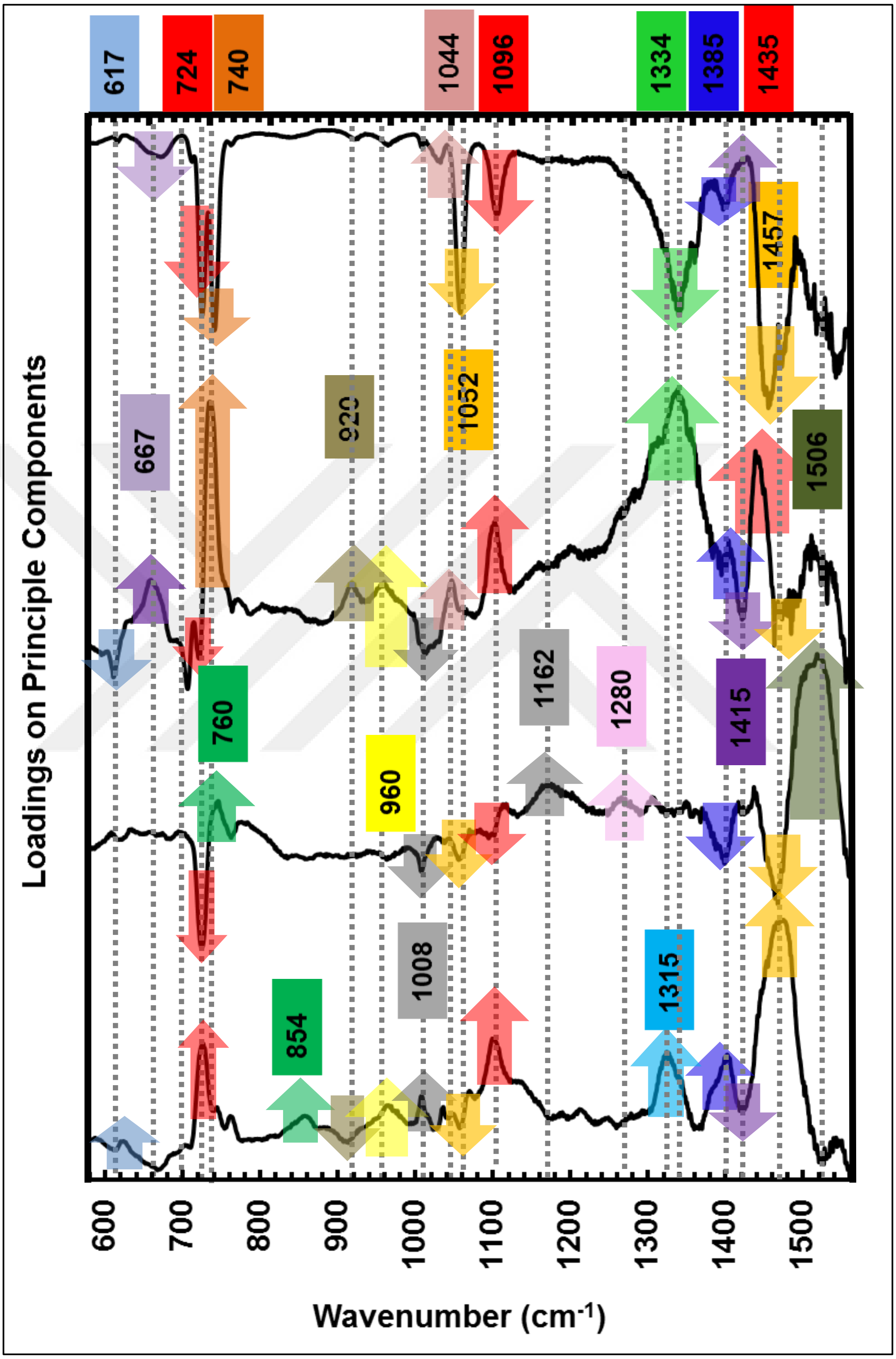

Figure 4.31. First four loading PC vectors obtained using PCA.

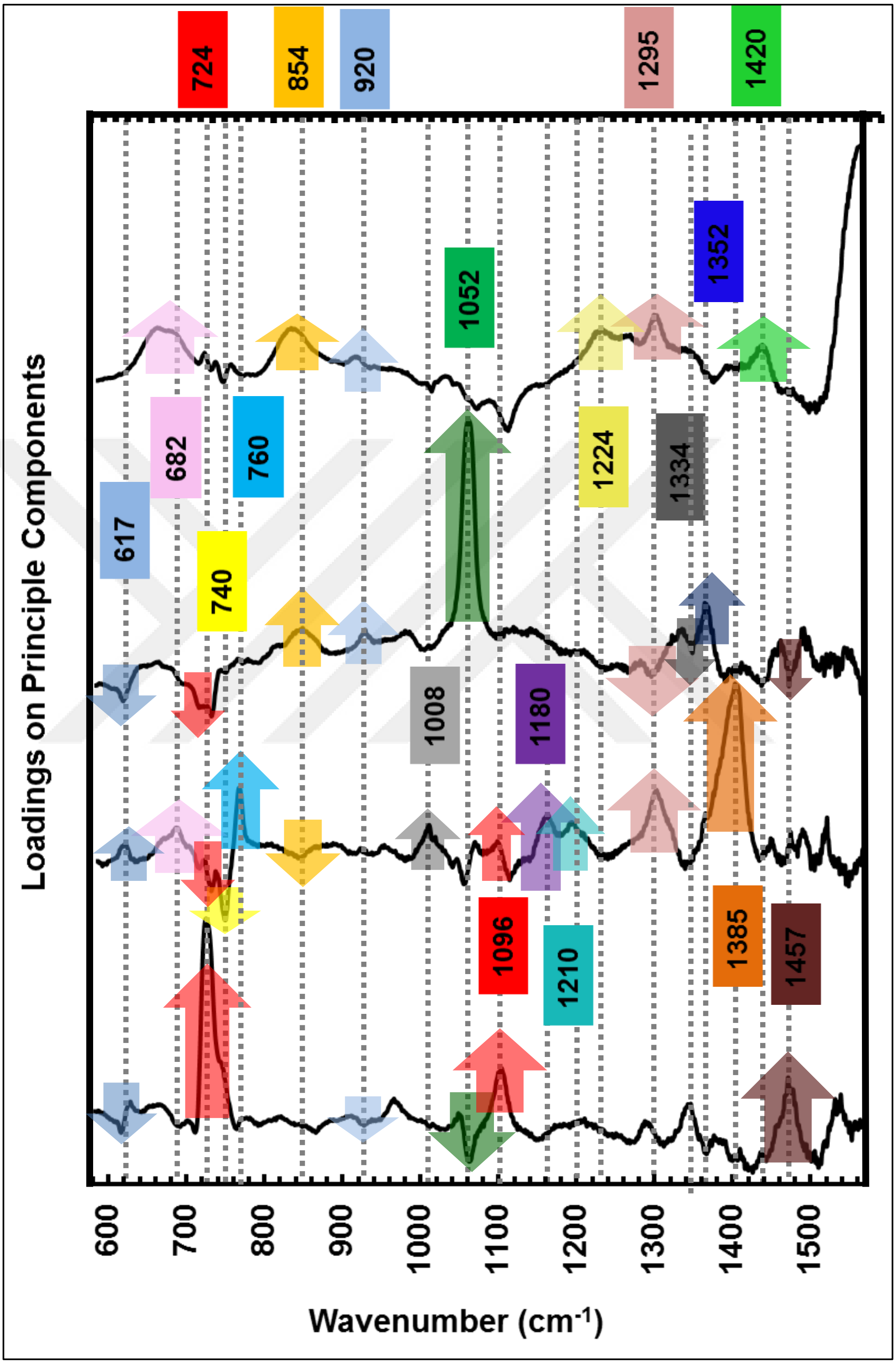

Figure 4.32. Last four loading PC vectors obtained using PCA.

The loadings exhibited the differences between the benign, malignant and healthy thyroid tissue samples. Their respective negative (down arrow) and positive (up arrow) bands in the loadings originated considerably the differentiation of the neoplasm and healthy sample.

The bands on the loading vectors can be attributed to biochemical components such as nucleic acids (724, 740, 1415 cm^{-1}), proteins (617, 667, 760, 854, 920, 1008, 1052, 1180, 1210, 1280, 1295, 1315, 1334, 1457 and 1506 cm^{-1}), metabolites (724 and 920 cm^{-1}), and lipids (960, 1096, 1385, 1435 and 1457 cm^{-1}). The tentative assignments of the bands observed on the spectra of tissues are given in Table 4.24.

Then, REGR factors derived by using PCA method applying on the specific bands at 667, 724, 740, 760, 854, 920, 960, 1008, 1052, 1096, 1180, 1210, 1280, 1295, 1315, 1334, 1385, 1415, 1435, and 1457 cm^{-1} instead of using the full spectral range. The derived factors were used in PC-LDA classification model, and the PCA and PC-LDA scatter plots were obtained and given in Figure. 4. 33-36.

Finally, LOO-CV method was used to obtain a predicted classification result by using the PC-LDA classification model. Table.4. 25 shows the predicted classification results of PC components of SERS spectra respective to tumorous (benign, malignant) and healthy tissue. The classification model was applied on the collected spectra in the full range of 582 to 1563 cm^{-1} and specific region at 667, 724, 740, 760, 854, 920, 960, 1008, 1044, 1096, 1180, 1210, 1295, 1315, 1334 and 1385 cm^{-1}.

Table 4.24. Tentative band assignment list for SERS spectra [33, 59, 60, 62, 63, 130, 145-147].

Band position (cm^{-1})	**Tentative Band Assignments**
425	Cholesterol
478	DNA / RNA
485	Uric acid / glycogen
524	S-S disulfide stretching in proteins
548	Cholestrol
570	Tyr / Cys / G
617	C-C twisting (protein)
627	Uric acid/ glycerol
667	C-S stretching mode of Cys (collagen type I)
687	G
725	Hypoxanthine/ ring breathing mode of DNA/RNA bases
738	T (ring breathing mode of DNA/RNA bases)
760	Ring breathing tryptophan (proteins)
810	Uric acid/ Phosphodiester, (RNA,DNA)/ Tyr
830	Tyr
854	C-C stretching of proline (collagen assignment)
885	Phospholipids, collagen
905	Protein/ glycogen
920	Lactic acid / protein
960	Cholesterol
1008	Phe
1030	Collagen /Phe
1053	C-O stretching, C-N stretching (protein)
1058	Lipids
1086	Phosphodiester groups in nucleic acids
1096	Lipids / nucleic acids
1126	Uric acid / lipids
1154	C-O stretching, C-N stretching (protein)
1180	C, G (DNA/RNA), Tyr (protein)
1210	Uric acid/ Amide III (collagen and protein) / Tyr / Phe
1245/1280	Amide III (collagen and protein)
1295	C
1315	Amide III (α-helix) / lipids
1334	Collagen
1385	Lipids
1397	Lipids / protein
1365	Nucleic acids
1415	A, G
1435	Lipids
1444	Lipids / collagen
1457	CH_2 deformation of lipids and proteins
1506	Cys
1536	Protein
1576	Nucleic acids

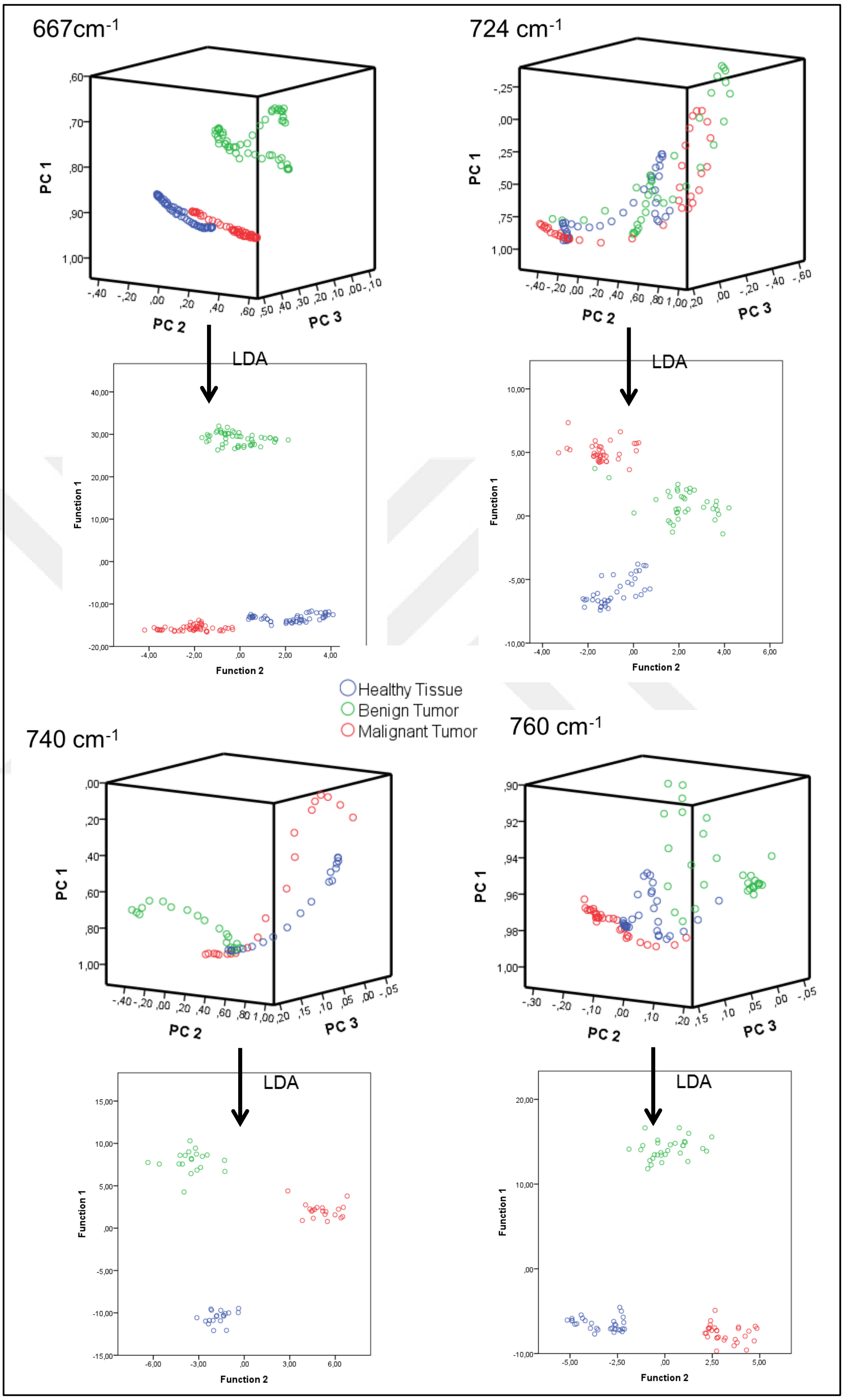

Figure 4.33. 3-D PCA and 2-D LDA scatter plots for PC components of SERS bands at, 667, 724, 740 and 760 cm^{-1}.

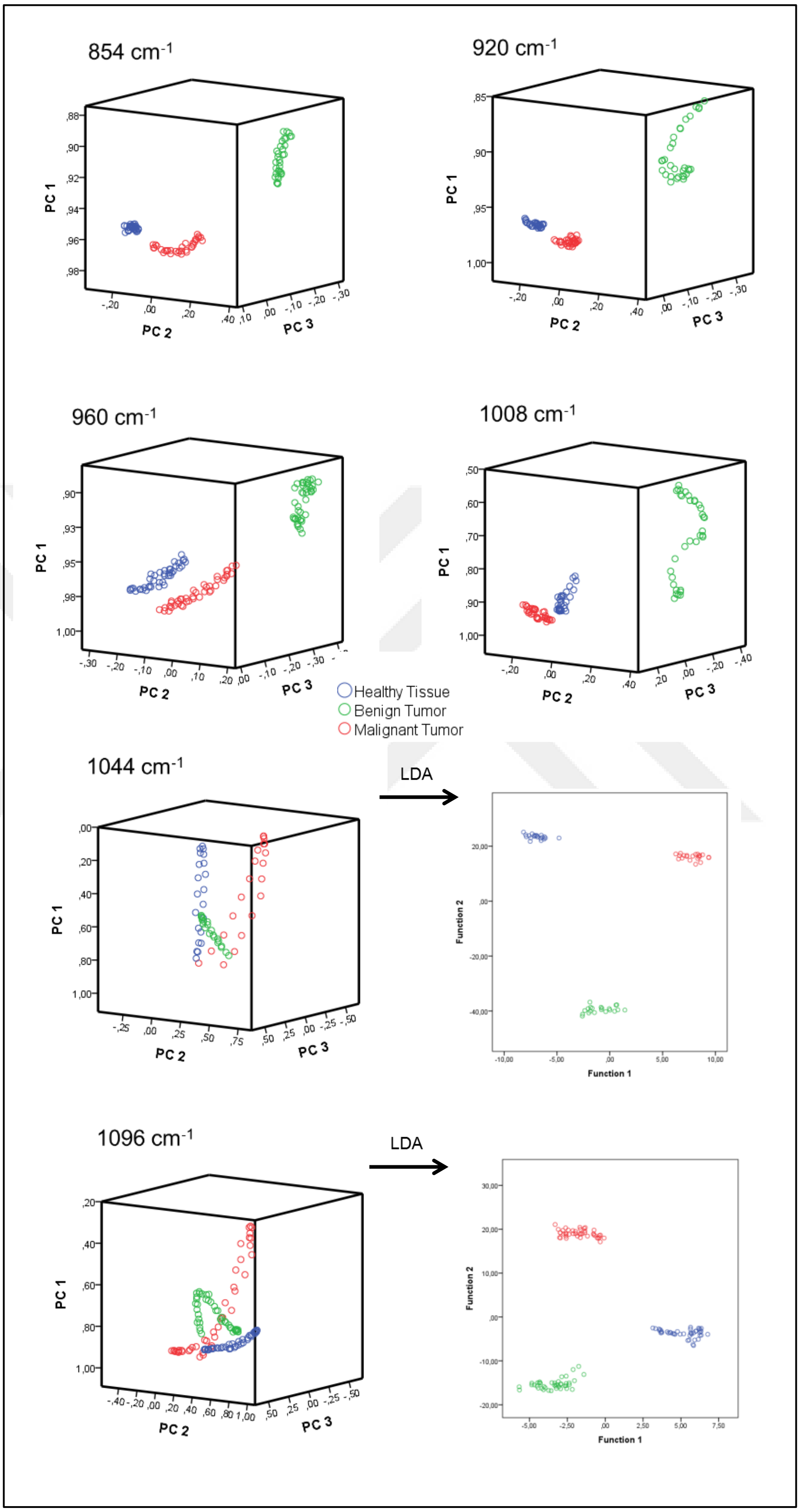

Figure 4.34. 3-D PCA and 2-D scatter plots for the PC components of SERS bands at 854, 920, 960, 1008, 1044 and 1096 cm^{-1}.

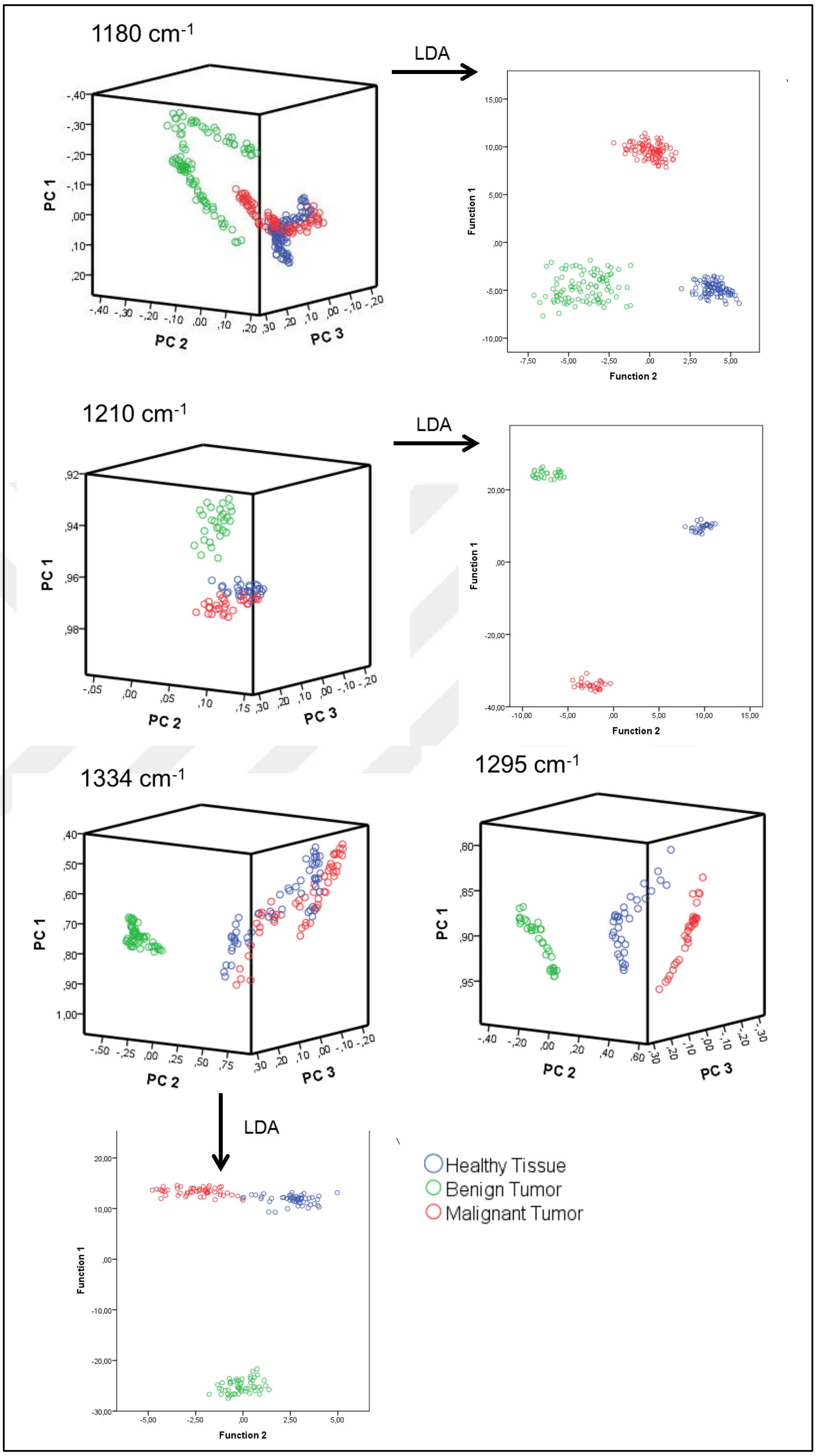

Figure 4.35. 3-D PCA and 2-D LDA scatter plots for the PC components of SERS bands at 1180, 1210, 1334 and 1295 cm^{-1}.

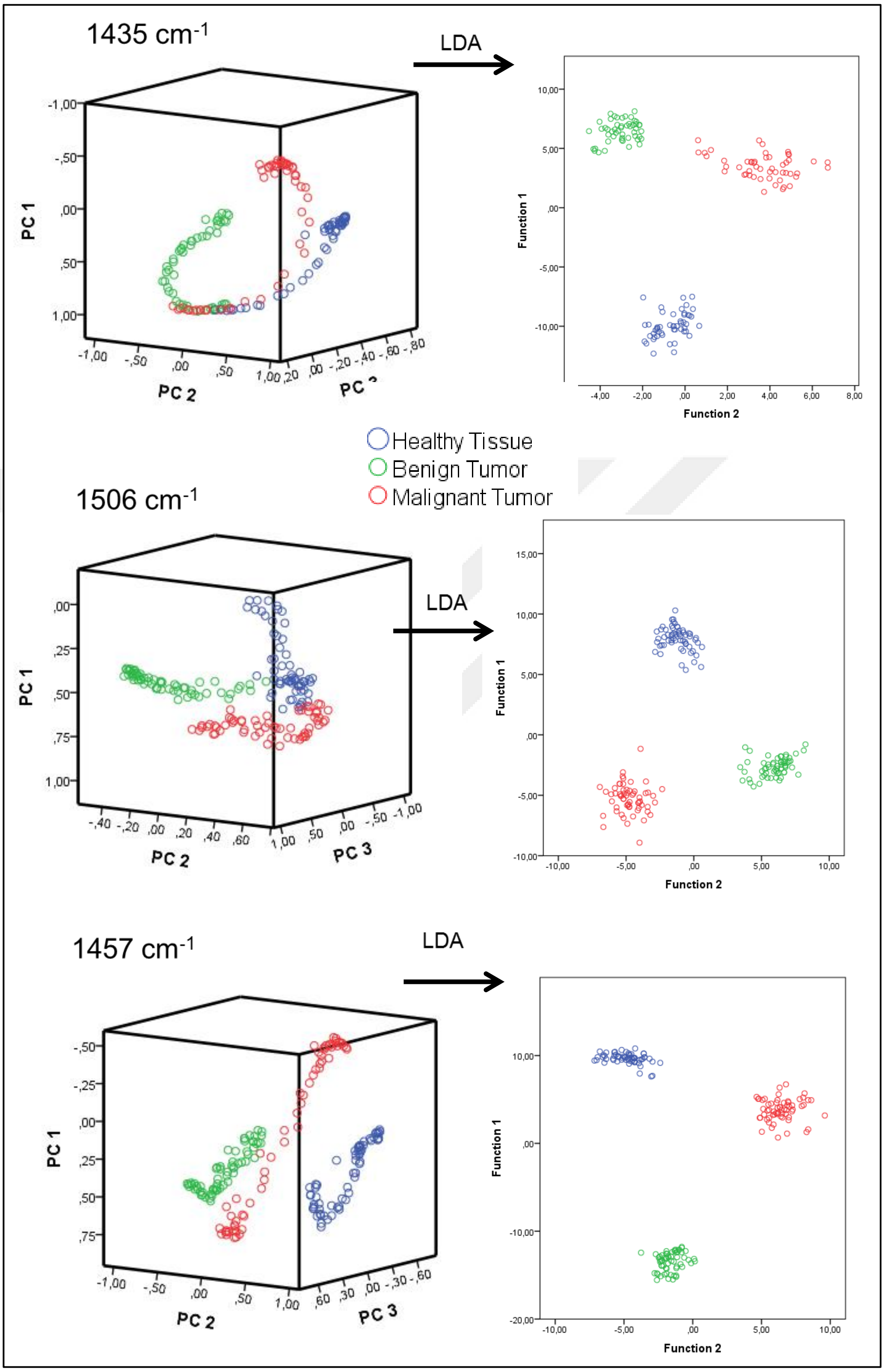

Figure 4.36. 3-D PCA and 2-D LDA scatter plots for the PC components of SERS bands at 1435, 1506, and 1457 cm^{-1}.

Table 4.25. Probability of predicted classification results obtained using LOO-CV method for tumorous and healthy tissue differentiation.

PCA-LDA Classification Results	**Healthy Tissue vs. Benign and Malignant Tumor**					
Cryosectioned-PDMS	Original Case			Cross-validation Case		
Wavenumber (cm^{-1})	Sensitivity	Specificity	Accuracy	Sensitivity	Specificity	Accuracy
582-1563	79	70	73	79	70	73
667	100	100	100	100	100	100
724	100	100	100	100	100	100
740	100	100	100	100	95	98
760	100	100	100	100	100	100
854	100	100	100	100	100	100
920	100	100	100	100	100	100
960	100	100	100	100	100	100
1008	100	100	100	100	100	100
1044	100	100	100	100	100	100
1096	100	100	100	100	100	100
1180	100	100	100	100	100	100
1210	100	100	100	100	100	100
1295	100	100	100	100	100	100
1315	100	100	100	100	100	100
1334	99	100	99	98	96	97
1385	100	100	100	100	100	100

The classification of tumorous tissues (benign and malignant) versus healthy tissues using PC-LDA methods in the spectral rage of 582 to 1563 cm^{-1} was obtained with the sensitivities of 79 per cent and 79 per cent and the specificities of 70 per cent and 70 per cent , and the accuracy of 73 per cent, and 73 per cent for original and cross validated cases, respectively. To increase the classification accuracy, the PC components of each significant SERS bands obtained from the tissue samples was used in PC-LDA classification model. The sensitivity, specificity and accuracy of classification results belongs to healthy tissues and tumor biopsies was obtained high as 100 per cent using PC components of each specific spectral bands except SERS band at 740 and 1334 cm^{-1}. The PC components of the spectra at 740 and 1334 cm^{-1} were classified with the accuracy of 98 per cent and 97 percent, respectively.

Two class predictions were also applied for the subgroups of tumorous tissue, benign and malignant, and healthy tissues. Table 4.26 gives the PC-LDA classification results for malignant, benign and healthy tissue samples using the bands at 617, 667, 724, 740, 760, 854, 920, 960, 1008, 1044, 1096, 1180, 1210, 1295, 1315, 1334 and 1385 cm^{-1}.

Table 4.26. Predicted values of classification results for malignant, benign and healthy tissues using PC-LDA algorithms.

	Wavenumber (cm^{-1})	**Cryosectioned- PDMS**							Wavenumber (cm^{-1})	
		Malignant	Surrounding (Healthy)		Sensitivity% Specificity% Accuracy%	Surrounding (Healthy)		Malignant Tumor		
Benign Tumor	582-1563	**94**	**79**	**100**	SN	100	100	100	1044	**Benign Tumor**
		91	**71**	**77**	SP	100	100	100		
		93	**76**	**91**	AC	100	100	100		
	667	100	100	100	SN	100	100	100	1096	
		100	100	100	SP	100	100	100		
		100	100	100	AC	100	100	100		
	724	100	100	100	SN	100	100	100	1180	
		100	100	100	SP	100	100	100		
		100	100	100	AC	100	100	100		
	740	**100**	100	100	SN	100	100	100	1210	
		95	100	100	SP	100	100	100		
		97	100	100	AC	100	100	100		
	760	100	100	100	SN	100	100	100	1295	
		100	100	100	SP	100	100	100		
		100	100	100	AC	100	100	100		
	854	100	100	100	SN	100	100	100	1315	
		100	100	100	SP	100	100	100		
		100	100	100	AC	100	100	100		
	920	100	100	100	SN	100	100	100	1334	
		100	100	100	SP	100	100	100		
		100	100	100	AC	100	100	100		
	960	100	100	100	SN	100	100	**96**	**1385**	
		100	100	100	SP	100	100	**96**		
		100	100	100	AC	100	100	**97**		
	1008	100	100	100	SN	**Malignant**	**Benign**	Sensitivity% (SN)		
		100	100	100	SP			Specificity% (SP)		
		100	100	100	AC			Accuracy% (AC)		
			Benign	**Malignant**						

Probability of correctly predicted performance of using PC-LDA classification algorithm for differentiation of tumorous and healthy tissues resulted with the sensitivities of 94, 79 and 100 per cent and the specificities of 79, 71 and 77 per cent, and accuracy of 93, 76 and 91 per cent for by using the data set in the spectral range of 582 to 1563 cm^{-1} between benign and malignant; benign and healthy, malignant and healthy, respectively.

The discrimination results of the diagnostic combinations of benign tumor versus malignant, benign tumors versus healthy tissues, and malignant tumors versus healthy tissues were achieved with the sensitivity, specificity and accuracy of 100, 95 and 97 per cent based on the PC components of SERS band at 740 cm^{-1} while the posterior probabilities based on the SERS band at 1385 cm^{-1} was obtained with the sensitivities of 96, 96 and 97 per cent, respectively.

4.3. *IN SITU* METHOD

In situ approach is another sampling, which involves the synthesis of SERS active AgNPs in the homogenized tissue. In the first approach discussed in the previous section, where already synthesized AgNPs are added onto the sliced tissue, the AgNPs and the molecular tissue components come into contact with AgNPs containing colloidal suspension is placed onto the tissue surface. Another possibility in the first approach is that some water-soluble tissue molecular components may diffuse into colloidal suspension added onto the tissue surface and come into contact with the AgNPs during the droplet drying process dominating the SERS spectrum. In the *in situ* approach, as the AgNPs are synthesized in the homogenized tissue, the possibility of diverse number of molecules coming into contact with AgNPs and their aggregates may increase influencing the spectral richness.

In the *in situ* approach, the influence of temperature the formation of AgNPs in homogenized tissue was also evaluated with or without a reducing agent. The attempt to reduce Ag$^+$ ions without addition of a reducing agent was not successful resulting in a weak SERS enhancement indicating that the formation of AgNPs was not enough or complete. Hydroxylamine chloride ($HONH_2{\cdot}HCl$) was selected to form AgNPs to increase the enhancement effect in the homogenized tissue inspired by the wet chemical synthesis method [126]. The development of *in situ* method involved the optimization of $AgNO_3$, $HONH_2{\cdot}HCl$ and NaOH concentrations, and instrumental parameters during SERS measurements. Then, the CV values of the spectra to optimize method parameters and the classification results by using PC-LDA model were obtained for three trials referring in terms of (i) intra-method reproducibility, (ii) inter-method reproducibility, (iii) accuracy, and (iv) SERS performance. Finally, the optimized method was evaluated using thyroid biopsies and the results were compared to the two other approaches.

4.3.1. Experimental Optimization

4.3.1.1. Temperature

First, the quality of the spectra obtained from the tissue sample by addition of only $AgNO_3$ solution at increasing temperatures at 25°C, 35°C, 45°C, 55°C, 65°C, 75°C and 85°C was observed. After the addition of a 50-µl volume from $3.55x10^{-2}$ M $AgNO_3$ solution into the 50-µl volume of homogenized tissue suspension, it was kept 30 minutes in a heated water bath. Then, a 5 µl volume of the mixture was placed on the CaF_2 slide and left to dry until SERS measurement. Figure 4.37 shows the averaged SERS spectra obtained at the increasing temperatures.

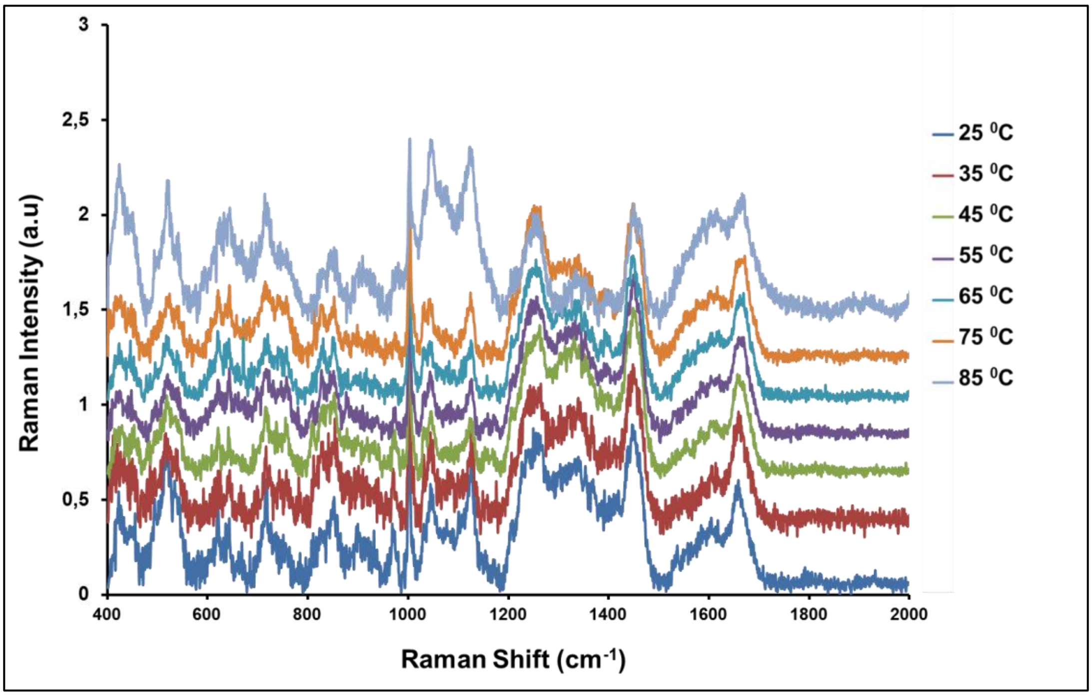

Figure 4.37. Mean SERS spectra obtained from each step of heating process.

As seen, the spectral pattern and the band intensity are almost the same at all temperatures. Interestingly, SERS enhancement effect was obtained from each sample without using any reducing agent but the obtained SERS spectra had very low SNR indicating the insufficient formation of AgNPs. Thus, addition of a reducing agent to enhance the reduction of Ag^+ ions in the tissue was evaluated.

4.3.1.2. Chemical Concentration

A range of concentrations of $AgNO_3$, $HONH_2 \cdot HCl$ and NaOH was used to optimize the method. The influence of the addition order of chemical solution on SERS signal quality was also studied. Thus, two set of experiments were performed simultaneously by changing the order of incorporation of chemicals to observe the quality of SERS spectra.

The different quantities and the addition order of the chemicals were optimized using two experimental set-ups. After the SERS spectra were collected, the mean SERS spectra were obtained as illustrated in Figure 4.38. Figure 4.38 (a) shows the optimized concentration and the addition order of the solution. The optimized in situ synthesis protocol includes the addition of a 10 μl volume of $3x10^{-2}$ M NaOH solution into a 10 μl volume of homogenized tissue suspension before addition a 10 μL volume of $4.36x10^{-1}$ M $HONH_2 \cdot HCl$ solution. Finally, a 10 μl volume of $3.55x10^{-2}$ M $AgNO_3$ solution was added into the mixture. The optimized order of the addition of agent solutions was found to be as NaOH, $HONH_2 \cdot HCl$ and $AgNO_3$, respectively. Figure 4.38 (b) shows the mean spectra obtained by using the solution with the optimized concentration but the addition order was $AgNO_3$, NaOH and $HONH_2 \cdot HCl$, respectively. As seen, the addition order of the reagent solutions influences the spectral quality. The high SNR in Figure 4.38 (a) clearly indicates the better formation of AgNPs in the homogenized tissue mixture. It is clear that addition of reducing agent first increases the chance reduction of those Ag+ ions into AgNPs before their binding to other molecular species present in the complex tissue mixture.

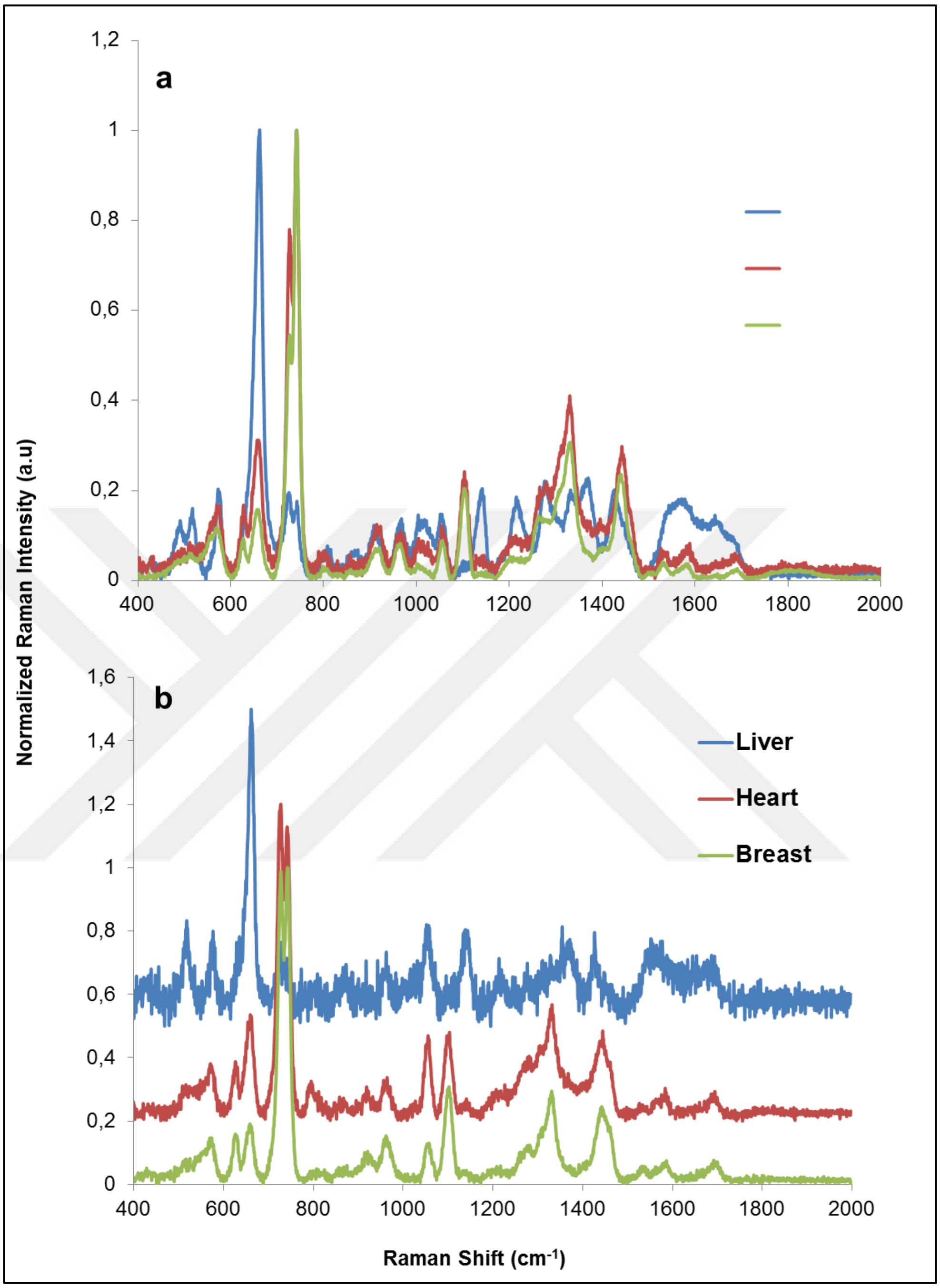

Figure 4.38. Mean SERS spectra of liver, heart and breast tissue using the addition order as NaOH, $HONH_2 \cdot HCl$ and $AgNO_3$ (a) and $AgNO_3$, NaOH and $HONH_2 \cdot HCl$ (b).

The AgNPs formed in the homogenized tissue were visualized with TEM. Figure 4.39 shows the representative AgNP TEM images formed in the tissue sample. As seen, the average size is around 25 nm, which can be considered as a suitable size for SERS enhancement.

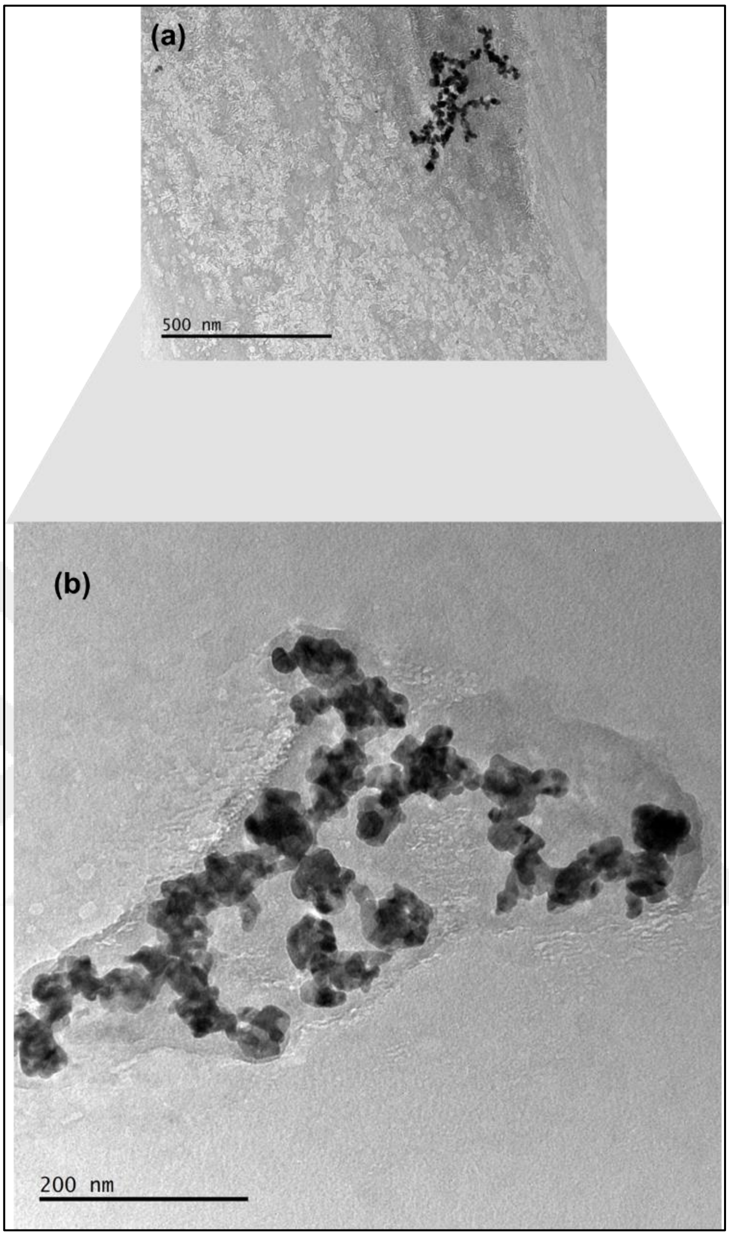

Figure 4.39. TEM images of AgNPs synthesized in situ homogenized bovine liver tissue specimen.

4.3.1.3. Acquisition of Point-by-Point versus Mapping

Since the AgNPs in the sample are not homogenously distributed in the prepared tissue sample, it is important to realize the influence of point-by-point acquisition versus mapping on spectral reproducibility. Thus, the acquisition type was also studied for optimization. SERS spectra were acquired from one, five and ten randomly selected points and a 10x10 points grid from three different spots on the sample with three trials conducted at different times as seen in Figure 4.40. Then, the CV values were calculated as shown in Table 4. 27 to compare their performance.

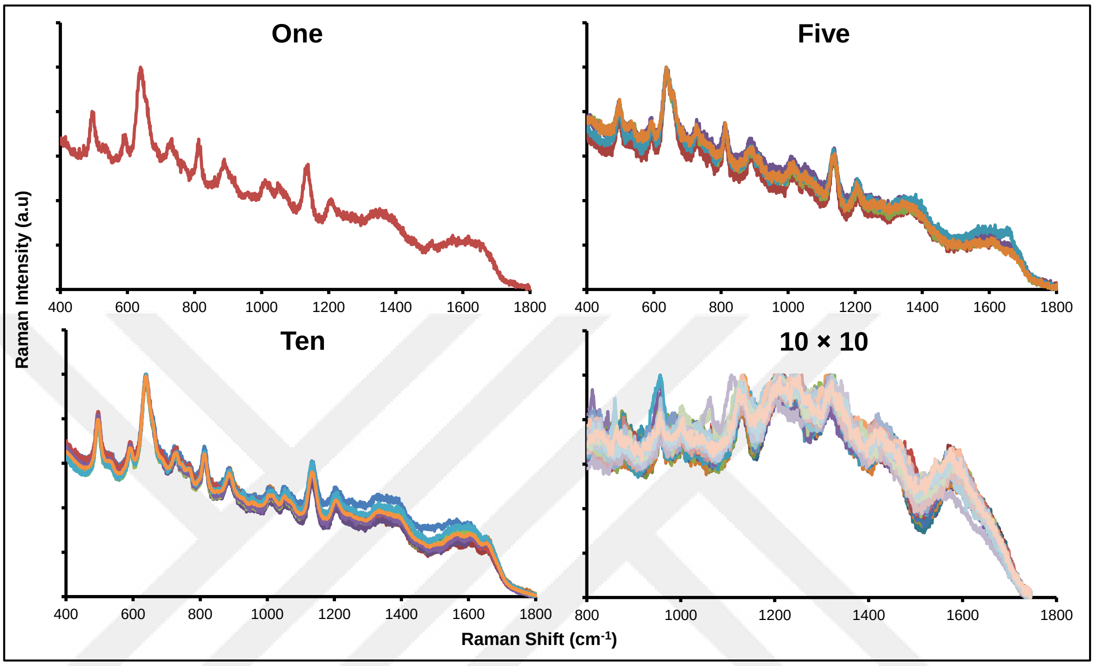

Figure 4.40. SERS spectra acquired from random selection of one point, five points, ten points and mapping of 10x10 points grid on the tissue surface.

Table 4.27. CV values of the spectra acquired from randomly selected one, five and ten points on the sample with three repetitions.

	1st Experiment				2nd Experiment				3rd Experiment				Total Average
Type of the acquisition	1st spot	2nd spot	3rd spot	Average	1st spot	2nd spot	3rd spot	Average	1st spot	2nd spot	3rd spot	Average	
Random selection of one point	10.62	4.99	9.38	18.3	8.75	11.86	5.66	10.27	6.31	7.04	6.51	9.91	8.69
Random selection of five points	8.55	5.68	12.8	7.12	7.78	7.39	6.73	2.92	6.93	6.71	7.62	9.43	2.94
Random selection of ten points	6.93	7.25	8.05	**4.04**	7.68	9.31	7.68	8.18	8.43	8.22	7.93	2.07	**2.61**
Mapping 10x10 points grid	11.92	15.63	17.94	17.74	14.36	12.74	10.45	5.04	11.89	14.59	16.63	4.48	24.46

In each trial, the CV value were variable but results were close to each other. Three experimental sets were performed at different times to observe the inter-method reproducibility. The average SERS spectrum for each experiment was obtained from the mean spectra of three spots and the comparison of the CV values is given in Table 4.28.

Table 4.28. CV values obtained from the mean spectra of the spots with three repetitions.

Bovine Liver	**1st Experiment**				**2nd Experiment**				**3rd Experiment**				**Total Average**			
	Random Selection Points			10x10 Points Grid	Random Selection Points			10x10 Points Grid	Random Selection Points			10x10 Points Grid				
Homgenized Tissue Specimen	One spectrum	Five Spectra	Ten Spectra	100 Spectra	One spectrum	Five Spectra	Ten Spectra	100 Spectra	One spectrum	Five Spectra	Ten Spectra	100 Spectra	One spectrum	Five Spectra	Ten Spectra	100 Spectra
	18.3	7.12	4.04	17. 74	10.27	2.92	8.18	5.04	9.91	9.43	2.07	4.48	8.69	2.94	2.61	24. 46

The lowest CV values were obtained as 2.61 and 2.94 belongs to randomly selected ten points and five points acquisition methods, respectively. The results demonstrated that the lowest CV value belongs to ten randomly selected acquisitions. The random selection of ten points to collect spectral information was selected as the optimum acquisition method due to its lower CV value indicating the high inter-method reproducibility.

Before proceeding with the further evaluation of the approach, the spectral quality of *in situ* and Crashed-liquefied methods was also evaluated. The Crashed-liquefied method involves the addition of colloidal AgNPs into the crashed and homogenized tissue..

4.3.2. Comparison of Signal Quality of *in situ* and Crashed-Liquefied Methods

The SERS spectra from ten randomly selected points were collected using each sampling method and their raw and mean spectra are presented on Figure 4.41.

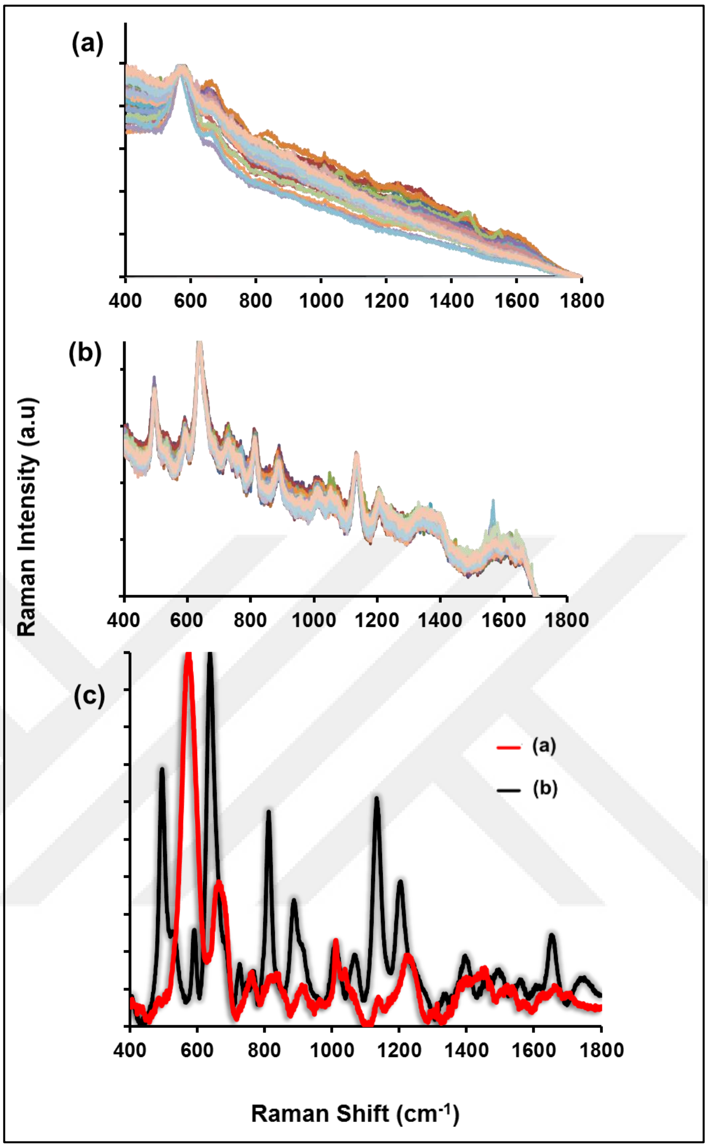

Figure 4.41. Raw SERS spectra of tissue by using Crashed-liquefied (a), and *in situ* sampling methods (b), and their mean SERS spectra.

As seen, it is clear that mean SERS spectra obtained from *in situ* method shows higher signal quality having high SNR and more spectral bands compared to the spectrum obtained from the Crashed-liqufied method. Many SERS band locations and intensities are different due to possibly differences in size and aggregation of colloidal nanoparticles, differences in the interaction of metal-analyte complexes, and differences in the position of analytes relative to the SERS substrate [148-151]. Finally, the developed *in situ* approach was applied on the sixty four thyroid biopsies to evaluate its performance for cancer diagnosis.

4.3.3. Evaluation of Thyroid Tumors with *in situ* Method

The *in situ* SERS-based approach for thyroid tissue differentiation was applied to 31 normal and 33 abnormal pathologically evaluated tissue samples obtained from thyroid disease patients. Table 4.29 lists the tissue type, the collected spectra per sample and pathological diagnostic results of tissue specimen examined in pathology. According to optimized experimental parameters for *in situ* SERS-based tissue sampling method, the spectral information belongs to biopsy sample was collected by randomly selected ten points (10 spectra for 64 biopsy samples, totally 640 spectra) using 15 mW (as adjusted in the software) of 830 nm laser equipped with 20× objective and 5s exposure time.

Table 4.29. Pathological evaluation of the specimens, number of biopsies, and number of spectra obtained per biopsy.

Sample type	**Samples**	**Spectra**
Adenomatous nodule	16	160
Follicular Adenoma	3	30
Papillary Thyroid Carcinoma	9	90
Hürthle cell adenoma	3	30
Multifocal Papillary Thyroid Carcinoma	1	10
Minimally Invasive Follicular Carcinoma	1	10
Normal thyroid tissue	31	310
Benign Tumor	22	220
Malignant Tumor	11	110
Total	64	640

The collected spectra were pre-processed by using cosmic ray filtering and normalization between the 0 and 1 through the WIRE.4.1 software. Figure 4.42 shows the comparison of mean spectra obtained from healthy and pathologically evaluated as benign tissues. Each spectrum on the figure is the average of ten spectra arbitrarily collected from the sample. As seen, there are similarities between the tissues deemed to be healthy and benign. However, although the tissue samples thought to be healthy, it may still contain tumorous cells. This could be the one reason behind the spectral differences.

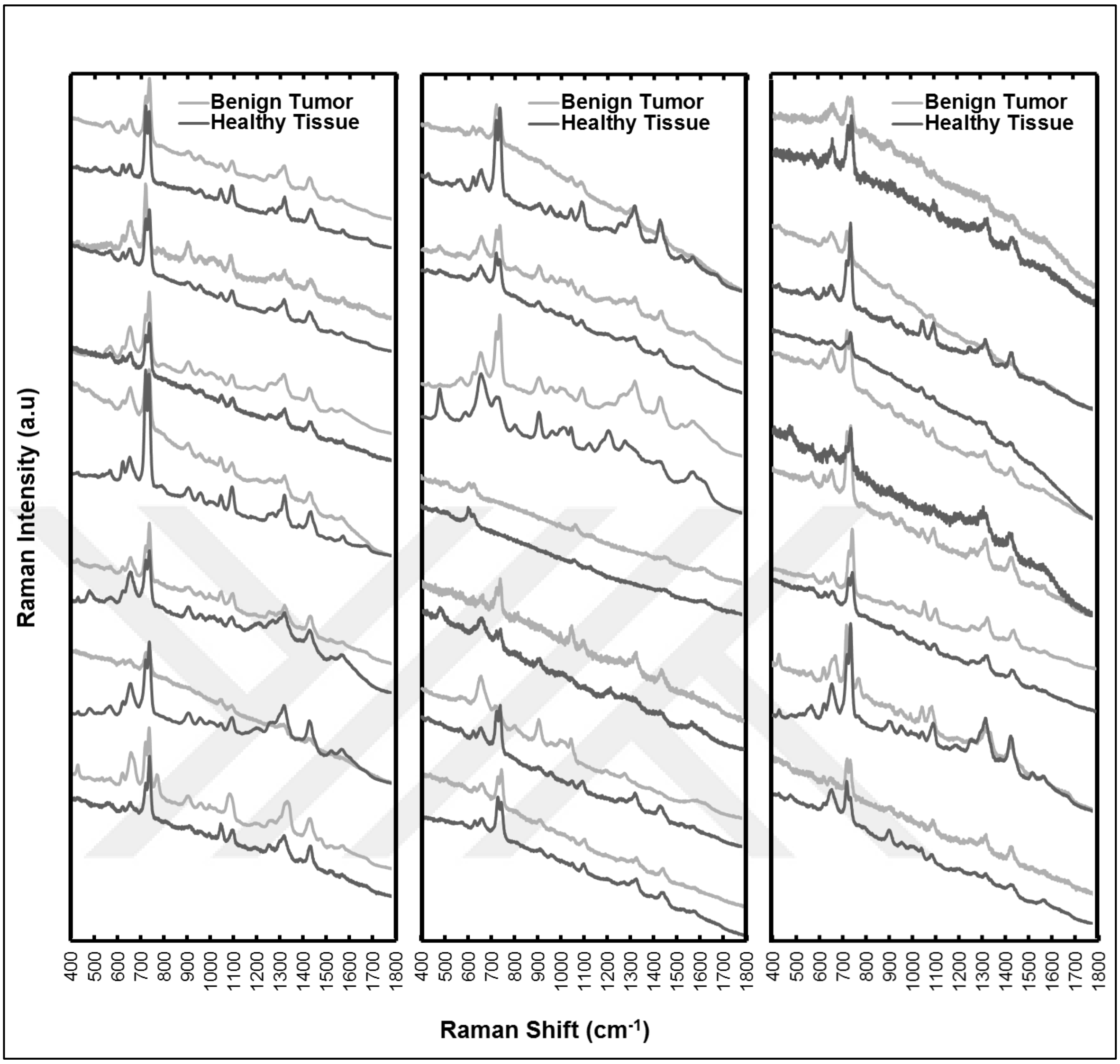

Figure 4.42. Mean SERS spectra of benign (n=22) and healthy (n=22) tissues using *in situ* approach.

The spectral patterns within the tissue samples were similar whereas the differences in the variations of patterns were increased among the samples. The same preprocessing parameters were applied to the spectral data belonging to the malignant and healthy tissues. The mean spectra belong to the malignant tumor and surrounding tissues obtained as seen in Figure. 4. 43.

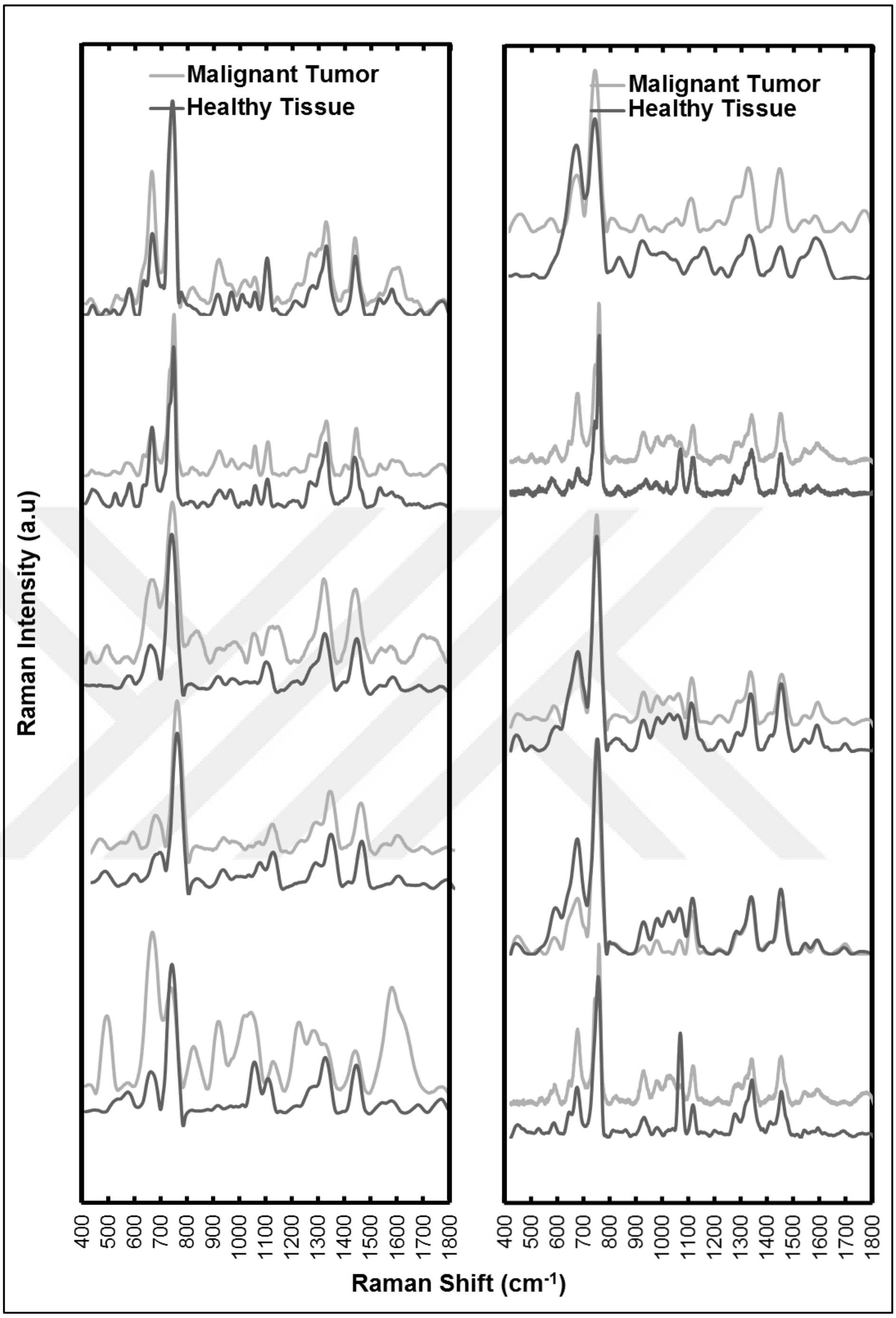

Figure 4.43. Mean SERS spectra of malignant (n=11) and healthy tissue specimen (n= 11) prepared with *in situ* SERS-based sampling method.

After the spectral information of each biopsy sample was collected, the multi high dimensional data needed to be minimized by using PCA method which was also applied on the spectral data related to the Cryosectioned-PDMS thyroid study in the previous section. However, the question of “Should a biopsy sample be represented by ten spectra or a mean of ten spectra in the PCA dimension reduction process?” should be clarified before proceeding to the text step. Thus, the multidimensional spectral dataset represented both by the ten spectra (10 spectra for each, totally 640 spectra, 640x1714) and by the average spectrum (64x1714) was reduced into new relative variants called as PCs. Twenty three significant PC vectors (eigenvalues greater than > 1) for representation by ten spectra (d=640x1714) and sixteen PC for representation by one averaged spectrum (d=64x1714) were extracted using the PCA, which are detailed in Table 4.30 and Table 4.31.

Table 4.30. Total variance explained PC vectors with percentage of explained variation of PCs for 640x1714 dimensional spectral data set.

Total Variance Explained							
PC	Total	% of Variance	Cumulative %	PC	Total	% of Variance	Cumulative %
1	1151.55	67.18	67.18	13	1.93	0.11	95.16
2	326.34	19.04	86.22	14	1.71	0.1	95.26
3	63.15	3.68	89.91	15	1.63	0.09	95.35
4	25.49	1.49	91.40	16	1.46	0.09	95.44
5	19.61	1.14	92.54	17	1.31	0.08	95.51
6	15.22	0.89	93.43	18	1.27	0.07	95.59
7	7.90	0.46	93.89	19	1.18	0.07	95.66
8	6.59	0.38	94.27	20	1.11	0.06	95.72
9	4.91	0.29	94.56	21	1.09	0.06	95.78
10	3.58	0.21	94.77	22	1.08	0.06	95.85
11	2.73	0.16	94.93	23	1.03	0.06	95.91

Table 4.31. Total variance explained PC vectors with percentage of explained variation of PCs for 64 x 1714 dimensional spectral data set.

Total Variance Explained							
PC	Total	% of Variance	Cumulative %	PC	Total	% of Variance	Cumulative %
1	1269.65	76.67	76.67	9	5.11	0.31	98.31
2	188.7	11.39	88.06	10	4.36	0.26	98.57
3	61.86	3.74	91.80	11	3.48	0.21	98.79
4	53.36	3.22	95.02	12	2.95	0.18	98.96
5	19.58	1.18	96.20	13	2.31	0.14	99.1
6	12.57	0.76	96.96	14	1.78	0.11	99.21
7	10.04	0.61	97.57	15	1.44	0.09	99.30
8	7.16	0.43	98.00	16	1.19	0.07	99.37

The PC components related to each data set were scatter plotted as seen in the Figure 4.44. The variances in the data within the groups were detectable even though the PC clusters related to each data set did not separate well using unsupervised PCA analysis method. It should be noted that PCA considers generating directions that maximize the variance in a data set without using class labels while LDA differentiates the variability within the dataset of the sample groups and the variability between the sample groups by maximizing the components for class separation [122].

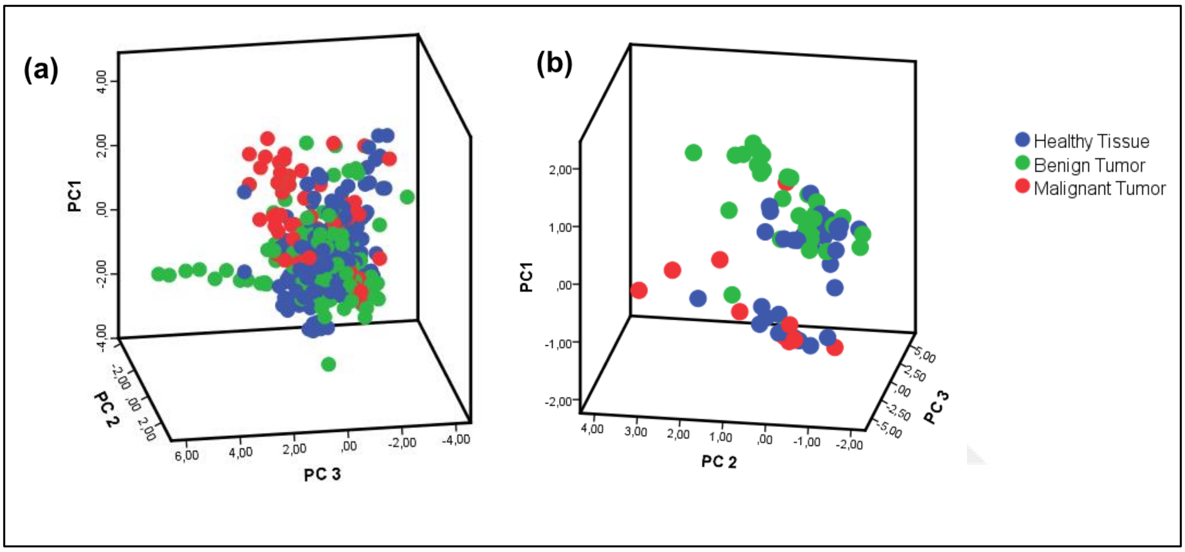

Figure 4.44. PCA scatter plots of two spectral data set, represented by ten spectra (a), and one averaged spectrum per biopsy (b), respectively.

LDA classification algorithm was applied on PCs with LOO-CV method to differentiate the biopsy samples according to their PC components derived from the representative of spectral data. Two SERS spectra of healthy tissue, three spectra of benign tumor and one spectra of malignant tumor sample was discarded from the SERS data before PC-LDA analysis due to relatively low SNR. The LDA scatter plot of the PC components of the spectral data set represented by one averaged spectrum, and ten spectra obtained as shown in Figure 4. 45.

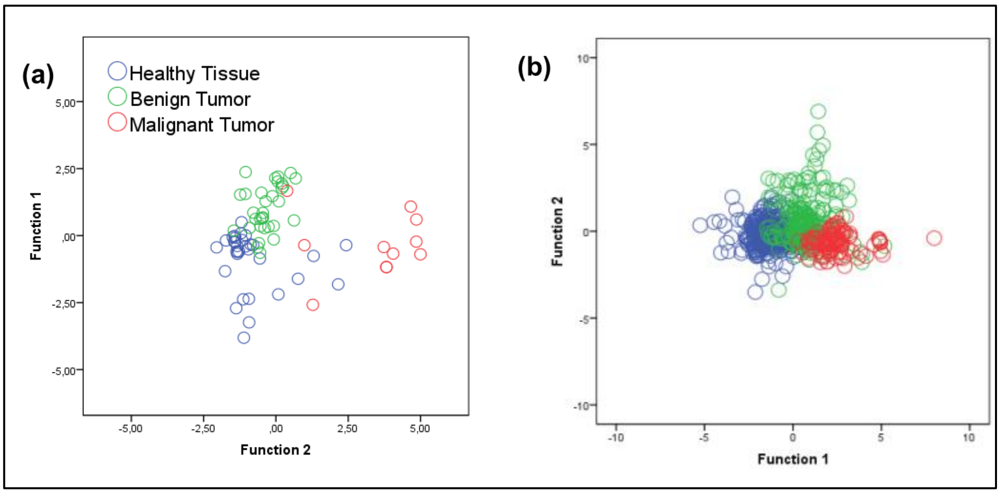

Figure 4.45. 2-D LDA scatter plots of SERS data set represented by one averaged spectrum (a), and ten spectra (b).

The predicted classification results of using PC-LDA differentiation model on the spectral data set represented by one averaged spectrum and ten spectra were obtained as detailed in Table 4.32 and Table 4. 3, respectively. The number of 1, 2 and 3 are the labels of the healthy tissue, benign tumor and malignant tumor, respectively.

Table 4.32. Classification results performing PC-LDA discrimination algorithms on the PCs obtained by ten spectra-representation (d=64x1714).

			Predicted Group Membership			Total
			1.00	2.00	3.00	
Original	Count	1.00	27	2	2	31
		2.00	5	17	0	22
		3.00	1	1	9	11
	%	1.00	87.1	6.5	6.5	100.0
		2.00	22.7	77.3	0.0	100.0
		3.00	9.1	9.1	81.8	100.0
Cross-validated	Count	1.00	24	2	5	31
		2.00	6	16	0	22
		3.00	3	3	5	11
	%	1.00	77.4	6.5	16.1	100.0
		2.00	27.3	72.7	0.0	100.0
		3.00	27.3	27.3	45.5	100.0

Table 4.33. Classification results performing PC-LDA discrimination algorithms on the PCs obtained by one averaged spectrum-representation (d=640x1714).

			Predicted Group Membership			Total
			1.00	2.00	3.00	
Original	Count	1.00	294	21	1	316
		2.00	25	159	27	211
		3.00	0	10	99	109
	%	1.00	93.0	6.6	.3	100.0
		2.00	11.8	75.4	12.8	100.0
		3.00	0.0	9.2	90.8	100.0
Cross-validated	Count	1.00	293	22	1	316
		2.00	28	141	42	211
		3.00	0	12	97	109
	%	1.00	92.7	7.0	.3	100.0
		2.00	13.3	66.8	19.9	100.0
		3.00	0.0	11.0	89.0	100.0

82.8 per cent of the original grouped cells and 70.3 per cent of cross-validated grouped cells are correctly classified with an average spectrum per biopsy sample, and 86.8 per cent of original grouped cells and 86.8 per cent of cross-validated grouped cells are correctly classified with ten spectra per biopsy sample. The predicted classification results show that the ten spectra per biopsy sample have a higher classification accuracy compared to an average spectrum. Thus, representative of ten spectra per biopsy was used to derive PC loading plots as seen in Figure. 4.46 and Figure 4.47. The first eight loading PC vectors indicate the most important diagnostic variables related to the differences in the SERS data. In addition, the positive and negative PC scores in the loadings underlie the biological differences representative of tissue samples.

The loading vectors were obtained to extract the significant differences in the spectra. Their respective negative (down arrow) and positive (up arrow) loadings originated from the variations between the spectra obtained from neoplasm and healthy tissue. It should be noted that the detailed information about the variations among the tissues is not the aim of this thesis but the differences can be examined in depth related to the tumor types. The PC loadings have bands which can be attributed to biochemical components such as nucleic acids (687 cm^{-1}), proteins (610, 675, 1005, 1170, 1278, 1452, 1656 and 1536 cm^{-1}), and lipids (425, 1058, 1100 and 1397 cm^{-1}).

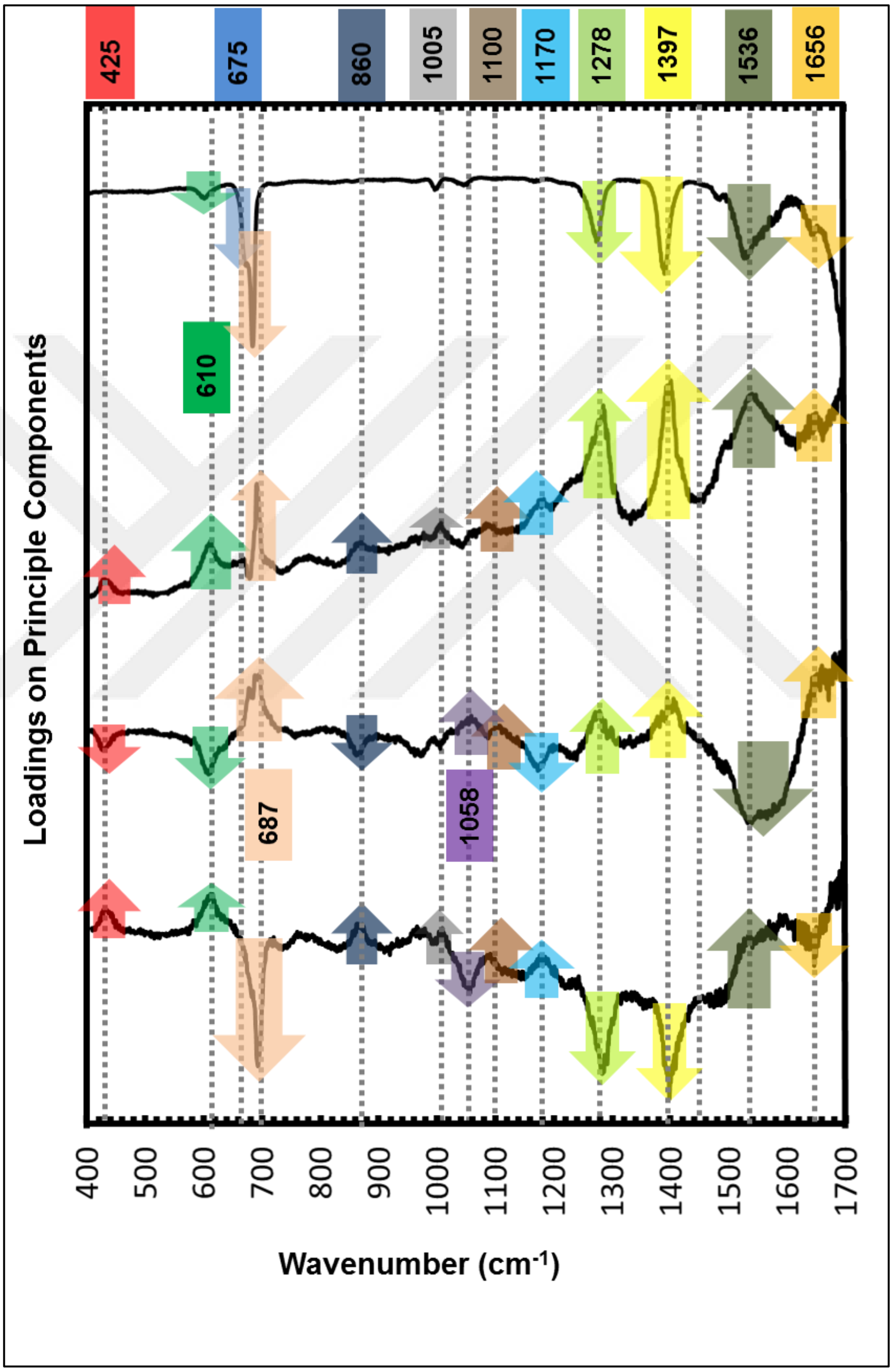

Figure 4.46. First four loading PC vectors calculated by PCA.

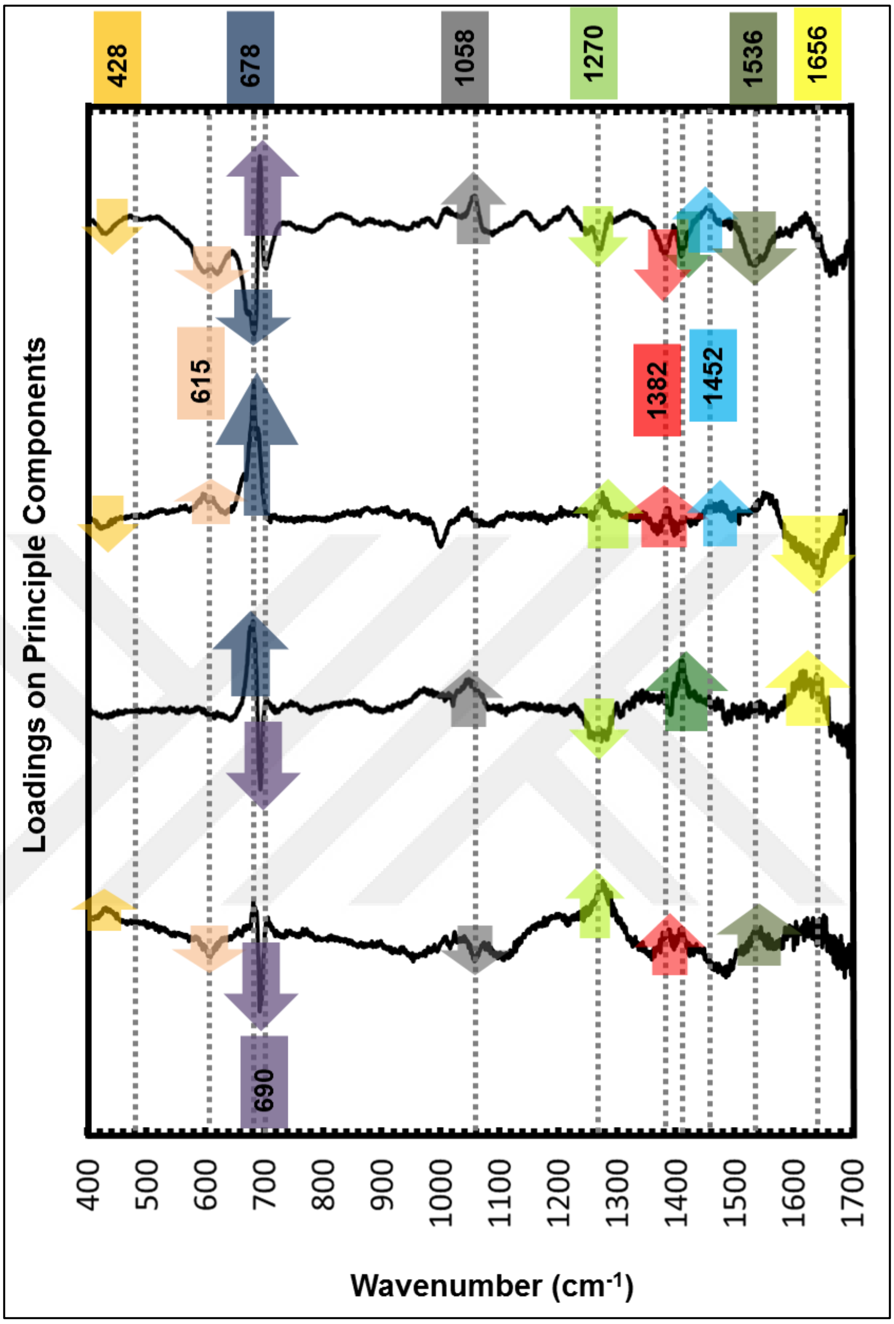

Figure 4.47. Last four loading PC vectors calculated by PCA.

Then, the PC coefficients placed in REGFR factors were extracted using the full spectral range in PC-LDA model. In addition, PCs related to SERS bands at 425, 610, 675, 687, 1005, 1058, 1100, 1170, 1278, 1397, 1452, 1536 and 1656 cm^{-1} appeared on the loading vectors were also used in PC-LDA classification model, and the PCA and LDA scatter plots were obtained as seen in the Figure 4. 48-4.51.

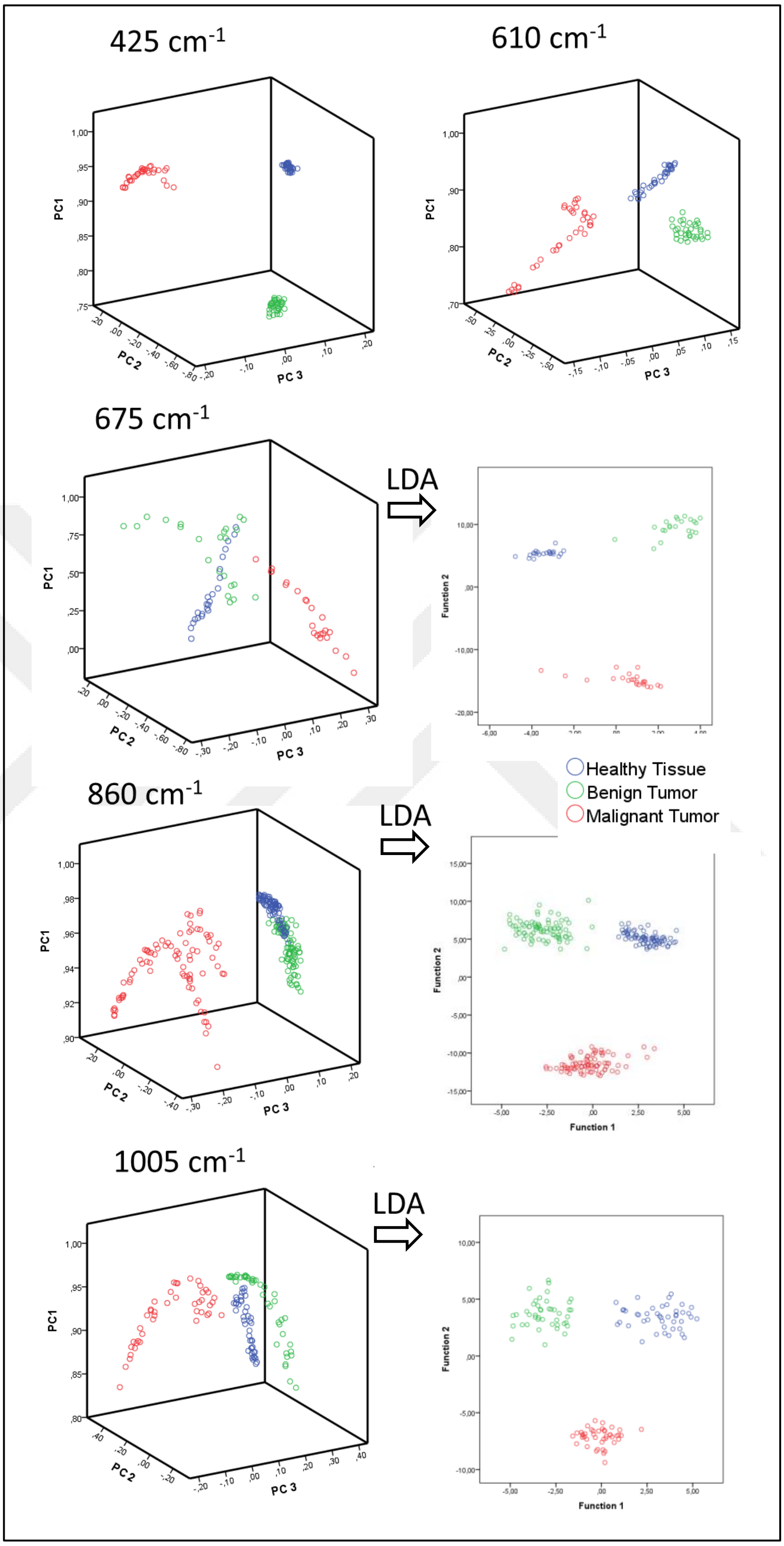

Figure 4.48. 3-D PCA and 2-D LDA scatter plots related to SERS bands at 425, 610, 675, 860 and 1005 cm^{-1}.

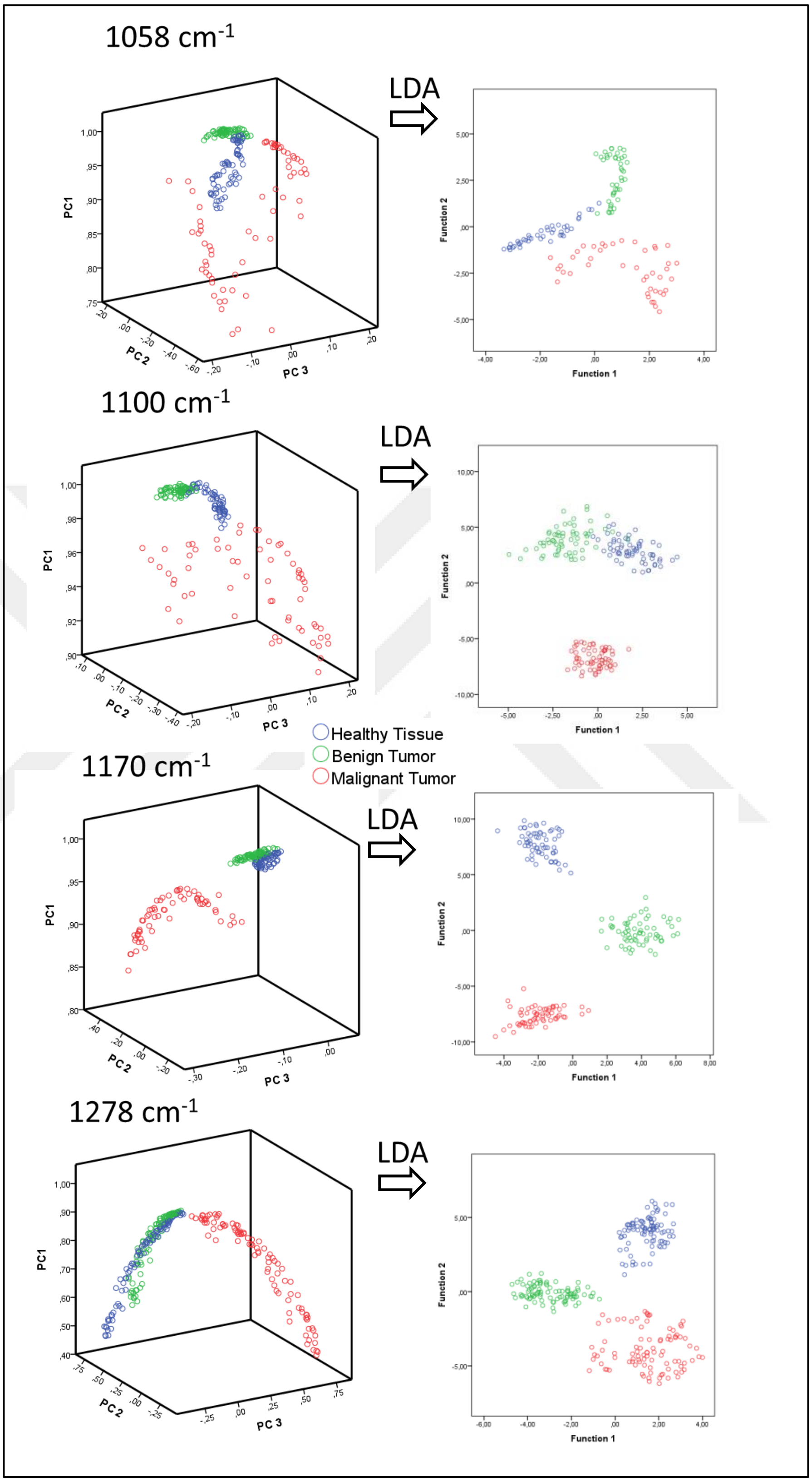

Figure 4.49. 3-D PCA and 2-D LDA scatter plots related to SERS bands at 1058,1100, 1170 and 1278 cm^{-1}.

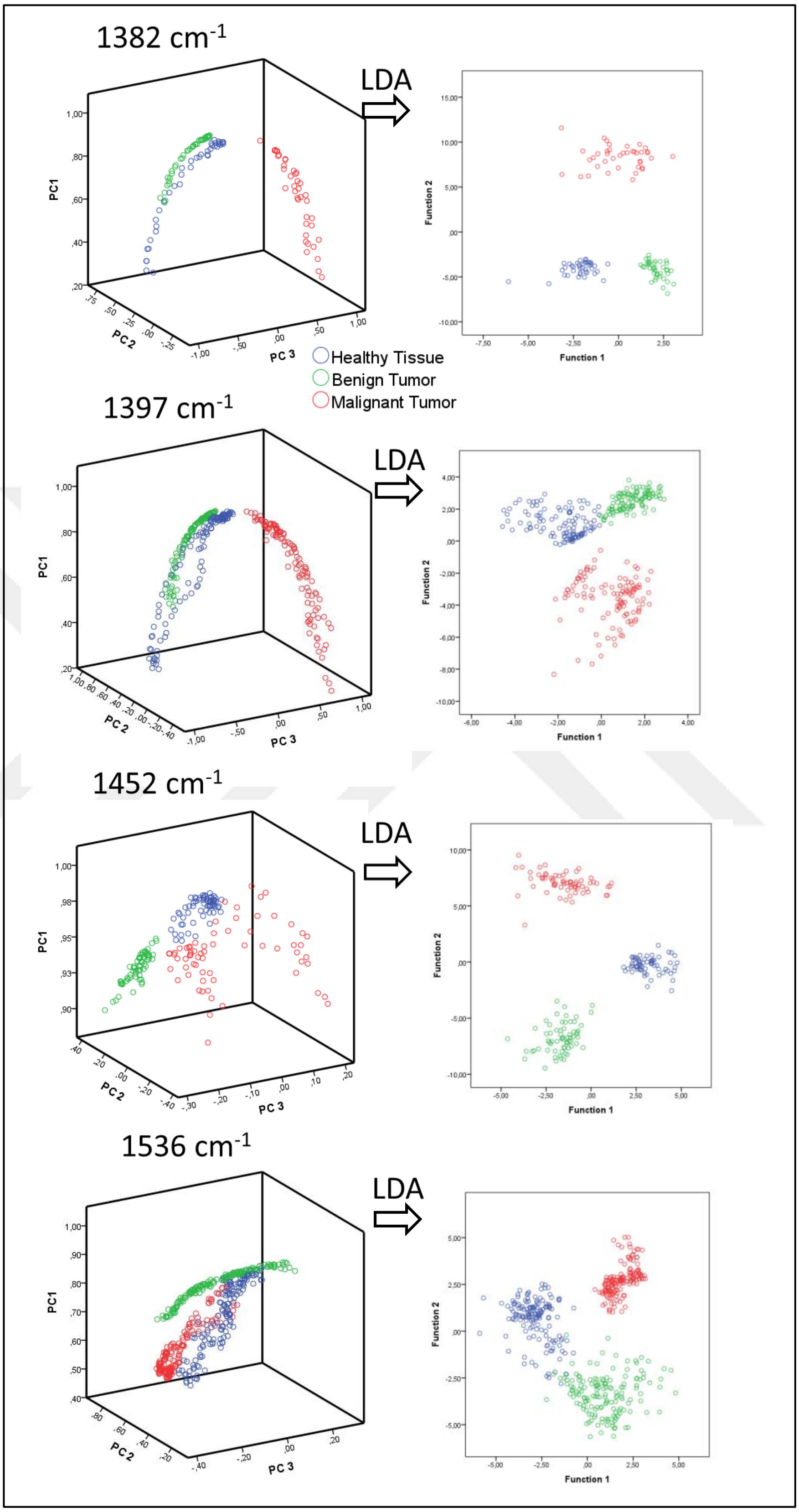

Figure 4.50. 3-D PCA and 2-D LDA scatter plots related to SERS bands at 1382, 1397, 1452 and 1536 cm^{-1}.

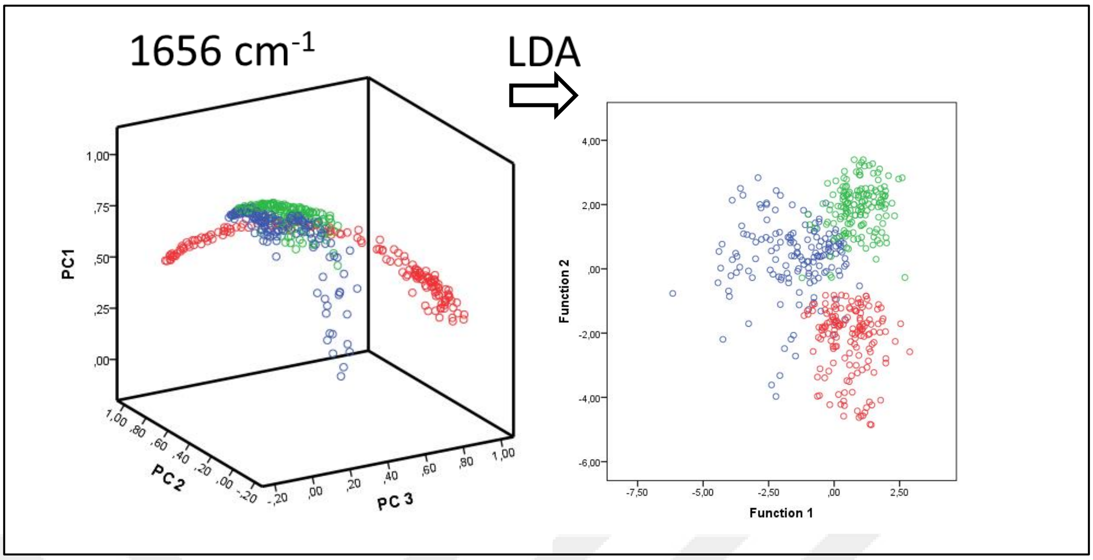

Figure 4.51. 3-D PCA and 2-D LDA scatter plots related to SERS bands 1656 cm^{-1}.

Even though PCA clusters are well separated for many relative SERS bands, LDA is used to derive a prediction value to differentiate the tissue types. The predicted classification results of PC components of the SERS spectra respective to tumorous (benign, malignant) and healthy (surrounding) tissues are detailed in Table 4.34.

The classification of tumorous and healthy tissues performing PC-LDA model on the spectra in the rage of 400 to 1800 cm^{-1} was obtained with the sensitivities of 92 per cent and 92 per cent and the specificities of 81 per cent and 81 per cent, and the accuracy of 87 per cent, and 87 per cent, respectively, indicating that the classification of normal and tumourous tissues is possible with a high diagnostic efficacy but still needs to be increased. Thus, the PC components of sigificant SERS bands obtained from the tissue samples was used in PC-LDA classification model. The sensitivity, specificity and accuracy of classification results belongs to healthy tissues and tumor biopsies was obtained 100 per cent using PC components of the bands at 425, 610, 860, 1005, 1170, 1382 and 1452 cm^{-1} while the tumorous and healthy tissues were classified with the sensitivities of 92, 99, 97, 95, 100, 99, 99, and 90 per cent and the specificities of 100, 100, 99, 98, 98, 99, 98 and 90 per cent, and accuracy of 96, 100, 98 96, 99, 99, 98 and 90 per cent for the bands at 675, 860, 1058, 1100, 1278, 1397, 1536 and 1656 cm^{-1}, respectively.

Table 4.34. Probability of predicted classification results obtained using LOO-CV method for tumorous and healthy tissue differentiation.

PC-LDA Classification Results	**Healthy Tissue versus Benign and Malignant Tumors**					
in situ	Original Case			Cross-validation Case		
Wavenumber (cm^{-1})	Sensitivity	Specificity	Accuracy	Sensitivity	Specificity	Accuracy
400-1800	92	81	87	92	81	87
425	100	100	100	100	100	100
610	100	100	100	100	100	100
675	100	100	100	92	100	96
860	100	100	100	99	100	100
1005	100	100	100	100	100	100
1058	100	99	100	97	99	98
1100	97	98	98	95	98	96
1170	100	100	100	100	100	100
1278	100	99	99	100	98	99
1382	100	100	100	100	100	100
1397	99	99	99	99	99	99
1452	100	100	100	100	100	100
1536	99	99	99	99	98	98
1656	91	91	91	90	90	90

The two class predictions were also applied for the subgroups of tumor (benign and malignant) and healthy tissues. Table 4.35 gives the PC-LDA classification results for malignant, benign and healthy tissue biopsy samples at the spectral bands of 425, 610, 675, 687, 1005, 1058, 1100, 1170, 1278, 1397, 1452, 1536 and 1656 cm^{-1}.

The probability of correctly predicted performance of using PC-LDA classification algorithm for differentiation of tumorous and healthy tissues was resulted in the sensitivities of 94, 92 and 100 per cent and the specificities of 79, 88 and 99 per cent, and accuracy of

87, 91 and 100 per cent by using the spectral range of 400 to 1800 cm^{-1} between benign and malignant; benign and healthy, malignant and healthy tissues, respectively.

The sensitivity, specificity and accuracy of classification results belongs to the healthy tissues and tumor biopsies for each diagnostic combination was obtained 100 per cent using PC components of the bands at 425, 610, 1005, 1170, 1382 and 1536 cm^{-1}.

Table 4.35. Predicted values of classification results for malignant, benign and healthy tissues using PC-LDA algorithms.

	Wavenumber (cm^{-1})	***in situ* Method**							**Wavenumber (cm^{-1})**	
		Malignant	**Surrounding (Healthy)**		Sensitivity%(SN) Specificity%(SP) Accuracy %(AC)	**Surrounding (Healthy)**		**Malignant**		
			Benign	**Malignant**		**Malignant**	**Benign**			
Benign Tumor	400-1800	**94**	**92**	**100**	SN	100	100	100	1170	**Benign Tumor**
		79	**88**	**99**	SP	100	100	100		
		87	**91**	**100**	AC	100	100	100		
	425	100	100	100	SN	100	100	100	1278	
		100	100	100	SP	97	100	100		
		100	100	100	AC	99	100	100		
	610	100	100	100	SN	100	100	100	1382	
		100	100	100	SP	100	100	100		
		100	100	100	AC	100	100	100		
	675	**95**	**81**	100	SN	100	**100**	99	1397	
		100	**94**	100	SP	100	**97**	100		
		97	**87**	100	AC	100	**99**	100		
	860	100	**100**	**81**	SN	100	100	100	1452	
		100	**98**	**100**	SP	99	99	100		
		100	**99**	**87**	AC	100	100	100		
	1005	100	100	100	SN	100	100	100	1536	
		100	100	100	SP	100	100	100		
		100	100	100	AC	100	100	100		
	1058	100	**97**	100	SN	100	100	**90**	1656	
		100	**97**	100	SP	100	100	**95**		
		100	**97**	100	AC	100	100	**93**		
	1100	100	**95**	100	SN					
		100	**100**	100	SP					
		100	**98**	100	AC					

The discrimination results of the PC components derived from the significant bands at 675, 1278 and 1452 cm^{-1} for the classification of benign and malignant tumors were achieved with the sensitivity of 95, 100 and 100 per cent, the specificity of 100, 97 and 99 per cent, and accuracy of 97, 99 and 100 per cent, respectively.

After REGR factors of the bands at 860, 1058, 1100, 1397 and 1452 cm^{-1} used in PC-LDA algorithms, the benign tumors were well differentiated from the healthy tissues with the diagnostic sensitivity of 81, 100, 97, 95, 100 per cent, the specificities of 100, 94, 98, 97, 100, 97 and 99 per cent, and accuracy of 87, 99, 97, 98, 99 and 100 per cent, respectively.

Finally, the malignant tumors and healthy tissues was classified with the sensitivities of 99 and 90 per cent, the specificities of 100 per cent and 95 per cent, and accuracy of 100 and 93 per cent for the SERS bands at 1397 an 1656 cm^{-1}, respectively.

4.4. CRASHED-LIQUEFIED METHOD

The Crashed-liquefied method developed in our laboratory earlier, which was used to differentiate brain [152] and kidney tissues [128], was also applied on the thyroid biopsies in this thesis. In our previous studies, the colloidal c-AgNP suspension was used. In this thesis, colloidal h-AgNP suspension was used for the reasons why explained above [132, 133]. The concentration of colloidal AgNP suspension used in this thyroid study was optimized before evaluating with the real biopsy samples.

4.4.1. Diagnosis of Kidney Tumors

The identification and the classification of 40 normal and 40 abnormal pathologically evaluated tissue samples obtained from kidney cancer patients at different stages were evaluated. The pattern recognition algorithm, PC-LDA was used for the evaluation of the tissue samples. The accuracy of the classification results was predicted using LOO-CV method.

SERS spectra were recorded from each type of normal and cancerous tissues. The mapping method of WIRE 2.0 software was applied to collect at least 10 spectra from randomly selected points from the dried sample composed of homogenized tissue and the colloidal AgNPs. The pathological stages of the cancer tissues according to TNM (tumor, node, and metastasis) classification were T1a, T1b, T2a, T2b, and T3a for RCC and T3 for TCC. The mean spectra of RCC tissue from the different stages T1a (120), T1b (160), T2a (30), T2b (10), T3a (60) with the mean spectra of TCC tissue from the T3 (20) stage tumor and the mean spectra of normal tissues (400) were normalized to the integrated area under the curve in the 400-1800 cm^{-1} range to enable a better comparison of the spectral shapes and the relative band intensities among the different tissue samples. Figure 4.52 shows the comparison of the normalized average SERS spectra from the normal, T1 (T1a-T1b), T2 (T2a-T2b), and T3 (T3a) stage cancer tissues. The major SERS bands, which can be attributed to biochemical constituents such as nucleic acids (478, 560, 723, 1086, 1334 cm^{-1}), proteins (524, 657, 804, 1031, 1050, 1214, 1300, 1395, 1443, 1585, 1704 cm^{-1}), carbohydrates (905 cm^{-1}) and lipids (961, 1128, 1443 cm^{-1}), were obtained from normal and abnormal tissue subjects.

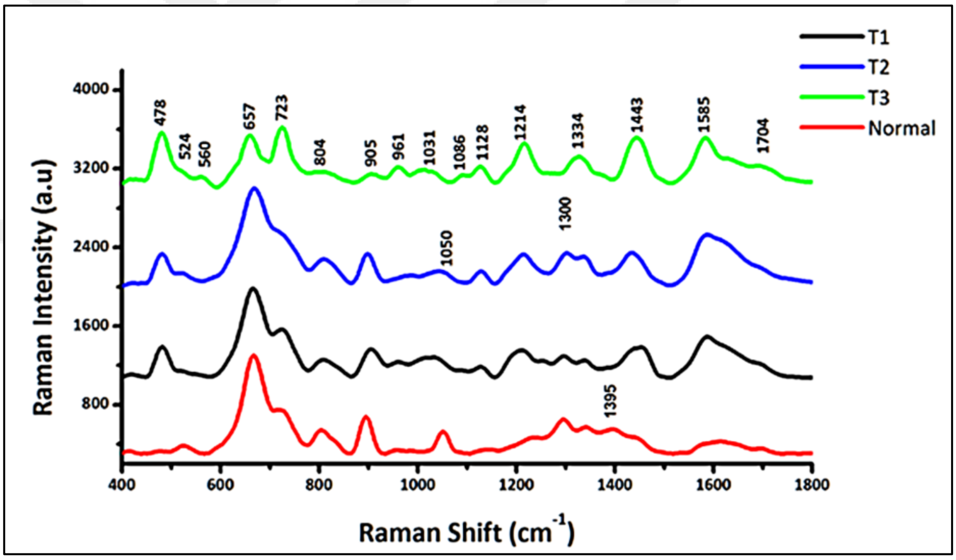

Figure 4.52. Mean SERS spectra obtained from normal tissues and cancerous tissues at T1 (T1a-T1b), T2 (T2a-T2b), T3 (T3a) stages.

Figure 4.54 shows that the normalized intensities of SERS bands at 478, 560, 723, 961, 1031, 1086, 1128, 1214, 1334, 1443, 1585 and 1704 cm^{-1} are higher for the tumor tissues than those of the normal tissues while the intensities of the SERS bands at 657, 1050, and 1395 cm^{-1} are higher on the spectra obtained from the normal tissues. The statistical significance of differences in the band intensities between the different pathology groups and normal group were identified using one-way ANOVA with a Tukey post-hoc test (significance level

$p < 0.05$). Error bars represent the standard deviation for SERS spectra obtained from each type of tissue. Abbreviated tentative assignments of Raman bands was placed under each column chart.

The significant decrease and increase in the amount of individual biomolecules is relative to the total SERS active components in the different tissue groups. These spectral intensity differences for the different pathological tissues and normal tissues could be evaluated for a better understanding of molecular changes between malignant and normal tissue types. As the detailed tentative assignments of Raman bands was established in Table 4.24. The band intensities at 478, 723, and 1334 cm^{-1}, which are primarily related to nucleic acids, were found to be increased in cancer groups, indicating that the uncontrolled fast replication of DNA in cancer cells is associated with an increased nucleic acid content in cancer cells, and the band intensity at 560 and 1086 cm^{-1} was obtained more intense in T3 stage of tumor tissues than the normal and T1-T2 stage of tumor tissues [153]. The SERS band at 961 cm^{-1}, which is associated with cholesterol, was found more intense for cancer tissues, especially T3 stage tumor sample. This increased intensity may be attributed to an increased cholesterol synthesis in cancer tissues.[154, 155] Phenylalanine related Raman bands at 1031, 1214, 1585 and 1704 cm^{-1} in cancer groups are associated with an increased amount in the phenylalanine contents relative to the total Raman-active components in cancer tissues [156, 157]. Thus, the study about the rate of uptake of amino acids, which is higher in cancer cells than normal supports the increased amino acids contents in malignant tissue [158]. The increased band intensity at 1128 cm^{-1} in cancer groups may be attributed to a higher percentage of fatty acid and lipid concentration in tumor tissue. The studies comprising the high levels of fatty acid synthesis related to tumor aggressiveness is consistent with our study results [159-161]. The SERS band of 1443 cm^{-1}, which is probably characteristic of collagen and phospholipids show a higher intense signal in malignant tissues, indicating that the collagen synthesis significantly increased in the cancerous tissue [162]. The SERS bands at 657, 1050, and 1395 cm^{-1}, enhanced in normal tissue are assigned to protein, and the SERS band of 524, 804 and 1300 cm^{-1}, which are probably defined as proteins or lipids, were obtained more intense in normal tissues compared to T1 and T3 stage tumor tissues even though the cancerous tissue in T2 stage was the most intense one. These results can be explained as the same SERS bands but different tentative assignments (serine, glutamic acid or lipids) for each tissue groups. In addition, the intensity of SERS band at 905 cm^{-1}, which is associated with protein or glycogen, was greater for normal tissues than tumor tissues in

T3 stage, whereas the greatest SERS band intensity was obtained in T1 and T2 stage of tumor tissues.

Renal cell carcinoma staging has been used as a significant prognostic factor for kidney cancer patients because the survival rate of patients with renal cancer is reduced from early stage to the late stage. PCA-LDA model was built to predict classification of tissue types and to improve the diagnostic utility of kidney cancer patients. The SERS spectra acquired from normal and abnormal tissues were processed for PCA-LDA analysis after the intensity of SERS spectra was scaled within a similar range using min-max normalization method to compare in a more precise manner relative band intensities among normal and cancerous tissue samples with different tumor stages. The significant PCs obtained using one-way ANOVA comparison test ($p < 0.05$) was used in LDA to generate a diagnostic assay. The scatter plot of the posterior probabilities based on the linear discriminant scores of the normal and the cancerous tissues using PCA-LDA diagnostic algorithm is provided on Figure 4.53 and Figure 4.55.

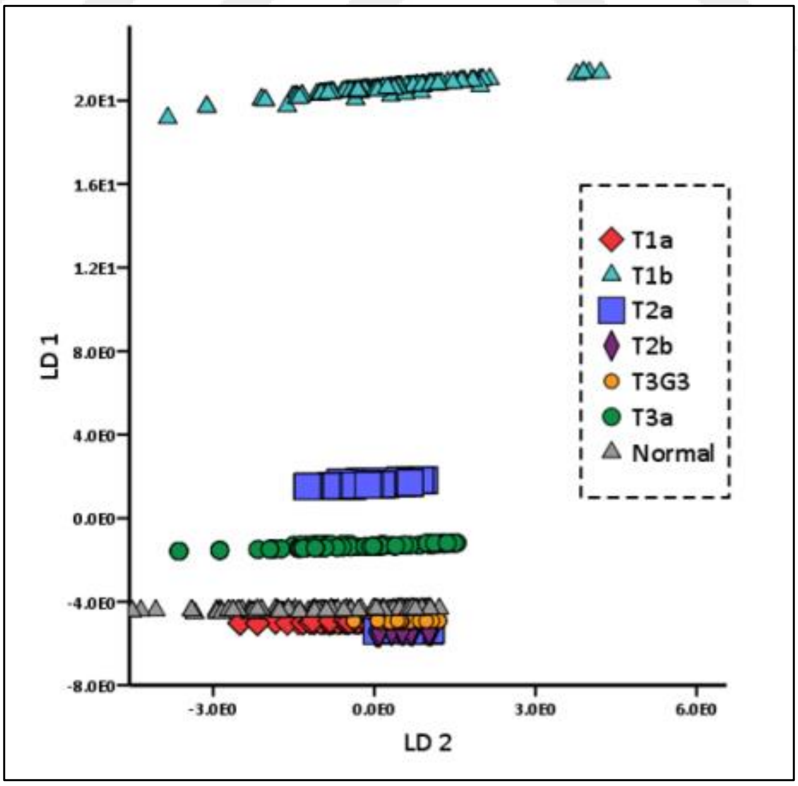

Figure 4.53. Scatter plot of posterior probabilities for the classification of tumor tissues and normal tissues.

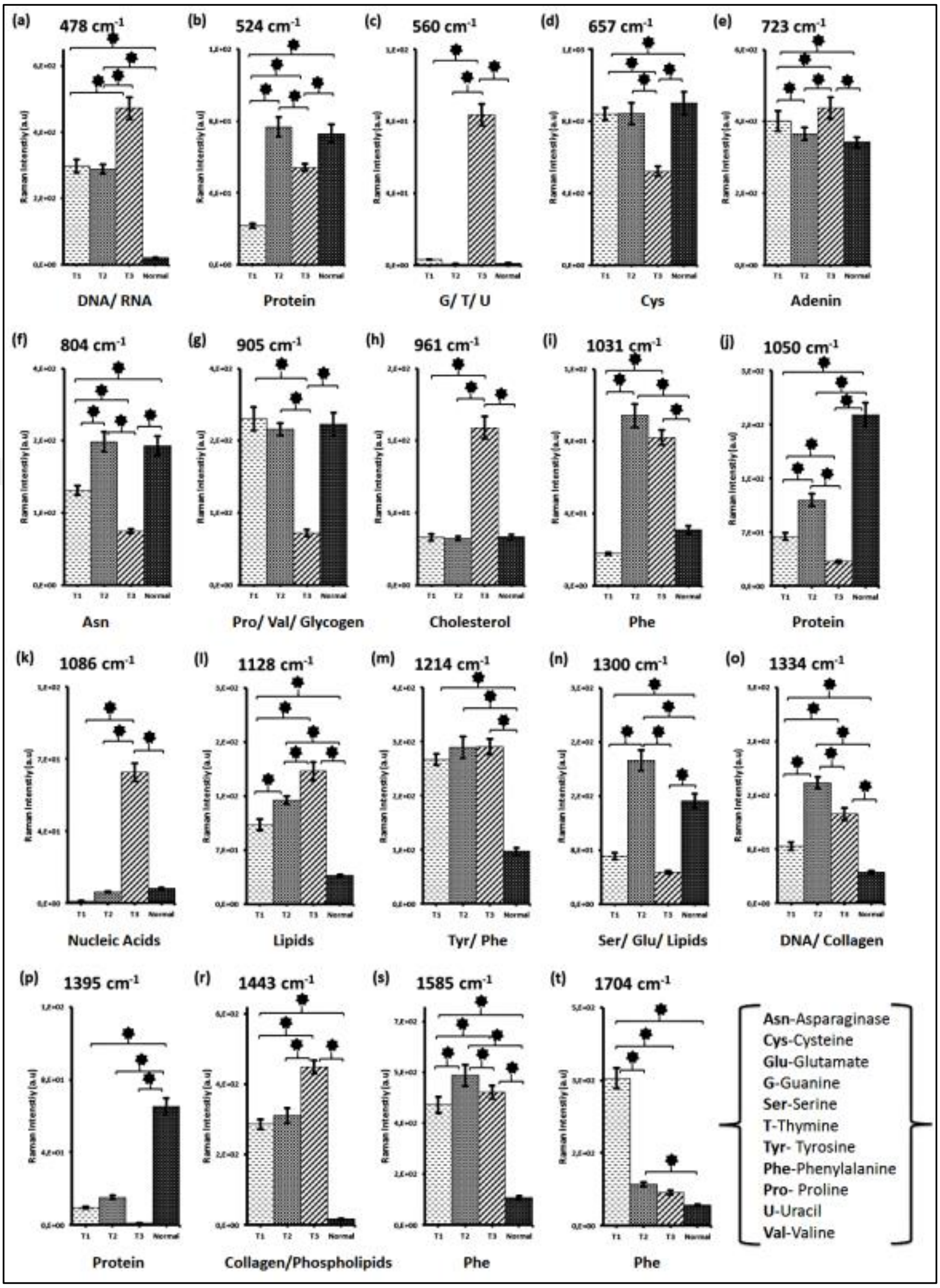

Figure 4.54. Column plots of the night teen significant SERS band intensities for the four tissue types (normal, T1, T2 and T3 stage cancer) (a) 478 cm^{-1}, (b) 524 cm-1, (c) 560 cm^{-1}, (d) 657 cm-^{1}, (e) 723 cm^{-1}, (f) 804 cm^{-1}, (g) 905 cm^{-1}, (h) 961 cm^{-1}, (i) 1031 cm^{-1}, (j) 1050 cm^{-1}, (k) 1086 cm^{-1},(l) 1128 cm^{-1},(m) 1214 cm^{-1}, (n) 1300 cm^{-1}, (o) 1334 cm^{-1}, (p) 1395 cm^{-1}, (r) 1443 cm^{-1}, (s) 1585 cm^{-1} and (t)1704 cm^{-1}.

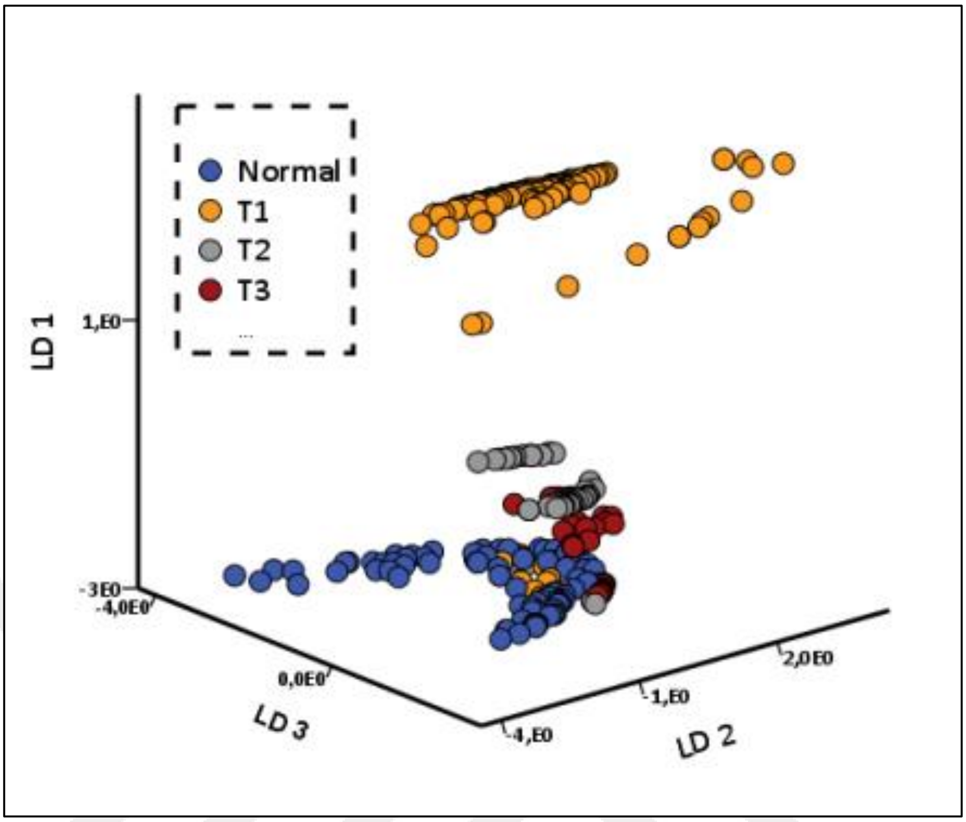

Figure 4.55. 3-D scatter plot of diagnostic probabilities of normal tissues and tumor tissues in T1, T2, and T3 stages.

The 3-D scatter plot of the diagnostic probabilities of LD1, LD2 and LD3 discriminants were shown in the Figure 4.61, illustrating a good classification among the different tumor stages and the normal tissue groups. Each dot on the plot is associated with the SERS spectra acquired from each type of tissue. The LDA scatter plot of the classification model developed to differentiate the cancerous and the normal tissue samples shows a good discrimination among normal and abnormal tissues in different tumor stages. The diagnostic performance of PCA-LDA models on the classification of tissue types has obtained with an improved accuracy by the selection of significant PCs and difference SERS bands ($p<0.05$). The discrimination results based on SERS spectra using LOO-CV method to evaluate the performance of the PCA-LDA models for the classification of different tumor stages in terms of sensitivity, specificity and 95 per cent confidence interval of accuracy was displayed in Table 4.36.

Table 4.36. LOO-CV Classification results of normal tissues and tumor tissues (T1a, T1b, T2a, T2b, T3a stages of RCC; T3 stage of TCC).

	T1b	**T2a**	**T2b**	**T3**	**T3a**	**Normal**	**LOOCV-CR**
T1a	100	100	65	89	100	65	SN
	100	100	100	100	100	70	SP
	100	100	88	93	100	69	AC
	T1b	100	100	100	100	100	SN
		100	100	100	100	100	SP
		100	100	100	100	100	AC
		T2a	100	100	100	100	SN
			100	100	100	100	SP
			100	100	100	100	AC
			T2b	88	100	80	SN
Classification Results (CR)				43	100	84	SP
				57	100	83	AC
Sensitivity % (SN)				**T3**	100	70	SN
					98	60	SP
Specificity % (SP)					98	62	AC
					T3a	100	SN
Accuracy (AC)						100	SP
						100	AC

The T1a stage tumors related to PCs, which were subtracted from SERS spectra, were well differentiated from T1b, T2a, T2b and T3a stage of RCC, T3 stage of TCC and the normal tissues with the diagnostic sensitivities of 100 per cent , 100 per cent , 65per cent , 100per cent , 8 9per cent and 65 per cent , the specificities of 100 per cent from all type of tumor stages and 70 per cent from the normal subjects, and the accuracy of 100 per cent , 100 per cent , 88 per cent , 93 per cent , 100 per cent and 69 per cent , respectively. The discrimination results of the diagnostic combinations of T1b stage tumor versus T2a, T2b and T3a stage of RCC, T3 stage of TCC and normal tissues, and T2a stage tumor versus T2b, T3a stage of RCC, T3 stage of TCC and the normal tissues were achieved with the sensitivity, specificity and accuracy of 100 per cent while the posterior probabilities of T2b stage tumor sample versus T3a stage of RCC, T3 stage of TCC and normal tissues were obtained with the sensitivities of 88 per cent , 100 per cent and 80 per cent , the specificities of 43 per cent , 100 per cent and 84 per cent , and the accuracy of 57 per cent, 100 per cent and 83 per cent , respectively. The T3a stage tumor subjects versus normal samples were diagnosed with the sensitivity, specificity, and accuracy of 100 per cent , and T3 stage tumors of TCC were classified with the sensitivity of 100 per cent and 70 per cent, the specificity of 98 per cent and 60 per cent, and the accuracy of 98 per cent and 62 per cent.

The T1, T2, and T3 stage tumors with normal tissue were also differentiated using PC-LDA models of the spectral data obtained from the normal and the abnormal tissue samples. As compared to the classification results in Table 4.37 were obtained among the different tissue classes with a diagnostic sensitivity of 89, 96, 94, 70, 97 and 98 per cent, specificity of 100, 100, 96, 83, 94 and 77 per cent, and accuracy of 99, 97, 95, 81, 95 and 85 per cent, respectively, for the classification between T1 and T2 stage cancer; T1 and T3 stage cancer; T1 stage cancer and normal tissues; T2 and T3 stage cancer; T2 stage cancer and normal groups; T3 stage cancer and normal tissue, respectively.

Table 4.37. LOO-CV classification results of normal and cancerous tissues in T1, T2 and T3 tumor stages.

	T1	**T2**	**Sensitivity % (SN)**	**T3**	**T2+T3**
			Specificity % (SP)		
			Accuracy % (AC)		
Normal	94	97	SN	98	98
	96	94	SP	77	86
	95	95	AC	85	90
	T1	89	SN	96	93
		100	SP	100	100
		85	AC	97	91
		T2	SN	70	
			SP	83	
			AC	81	

The classification of tumor tissues in advanced tumor stages (T2-T3) with tumor tissues in early stage (T1), and normal tissues was obtained with the sensitivities of 93 and 100 per cent and the specificities of 98 and 86 per cent, and the accuracy of 91, and 90 per cent, respectively, indicating that the classifying of normal tissues, early stage of tumor tissues and advanced stage of tumor tissues is possible with a high diagnostic efficacy.

4.4.2. Diagnosis of Thyroid Tumors

The concentration of colloidal h-AgNP suspension needed to be optimized before evaluating with thyroid biopsies. The final suspension concentration obtained by using the hydroxylamine chloride reduction method was named as 1×. Then, the suspension was concentrated to 8×, 16× and 32×, and each concentrated suspension was mixed with the same volume of the homogenized tissue suspension. Figure 4.56 shows the comparison of the SERS spectra obtained at increasing colloidal suspension concentration.

Table 4.38 shows type of tissues, the number of tissue samples and spectra collected from each tissue sample

Table 4.38. Pathological evaluation of the specimens, number of biopsies, and number of spectra obtained per biopsy

Sample type	**Samples**	**Spectra**
Normal thyroid tissue	31	310
Adenomatous nodule	16	160
Follicular Adenoma	3	30
Papillary Thyroid Carcinoma	9	90
Hürthle cell adenoma	3	30
Multifocal Papillary Thyroid Carcinoma	1	10
Minimally Invasive Follicular Carcinoma	1	10
Total	64	640

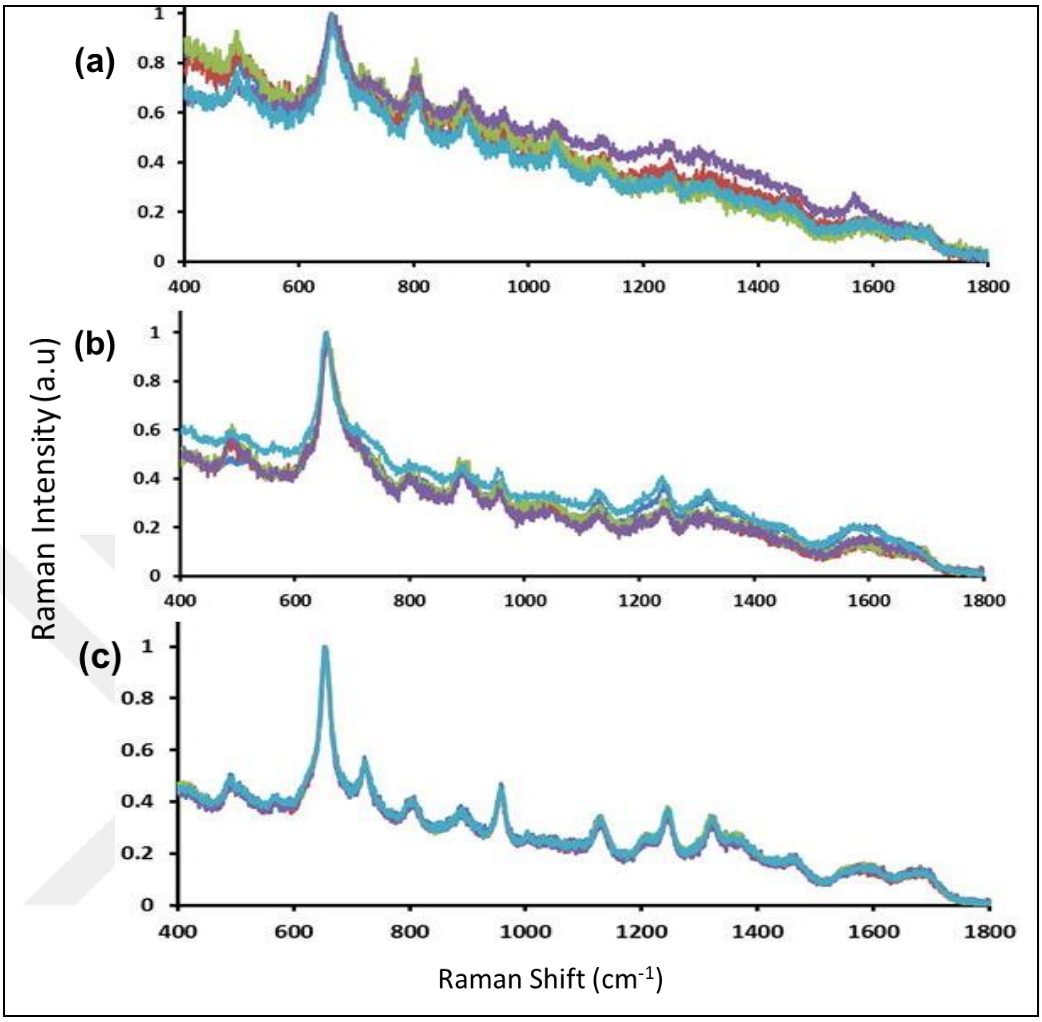

Figure 4.56. SERS spectra of tissue using 8× (a), 16× (b), and 32× (c) concentrated colloidal AgNP suspension.

A high quality SERS spectra with the use of 32× concentrated suspension was obtained. Thus, 32× concentrated AgNP suspension was used during for the rest of the study.

Figure 4.57 and Figure 4.58 show the mean spectra from the collected spectra of benign, malignant and health tissues. Cosmic ray filtering and normalization of the data between the 0 and 1 were obtained through the WIRE.4.1 software. The inspection of Figure 4.57 reveal that the spectral patterns of benign and healthy tissues within the same sample are similar while the variations in the pattern were increasing among the samples.

.

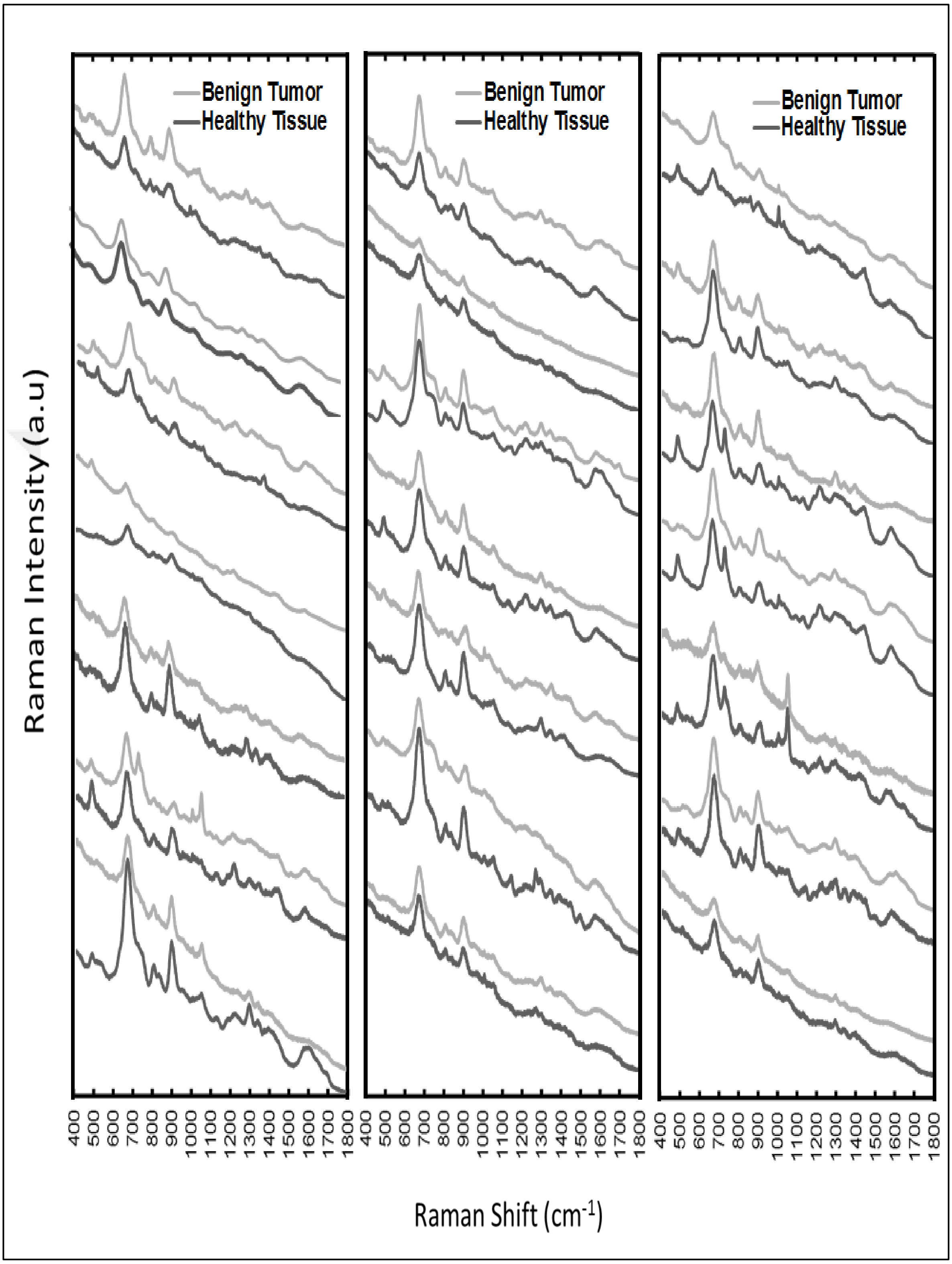

Figure 4.57. Mean SERS spectra of benign tumors (n=22) and healthy tissue specimen (n= 22) prepared using Crashed-liquefied tissue sampling method.

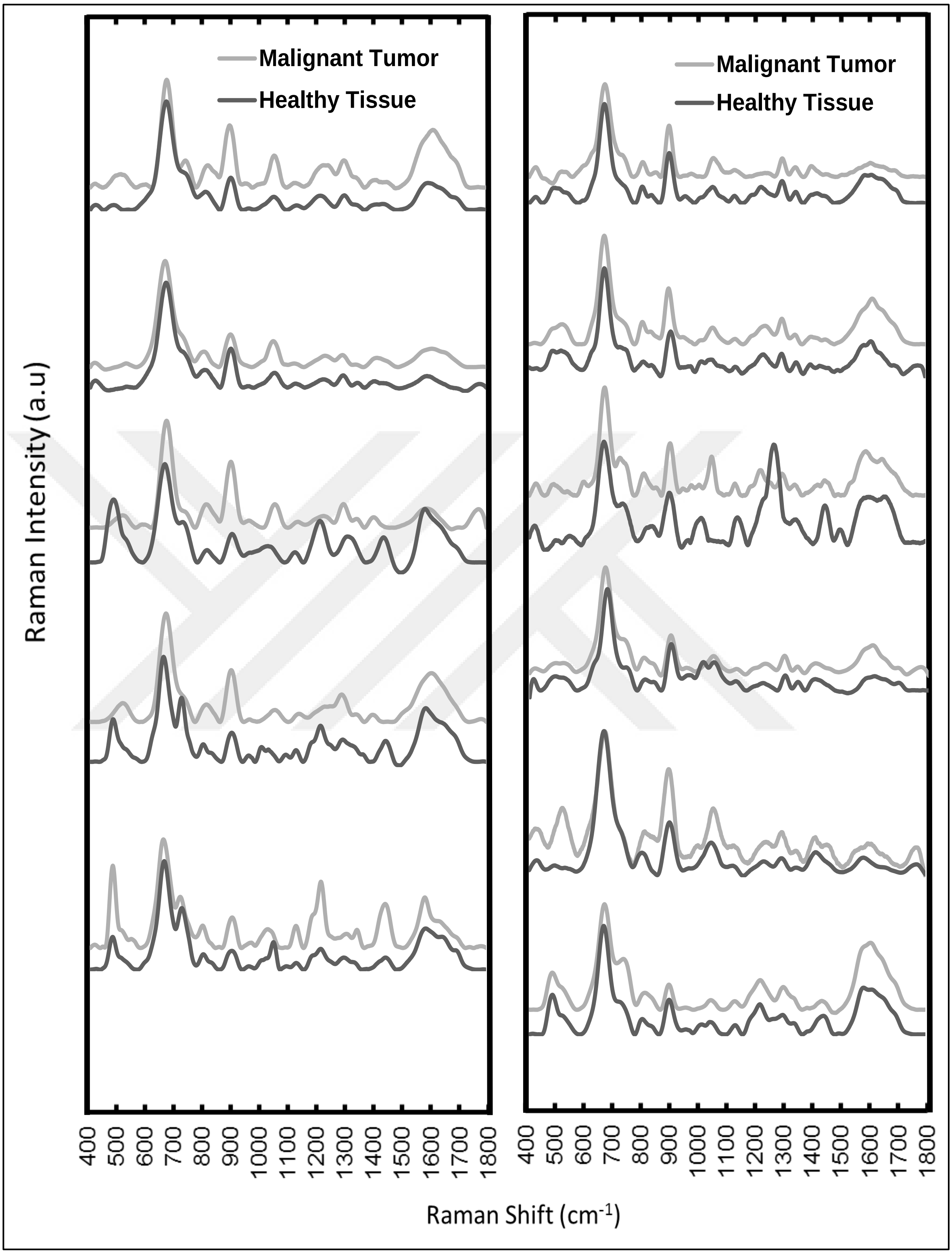

Figure 4.58. Mean SERS spectra of malignant tumors (n=11) and healthy tissue specimen (n= 11) prepared using crashed-liquefied tissue sampling method.

Before using that multidimensional data in PCA to reduce the dimension, there is a prior question to be answered similar to the question asked in the previous section. “Would be a biopsy sample represented by the ten spectra or a mean of ten spectra in the classification model?” Thus, a comparison of using one averaged spectrum and ten spectra for Crashed-liquefied sampling method was also performed using PCA-LDA classification model. The multidimensional spectral dataset represented both by the ten spectra (10 spectra for each, totally 640 spectra, 640x1714) and by the average spectrum (64x1714) was reduced into new relative variants as PCs. Nineteen significant PC components (eigenvalues greater than > 1) (for 640x1714 dimension) and eighteen PC components (for 62x1714 dimension) were extracted by using the PCA as illustrated in Table 4.39 and Table 4.40.

Table 4.39. Total variance explained PC vectors with percentage of explained variation of PCs for 620x1714 dimensional spectral data set.

Total Variance Explained							
PC	Total	% of Variance	Cumulative %	PC	Total	% of Variance	Cumulative %
1	934.29	54.51	54.51	7	13.85	0.81	93.19
2	422.58	24.65	79.16	8	10.74	0.63	93.81
3	121.57	7.09	86.26	9	7.12	0.42	94.23
4	58.09	3.39	89.65	10	5.6	0.33	94.56
5	25.56	1.49	91.14	11	4.14	0.24	94.8
6	21.29	1.24	92.38	12	3.64	0.21	95.01
7	13.85	0.81	93.19	13	2.6	0.15	95.16
8	10.74	0.63	93.81	14	2.42	0.14	95.3

Table 4.40. Total variance explained PC vectors with percentage of explained variation of PCs for 64x1714 dimensional spectral data set.

Total Variance Explained							
PC	Total	% of Variance	Cumulative %	PC	Total	% of Variance	Cumulative %
1	1010.32	59.08	59.08	10	5.93	0.35	98.21
2	421.00	24.62	83.7	11	4.28	0.25	98.46
3	111.24	6.51	90.21	12	3.62	0.21	98.67
4	50.93	2.98	93.19	13	2.65	0.15	98.82
5	27.94	1.63	94.82	14	2.06	0.12	98.94
6	17.79	1.04	95.86	15	1.83	0.11	99.05
7	14.34	0.84	96.7	16	1.33	0.08	99.13
8	11.2	0.66	97.35	17	1.16	0.07	99.20
9	8.64	0.51	97.86	18	1.12	0.07	99.26

The three REGR factors derived by using PCA performing on the spectra in the range of 400 to 1800 cm^{-1} were scatter plotted as shown in Figure. 4.59.

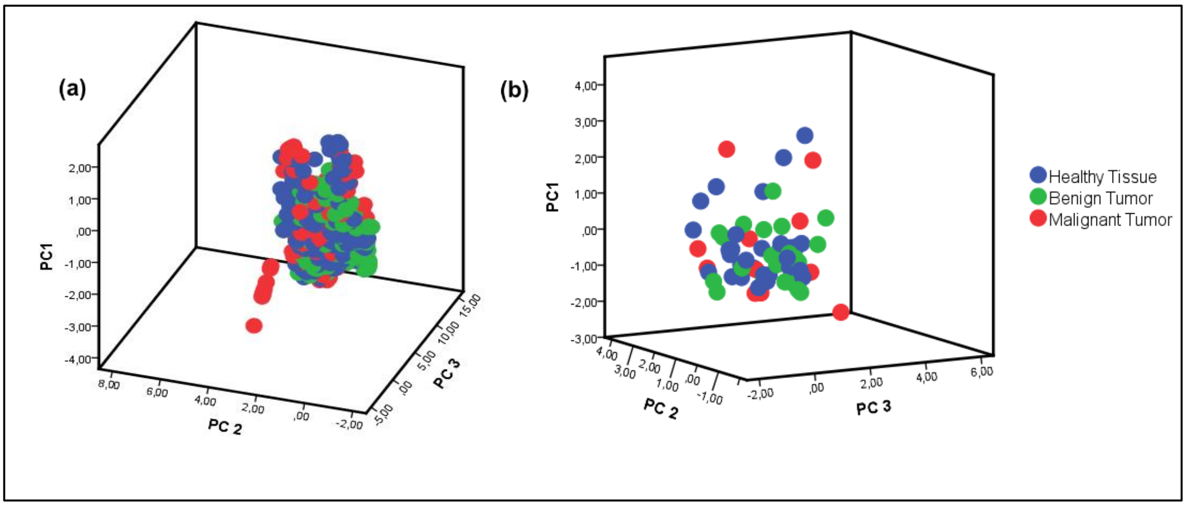

Figure 4.59. PCA scatter plots of two spectral data set (d=640x1714 and d=64x1714, respectively)

The PC clusters of each SERS data were not separated well, which might be due to the increased variances within the clusters. Then, LDA classification algorithm was applied on PCs with LOO-CV method to provide a predicted classification result explained with the terms of sensitivity, specificity and accuracy. The LDA scatter plots as shown in Figure 4.60 was obtained for each SERS data set.

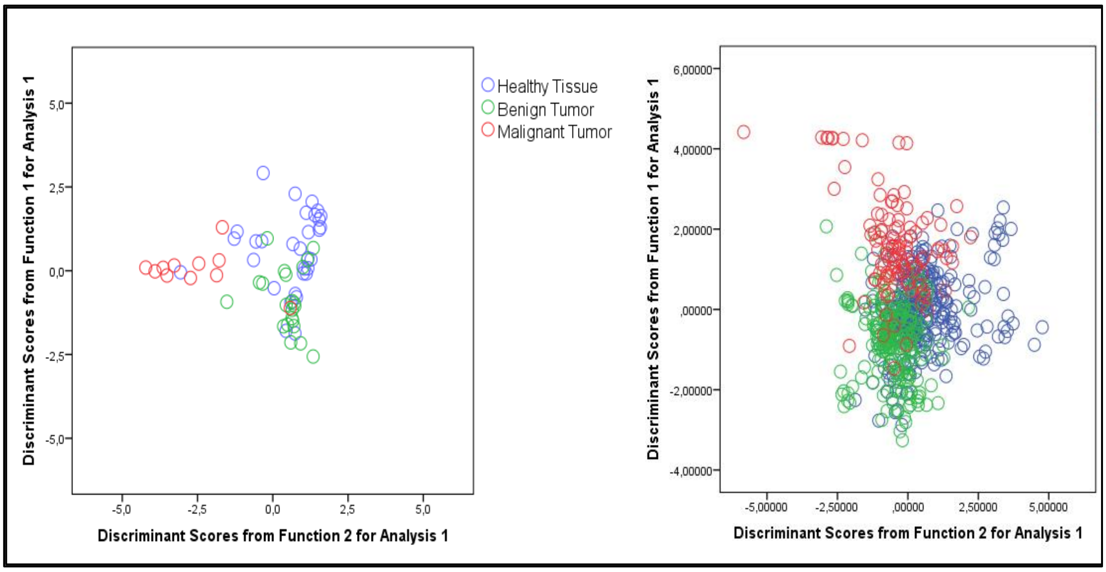

Figure 4.60. 2-D LDA scatter plots for the spectral data set represented by one averaged spectrum (left), and ten spectra (right).

The predicted classification results of using PC-LDA differentiation model on the spectral data represented by one averaged spectrum and ten spectra were obtained as detailed in Table 4.41 and Table 4.42, respectively. The number of 1, 2 and 3 are the labels healthy tissue, benign tumor and malignant tumor, respectively.

Table 4.41. Classification results of using PC- LDA discrimination algorithms performed on the PCs extracted from the spectral data (d=62x1714).

			Predicted Group Membership			**Total**
			1.00	2.00	3.00	
Original	Count	1.00	22	6	3	31
		2.00	6	15	1	22
		3.00	0	1	10	11
	%	1.00	71.0	19.4	9.7	100.0
		2.00	27.3	68.2	4.5	100.0
		3.00	0.0	9.1	90.9	100.0
Cross-validated	Count	1.00	22	6	3	31
		2.00	6	15	1	22
		3.00	0	1	10	11
	%	1.00	71.0	19.4	9.7	100.0
		2.00	27.3	68.2	4.5	100.0
		3.00	0.0	9.1	90.9	100.0

Table 4.42. Classification results of using PC- LDA discrimination algorithms performed on the PCs extracted from the spectral data (d=620x1714).

			Predicted Group Membership			Total
			1.00	2.00	3.00	
Original	Count	1.00	191	83	34	308
		2.00	37	169	11	217
		3.00	16	9	84	109
	%	1.00	62.0	26.9	11.0	100.0
		2.00	17.1	77.9	5.1	100.0
		3.00	14.7	8.3	77.1	100.0
Cross-validated	Count	1.00	191	83	34	308
		2.00	37	169	11	217
		3.00	16	9	84	109
	%	1.00	62.0	26.9	11.0	100.0
		2.00	17.1	77.9	5.1	100.0
		3.00	14.7	8.3	77.1	100.0

73.4 per cent of original grouped cells and 73.4 per cent of cross-validated grouped cells are correctly classified for the data with an average spectrum per biopsy sample, and 70 per cent of original grouped cells and 70 per cent of cross-validated grouped cells are correctly classified for SERS data with ten spectra per biopsy sample. The predicted classification results with an average spectrum per biopsy sample have a higher degree of accuracy than the spectral data with ten spectra per biopsy sample. Thus, an average spectrum representing the each sample prepared by using Crashed-liquefying method was selected as the optimum parameter for the next coming applications.

The first eight loading PC vectors as seen in Figure 4.61 and Figure 4.62 were extracted using PCA to figure out the variances between the variables (wavenumber) in the SERS data for tumorous and healthy tissues coloring rows to indicate the most important diagnostic variables related to differences in the spectra.

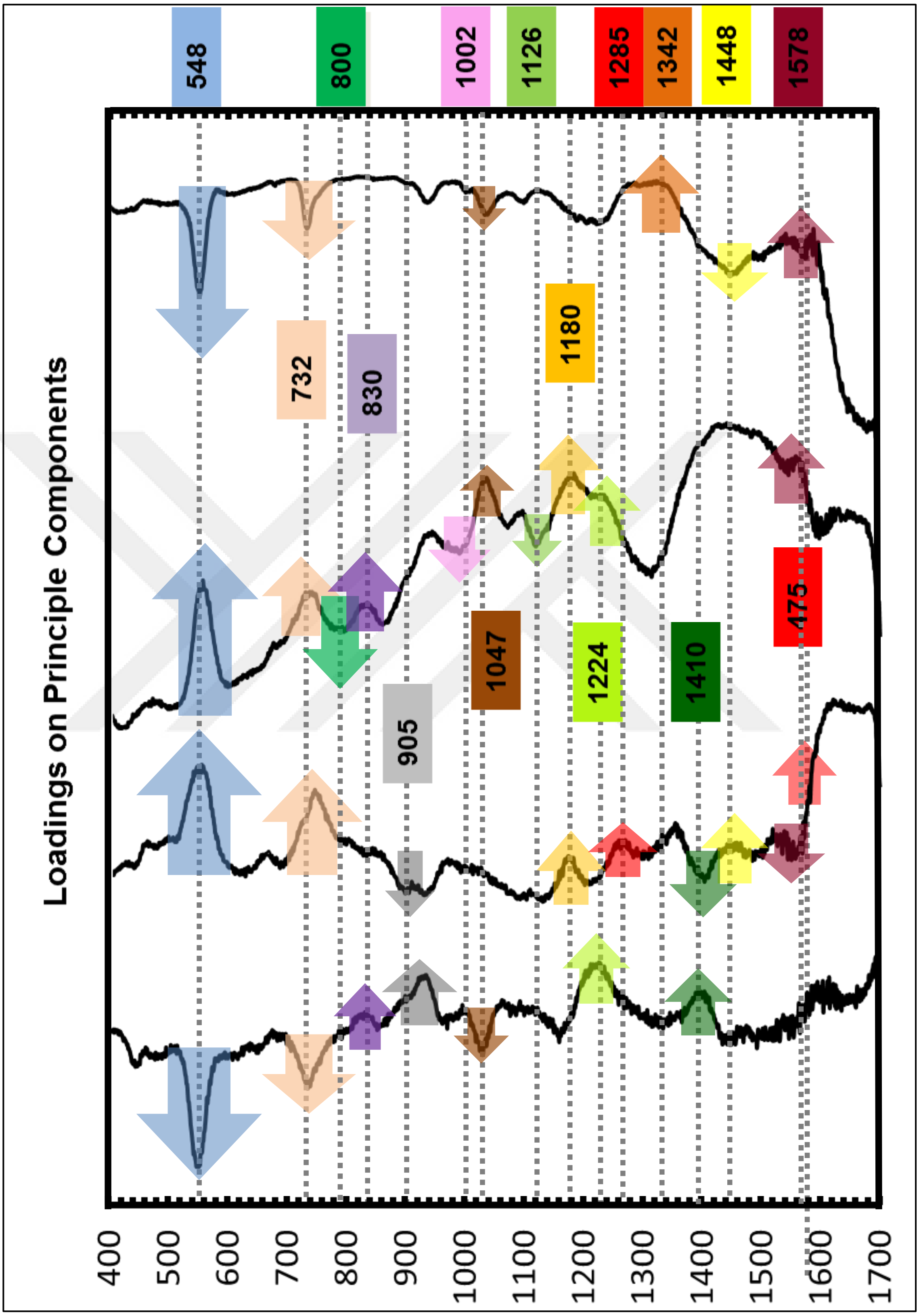

Figure 4.61. First four loading PC vectors calculated by PCA.

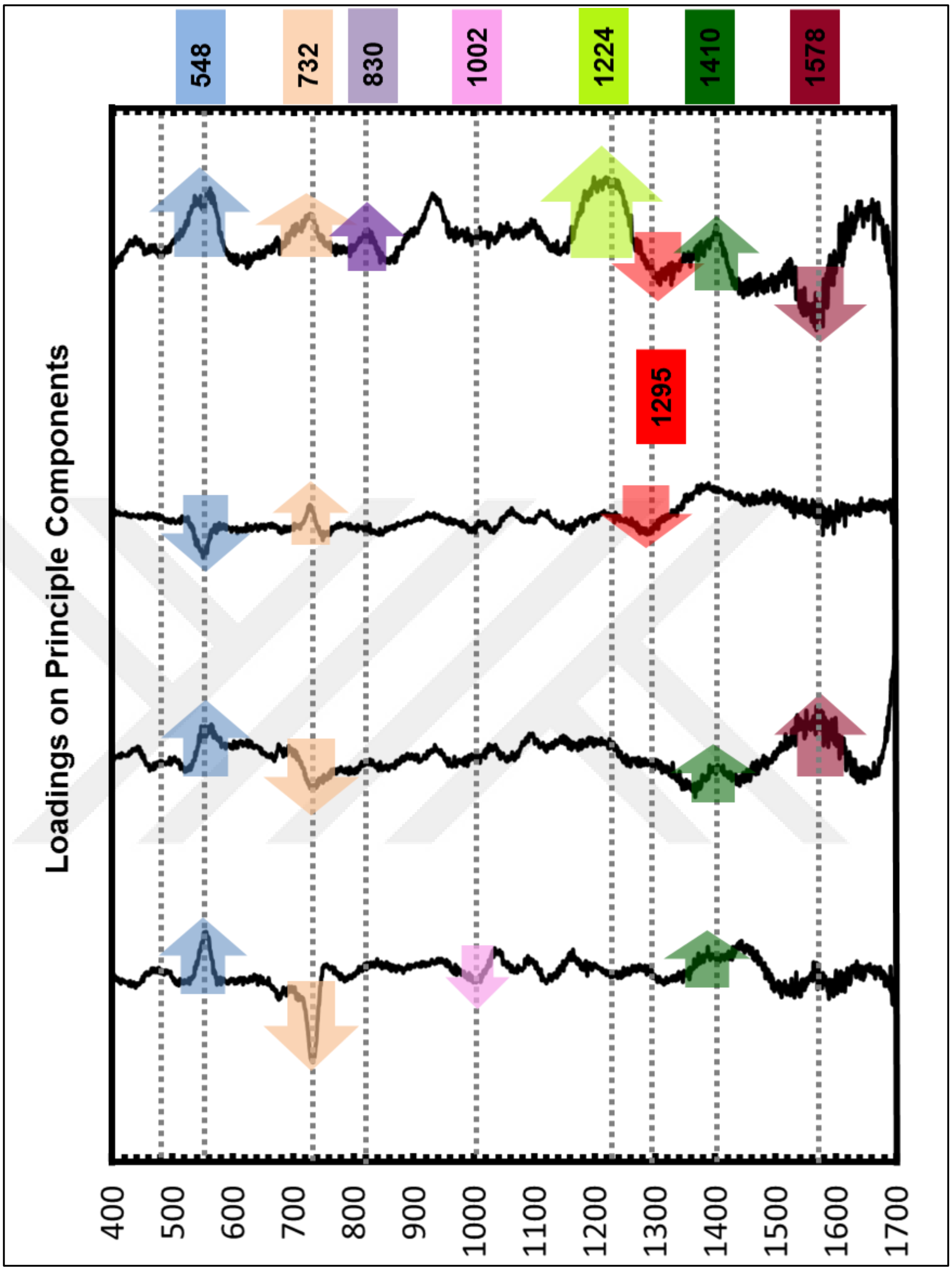

Figure 4.62. Last four PC loading plots.

The prominent spectral variations on the loadings can be assigned to the biochemical components such as nucleic acids (732, 805, 1410 and 1578 cm^{-1}), proteins (830, 905, 1002, 1047, 1180 and 1285) and 1506 cm^{-1}), metabolites (1126 cm^{-1}), and lipids (548, 1126 and 1448 cm^{-1}). After the REGFR factors extracted by using PCA applied on the specific bands at 475, 548, 732, 805, 830, 905, 1002, and 1047 cm^{-1} were used in the PC -LDA classification algorithms, and the scatter plot of PCA and LDA were obtained as seen in Figure 4.63- 4.65.

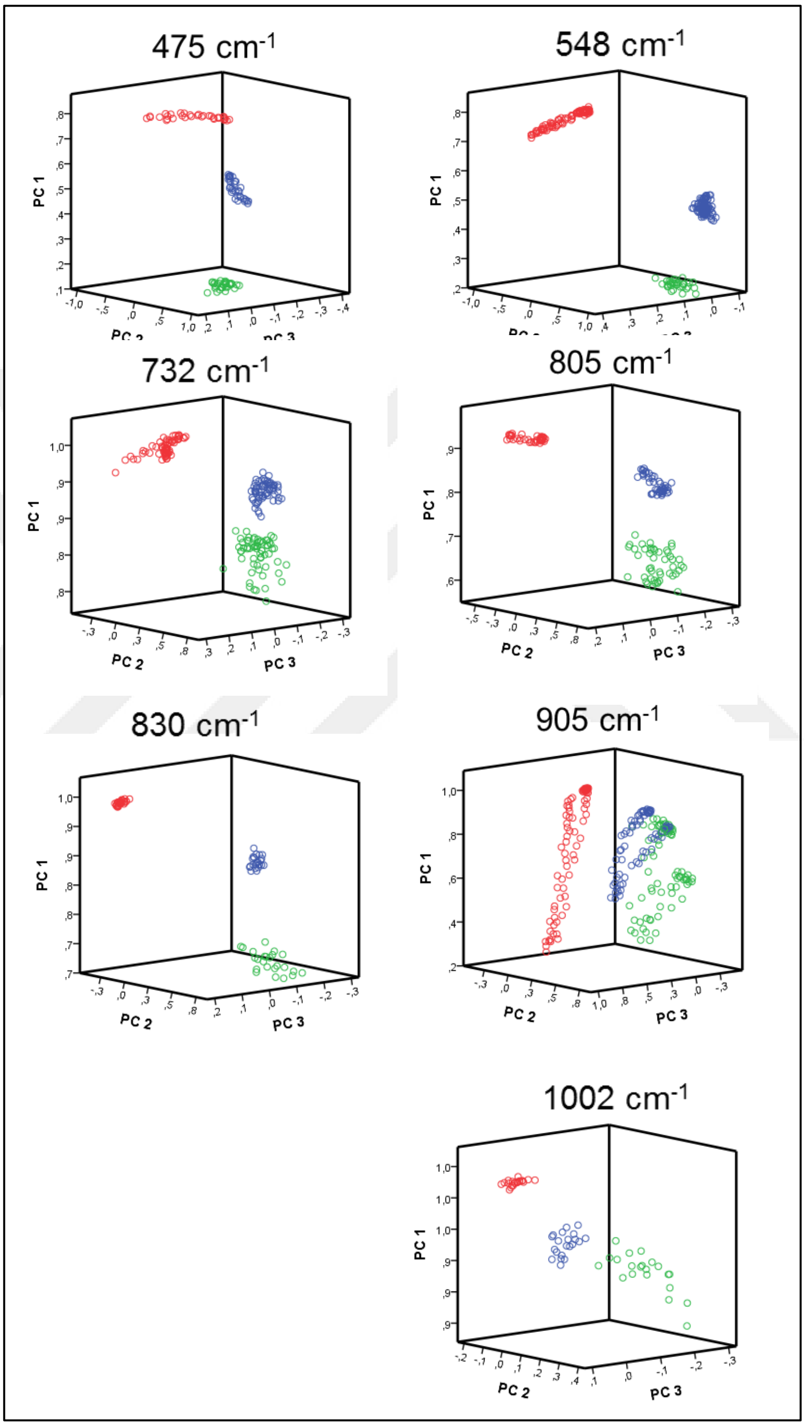

Figure 4.63. 3-D PCA scatter plot belongs to SERS bands at 475, 548, 732, 805, 830, 905, and 1002 cm^{-1}.

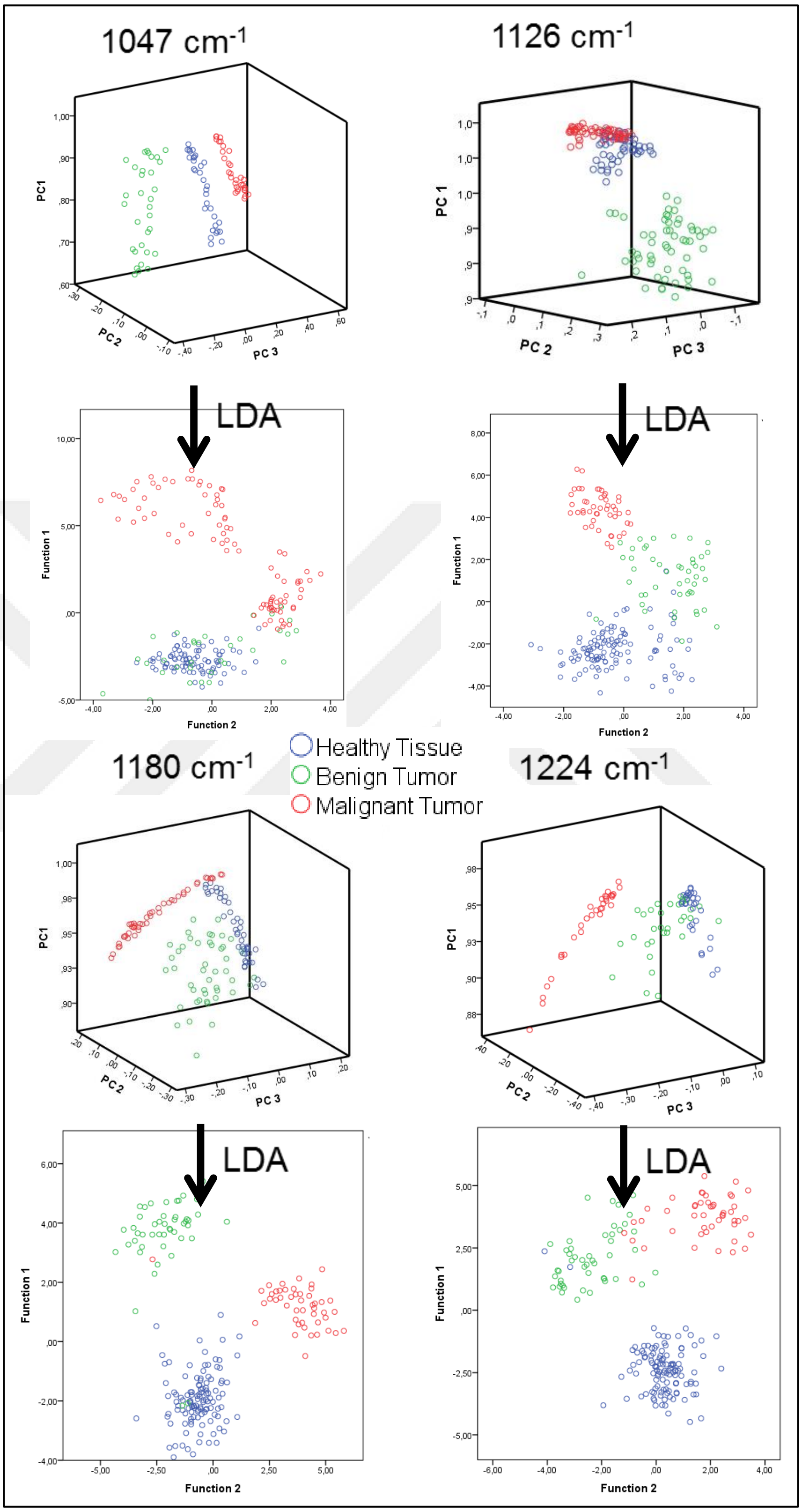

Figure 4.64. 3-D PCA scatter plot belongs to SERS bands at 1047, 1126, 1180 and 1224 cm^{-1}.

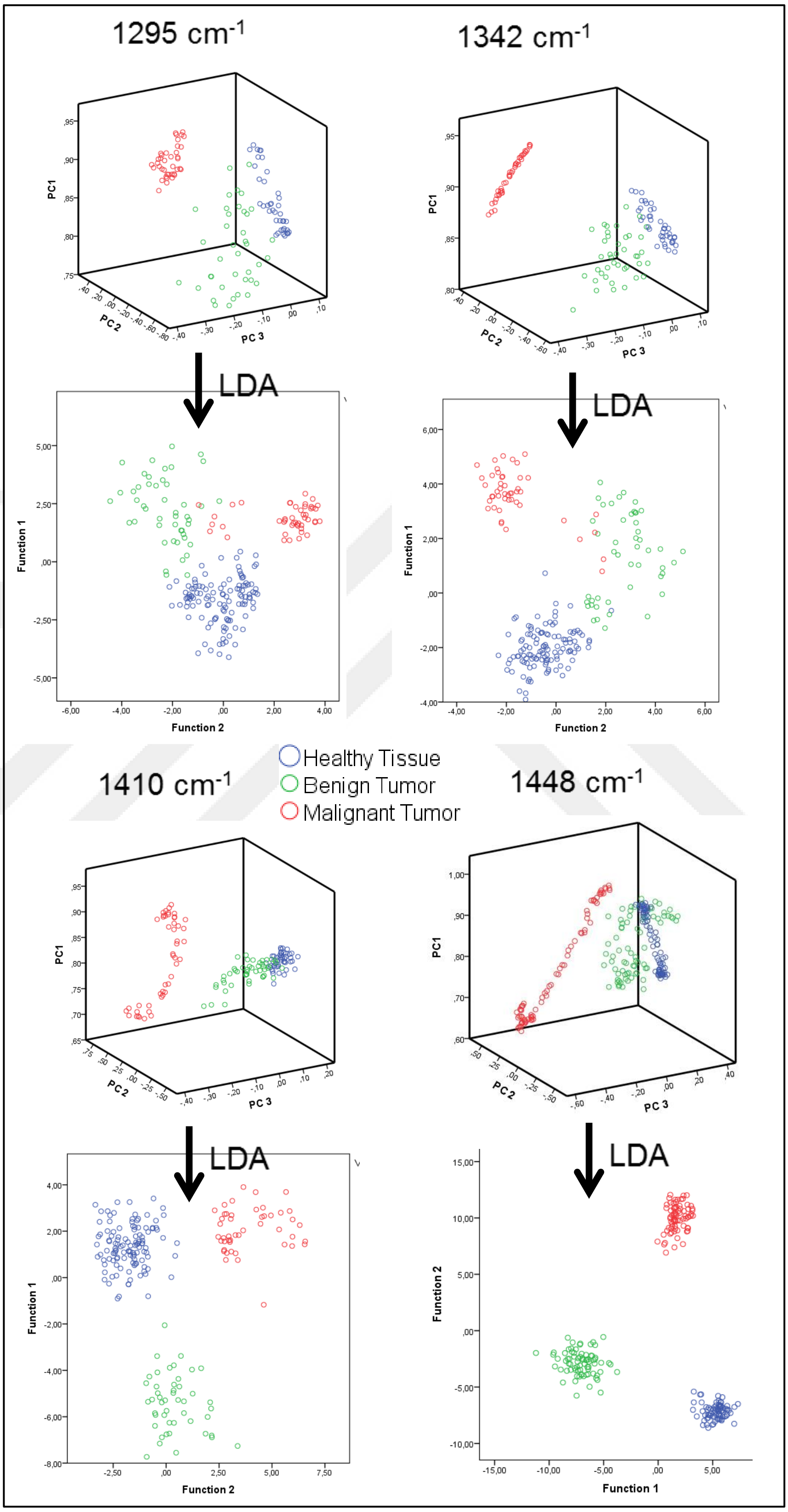

Figure 4.65. 3-D PCA and 2-D LDA scatter plots related to SERS bands at 1295, 1342, 1410 and 1448 cm^{-1}.

The classification of original and cross-validation cases of tumorous and healthy tissues using PC-LDA methods on the SERS data set in the spectral rage of 400 to 1800 cm^{-1}was obtained with the sensitivities of 79 and 79 per cent and the specificities of 70 and 70 per cent, and the accuracy of 73 per cent, and 73, respectively. Thus, the PC components of sigificant SERS bands obtained from the tissue samples was used in PC-LDA classification model to increase the classification accuracy. Table 4.43 shows the performance results after using specific spectra regions belong to the biopsies.

Table 4.43. Probability of predicted classification results obtained using LOO-CV method for tumorous and healthy tissue differentiation.

PCA-LDA Classification Results	**Benign and Malignant Tumors vs. Healthy Tissue**					
Crashed-Liquefied Method	Original Case			Cross-validation Case		
Spectral Range/ Raman bands (cm^{-1})	Sensitivity	Specificity	Accuracy	Sensitivity	Specificity	Accuracy
400-1800	79	70	73	79	70	73
548	100	100	100	100	100	100
732	100	100	100	100	100	100
805	100	100	100	100	100	100
830	100	100	100	100	100	100
905	96	88	93	96	88	93
1002	100	100	100	100	100	100
1047	100	100	100	100	100	100
1126	91	78	86	91	78	86
1180	99	95	97	99	95	97
1224	95	78	88	95	78	88
1295	100	100	100	100	100	100
1342	100	100	100	100	100	100
1410	100	100	100	100	100	100
1448	100	100	100	100	100	100
1578	89	95	91	89	95	91

The PCs of the bands at 548, 732, 805, 830, 1002, 1047, 1295, 1342, 1410 and 1448 cm^{-1} were discriminated with the accuracy of 100 per cent while the tumorous and healthy tissues was classified with the sensitivities of 96, 91, 99, 89 and 95 per cent and the specificities of 88, 78, 95, 95 and 78 per cent, and accuracy of 93, 86, 97, 91 and 88 per cent for the bands at 905, 1126, 1180, 1578 and 1224 cm^{-1}, respectivly.

The two class predictions were also applied for the subgroups of tumorous tissue, benign and malignant, and healthy tissues. Table 4.44 gives the PC-LDA classification results for malignant, benign and healthy tissue biopsy samples performed on the SERS data in the spectral range in which bands at 548, 732, 805, 830, 1002, 1047, 1126, 1180, 1224, 1295, 1342, 1410, 1448 and 1578 cm^{-1}.

The probability of correctly predicted performance of using PC-LDA classification algorithm for differentiation of tumorous and healthy tissues was resulted with the sensitivities of 94, 79 and 100 per cent and the specificities of 79, 71 and 77 per cent, and accuracy of 93, 76 and 91 per cent for by using the SERS data set in spectral range of 582 to 1563 cm^{-1} between benign and malignant; benign and healthy, malignant and healthy, respectively.

The sensitivity, specificity and accuracy of classification results belongs to the healthy tissues and tumor biopsies for each diagnostic combination was obtained 100 per cent using PCs of the bands at 543, 732, 805, 830, 1002 and 1047 cm^{-1}. After REGR factors of SERS bands at 1295, 1342, 1410, 1448 and 1578 cm^{-1} used in PC-LDA algorithms, the benign tumors were well differentiated from the healthy tissues with the diagnostic sensitivity of, 92, 90, 74, 73 and 78 per cent, the specificities of, 100, 100,100, 60 and 95 per cent, and the accuracy of 96, 95, 86, 66 and10 86 per cent, respectively.

Finally, diagnostic combinations of malignant tumors and healthy tissues was classified with the sensitivities of 76 and 91 per cent, the specificities of 83 per cent and 97 per cent, and accuracy of 80 and 94 per cent for the SERS bands at 905 an 1224 cm^{-1}, respectively.

Table 4.44. Predicted values of classification results for malignant, benign and healthy tissues using PC-LDA algorithms.

		Crashed-Liquefied Method								
	Raman Bands (cm^{-1})	**Malignant Tumor**	**Surrounding (Healthy) Tissue**		**Sensitivity % (SN)** **Specificity % (SP)** **Accuracy % (AC)**	**Surrounding (Healthy) Tissue**		**Malignant Tumor**	Raman Bands (cm^{-1})	
Benign Tumor	(400-1800)	**94**	**79**	**100**	SN	100	100	**76**	1126	**Benign Tumor**
		91	**71**	**77**	SP	100	100	**83**		
		93	**76**	**91**	AC	100	100	**80**		
	548	100	100	100	SN	100	100	**91**	1180	
		100	100	100	SP	100	100	**97**		
		100	100	100	AC	100	100	**94**		
	732	100	100	100	SN	100	**75**	100	1224	
		100	100	100	SP	100	**90**	100		
		100	100	100	AC	100	**82**	100		
	805	100	100	100	SN	100	**92**	100	1295	
		100	100	100	SP	100	**100**	100		
		100	100	100	AC	100	**96**	100		
	830	100	100	100	SN	100	**90**	100	1342	
		100	100	100	SP	100	**100**	100		
		100	100	100	AC	100	**95**	100		
	905	100	88	100	SN	100	**74**	100	1410	
		100	93	100	SP	100	**100**	100		
		100	90	100	AC	100	**86**	100		
	1002	100	100	100	SN	100	**73**	100	1448	
		100	100	100	SP	100	**60**	100		
		100	100	100	AC	100	**66**	100		
	1047	100	100	100	SN	100	**78**	100	1578	
		100	100	100	SP	100	**95**	100		
		100	100	100	AC	100	**86**	100		
			Benign Tumor	**Malignant Tumor**		**Benign Tumor**	**Malignant Tumor**			

4.5. COMPARISON OF METHODS

The two developed SERS-based cancer diagnosis methods, Cryosectioned-PDMS, *in situ*, were compared to the previously developed method of Crashed-liquefied.

4.5.1. Intra-and Inter Method Reproducibility

The spot-to-spot variations were obtained with the maximum difference between 5 and 11 per cent, 3 and 10 percent and 20 and 25 per cent while sample-to-sample variations were between 2 and 4 per cent, 3 and 4 per cent and 20 and 25 per cent for Cryosectioned-PDMS, *in situ* and Crashed-liquefied method, respectively, are presented in Table 4.45.

Table 4.45. CV values for three types of sampling method [152].

Methods	**Averaged CV Values**	
	Spot-to-Spot	**Sample-to-Sample**
Cryosectioned-PDMS	5-11	2-4
in situ	3-10	3-4
Crashed-Liquefied	20-25	20-25

The CV values for the developed methods are quite lower than the previous tissue sampling method. The CV values between 3 and 10 per cent, and 5 and 11 per cent demonstrate that CV values of SERS measurements are quite low among the spots which indicates the high intra-method reproducibility of *in situ* and Cryosectioned-PDMS methods. Moreover, the CV values between 3 and 4, and 2 and 4, which shows the sample-to-sample variation is quite low for the methods of *in situ* and Cryosectioned-PDMS, respectively, pointing to high inter-method reproducibility of *in situ* and Cryosectioned-PDMS methods .

4.5.2. A Preliminary Study

The methods with the optimized parameters were applied on a benign thyroid tumor and healthy tissue surrounding the tumor. The diagnosis of benign tumors is also parallel with the aim of this thesis study because benign tumors, which are the non-cancerous abnormal growth but have a potential to become malignant. However, this preliminary comparison study of the new developed sampling methods with Crashed-liquefied method mainly focused on method dependent PC-LDA classification accuracy and spectral patterns due to the differences in bringing tissue components together with the SERS active substrates. All sampling methods were evaluated for PC-LDA model performance testing.

4.5.2.1. Method Dependent PC-LDA Classification

The spectra obtained by using *in situ* approach were used in PCA method. The nineteen PCs were extracted using the factor analysis to reduce the spectral dimension (d=1715). The first five PCs including 80.40 per cent of the variance were used in PCA classification algorithm as detailed in Table 4.46. Then, the PCA and LDA scatter plot of PCs constructed from the spectra of benign tumor and healthy tissue were obtained as shown in Figure 4.66.

Table 4.46. Eigenvalues and the percentage of explained variation of PCs.

PC	Eigenvalue	Explained Variation %
1st PC	5.61E+01	56.07
2nd PC	6.87E+01	68.67
3rd PC	7.57E+01	75.71
4th PC	8.04E+01	80.4
5th PC	1.81E+00	83.41

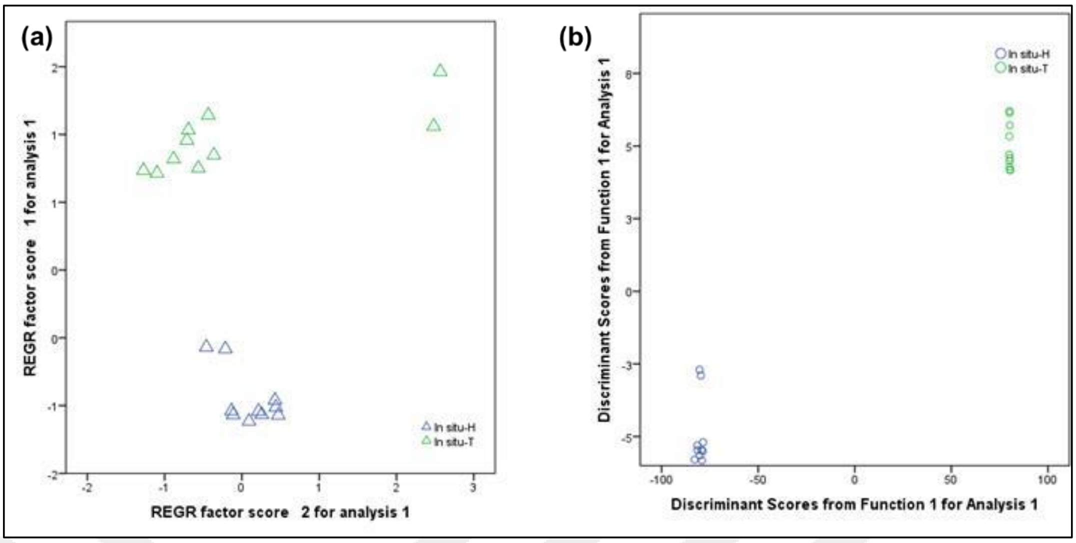

Figure 4.66. 2-D PCA and LDA scatter plots constructed from the spectra acquired from benign tumor and healthy tissue.

The clustering differences from the scatter plots are clear. LDA provided an increased classification of the groups within variables. The classification accuracy was obtained as 100 per cent to differentiate healthy and benign tumor tissues.

The method of Crashed-liquefied was also applied on the benign and healthy tissues. Spectral dimension (d=1715) were reduced to twenty three PCs extracted by using the factor analysis. First five PCs including 73.51 per cent of the variance was used in PCA classification algorithms as detailed in Table 4.47.

Table 4.47. Eigenvalues and the percentage of explained variation of PCs.

PC	**Eigenvalue**	**Explained Variation %**
1st PC	2.95E+01	29.51
2nd PC	4.92E+01	49.20
3rd PC	6.10E+01	61.01
4th PC	6.80E+01	67.97
5th PC	7.35E+01	73.51

Then, the PCA and LDA scatter plot of PCs related to the SERS spectra of benign and healhyt tissue were obtained as shown in Figure 4.67.

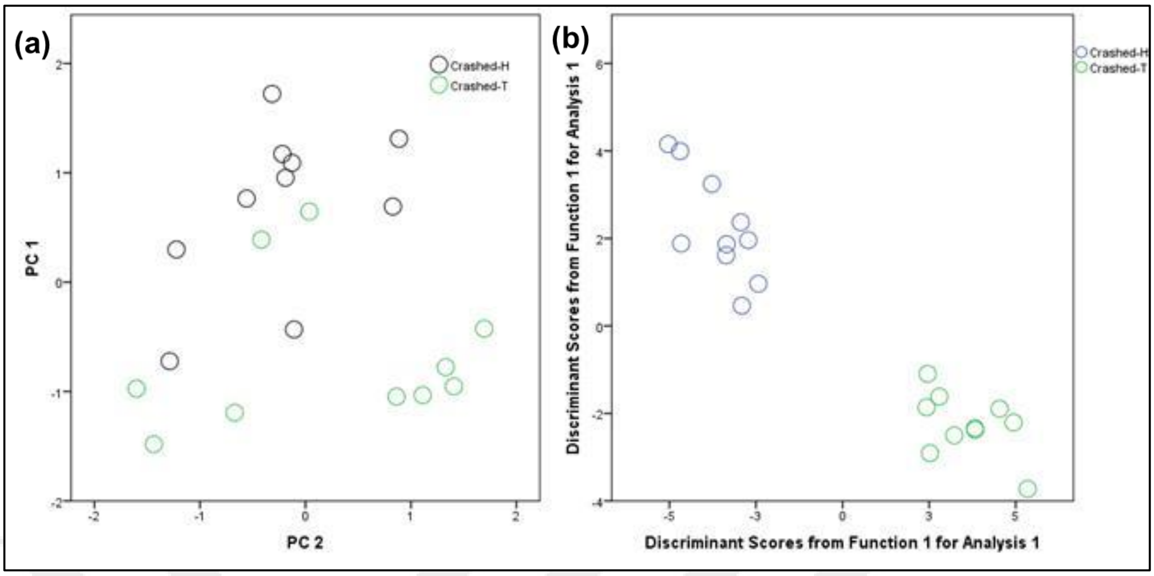

Figure 4.67. 2-D PCA and LDA scatter plots constructed from SERS spectra acquired from benign tumor and healthy tissue.

The clusters in the PCA scatter plot was not separated well but the clusters were classified well in LDA scatter plot. Finally, the Cryosectioned-PDMS method was applied to the tissue samples. The thirteen PCs were extracted using the factor analysis to reduce the spectral dimension. First, the two PC components including 91.59 per cent of the variance were used in PCA classification algorithms as detailed in Table 4.48. Then, the PCA and LDA scatter plot of two PC components were obtained as shown in Figure 4.68.

Table 4.48. Eigenvalues and the percentage of explained variation of PCs.

PC	**Eigenvalue**	**Explained Variation %**
1st PC	7.23E+01	72.32
2nd PC	9.16E+01	91.59

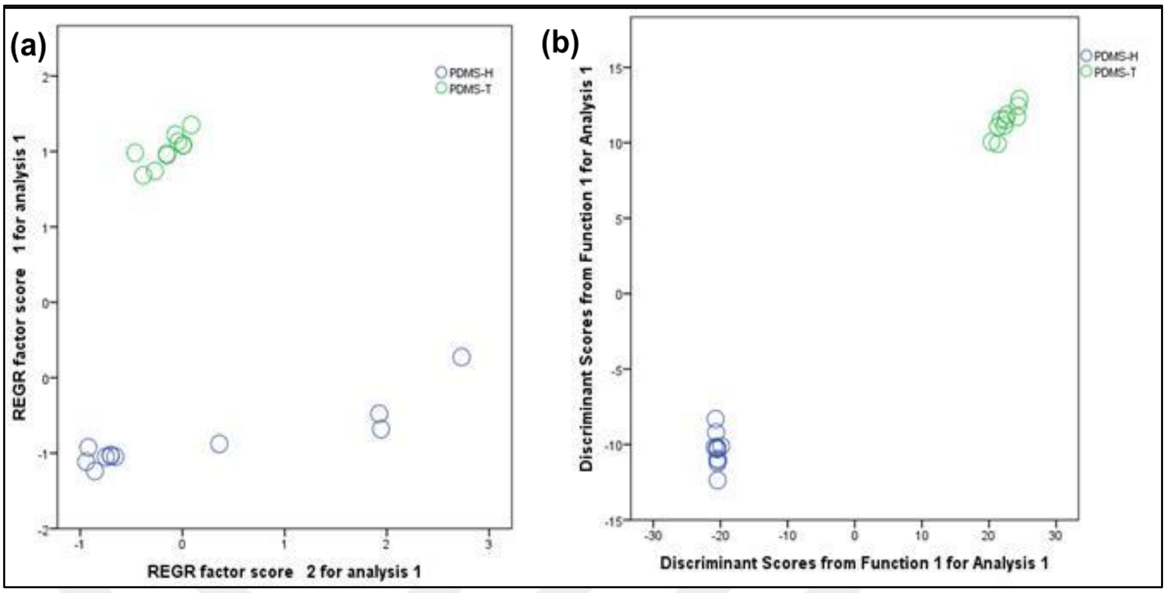

Figure 4.68**.** 2-D PCA and LDA scatter plots constructed from SERS spectra acquired from benign tumor and healthy tissue.

Finally, the performance measurements were obtained using PC-LDA classification algorithms with LOO-CV method in the spectra obtained by using three methods of *in situ*, Cryosectioned-PDMS and Crashed-liquefied as shown in Table 4.49.

Tablo 4.49. Classification performance of PCA and PC-LDA models for each approach.

METHOD	**PCA**	**LDA**		
		Sensitivity %	**Specificity %**	**Accuracy %**
in situ	Well grouped	100/100	100/100	100/100
Cryosectioned-PDMS	Well grouped	100/100	100/100	100/100
Crashed-Liquefied	Not well grouped	100/100	100/100	100/100

While the PC components belong to the methods of *in situ* and Cryosectioned-PDMS were well separated in PCA scatter plot, the variables obtained by using Crashed-liquefied method were not well seperetad, which means the difference in the variables were not significant as well as the results obtained by other methods. On the other hand, LDA algorithm provided a well clustering with the sensitivity, specificty and accuracy of 100 per cent for each method. Finally, the methods were compared based on their spectral patterns.

4.5.2.2. Method Dependent SERS Spectral Patterns

The differences in the patterns of the spectra obtained by using each approach also need to be evaluated. Even though the experimental optimization were employed for each method, the spectra were collected from three spots on the sample surface in this preliminary investigation to increase the reliability of the differences in the band locations and intensities which could be attributed to the key challenge of SERS signal reproducibility due to the chaotic distribution of the AgNPs in the sample. The mean spectra of benign and healthy tissues were calculated from the three mean spectra of the spots, and the calculated mean spectra belongs to tissue are given in Figure 4.69 with the mean spectra of each spot as a comparison for the *in situ* appoach. The shadow area in the mean spectra (d) shows the deviations between three mean spectra (a-c) obtained from the spots.

The spectral pattern is similar for each tissue type but has differences in the intensity of the bands. This might be due to differences in the formation of analyte-AgNPs complex and AgNPs aggregates, and the heterogeneity of the tissue structure. Then, the mean spectra were calculated from the three mean spectra obtained from the spots.

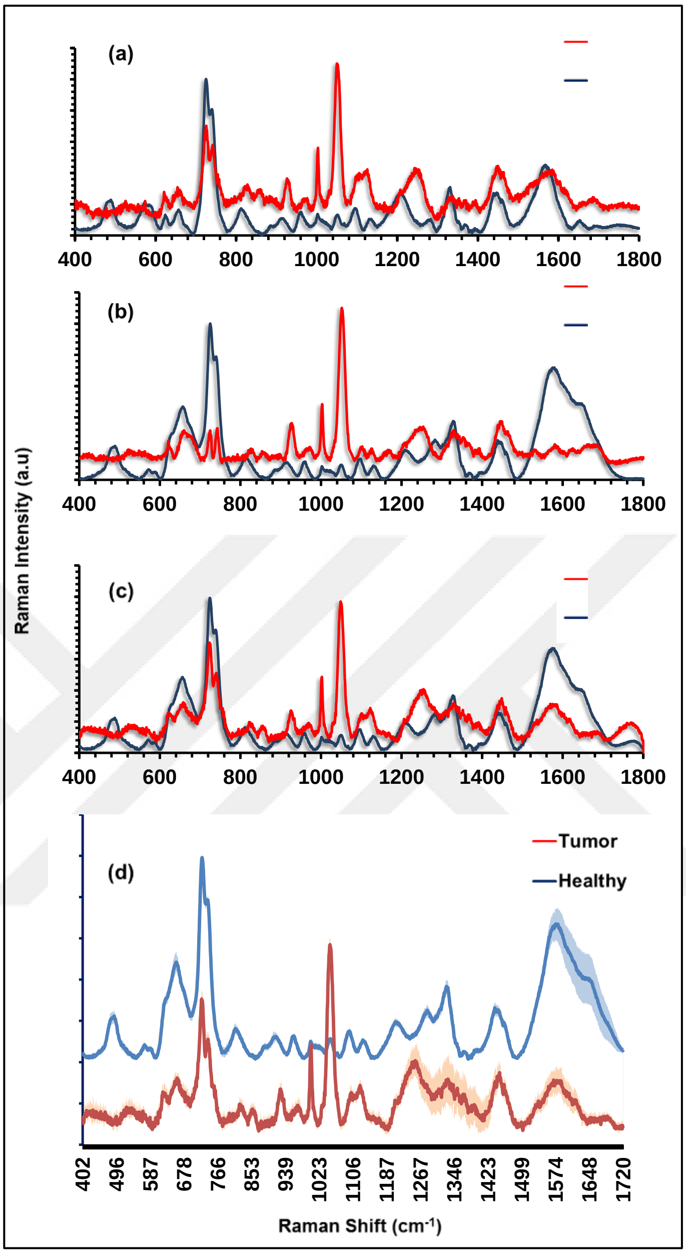

Figure 4.69. Mean SERS spectra of benign tumor and healthy tissue obtained from three spots (a-c), and their mean spectra (d) using *in situ* method.

The final mean spectra of benign and healthy tissues obtained from the Crashed-liquefied method are given in Figure 4.70.As seen in the figure, the increased standard deviation in the spectra between the 400 and 500 cm^{-1} range could be attributed to the applied intelligent fitting baseline correction because there were no observable peaks in the 400 to 500 cm^{-1} region in the mean spectra of the tumorous tissues. This indicates to why the raw data instead of pre-processing with baseline correction and smoothing needs to be used in the classification models. However, if the data is quite noisy to understand the band characteristics of the spectra, it would be better to use the process of baseline correction, smoothing and noisy reduction. Intelligent fitting of WIRE 4.1 software was progressed by cropping the original signal under a given polynomial order; a suitable polynomial is obtained by fitting the original signal with the least squares criterion [163].

Finally, the Cryosectioned-PDMS method was applied to the thyroid benign tumor and healthy tissue samples. The mean spectra of each spot and the mean spectra calculated from those are illustrated in Figure 4.71.

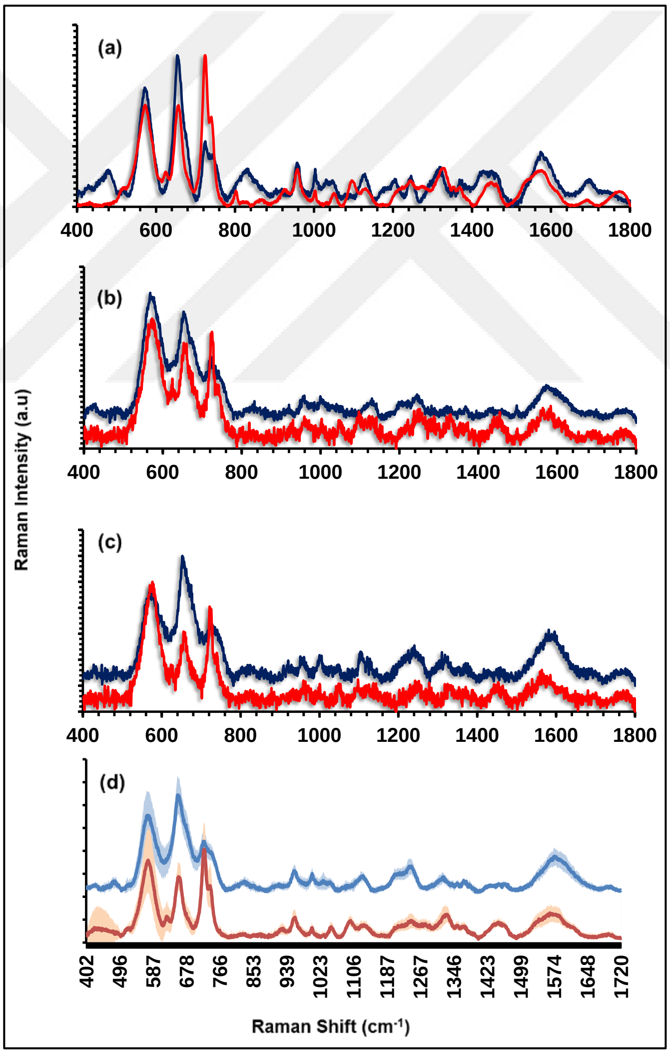

Figure 4.70. Mean spectra of benign tumor and healthy tissue specimen of three spots (a-c), and their mean spectra (d) using Crashed-liquefied method. The shadowed area in the spectra shows the deviations of the intensities related to the mean spectra of the spots.

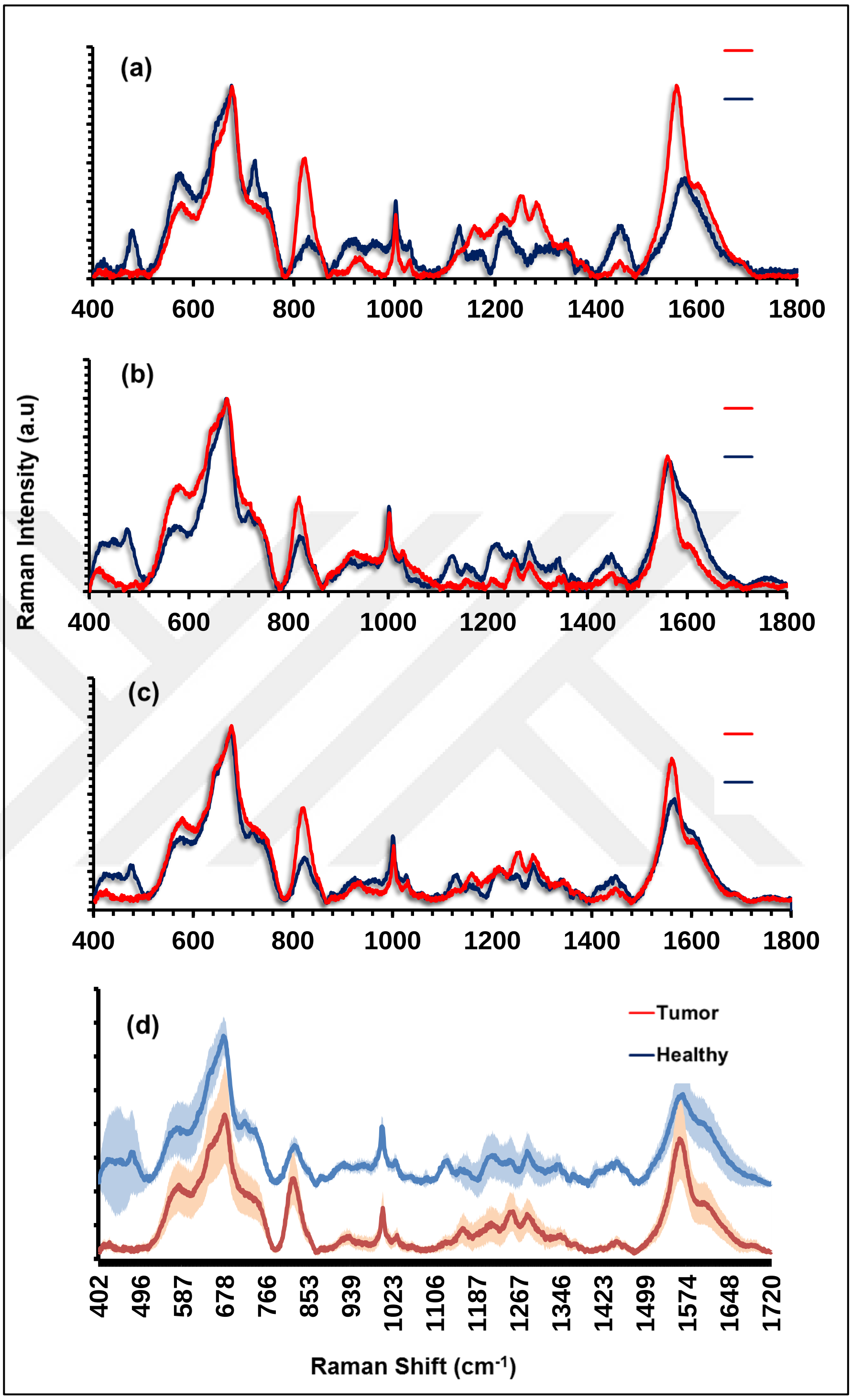

Figure 4.71. Mean spectra of benign tumor and healthy tissue specimen of three spots (a-c), and their mean spectra (d) using Cryosectioned- PDMS method. The shadow area in the spectra shows the deviations of intensities among the mean spectra of each spot.

A similar increased standart deviation was observed in the same region that was probably due to the same reason related to the diffences in the spectral pattern intensity and shape in the spetrum of healhty tissue and benign tumor. The mean spectra of the benign tumor and healthy tissue utilized with each sampling method are given as a comparison in Figure 4.72.

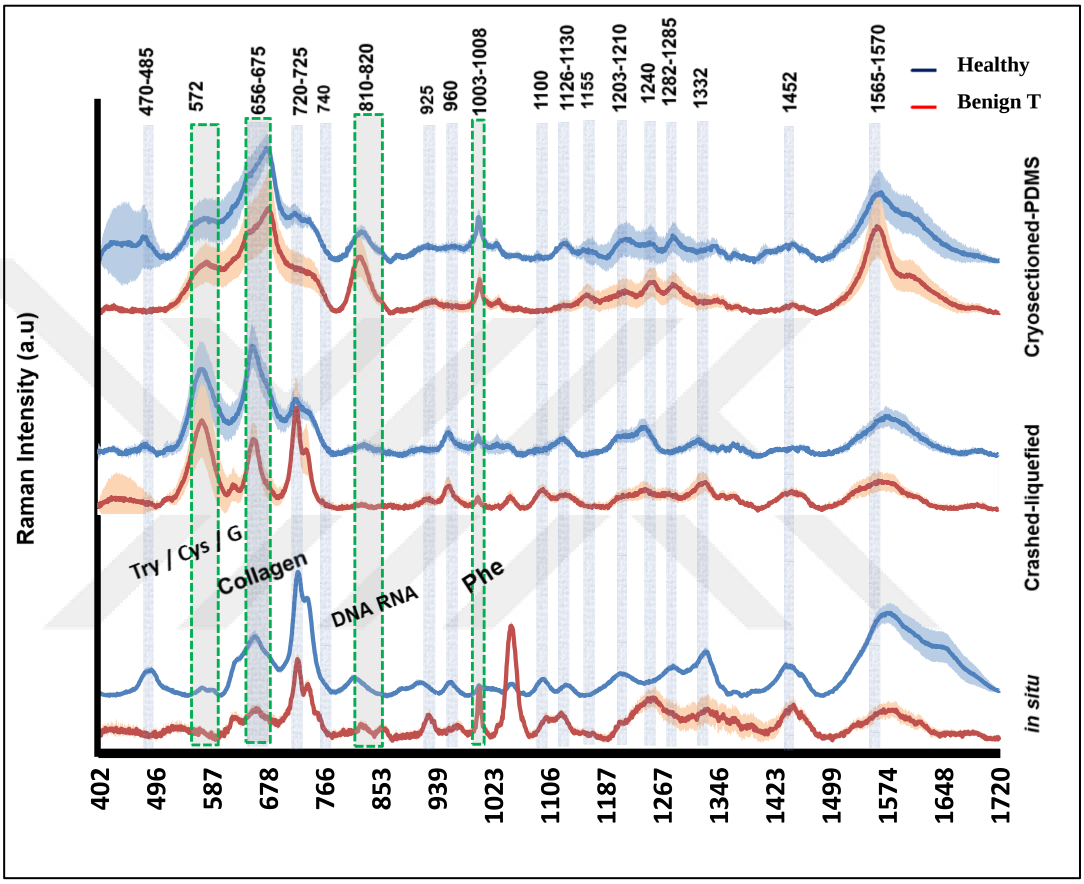

Figure 4.72. Mean spectra of benign tumor and healthy tissue as a comparison.

The four SERS bands at 572, 656, 810 and 1003 cm^{-1} were significantly different than the other bands compared to the column plotted against the band intensities. They can probably be assigned to tyrosine, cystein or guanine for 572 cm^{-1}, collagen for 656-675 cm^{-1}, DNA/RNA for 810-820 cm^{-1}, and phenyalanine for 1003-1008 cm^{-1} [33, 130, 147]. Then, total of the twenty-five prominent SERS bands, twelve of them were common for each method were obtained from benign tumor and surrounding (healthy) tissues, and the band intensity column plots related to three mean spectra for each sampling method are illustrated in Figure 4.73 to 4.75.

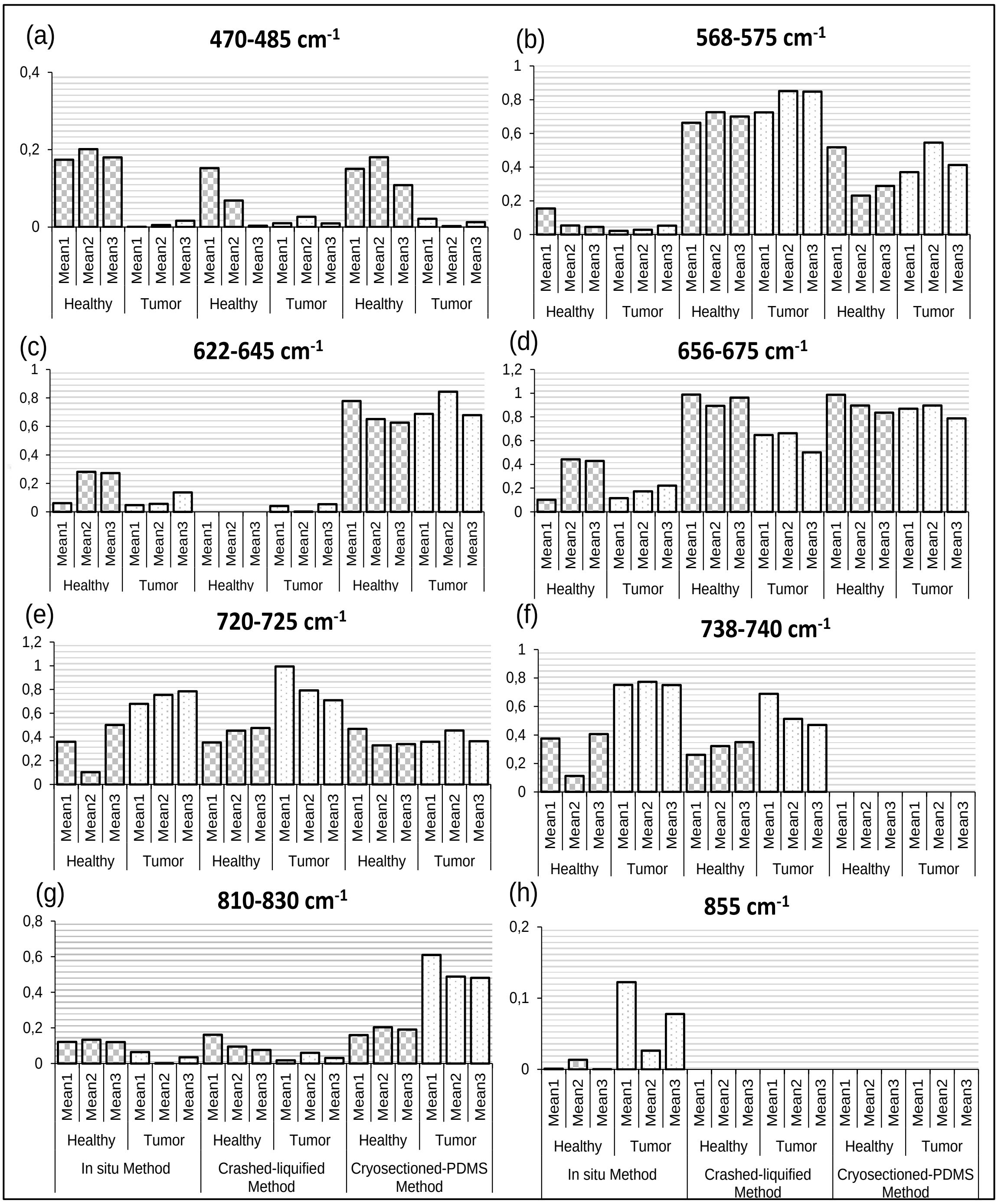

Figure 4.73 .Column plots of the SERS band intensities in the spectral region of 470-485 cm^{-1} (a), 568-575 cm^{-1} (b), 622-645 cm^{-1} (c), 656-675 cm^{-1} (d), 720-725 cm^{-1} (e), 738-740 cm^{-1} (f), 810-830 cm^{-1} (g) and 855 cm^{-1} (h).

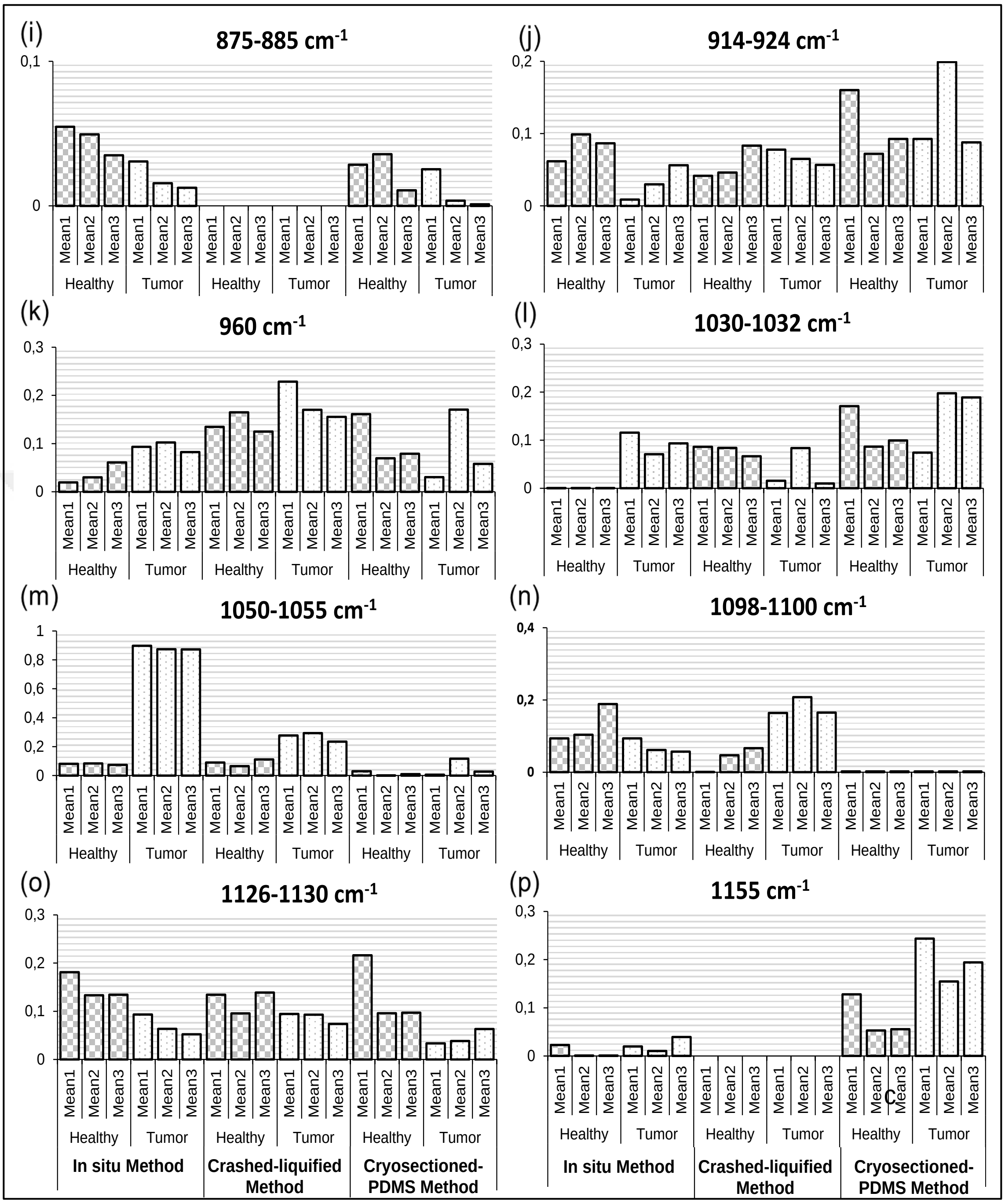

Figure 4.74. Column plots of the SERS band intensities in the spectral region of 875-885 cm^{-1} (i),914-924 cm^{-1} (j), 960 cm^{-1} (k), 1030-1032 cm^{-1} (l), 1055-1055 cm^{-1} (m), 1098-1100 cm^{-1} (n), 1126-1130 cm^{-1} (o) and 1155 cm^{-1} (p).

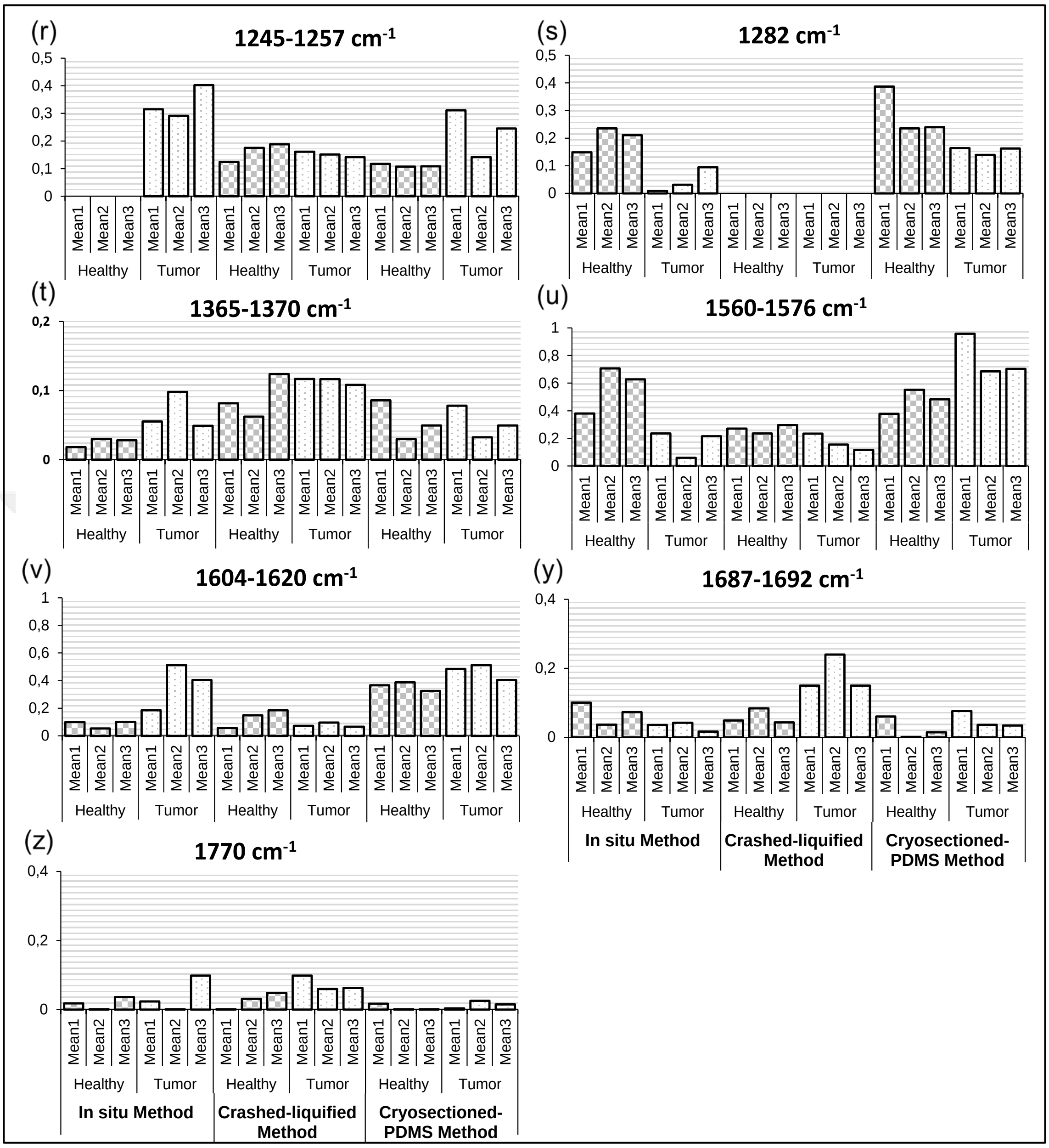

Figure 4.75.Column plots of the SERS band intensities in the spectral region of 1245-1257 cm^{-1} (r), 1282 cm^{-1} (s), 1365-1370 cm^{-1} (t), 1560-1576 cm^{-1} (u), 1604-1620 cm^{-1} (v), 1687-1692 cm^{-1} (y) and 1770 cm^{-1} (z).

It should be noted that prominant SERS bands located in the spectral region of 470 to 485, 656 to 675, 720 to725, 738 to 740, 875 to 885, 1003 to 1008, 1050 to 1055, 1126 to 1130, 1155, 1203 to 1210, 1282 to 1285, 1604 to 1620 cm^{-1} were commonly observed on the spectra of benign and healthy tissues studied with each approach. Although one spot spectra collection was enough for the optimized conditions of each approach, the spectra were collected from three different spots in this preliminary comparison study of three methods. The band intenstiy differences were obtained more for the *in situ* method compared to other methods that means the increased variations between the variables may provide high classification accuracy. However, it should be noted that this was a preliminary study performed by three methods after their optimizations. It could be used as a preliminary model study of possible SERS-biomarkers for diagnosis of benign tumor and healthy tissues. The extensive study to compare each method was obtained with sixty four thyroid tissues.

4.5.3. An Extensive Study

Each approach method was applied on thyroid tumor biopsies and healthy tissues. Each approach was compared by their spectral pattern, classification accuracy by using PC-LDA diagnostic model and method reproducibility. The common prominent bands which are presented in each method were determined to compare the classification accuracy related to these bands.

4.5.3.1. Method Dependent SERS Spectral Patterns

PC loading vectors were extracted performing PCA algorithm on the high dimensional spectral data. The loading plots explain the significant variances in the SERS data including the spectra obtained from malignant, benign and healthy tissues (64 biopsies). The significant variations were in the bands at 667, 724, 740, 760, 854, 920, 960, 1008, 1052, 1096, 1180, 1210, 1280, 1295, 1315, 1334, 1385, 1415, 1435, 1457 and 1506 cm^{-1} for Cryosectioned-PDMS method; 425, 610, 675, 687, 1005, 1058, 1100, 1170, 1278, 1397, 1452, 1536 and 1656 cm^{-1} for *in situ* method, and 548, 732, 805, 830, 1002, 1047, 1126, 1180, 1224, 1295, 1342, 1410, 1448 and 1578 cm^{-1} for the Crashed-liquefied method. The total of 21, 13, and 14 number of characteristic bands originated from the biopsies was obtained for the sampling methods of Cryosectioned-PDMS, *in situ* and Crashed-liquefied, respectively. The spectra related to Cryosectioned-PDMS method has the richest spectral pattern compared to other methods. The commonly observed SERS bands from three methods are given in Table.4.50 as a comparison.

Table 4.50. Common SERS bands in the methods.

<table>
<tr><th></th><th>Crashed-Liquefied</th><th>Cryosectioned-PDMS</th><th><i>in situ</i></th><th>Crashed-Liquefied</th></tr>
<tr><td rowspan="12">Raman Bands (cm-^{1})</td><td></td><td colspan="2">667-675</td><td></td></tr>
<tr><td colspan="2">724-732</td><td></td><td></td></tr>
<tr><td></td><td colspan="2">854-860</td><td></td></tr>
<tr><td colspan="3">1002-1008</td><td></td></tr>
<tr><td colspan="3">1044-1058</td><td></td></tr>
<tr><td></td><td colspan="2">1096-1100</td><td></td></tr>
<tr><td colspan="3">1170-1180</td><td></td></tr>
<tr><td colspan="3">1278-1295</td><td></td></tr>
<tr><td colspan="2">1334-1342</td><td></td><td></td></tr>
<tr><td></td><td colspan="2">1382-1385</td><td></td></tr>
<tr><td></td><td></td><td colspan="2">1397-1410</td></tr>
<tr><td></td><td></td><td colspan="2">1448-1452</td></tr>
</table>

The bands in the spectral range of 667 to 675 cm^{-1}, 854 to 860 cm^{-1}, 1096 to 1100cm^{-1} and 1382 to 1385 cm^{-1} can be assigned to C-S stretch frequencies of the cysteine residue in proteins, C-C backbone stretching vibrations, C-N stretch of lipids, and symmetric CH_3 stretching vibration of lipids, respectively, were obtained both in the use of Cryosectioned-PDMS and *in situ* method [145, 146].

SERS bands in the region of 724 to 732 cm^{-1} and 1334 to 1342 cm^{-1} can be assigned to ring breathing mode of DNA and RNA bases, and CH_3CH_2 wagging mode of collagen & polynucleotidechain (DNA purine bases), respectively, for the Crashed-liquefied and Cryosectioned-PDMS method [63, 147].

The major SERS bands in the region of 1397 to 1410 cm^{-1}, assigned to CH_2 deformation and the ester linkage C=O stretching vibrations in lipids and 1448 to 1452 cm^{-1}, assigned to CH_2 deformation in lipids, were acquired by using Crashed-liquefied and *in situ* methods [33, 47].

SERS bands in the region of 1002 to 1008 cm^{-1}, 1044 to 1058 cm^{-1}, 1170 to 1180 cm^{-1}, 1278 to 1295 cm^{-1}, can be attributed to Phenylalanine, C-O stretching vibrations in protein, Tyrosine, and Amide III, respectively, were acquired common in the use of each method [59, 130, 145, 147]. Figure 4.76 shows the spectral relativeness of the common prominent bands obtained by using three approaches.

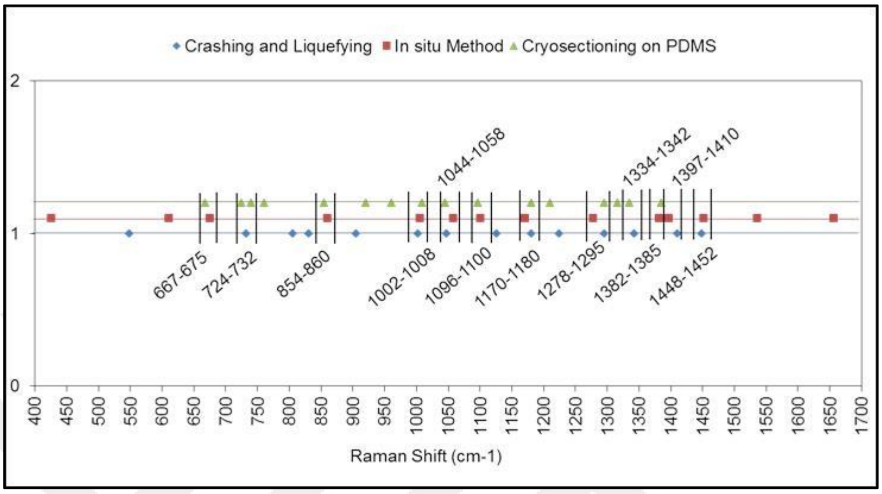

Figure 4.76. Common spectral bands on the spectra of tissues obtained with both approaches.

From the results, the method of Cryosectioning-PDMS and *in situ* had two more different bands, which were not appeared in the spectra obtained by using the Crashed-liquefied method.

The differences in the spectral pattern (band position/ band intensity) are probably related to using different tissue sampling methods, mechanical homogenization of snap-frozen tissue (Crashed-liquefied method), cryosectioning tissue specimen (Cryosectioned-PDMS method), and ultrasonic homogenization of tissue specimen (*in situ* method), affecting the interaction of the intra- and extra-cellular components in the tissue sample with the SERS active substrates. The differences in the SERS band intensities could be related to the concentration of the assigned biomolecule or/with the chaotic distribution of AgNPs on the tissue surface and in the homogenized tissue specimen.

It is clear that the best approach is expected to have the following properties; high reproducibility, rich spectral pattern, low cost, minimal sample preparation steps and high classification accuracy. Thus, the developed methods were compared using these parameters. The spot-to-spot variations were obtained with the maximum difference between the 5 and 11 per cent, 3 and 10 percent and 20 and 25 per cent while sample-to-sample variations were 2 and 4 per cent, 3 and 4 per cent and 20 and 25 per cent for Cryosectioned-PDMS, *in situ* and Crashed-liquefied method, respectively. Cryosectioned-PDMS and *in situ* has fairly equal benefits with close CV values indicating higher inter-method reproducibility. However, all methods are similar from the point of minimal sample preparation but Cryosectioned-PDMS method requires a qualified person with cryostat sectioning.

4.5.3.2. Method Dependent PC-LDA Classification

The PC-LDA classification model was applied on the data obtained from the three approaches. The diagnostic algorithm of PC-LDA was performed on the data both in full spectra region and specific region having characteristic features related to the tissue specimen. The validation of the multi-class diagnostic algorithm was calculated by LOO-CV method. The comparison among the predicted classification results for differentiation of malignant, benign and healthy tissue of three approaches are shown in Table 4.51.

The predicted classification was based on testing one point data while the others were used in the training test (LOO-CV). The healthy and disease tissues (benign and malignant tumor) were classified according to their coefficients in the factors extracted by using PCA algorithm performed on the spectral data. The probability of correctly predicted performance of using multi-class PC-LDA diagnostic algorithm for classifying healthy tissues versus benign and malignant were resulted with the sensitivities of 94, 79 and 100 per cent and the specificities of 79, 71 and 77 per cent, and accuracy of 93, 76 and 91 per cent for by using the data set in spectral range of 582 to 1563 cm^{-1} for the Cryosectioned-PDMS approach. In addition, the diagnosis of multiple tissue types was obtained same as the predicted performance of PC-LDA model performed on the data obtained by using Crashed-Liquefied approach. However, the probability of correctly predicted performance was resulted with the sensitivities of 94 per cent, 92 per cent and 100 per cent and the specificities of 79 per cent, 88 per cent and 99 per cent, and accuracy of 87, 91 and 100 per cent for the *in situ* approach.

Table 4.51. Comparison of the predicted classification performance of PC-LDA diagnostic model for healthy versus disease tissues (benign and malignant).

Cryosectioned-PDMS				Total Spectra=Sample number x Averaged Spectrum
Count	Healthy	Benign	Malignant	
Healthy	22	6	3	31
Benign	6	15	1	22
Malignant	0	1	10	11
Healthy	**71**	19,4	9,7	100
Benign	27,3	**68,2**	4,5	100
Malignant	0	9,1	**90,9**	100
Cross Validation Results		Sensitivity %	Specificity %	Accuracy %
Healthy vs Benign and Malignant		**79**	**70**	73
in situ				Total Spectra=Sample number x Ten Spectra
Count	Healthy	Benign	Malignant	
Healthy	293	22	1	316
Benign	28	141	42	211
Malignant	0	12	97	109
Healthy	**92,7**	7	0,3	100
Benign	13,3	**66,8**	19,9	100
Malignant	0	11	**89**	100
Cross Validation Results		Sensitivity %	Specificity %	Accuracy %
Healthy vs Benign and Malignant		**92**	**81**	**87**
Crashed-Liquefied				Total Spectra=Sample number x Averaged Spectrum
Count	Healthy	Benign	Malignant	
Healthy	22	6	3	31
Benign	6	15	1	22
Malignant	0	1	10	11
Healthy	**71**	19,4	9,7	100
Benign	27,3	**68,2**	4,5	100
Malignant	0	9,1	**90,9**	100
Cross Validation Results		Sensitivity %	Specificity %	Accuracy %
Healthy vs Benign and Malignant		**79**	**70**	**73**

Two-class model of PC-LDA were performed on the spectra of healthy, benign and malignant tissues. The predicted grouping results of the diagnostic algorithm by using LOO-CV were calculated for two cluster differentiating as benign vs. healthy, healthy vs. malignant, and benign vs. malignant. The performance values were detailed in Table 4.52. The obtained results indicated that the best clustering was obtained by using the data of the *in situ* approach for classifying healthy vs. malignant tissue with the sensitivity of 100, specificity of 99 and accuracy of 100 per cent. In addition, the *in situ* has the best classification performance for healthy vs. benign tissue diagnosis, which is the sensitivity of 92, specificity of 88, and accuracy of 91 per cent. However, benign vs. malignant differentiating was obtained with the sensitivity of 94, specificity of 91, and accuracy of 93 per cent which is higher in the performance results for the Cryosectioned-PDMS and Crashed-liquefied compared to the *in situ*. Two-class diagnostic classification model was also applied on the specific spectra regions related to the prominent SERS bands for each approach. The detailed performance results are given in Table 4.53. The predicted classifications related to the PC components of SERS bands at 740 and 1385 cm^{-1} for benign and malignant tumors, and malignant tumors and healthy tissues were resulted with the accuracy of 97 and 97 per cent, respectively, for the Cryosectioned-PDMS method. On the other hand, the PCs related to the other bands were differentiated with the sensitivity, specificity and accuracy of 100 per cent for malignant and benign tumors with healthy tissues.

There are eight diagnostic combinations classified with the accuracy under 100 per cent in the range of 87 to 98 per cent using *in situ* based approach while Cryosectioned-PDMS has two with the accuracy of 97 per cent. Benign versus healthy tissues were classified based on the bands at 675, 860, 1058, 1100, and 1397cm^{-1} with the accuracy of 87, 99, 97, 98, and 99 per cent, respectively while benign versus malignant tumors were differentiated with the accuracy of 97 and 99 per cent for 675 and 1278 cm^{-1}, respectively. Malignant tumors and healthy tissues were classified with the accuracy of 93 per cent for the band at 1656 cm^{-1}.

Table 4.52. Comparison of the performance of two-group based classification of PC-LDA model with LOO-CV.

Cryosectioned-PDMS				***in situ***				**Crashed-Liquefied**			
Count	Healthy	Benign	Malignant	Count	Healthy	Benign	Malignant	Count	Healthy	Benign	Malignant
Healthy	22	6	3	Healthy	294	21	1	Healthy	22	6	3
Benign	6	15	1	Benign	25	159	27	Benign	6	15	1
Malignant	0	1	10	Malignant	0	10	99	Malignant	0	1	10
Sensitivity % (SN)	Healthy	79	100	Sensitivity % (SN)	Healthy	**92**	**100**	Sensitivity % (SN)	Healthy	79	**100**
Specificity % (SP)		71	77	Specificity % (SP)		**88**	**99**	Specificity % (SP)		71	77
Accuracy % (AC)		76	91	Accuracy % (AC)		**91**	**100**	Accuracy % (AC)		76	91
%	SN	Benign	**94**	%	SN	Benign	94	%	SN	Benign	**94**
	SP		**91**		SP		79		SP		**91**
	AC		**93**		AC		87		AC		**93**

Table 4.53. Performance results under the accuracy of 100 per cent by using PC-LDA classification model on the specific spectral regions for each approach.

	Sensitivity % Specificity % Accuracy %	**Crashed-Liquefied**		
	WN	**Malignant**	**Healthy**	
Benign Tumor	(400-1800)	94	79	100
		91	71	77
		93	76	91
	548	100	**88**	100
		100	**93**	100
		100	**90**	100
	1126	100	100	**76**
		100	100	**83**
		100	100	**80**
	1180	100	100	**91**
		100	100	**97**
		100	100	**94**
	1224	100	**75**	100
		100	**90**	100
		100	**82**	100
	1295	100	**92**	100
		100	**100**	100
		100	**96**	100
	1342	100	**90**	100
		100	**100**	100
		100	**95**	100
	1410	100	**74**	100
		100	**100**	100
		100	**86**	100
	1448	100	**73**	100
		100	**60**	100
		100	**66**	100
	1578	100	**78**	100
		100	**95**	100
		100	**86**	100
			Benign	**Malignant**	

WN: Wavenumber (cm^{-1})

Sensitivity % Specificity % Accuracy %	***in situ***			
WN	**Malignant**	**Healthy**		
(400-1800)	94	92	100	**Benign Tumor**
	79	88	99	
	87	91	100	
675	**95**	**81**	100	
	100	**94**	100	
	97	**87**	100	
1058	100	**97**	100	
	100	**97**	100	
	100	**97**	100	
1100	100	**95**	100	
	100	**100**	100	
	100	**98**	100	
1170	**100**	100	100	
	97	100	100	
	99	100	100	
1278	100	**100**	**99**	
	100	**97**	**100**	
	100	**99**	**100**	
1382	100	100	**90**	
	100	100	**95**	
	100	100	**93**	
Cryosectioned-PDMS				
582-1563	**94**	**79**	**100**	
	91	**71**	**77**	
	93	**76**	**91**	
740	**100**	100	100	
	95	100	100	
	97	100	100	
1385	100	100	**96**	
	100	100	**96**	
	100	100	**97**	
	Malignant	**Benign**		

The classification accuracy of tumors and healthy tissues using the Crashed-liquefied method was obtained under 100 per cent for the bands at 905, 1224, 1295, 1342, 1410, 1448 and 1578 cm^{-1} with the accuracy of 90, 82, 96, 95,86, 66 and 86 per cent for the benign versus healthy tissues, respectively. Malignant tumors and healthy tissue were differentiated with the accuracy of 80 and 94 per cent for the SERS bands at 1126 and 1180 cm^{-1}.

Two-diagnostic combinations for the Cryosectioned-PDMS method, eight and nine combinations for the methods of the *in situ* and Crashed-liquefied, respectively, were classified with the predicted accuracy under 100 per cent. As a conclusion, the Cryosectioned-PDMS method obviously gave better classification results compared to other methods of the *in situ* and Crashed-liquefied if a specific spectral region was used in the model instead of full spectral region. However, the *in situ* indicated better classification accuracy compared to other methods for malignant vs. healthy and benign vs. healthy diagnostic combination by using full spectral region while the best classification performance for benign and malignant biopsy samples was obtained for with the Cryosectioned-PDMS and Crashed-liquefied methods by using the full spectral region.

It should be reminded that significant PC components were used in LDA method which means that significant differences in the variables as component coefficients were grouped by using LDA. The commonly observed SERS bands on the spectra for each approach were selected, and their band intensity column graphs to make a comparison among the tissue types (healthy, benign and malignant) were obtained as seen in Figure 4.77. However, the statistical comparison of the methods related to the specific band regions were obtained by using PC-LDA and LOO-CV method, and the predicted results of the other specific regions clustered with the accuracy of under 100 per cent were detailed in Table 4.53 above. The SERS bands in the region of 1002 to 1008, 1044 to 1058, 1170 to 1180 and 1278 to 1295 cm^{-1} were commonly appeared as major on the PCA loading vectors for each approach. The band intensity column graph belongs to these SERS bands of healthy, benign and malignant tissues for each approach are shown in Figure 4.77. The component coefficients in the first PC loading related to each type of tissue and approach were used to obtain the graph. The standard deviation bars related to each tissue type (malignant, benign and healthy) at the specific spectra region were displayed on each column.

SERS bands in the region of 1002 to 1008 cm^{-1}, 1044 to 1058 cm^{-1}, 1170 to 1180 cm^{-1}, 1278 to 1295 cm^{-1}, probably assigned to ν(C-C) stretching in Phenylalanine, C-O and C-N stretching vibrations in protein, C-H bend vibration in Tyrosine and ν_{as} stretching vibration in nucleic acids, and CH_2 twisting mode and CH_2 wagging vibrations in Amide III, respectively [45, 108, 130, 164-167].

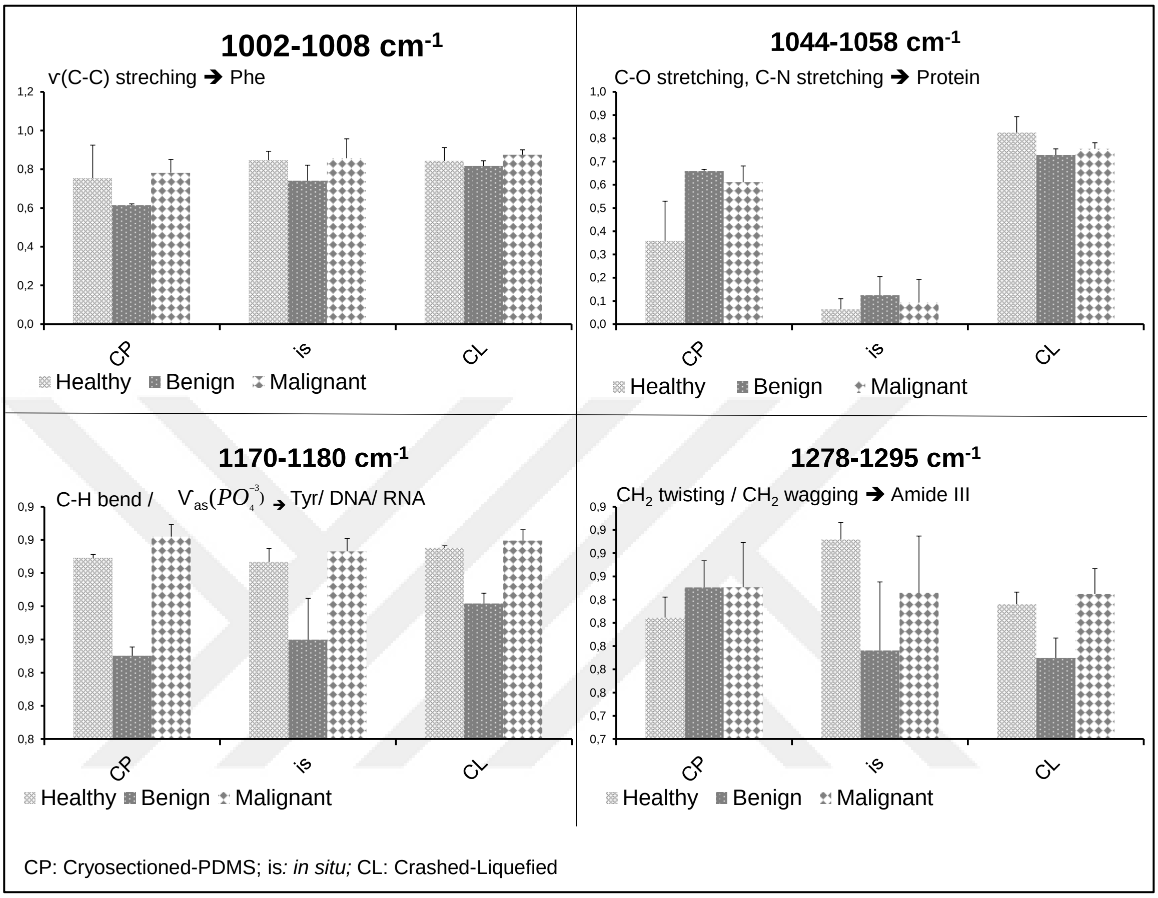

Figure 4.77. Comparison of band intensities in the region of 1002-1008, 1044-1058, 1170-1180 and 1278-1295 cm-1 for healthy, benign and malignant tumor tissues evaluated by three approaches.

The bands in the region of 1002 to 1008 cm^{-1} region was found more intense for malignant tumors rather than benign tumor and healthy tissues. That result is in-line with the result of 1170-1180 cm^{-1} region while the lesser band intensity was obtained in the benign tumors. The band intensity of 1278-1295 cm^{-1} region were higher for benign and malignant tumors that healthy tissue for the Cryosectioned-PDMS method. That result is in-line with the result of a SERS based cancer study in the literature [136]. The different results among the methods for the same band are related to the different sample and substrate preparation. The *in situ* and Crashed-liquefied sampling methods are novel methods, which use a different protocol. That is why the results of these approaches could not be comprised with the literature studies as well as the results of the Cryosectioned-PDMS method because sectioned tissues are the most common tissue sampling type. For instance, the difference for 1278-1295 cm^{-1} band region among the tissue types was similar for the *in situ* and Crashed-liquefied method while it was different for the Cryosectioned-PDMS method. However, the other bands were mostly similar for each method. Similarity means that the relation of the band intensities (more/less intense) between the tissue types.

The method dependent classification accuracy using the full spectra and specific spectral regions based on each approach were compared to each other in the previous section. The specific common prominent bands appeared on the PCA loadings evaluated with sixty four biopsy tissues after applying three approaches, were also used in the PC-LDA classification algorithm. The performance comparison of using PC-LDA model utilizing the common major bands is shown in Table 4.58 below. The richest spectral pattern was obtained belonging to the Cryosectioned-PDMS method displaying both high method reproducibility and ability to be used in diagnostic models. It also mentioned that the method dependent classification accuracy was dependent on the specific band regions that would like to be used as SERS-biomarkers regarding to the cancer and tissue type. As a result, the Cryosectioned-PDMS approach is the best to apply on thyroid biopsies using for specific spectra region while the *in situ* for full spectra region resulted as the best.

Table 4.54. Performance results of PC-LDA diagnostic function applied on the data in the specific spectra region.

	(1002-1008) cm^{-1}	**(1044-1058) cm^{-1}**	**(1170-1180) cm^{-1}**	**(1278-1295) cm^{-1}**
Cryosectioned-PDMS	100%	100%	100%	100%
in situ	100%	Benign vs. Healthy 97%	Benign vs. Malignant 99%	Benign vs. Healthy 99%
Crashed-Liquefied	100%	100%	Healthy vs. Malignant 94%	Benign vs. Healthy 96%

The four band regions were classified with the accuracy of 100 per cent for the Cryosectioned-PDMS method while two-class diagnosis of benign and healthy tissues were obtained as 97 per cent and 99 per cent for the *in situ* approach by using the bands in the region of 1044 to 1058 cm^{-1} and 1278 to 1295 cm^{-1}, respectively. In addition, the loading coefficients belong to 1044-1058 cm^{-1} region were classified with the accuracy of 100 per cent for each two-class diagnostic combination for the Crashed-liquefied method whereas it was obtained with the accuracy of 96 per cent for the coefficients regarding to 1278-1295 cm^{-1} region for the benign and healthy tissue differentiation. However, benign and healthy tissues were classified correctly with the accuracy of 99 per cent for the same region for the *in situ* approach. The performance results were obtained with the accuracy of 99 and 94 per cent for the *in situ* and Crashed-liquefied approach for the diagnosis of benign vs. malignant tissues and healthy vs. malignant tissues, respectively. When the approaches were compared, the best diagnostic performance was obtained using the data of the Cryosectioned-PDMS approach while the second best is the *in situ* based on the common major SERS bands. If these common bands as SERS-biomarkers were used to identify the tissue status, the Cryosectioned-PDMS approach would perform generally higher classification accuracy compare to the others.

5. CONCLUSIONS AND OUTLOOK

In this thesis, the applicability of SERS in cancer diagnosis using a systematic approach was presented. Two novel approaches were developed, and three alternative approaches including one existing were evaluated using human thyroid biopsies. Finally, the results obtained from three approaches were compared with inter- and intra-method reproducibility, spectral richness, and classification accuracy.

With Cryosectioned-PDMS approach, the following parameters were found to be optimal. The thickness of the PDMS layer should be at least in 1.8 mm to cover the glass slide to prevent the background. A 20 × objective and 830 nm laser with 30 mW power (as adjusted in the software) and 2s exposure time were found to be suitable. The minimum thickness of the sectioned tissue to place on the glass slide should be 5-µm. The mapping of 10 x 10 points array using fast StreamHR method, using 16 × concentrated colloidal AgNPs suspension, and arranging the Raman shift range with a median value of 1100 (from ~580 to 1560 cm^{-1}) were necessary. The most striking result to emerge from the observations is that placement of a PDMS layer over glass slide works better than CaF_2 slide and Al-foil with a 2.7 per cent variation indicating higher reproducibility while the variation was 11.7 and 14.9 upon placing sliced tissue on Al-foil and CaF_2 slide, respectively. Finally, this sampling approach was used for the classification of 64 biopsy samples involving 22 benign, 11 malignant and 31 healthy tissue samples. By performing PC-LDA classification algorithm on the spectral data in the range of 582 to 1563 cm^{-1}, the sensitivities of 94, 79 and 100 per cent and the specificities of 79, 71 and 77 per cent, and accuracy of 93, 76 and 91 per cent for between benign and malignant; benign and healthy, malignant and healthy, respectively, were obtained. However, the sensitivity, specificity and accuracy of classification of healthy and tumor biopsies was obtained 100 per cent using component coefficients of the bands at 617, 667, 724, 760, 854, 920, 960, 1008, 1052, 1096, 1180, 1210, 1280, 1295, 1315, 1334, 1415, 1435, 1457 and 1506 cm^{-1} except two SERS bands at 740 and 1385 cm^{-1}.The results of the Cryosectioned-PDMS approach showed a high inter- and intra-method reproducibility and a high classification accuracy using PC-LDA model on the full spectra region and specific spectral regions.

In the second approach, called *in situ*, the AgNPs were synthesized in the homogenized tissue to increase the possibility of molecular components and molecular species forming the tissue with the AgNPs. A biopsy sample about 2x2x2 mm^3 was homogenized, and a 10-µl from each of $3.55x10^{-2}$ M $HONH_2 \cdot HCl$, $3x10^{-2}$ M NaOH and $4.36x10^{-1}$ M $AgNO_3$ was added into the homogenized tissue suspension for the reduction of Ag^+ into AgNPs. Then, the mixture of homogenized tissue and AgNPs was placed onto a CaF_2 slide. The point-to-point, spot-to-spot and sample-to-sample reproducibility referring to intra-and inter-method reproducibility were found to be satisfactory by acquiring ten spectra arbitrarily chosen points on a dried homogenized tissue-AgNPs mixture. A laser at 830 nm with 15 mW (adjusted power in the software), a 20× objective, and 5s exposure time yielded the best spectrum. After the optimization study, the same thyroid biopsy samples mentioned above were used for the evaluation of the approach. Ten spectra obtained from each sample were collected and used in the PC-LDA model. The probability of correctly predicted performance was obtained with the sensitivities of 94, 92 and 100 per cent and the specificities of 79, 88 and 99 per cent, and accuracy of 87, 91 and 100 per cent for the benign vs. malignant, healthy vs. benign and healthy vs. malignant tissues, respectively.

The sensitivity, specificity and accuracy of classification results from healthy tissues and tumor biopsies were obtained as 100 per cent using PC components of the bands at 425, 610, 860, 1005, 1170, 1382 and 1452 cm^{-1} while the eight diagnostic combination of the bands at 675, 860, 1058, 1100, 1278, 1397 and 1656 cm^{-1}between benign vs. malignant, healthy vs. benign and healthy vs. malignant were in the accuracy range of 87 to 99 per cent. The benign vs. healthy tissues were classified based on the bands at 675, 860, 1058, 1100, and 1397 cm^{-1} with an accuracy of 87, 99, 97, 98, and 99 per cent, respectively, while benign vs. malignant tumors were differentiated with an accuracy of 97 and 99 per cent based on the bands at 675 and 1278 cm^{-1}, respectively. Malignant tumors and healthy tissues were classified with an accuracy of 93 per cent for the band at 1656 cm^{-1}.

The evaluation of the full spectral region from 400 to 1800 cm^{-1} indicates that the best discrimination for healthy vs. benign, and healthy vs. malignant tissues is achieved with the *in situ* approach whereas the best discrimination for benign vs. malignant is achieved with the Cryosectioned-PDMS approach.

In order to compare the performance of the sampling approaches studied in this thesis, the Crashed-liquefied approach previously developed by our group was also evaluated. As different from our previous study, the colloidal suspension containing h-AgNPs instead of c-AgNPs was used with the homogenized tissue. A 200-µl volume of 32 × concentrated h-AgNPs was mixed with the homogenized tissue with the same thyroid biopsies used in other approaches. Performing PC-LDA classification algorithm on the spectral data in the range of 400 to 1800 cm^{-1} discriminated benign vs. malignant; benign vs. healthy; malignant vs. healthy tissues with the sensitivities of 94, 79 and 100 per cent and the specificities of 79, 71 and 77 per cent, and accuracy of 93, 76 and 91 per cent, respectively. However, component coefficients of SERS bands at 548, 732, 805, 830, 1002, 1047, 1295, 1342, 1410 and 1448 cm^{-1} for the tumorous and healthy tissues was classified with the sensitivity, specificity and accuracy of 100 per cent while the results was obtained with sensitivities of 96, 91, 99, 89 and 95 per cent and the specificities of 88, 78, 95, 95 and 78 per cent, and accuracy of 93, 86, 97, 91 and 88 per cent for the SERS bands at 905, 1126, 1180, 1578 and 1224 cm^{-1}, respectively. Seven diagnostic combinations between the benign and healthy tissues for the bands at 905, 1224, 1295, 1342, 1410, 1448 and 1578 cm^{-1} were classified with an accuracy of under 100 per cent, which are 90, 82, 96, 95, 86, 66 and 86 per cent, respectively. In addition, two diagnostic combinations between the malignant tumors and healthy tissues for the bands at 1126 and 1180 cm^{-1} were differentiated with an accuracy of 80 and 94 per cent, respectively.

As a result, a total of nine diagnostic combinations for the Crashed-liquefied approach were classified with an accuracy under 100 per cent while it was two and eight for the Cryosectioned-PDMS and *in situ* approaches, respectively. Therefore, the classification results of using full spectra region obtained by using the Crashed-liquefied approach for the differentation of healthy vs. benign and malignant tissue were close to the results obtained with the Cryosectioned-PDMS.

The CV values between 3 and 10 per cent, and 5 and 11 per cent for *in situ* and Cryosectioned-PDMS approaches, respectively, indicate that SERS measurements have high intra-method reproducibility. Moreover, the CV values calculated to evaluate the sample-to-sample variations are found between 3 and 4, and 2 and 4 indicate that *in situ* and Cryosectioned-PDMS approaches have high inter-method reproducibility.

A total of twenty one, thirteen, and fourteen prominent characteristic bands of the tissues were obtained for the methods of Cryosectioned-PDMS, *in situ* and Crashed- liquefied, respectively. Based on these results, one can claim that the SERS spectra obtained with the

Cryosectioned-PDMS method has the richest SERS spectrum compared to the spectra obtained with the other sampling methods.

The results indicate that the best clustering is obtained with the data from the *in situ* approach for the classification of healthy vs. malignant tissue with a sensitivity of 100, specificity of 99 and accuracy of 100 per cent. In addition, the i*n situ* method has the best classification performance for the diagnosis of healthy vs. benign tissue with a sensitivity of 92, specificity of 88, and accuracy of 91 per cent. However, benign vs. malignant differentiating was obtained with a sensitivity of 94, specificity of 91, and accuracy of 93 per cent, which were higher in the Cryosectioned-PDMS and Crashed-liquefied approaches. However, the Cryosectioned-PDMS method obviously gave better classification results compared to other methods when a specific spectra region was used in the model instead of the full spectra region. It should be noted that only four SERS bands were obtained in common, which means that specific spectra region still depends on the observer and the defined SERS-biomarkers related to the type of cancer tissue.

Each method is almost similar with their minimum sample preparation steps but the Cryosectioned-PDMS method requires a qualified person with cryostat sectioning. On the other hand, the methods of Crashed-liquefied and *in situ* based sampling use CaF_2, which is fragile and quite expensive to use in routine clinic applications. Multiple samples can be process using the same CaF_2 slide but still it can be costly for routine use.

Despite the spectral patterns of tissues are similar, it still seems necessary to arrange the Raman shift range based on cancer type to be studied with the Cryosectioned-PDMS approach because StreamHR fast mapping method can be adjusted to a reduced spectral range.

The concept of *in situ* synthesis of AgNPs in homogenized tissue specimen and Cryosectioned-PDMS approaches have a potential in clinical cancer diagnosis applications. However, more work is needed to clarify whether full spectrum or a certain spectral region is necessary for the diagnostic procedure. The data generated using the all methods studied in this thesis should also be evaluated by using different classification algorithms such as neural networks, kernel estimation, least squares regression, multinomial logistic regression, support vector machines and Bayesian classifications. The important point is that the developed methodologies have only been applied to thyroid tumors and other types of tumors should also be studied. As future study, the evaluation of the metabolites obbtained from tisues and tumors can be an important point to consider.

This study is differing from the literature with being a more comprehensive and systematic study that explores the method dependent reproducibility of the approaches. The results indicate the method dependent changes in the classification accuracy and spectral patterns. Moreover, one research article related to SERS-based sampling method for cancer cell differentiation was published, whereas a book chapter on label-free detection of cancer from proteins, cells and tissues using SERS was submitted (150). A poster presentation of the outcomes related to cryosectioned-PDMS sampling method exploring rat tumors in Raman4Clinics Annual Meeting, Leibniz Institute of Photonic Technology was performed. Two research articles related to the outcomes of the thesis is in progress. Indeed, throughout the study of this thesis, from 2014 to 2017, other groups also reported the potential use of SERS in cancer diagnosis (144, 166-175). In conclusion, SERS can be used as an alternative or supporting technique for accurate cancer diagnosis. However, it is clear that more validation studies using different cancer types are needed. All of the three alternative SERS based cancer diagnosis approaches developed in this thesis are quite comparable and their further evaluations can provide new opportunities in cancer.

REFERENCES

1. Hanahan D, Weinberg RA. The hallmarks of cancer. *Cell*. 2000;100(1):57-70.

2. Torre LA, Bray F, Siegel RL, Ferlay J, Lortet-Tieulent J, Jemal A. Global cancer statistics, 2012. *CA: A Cancer Journal for Clinicians*. 2015;65(2):87-108.

3. Siegel R, Ma J, Zou Z, Jemal A. Cancer statistics, 2014. *CA: A Cancer Journal for Clinicians*. 2014;64(1):9-29.

4. Levy DA, Slaton JW, Swanson DA, Dinney CP. Stage specific guidelines for surveillance after radical nephrectomy for local renal cell carcinoma. *The Journal of Urology*. 1998;159(4):1163-7.

5. Lam JS, Leppert JT, Figlin RA, Belldegrun AS. Surveillance following radical or partial nephrectomy for renal cell carcinoma. *Current Urology Reports*. 2005;6(1):7-18.

6. Hafez KS, Fergany AF, Novick AC. Nephron sparing surgery for localized renal cell carcinoma: Impact of tumor size on patient survival, tumor recurrence and tnm staging. *The Journal of Urology*. 1999;162(6):1930-3.

7. Patard J-J, Shvarts O, Lam JS, Pantuck AJ, Kim HL, Ficarra V, Cindolo L, Han K-r, De La Taille A, Tostain J. Safety and efficacy of partial nephrectomy for all t1 tumors based on an international multicenter experience. *The Journal of Urology*. 2004;171(6):2181-5.

8. McDougall IR. *Management of thyroid cancer and related nodular disease*. Standford, CA, USA: Springer Science & Business Media; 2006.

9. Cooper D, Doherty G, Haugen B, Kloos R, Lee S, Mandel S, Mazzaferri E, McIver B, Pacini F, Schlumberger M. American thyroid association (ata) guidelines taskforce on thyroid nodules and differentiated thyroid cancer. Revised american thyroid association management guidelines for patients with thyroid nodules and differentiated thyroid cancer. *Thyroid.* 2009;19(11):1167-214.

10. Gharib H, Papini E, Paschke R, Duick D, Valcavi R, Hegedüs L, Vitti P. American association of clinical endocrinologists, associazione medici endocrinologi, and european thyroid association medical guidelines for clinical practice for the diagnosis and management of thyroid nodules. *Endocrine Practice.* 2010;16(Supplement 1):1-43.

11. Udelsman R, Chen H. The current management of thyroid cancer. *Advances in Surgery.* 1999;33:1-27.

12. Chiacchio S, Lorenzoni A, Boni G, Rubello D, Elisei R, Mariani G. Anaplastic thyroid cancer: Prevalence, diagnosis and treatment. *Minerva Endocrinologica.* 2008;33(4):341-57.

13. Hedinger C. *Histological typing of thyroid tumours*. Wales, UK: Springer Science & Business Media; 2012.

14. Rout P, Shariff S. Diagnostic value of qualitative and quantitative variables in thyroid lesions. *Cytopathology.* 1999;10(3):171-9.

15. Nikiforov YE, Ohori NP, Hodak SP, Carty SE, LeBeau SO, Ferris RL, Yip L, Seethala RR, Tublin ME, Stang MT. Impact of mutational testing on the diagnosis and management of patients with cytologically indeterminate thyroid nodules: A prospective analysis of 1056 fna samples. *The Journal of Clinical Endocrinology & Metabolism.* 2011;96(11):3390-7.

16. Nikiforov YE, Steward DL, Robinson-Smith TM, Haugen BR, Klopper JP, Zhu Z, Fagin JA, Falciglia M, Weber K, Nikiforova MN. Molecular testing for mutations in improving the fine-needle aspiration diagnosis of thyroid nodules. *The Journal of Clinical Endocrinology & Metabolism.* 2009;94(6):2092-8.

17. Beaudenon-Huibregtse S, Alexander EK, Guttler RB, Hershman JM, Babu V, Blevins TC, Moore P, Andruss B, Labourier E. Centralized molecular testing for oncogenic gene mutations complements the local cytopathologic diagnosis of thyroid nodules. *Thyroid.* 2014;24(10):1479-87.

18. Rex DK, Johnson DA, Anderson JC, Schoenfeld PS, Burke CA, Inadomi JM. American college of gastroenterology guidelines for colorectal cancer screening 2008. *The American Journal of Gastroenterology.* 2009;104(3):739-50.

19. Schiffman M, Herrero R, Hildesheim A, Sherman ME, Bratti M, Wacholder S, Alfaro M, Hutchinson M, Morales J, Greenberg MD. Hpv DNA testing in cervical cancer screening: Results from women in a high-risk province of costa rica. *Jama.* 2000;283(1):87-93.

20. Chastre J, Fagon JY. Invasive diagnostic testing should be routinely used to manage ventilated patients with suspected pneumonia. *American Journal of Respiratory and Critical Care Medicine.* 1994;150(2):570-4.

21. Suvarna KS, Layton C, Bancroft JD. *Bancroft's theory and practice of histological techniques.* Philadelphia, PA, USA: Elsevier Health Sciences; 2012.

22. Saha K, Raychaudhuri G, Chattopadhyay BK, Das I. Comparative evaluation of six cytological grading systems in breast carcinoma. *Journal of Cytology/Indian Academy of Cytologists.* 2013;30(2):87-93.

23. Srinivasan M, Sedmak D, Jewell S. Effect of fixatives and tissue processing on the content and integrity of nucleic acids. *The American Journal of Pathology.* 2002;161(6):1961-71.

24. Yaziji H, Barry T. Diagnostic immunohistochemistry: What can go wrong? *Advances in Anatomic Pathology.* 2006;13(5):238-46.

25. Bresters D, Schipper M, Reesink H, Boeser-Nunnink B, Cuypers H. The duration of fixation influences the yield of hcv cdna-pcr products from formalin-fixed, paraffin-embedded liver tissue. *Journal of Virological Methods.* 1994;48(2-3):267-72.

26. Titford M. Safety considerations in the use of fixatives. *Journal of Histotechnology.* 2001;24(3):165-71.

27. McGhee JD, Von Hippel PH. Formaldehyde as a probe of DNA structure. 3. Equilibrium denaturation of DNA and synthetic polynucleotides. *Biochemistry.* 1977;16(15):3267-76.

28. Kerawala CJ, Ong TK. Relocating the site of frozen sections—is there room for improvement? *Head & Neck.* 2001;23(3):230-2.

29. Cornett DS, Reyzer ML, Chaurand P, Caprioli RM. Maldi imaging mass spectrometry: Molecular snapshots of biochemical systems. *Nature Methods.* 2007;4(10):828-833

30. Siesler HW, Ozaki Y, Kawata S, Heise HM. *Near-infrared spectroscopy: Principles, Instruments, Applications*. Weinheim, Germany: John Wiley & Sons; 2008.

31. Albrecht C. Joseph r. Lakowicz: Principles of fluorescence spectroscopy. *Analytical and Bioanalytical Chemistry.* 2008;390(5):1223-4.

32. Lewis IR, Edwards H. *Handbook of raman spectroscopy: From the research laboratory to the process line*. Boca Raton: CRC Press; 2001.

33. Kong K, Kendall C, Stone N, Notingher I. Raman spectroscopy for medical diagnostics—from in-vitro biofluid assays to in-vivo cancer detection. *Advanced Drug Delivery Reviews.* 2015;89:121-34.

34. Wulfkuhle JD, Liotta LA, Petricoin EF. Early detection: Proteomic applications for the early detection of cancer. *Nature Reviews Cancer.* 2003;3(4):267-275.

35. Leblond F, Davis SC, Valdés PA, Pogue BW. Pre-clinical whole-body fluorescence imaging: Review of instruments, methods and applications. *Journal of Photochemistry and Photobiology B: Biology.* 2010;98(1):77-94.

36. Bremer C, Ntziachristos V, Weissleder R. Optical-based molecular imaging: Contrast agents and potential medical applications. *European Radiology.* 2003;13(2):231-43.

37. Müller H, Michoux N, Bandon D, Geissbuhler A. A review of content-based image retrieval systems in medical applications—clinical benefits and future directions. *International Journal of Medical Informatics.* 2004;73(1):1-23.

38. Lane LA, Qian X, Nie S. Sers nanoparticles in medicine: From label-free detection to spectroscopic tagging. *Chemical Reviews.* 2015;115(19):10489-529.

39. Weiss S. Fluorescence spectroscopy of single biomolecules. *Science.* 1999;283(5408):1676-83.

40. Wang M, Mi C-C, Wang W-X, Liu C-H, Wu Y-F, Xu Z-R, Mao C-B, Xu S-K. Immunolabeling and nir-excited fluorescent imaging of hela cells by using nayf4: Yb, er upconversion nanoparticles. *Acs Nano.* 2009;3(6):1580-6.

41. Park J-H, Gu L, Von Maltzahn G, Ruoslahti E, Bhatia SN, Sailor MJ. Biodegradable luminescent porous silicon nanoparticles for in vivo applications. *Nature Materials.* 2009;8(4):331-336.

42. Gustafsson JO, Oehler MK, Ruszkiewicz A, McColl SR, Hoffmann P. Maldi imaging mass spectrometry (maldi-ims)—application of spatial proteomics for ovarian cancer classification and diagnosis. *International Journal of Molecular Sciences.* 2011;12(1):773-94.

43. Lui H, Zhao J, McLean D, Zeng H. Real-time raman spectroscopy for in vivo skin cancer diagnosis. *Cancer Research.* 2012;72(10):2491-500.

44. Manoharan R, Shafer K, Perelman L, Wu J, Chen K, Deinum G, Fitzmaurice M, Myles J, Crowe J, Dasarl RR. Raman spectroscopy and fluorescence photon migration for breast cancer diagnosis and imaging. *Photochemistry and Photobiology*. 1998;67(1):15-22.

45. Barroso E, Smits R, Bakker Schut T, Ten Hove I, Hardillo J, Wolvius E, Baatenburg de Jong R, Koljenovic S, Puppels G. Discrimination between oral cancer and healthy tissue based on water content determined by raman spectroscopy. *Analytical Chemistry*. 2015;87(4):2419-26.

46. Anwar S, Firdous S, Rehman A-u, Nawaz M. Optical diagnostic of breast cancer using raman, polarimetric and fluorescence spectroscopy. *Laser Physics Letters.* 2015;12(4):045601.

47. Barroso EM, Smits RWH, Bakker Schut T, ten Hove I, Hardillo JA, Wolvius EB, Baatenburg de Jong R, Koljenović S, Puppels GJ. Discrimination between oral cancer and healthy tissue based on water content determined by raman spectroscopy. *Analytical Chemistry.* 2015;87(4):2419-26.

48. Brozek-Pluska B, Kopec M, Niedzwiecka I, Morawiec-Sztandera A. Label-free determination of lipid composition and secondary protein structure of human salivary noncancerous and cancerous tissues by raman microspectroscopy. *Analyst.* 2015. (2015). Label-free determination of lipid composition and secondary protein structure of human salivary noncancerous and cancerous tissues by Raman microspectroscopy. Analyst, 140(7), 2107-2113.

49. Surmacki J, Brozek-Pluska B, Kordek R, Abramczyk H. The lipid-reactive oxygen species phenotype of breast cancer. Raman spectroscopy and mapping, pca and plsda for invasive ductal carcinoma and invasive lobular carcinoma. Molecular tumorigenic mechanisms beyond warburg effect. *Analyst.* 2015;140(7):2121-33.

50. Tolles WM, Nibler J, McDonald J, Harvey A. A review of the theory and application of coherent anti-stokes raman spectroscopy (cars). *Applied Spectroscopy.* 1977;31(4):253-71.

51. Freudiger CW, Min W, Saar BG, Lu S, Holtom GR, He C, Tsai JC, Kang JX, Xie XS. Label-free biomedical imaging with high sensitivity by stimulated raman scattering microscopy. *Science.* 2008;322(5909):1857-61.

52. Aina A, Hargreaves MD, Matousek P, Burley JC. Transmission raman spectroscopy as a tool for quantifying polymorphic content of pharmaceutical formulations. *Analyst.* 2010;135(9):2328-33.

53. Nan X, Tonary AM, Stolow A, Xie XS, Pezacki JP. Intracellular imaging of hcv rna and cellular lipids by using simultaneous two-photon fluorescence and coherent anti-stokes raman scattering microscopies. *ChemBioChem.* 2006;7(12):1895-7.

54. Rinia HA, Burger KN, Bonn M, Müller M. Quantitative label-free imaging of lipid composition and packing of individual cellular lipid droplets using multiplex cars microscopy. *Biophysical Journal.* 2008;95(10):4908-14.

55. Fu Y, Wang H, Huff TB, Shi R, Cheng JX. Coherent anti-stokes raman scattering imaging of myelin degradation reveals a calcium-dependent pathway in lyso-ptdcho-induced demyelination. *Journal of Neuroscience Research.* 2007;85(13):2870-81.

56. Freudiger CW, Min W, Holtom GR, Xu B, Dantus M, Xie XS. Highly specific label-free molecular imaging with spectrally tailored excitation-stimulated raman scattering (ste-srs) microscopy. *Nature Photonics.* 2011;5(2):103-109.

57. Stone N, Baker R, Rogers K, Parker AW, Matousek P. Subsurface probing of calcifications with spatially offset raman spectroscopy (sors): Future possibilities for the diagnosis of breast cancer. *Analyst.* 2007;132(9):899-905.

58. Kneipp K, Kneipp H. Single molecule raman scattering. *Applied Spectroscopy.* 2006;60(12):322A-34A.

59. Lin D, Feng S, Pan J, Chen Y, Lin J, Chen G, Xie S, Zeng H, Chen R. Colorectal cancer detection by gold nanoparticle based surface-enhanced raman spectroscopy of blood serum and statistical analysis. *Optics Express.* 2011;19(14):13565-77.

60. Feng S, Chen R, Lin J, Pan J, Chen G, Li Y, Cheng M, Huang Z, Chen J, Zeng H. Nasopharyngeal cancer detection based on blood plasma surface-enhanced raman spectroscopy and multivariate analysis. *Biosensors and Bioelectronics.* 2010;25(11):2414-9.

61. Li Z, Li C, Lin D, Huang Z, Pan J, Chen G, Lin J, Liu N, Yu Y, Feng S. Surface-enhanced raman spectroscopy for differentiation between benign and malignant thyroid tissues. *Laser Physics Letters.* 2014;11(4):045602.

62. Feng S, Lin J, Huang Z, Chen G, Chen W, Wang Y, Chen R, Zeng H. Esophageal cancer detection based on tissue surface-enhanced raman spectroscopy and multivariate analysis. *Applied Physics Letters.* 2013;102(4):043702.

63. Feng S, Chen R, Lin J, Pan J, Wu Y, Li Y, Chen J, Zeng H. Gastric cancer detection based on blood plasma surface-enhanced raman spectroscopy excited by polarized laser light. *Biosensors and Bioelectronics.* 2011;26(7):3167-74.

64. Li Y, Qi X, Lei C, Yue Q, Zhang S. Simultaneous sers detection and imaging of two biomarkers on the cancer cell surface by self-assembly of branched DNA–gold nanoaggregates. *Chemical Communications.* 2014;50(69):9907-9.

65. Boca-Farcau S, Potara M, Simon T, Juhem A, Baldeck P, Astilean S. Folic acid-conjugated, sers-labeled silver nanotriangles for multimodal detection and targeted photothermal treatment on human ovarian cancer cells. *Molecular Pharmaceutics.* 2013;11(2):391-9.

66. Liu Y, Huang L-q, Wang J, Yuan L, Zhang W-w, Wang L, Zhu J. Fabrication of silver ordered nanoarrays sers-active substrates and their applications in bladder cancer cells detection. *Spectroscopy and Spectral Analysis.* 2012;32(2):386-90.

67. Li X, Yang T, Lin J. Spectral analysis of human saliva for detection of lung cancer using surface-enhanced raman spectroscopy. *Journal of Biomedical Optics.* 2012;17(3):037003.

68. Mert S, Culha M. Surface-enhanced raman scattering-based detection of cancerous renal cells. *Applied Spectroscopy.* 2014;68(6):617-24.

69. Willard HH, Merritt Jr LL, Dean JA, Settle Jr FA. Seattle, USA: Instrumental methods of analysis. 1988.

70. Nakamoto K. *Infrared and raman spectra of inorganic and coordination compounds*. Washington, USA: Wiley; 1977.

71. Colthup N. *Introduction to infrared and raman spectroscopy*. New York, USA: Elsevier; 2012.

72. Chang R. *Physical chemistry for the biosciences*. California, USA: University Science Books; 2005.

73. Nakamoto K. *Infrared spectra of inorganic and coordination compounds*. New York, USA: Wiley; 1970.

74. Fleischmann M, Hendra PJ, McQuillan AJ. Raman spectra of pyridine adsorbed at a silver electrode. *Chemical Physics Letters.* 1974;26(2):163-6.

75. Jeanmaire DL, Van Duyne RP. Surface raman spectroelectrochemistry: Part i. Heterocyclic, aromatic, and aliphatic amines adsorbed on the anodized silver electrode. *Journal of Electroanalytical Chemistry and Interfacial Electrochemistry.* 1977;84(1):1-20.

76. Van Duyne R. Raman applications of raman spectroscopy in electrochemistry. *Le Journal de Physique Colloques.* 1977;38(C5):C5-239-C5-52.

77. Albrecht MG, Creighton JA. Anomalously intense raman spectra of pyridine at a silver electrode. *Journal of the American Chemical Society.* 1977;99(15):5215-7.

78. Kambhampati P, Child C, Foster MC, Campion A. On the chemical mechanism of surface enhanced raman scattering: Experiment and theory. *The Journal of Chemical Physics.* 1998;108(12):5013-26.

79. Lombardi JR, Birke RL. A unified approach to surface-enhanced raman spectroscopy. *The Journal of Physical Chemistry C.* 2008;112(14):5605-17.

80. Morton SM, Ewusi-Annan E, Jensen L. Controlling the non-resonant chemical mechanism of sers using a molecular photoswitch. *Physical Chemistry Chemical Physics.* 2009;11(34):7424-9.

81. Van Duyne RP. Laser excitation of raman scattering from adsorbed molecules on electrode surfaces. *Chemical and Biochemical Applications of Lasers.* 1979;4:101-389.

82. Vo-Dinh T. Surface-enhanced raman spectroscopy using metallic nanostructures. *TrAC Trends in Analytical Chemistry.* 1998;17(8):557-82.

83. Doering WE, Nie S. Single-molecule and single-nanoparticle sers: Examining the roles of surface active sites and chemical enhancement. *The Journal of Physical Chemistry B.* 2002;106(2):311-7.

84. Moores A, Goettmann F. The plasmon band in noble metal nanoparticles: An introduction to theory and applications. *New Journal of Chemistry.* 2006;30(8):1121-32.

85. Moskovits M. Surface roughness and the enhanced intensity of raman scattering by molecules adsorbed on metals. *The Journal of Chemical Physics.* 1978;69(9):4159-61.

86. Zhang X, Chen YL, Liu R-S, Tsai DP. Plasmonic photocatalysis. *Reports on Progress in Physics.* 2013;76(4):046401.

87. Maier SA, Atwater HA. Plasmonics: Localization and guiding of electromagnetic energy in metal/dielectric structures. *Journal of Applied Physics.* 2005;98(1):10.

88. Haes AJ, Haynes CL, McFarland AD, Schatz GC, Van Duyne RP, Zou S. Plasmonic materials for surface-enhanced sensing and spectroscopy. *MRS Bulletin.* 2005;30(5):368-75.

89. Lu X, Rycenga M, Skrabalak SE, Wiley B, Xia Y. Chemical synthesis of novel plasmonic nanoparticles. *Annual Review of Physical Chemistry.* 2009;60:167-92.

90. Rycenga M, Cobley CM, Zeng J, Li W, Moran CH, Zhang Q, Qin D, Xia Y. Controlling the synthesis and assembly of silver nanostructures for plasmonic applications. *Chemical Reviews.* 2011;111(6):3669-712.

91. Radziuk D, Moehwald H. Prospects for plasmonic hot spots in single molecule sers towards the chemical imaging of live cells. *Physical Chemistry Chemical Physics.* 2015;17(33):21072-93.

92. Le Ru E, Etchegoin P. *Principles of surface-enhanced raman spectroscopy: and related plasmonic effects*. Oxford, UK: Elsevier; 2008.

93. Lee SY, Hung L, Lang GS, Cornett JE, Mayergoyz ID, Rabin O. Dispersion in the sers enhancement with silver nanocube dimers. *Acs Nano.* 2010;4(10):5763-72.

94. Ravindranath SP, Wang Y, Irudayaraj J. Sers driven cross-platform based multiplex pathogen detection. *Sensors and Actuators B: Chemical.* 2011;152(2):183-90.

95. Shanmukh S, Jones L, Driskell J, Zhao Y, Dluhy R, Tripp RA. Rapid and sensitive detection of respiratory virus molecular signatures using a silver nanorod array sers substrate. *Nano Letters.* 2006;6(11):2630-6.

96. Kahraman M, Zamaleeva AI, Fakhrullin RF, Culha M. Layer-by-layer coating of bacteria with noble metal nanoparticles for surface-enhanced raman scattering. *Analytical and Bioanalytical Chemistry.* 2009;395(8):25592567.

97. Lee S, Chon H, Lee J, Ko J, Chung BH, Lim DW, Choo J. Rapid and sensitive phenotypic marker detection on breast cancer cells using surface-enhanced raman scattering (sers) imaging. *Biosensors and Bioelectronics.* 2014;51:238-43.

98. Ock K, Jeon WI, Ganbold EO, Kim M, Park J, Seo JH, Cho K, Joo S-W, Lee SY. Real-time monitoring of glutathione-triggered thiopurine anticancer drug release in live cells investigated by surface-enhanced raman scattering. *Analytical Chemistry.* 2012;84(5):2172-8.

99. Cole JR, Mirin NA, Knight MW, Goodrich GP, Halas NJ. Photothermal efficiencies of nanoshells and nanorods for clinical therapeutic applications. *The Journal of Physical Chemistry C.* 2009;113(28):12090-4.

100. Prentice BM, Caprioli RM, Vuiblet V. Label-free molecular imaging of the kidney. *Kidney International.* 2017;92(3):580-98.

101. Yu Y, Lin J, Lin D, Feng S, Chen W, Huang Z, Huang H, Chen R. Leukemia cells detection based on electroporation assisted surface-enhanced raman scattering. *Biomedical Optics Express.* 2017;8(9):4108-21.

102. Perumal J, Balasundaram G, Mahyuddin AP, Choolani M, Olivo M. Sers-based quantitative detection of ovarian cancer prognostic factor haptoglobin. *International Journal of Nanomedicine.* 2015;10:1831-40.

103. Leray A, Brulé T, Buret M, Des Francs GC, Bouhelier A, Dereux A, Finot E. Sorting of single biomolecules based on fourier polar representation of surface enhanced raman spectra. *Scientific Reports.* 2016;6:20383.

104. Yolken RH. Enzyme immunoassays for the detection of infectious antigens in body fluids: Current limitations and future prospects. *Reviews of Infectious Diseases.* 1982;4(1):35-68.

105. Krasnoslobodtsev AV, Torres MP, Kaur S, Vlassiouk IV, Lipert RJ, Jain M, Batra SK, Lyubchenko YL. Nano-immunoassay with improved performance for detection of cancer biomarkers. *Nanomedicine: Nanotechnology, Biology and Medicine.* 2015;11(1):167-73.

106. Wu L, Wang Z, Zong S, Chen H, Wang C, Xu S, Cui Y. Simultaneous evaluation of p53 and p21 expression level for early cancer diagnosis using sers technique. *Analyst.* 2013;138(12):3450-6.

107. Sha MY, Xu H, Natan MJ, Cromer R. Surface-enhanced raman scattering tags for rapid and homogeneous detection of circulating tumor cells in the presence of human whole blood. *Journal of the American Chemical Society.* 2008;130(51):17214-5.

108. Pînzaru SC, Andronie L, Domsa I, Cozar O, Astilean S. Bridging biomolecules with nanoparticles: Surface-enhanced raman scattering from colon carcinoma and normal tissue. *Journal of Raman Spectroscopy.* 2008;39(3):331-4.

109. Feng S, Lin J, Cheng M, Li Y-Z, Chen G, Huang Z, Yu Y, Chen R, Zeng H. Gold nanoparticle based surface-enhanced raman scattering spectroscopy of cancerous and normal nasopharyngeal tissues under near-infrared laser excitation. *Applied Spectroscopy.* 2009;63(10):1089-94.

110. Yan B, Reinhard BrM. Identification of tumor cells through spectroscopic profiling of the cellular surface chemistry. *The Journal of Physical Chemistry Letters.* 2010;1(10):1595-8.

111. Schaeberle MD, Kalasinsky VF, Luke JL, Lewis EN, Levin IW, Treado PJ. Raman chemical imaging: Histopathology of inclusions in human breast tissue. *Analytical Chemistry.* 1996;68(11):1829-33.

112. Stone N, Faulds K, Graham D, Matousek P. Prospects of deep raman spectroscopy for noninvasive detection of conjugated surface enhanced resonance raman scattering nanoparticles buried within 25 mm of mammalian tissue. *Analytical Chemistry.* 2010;82(10):3969-73.

113. Alvarez-Puebla RA, Liz-Marzán LM. Sers-based diagnosis and biodetection. *Small.* 2010;6(5):604-10.

114. Shabihkhani M, Lucey GM, Wei B, Mareninov S, Lou JJ, Vinters HV, Singer EJ, Cloughesy TF, Yong WH. The procurement, storage, and quality assurance of frozen blood and tissue biospecimens in pathology, biorepository, and biobank settings. *Clinical Biochemistry.* 2014;47(4-5):258-66.

115. Tfayli A, Gobinet C, Vrabie V, Huez R, Manfait M, Piot O. Digital dewaxing of raman signals: Discrimination between nevi and melanoma spectra obtained from paraffin-embedded skin biopsies. *Applied Spectroscopy.* 2009;63(5):564-70.

116. Chan JW, Taylor DS, Thompson DL. The effect of cell fixation on the discrimination of normal and leukemia cells with laser tweezers raman spectroscopy. *Biopolymers.* 2009;91(2):132-9.

117. Vo-Dinh T, Wang HN, Scaffidi J. Plasmonic nanoprobes for sers biosensing and bioimaging. *Journal of Biophotonics.* 2010;3(1-2):89-102.

118. Skoog DA, Holler FJ, Crouch SR. *Principles of Instrumental Analysis*. Boston, USA: Cengage learning; 2017.

119. Abdi H. Coefficient of variation. *Encyclopedia of Research Design.* 2010;1:169-71.

120. Wold S, Esbensen K, Geladi P. Principal component analysis. *Chemometrics and Intelligent Laboratory Systems.* 1987;2(1-3):37-52.

121. Moore B. Principal component analysis in linear systems: Controllability, observability, and model reduction. *IEEE Transactions on Automatic Control.* 1981;26(1):17-32.

122. Martin FL, German MJ, Wit E, Fearn T, Ragavan N, Pollock HM. Identifying variables responsible for clustering in discriminant analysis of data from infrared microspectroscopy of a biological sample. *Journal of Computational Biology.* 2007;14(9):1176-84.

123. Huefner A, Kuan W-L, Müller KH, Skepper JN, Barker RA, Mahajan S. Characterization and visualization of vesicles in the endo-lysosomal pathway with surface-enhanced raman spectroscopy and chemometrics. *Acs Nano.* 2015;10(1):307-16.

124. Refaeilzadeh P, Tang L, Liu H. Cross-validation. *Encyclopedia of Database Systems*: Springer; 2009. pp. 532-8.

125. Sackett DL, Straus SE. Finding and applying evidence during clinical rounds: The evidence cart. *Jama.* 1998; 280(15):1336-8.

126. Leopold N, Lendl B. A new method for fast preparation of highly surface-enhanced raman scattering (sers) active silver colloids at room temperature by reduction of silver nitrate with hydroxylamine hydrochloride. *The Journal of Physical Chemistry B.* 2003;107(24):5723-7.

127. Lee P, Meisel D. Adsorption and surface-enhanced raman of dyes on silver and gold sols. *The Journal of Physical Chemistry.* 1982;86(17):3391-5.

128. Mert S, Özbek E, Ötünçtemur A, Çulha M. Kidney tumor staging using surface-enhanced raman scattering. *Journal of Biomedical Optics.* 2015;20(4):047002-1:10.

129. Joliffe I, Morgan B. Principal component analysis and exploratory factor analysis. *Statistical Methods in Medical Research.* 1992;1(1):69-95.

130. Teh S, Zheng W, Ho K, Teh M, Yeoh K, Huang Z. Diagnostic potential of near-infrared raman spectroscopy in the stomach: Differentiating dysplasia from normal tissue. *British Journal of Cancer.* 2008;98(2):457-65.

131. Guerrini L, Graham D. Molecularly-mediated assemblies of plasmonic nanoparticles for surface-enhanced raman spectroscopy applications. *Chemical Society Reviews.* 2012;41(21):7085-107.

132. Bonifacio A, Dalla Marta S, Spizzo R, Cervo S, Steffan A, Colombatti A, Sergo V. Surface-enhanced raman spectroscopy of blood plasma and serum using ag and au nanoparticles: A systematic study. *Analytical and Bioanalytical Chemistry.* 2014;406(9-10):2355-65.

133. Larmour I, Faulds K, Graham D. Sers activity and stability of the most frequently used silver colloids. *Journal of Raman Spectroscopy.* 2012;43(2):202-6.

134. Wang SS, Sherman ME, Rader JS, Carreon J, Schiffman M, Baker CC. Cervical tissue collection methods for rna preservation: Comparison of snap-frozen, ethanol-fixed, and rnalater-fixation. *Diagnostic Molecular Pathology.* 2006;15(3):144-8.

135. Micke P, Ohshima M, Tahmasebpoor S, Ren Z-P, Östman A, Pontén F, Botling J. Biobanking of fresh frozen tissue: Rna is stable in nonfixed surgical specimens. *Laboratory Investigation.* 2006;86(2):202-211.

136. Li Y, Pan J, Chen G, Li C, Lin S, Shao Y, Feng S, Huang Z, Xie S, Zeng H. Micro-raman spectroscopy study of cancerous and normal nasopharyngeal tissues. *Journal of Biomedical Optics.* 2013;18(2):027003.

137. Pergolese B, Bonifacio A, Bigotto A. Sers studies of the adsorption of guanine derivatives on gold colloidal nanoparticles. *Physical Chemistry Chemical Physics.* 2005;7(20):3610-3.

138. Narahara T, Kobayashi S, Hattori M, Shimpuku Y, van den Enden GJ, Kahlman JA, van Dijk M, van Woudenberg R. Optical disc system for digital video recording. *Japanese Journal of Applied Physics.* 2000;39(2S):912-19.

139. Keskin S, Çulha M. Label-free detection of proteins from dried-suspended droplets using surface enhanced raman scattering. *Analyst.* 2012;137(11):2651-7.

140. Avci E, Culha M. Influence of droplet drying configuration on surface-enhanced raman scattering performance. *RSC Advances.* 2013;3(39):17829-36.

141. Shen X, Ho C-M, Wong T-S. Minimal size of coffee ring structure. *The Journal of Physical Chemistry B.* 2010;114(16):5269-74.

142. Betz JF, Wei WY, Cheng Y, White IM, Rubloff GW. Simple sers substrates: Powerful, portable, and full of potential. *Physical Chemistry Chemical Physics.* 2014;16(6):2224-39.

143. Gutés A, Carraro C, Maboudian R. Silver dendrites from galvanic displacement on commercial aluminum foil as an effective sers substrate. *Journal of the American Chemical Society.* 2010;132(5):1476-7.

144. Huang Z, Meng G, Huang Q, Yang Y, Zhu C, Tang C. Improved sers performance from au nanopillar arrays by abridging the pillar tip spacing by ag sputtering. *Advanced Materials.* 2010;22(37):4136-9.

145. De Gelder J, De Gussem K, Vandenabeele P, Moens L. Reference database of raman spectra of biological molecules. *Journal of Raman Spectroscopy.* 2007;38(9):1133-47.

146. Dai WY, Lee S, Hsu YC. Discrimination between oral cancer and healthy cells based on the adenine signature detected by using raman spectroscopy. *Journal of Raman Spectroscopy.* 2017;49(2):336-342.

147. Movasaghi Z, Rehman S, Rehman IU. Raman spectroscopy of biological tissues. *Applied Spectroscopy Reviews.* 2007;42(5):493-541.

148. Smith W. Practical understanding and use of surface enhanced raman scattering/surface enhanced resonance raman scattering in chemical and biological analysis. *Chemical Society Reviews.* 2008;37(5):955-64.

149. Haynes CL, McFarland AD, Duyne RPV. Surface-enhanced raman spectroscopy. *ACS Publications*; 2005; 338-46A.

150. Aroca R. *Surface-enhanced vibrational spectroscopy*. Ontario: Canada: John Wiley & Sons; 2006.

151. Nguyen BH, Nguyen VH, Tran HN. Rich variety of substrates for surface enhanced raman spectroscopy. *Advances in Natural Sciences: Nanoscience and Nanotechnology.* 2016;7(3):033001.

152. Aydin Ö, Altaş M, Kahraman M, Bayrak ÖF, Çulha M. Differentiation of healthy brain tissue and tumors using surface-enhanced raman scattering. *Applied Spectroscopy.* 2009;63(10):1095-100.

153. Banki F, Yacoub WN, Hagen JA, Mason RJ, Ayazi S, DeMeester SR, Lipham JC, Danenberg K, Danenberg P, DeMeester TR. Plasma DNA is more reliable than carcinoembryonic antigen for diagnosis of recurrent esophageal cancer. *Journal of the American College of Surgeons.* 2008;207(1):30-5.

154. Gebhard R, Clayman R, Prigge W, Figenshau R, Staley N, Reesey C, Bear A. Abnormal cholesterol metabolism in renal clear cell carcinoma. *Journal of Lipid Research.* 1987;28(10):1177-84.

155. Hager MH, Solomon KR, Freeman MR. The role of cholesterol in prostate cancer. *Current Opinion in Clinical Nutrition & Metabolic Care.* 2006;9(4):379-85.

156. Stone N, Stavroulaki P, Kendall C, Birchall M, Barr H. Raman spectroscopy for early detection of laryngeal malignancy: Preliminary results. *The Laryngoscope.* 2000;110(10):1756-63.

157. Huang Z, McWilliams A, Lui H, McLean DI, Lam S, Zeng H. Near-infrared raman spectroscopy for optical diagnosis of lung cancer. *International Journal of Cancer.* 2003;107(6):1047-52.

158. Wang L-B, Shen J-G, Zhang S-Z, Ding K-F, Zheng S. Amino acid uptake in arterio-venous serum of normal and cancerous colon tissues. *World Journal of Gastroenterology.* 2004;10(9):1297-300.

159. Alo PL, Visca P, Marci A, Mangoni A, Botti C, Di Tondo U. Expression of fatty acid synthase (fas) as a predictor of recurrence in stage i breast carcinoma patients. *Cancer.* 1996;77(3):474-82.

160. Jensen V, Ladekarl M, Holm-Nielsen P, Melsen F, Sœrensen FB. The prognostic value of oncogenic antigen 519 (oa-519) expression and proliferative activity detected by antibody mib-i in node-negative breast cancer. *The Journal of Pathology.* 1995;176(4):343-52.

161. Shurbaji MS, Kalbfleisch JH, Thurmond TS. Immunohistochemical detection of a fatty acid synthase (oa-519) as a predictor of progression of prostate cancer. *Human Pathology.* 1996;27(9):917-21.

162. Burns-Cox N, Avery N, Gingell J, Bailey A. Changes in collagen metabolism in prostate cancer: A host response that may alter progression. *The Journal of Urology.* 2001;166(5):1698-701.

163. Miao S, Koenders E, Knobbe A. Automatic baseline correction of strain gauge signals. *Structural Control and Health Monitoring.* 2015;22(1):36-49.

164. Huang Z, Li Z, Chen R, Chen G, Lin D, Xi G, Chen Y, Lin H, Lei J, editors. The application of silver nanoparticle based sers in diagnosing thyroid tissue. *Journal of Physics: Conference Series; 2011*: IOP Publishing.

165. Salehi M, Steinigeweg D, Ströbel P, Marx A, Packeisen J, Schlücker S. Rapid immuno-sers microscopy for tissue imaging with single-nanoparticle sensitivity. *Journal of Biophotonics.* 2013;6(10):785-92.

166. Velickaa M, Radzvilaitea M, Ceponkusa J, Urbonienea V, Pucetaitea M, Jankeviciusb F, Steinera G, Sablinskasa V, editors. Assignment of vibrational spectral bands of kidney tissue by means of low temperature sers spectroscopy. *Proc of SPIE.* 2017;(10068):100681W

167. Wolthuis R, van Aken M, Fountas K, Robinson Jr JS, Bruining HA, Puppels GJ. Determination of water concentration in brain tissue by raman spectroscopy. *Analytical Chemistry.* 2001;73(16):3915-20.

APPENDIX A: APPROVAL OF ETHICAL BOARD

T.C. YEDİTEPE ÜNİVERSİTESİ

Sayı : 37068608-6100-15-1174 **25/02/2016**
Konu: Klinik Araştırmalar
Etik kurul Başvurusu hk.

İlgili Makama (Sevda Mert)

Yeditepe Üniversitesi Genetik ve Biyomühendislik Bölümü Prof. Dr. Mustafa Çulha'nın sorumlu olduğu **"Yüzeyde zenginleştirilmiş Raman saçılmasına dayalı patolojik tanı metotların geliştirilmesi"** isimli araştırma projesine ait Klinik Araştırmalar Etik Kurulu (KAEK) Başvuru Dosyası (**1159** kayıt Numaralı KAEK Başvuru Dosyası), Yeditepe Üniversitesi Klinik Araştırmalar Etik Kurulu tarafından **24.02.2016** tarihli toplantıda incelenmiştir.

Kurul tarafından yapılan inceleme sonucu, yukarıdaki isimi belirtilen çalışmanın yapılmasının etik ve bilimsel açıdan uygun olduğuna karar verilmiştir (**KAEK Karar No: 587**).

Prof. Dr. Turgay ÇELİK
Yeditepe Üniversitesi
Klinik Araştırmalar Etik Kurulu Başkanı

Yeditepe Üniversitesi 26 Ağustos Yerleşimi, İnönü Mahallesi Kayışdağı Caddesi 34755 Ataşehir / İstanbul
T. 0216 578 00 00 www.yeditepe.edu.tr F. 0216 578 02 99